



Universiteit  
Antwerpen

Faculteit Wetenschappen

Departement Chemie

# **Bio(inspired) strategies for the electro-sensing of $\beta$ -lactam antibiotics**

Proefschrift voorgelegd tot het behalen van de graad van

**Doctor in de Wetenschappen: Chemie**

aan de Universiteit Antwerpen, te verdedigen door

**Fabio Bottari**

Promoter: Prof. Dr. K. De Wael

Co-promoter: Prof. Dr. R. Blust

Antwerpen

2019



## Table of contents

<b>Aim of the thesis</b>	<b>8</b>
<b>General outline</b>	<b>9</b>
<i>List of abbreviations</i>	12
<b>Chapter 1</b>	
<b><math>\beta</math>-lactam antibiotics residues: an introduction</b>	<b>15</b>
Structure and classification of $\beta$ -lactams antibiotics	15
Use of antimicrobials in diary industries	17
Mechanisms of resistance	19
Current analytical methods for $\beta$ -lactam antibiotics	20
Sensors and biosensors	22
Electrochemical biosensors	24
Antibodies	24
Enzymes	25
Proteins	26
Aptamers	27
Molecularly imprinted polymers	29
Photoelectrochemistry-based strategies	31
Comparison of different analytical strategy for antibiotic residues	31
A new scenario: the electrochemical fingerprint for the identification of antibiotics residues	32
Cephalosporins	33
Penicillins	37
References	39
<b>Chapter 2</b>	
<b>Electrochemical fingerprinting of nafcillin and isoxazolyl penicillins</b>	<b>51</b>
Materials and methods	53
Reagents and materials	53
Instrumentation	53
Results and discussion	54

Nafcillin	54
Isoxazolyl penicillins	58
Conclusions	64
References	65

## Chapter 3

<b>Aptamers: bioreceptors for antibiotics identification</b>	<b>68</b>
Aptamers: selection strategies	68
Aptamers for $\beta$ -lactam antibiotics: the state of the art	74
Flu-Mag SELEX for nafcillin and cephalexin	77
Materials and methods	78
Flu-Mag SELEX	78
Reagents	78
Instrumentation	78
SELEX protocol	79
Immobilization of antibiotics onto magnetic beads	79
Selection round	79
Ethanol precipitation of ssDNA	79
PCR	80
dsDNA strand separation	80
Modified Graphene oxide (GO) SELEX	81
Adsorption test protocol	81
Results and discussion	82
Target immobilization on amine coated magnetic beads	82
ssDNA recovery optimization	83
PCR amplification	84
SELEX recovery rates	85
Modified GO-SELEX	87
ssDNA-GO ratio optimization	88
Influence of salts concentration on the ssDNA-GO interaction	89
Influence of buffer pH on the ssDNA-GO interaction	91

NAF GO-SELEX: optimization of the binding buffer	95
Conclusions	95
References	96

## Chapter 4

<b>Characterization of aptamers for small organic molecules</b>	<b>104</b>
A multi-faceted approach to study aptamer affinity	105
Materials and Methods	107
Aptamers and reagents	107
AuNPs synthesis	107
AuNPs colorimetric assay	108
ITC protocol	108
ITC with AuNPs	108
Native nESI-MS protocol	109
<sup>1</sup> H-NMR protocol	109
Results and Discussion	110
Colorimetric AuNPs assay	110
Aptamer binding in solution	113
Characterization of MN4 aptamer binding with quinine	117
Effect of AuNPs on ampicillin-binding aptamers	119
Conclusions	122
References	123

## Chapter 5

<b>Biomimetic receptors for antibiotics electroensing</b>	<b>127</b>
Material and Methods	129
Reagents	129
Rational monomer design	129
Electrochemical measurements	129
Conductive imprinted polymers for the direct electrochemical detection of cefquinome	130
Experimental section	130

Reagents	130
Rational monomer design	131
Electrochemical measurements	131
Analytical protocol	131
Electrode characterization	131
Results and discussion	132
Cefquinome electrochemical behaviour	132
4-ABA electropolymerization study	132
Optimization of the pH	133
Optimization of scan rate, monomer concentration and number of CV cycles	136
MWCNTs	138
CFQ-MIP synthesis protocol	140
Analytical protocol and calibration plot	143
Interference study	143
Conclusions	144
Electropolymerized o-phenylenediamine on graphite promoting the electrochemical detection of nafcillin	146
Experimental Section	146
Reagents	146
Rational monomer design	146
Analytical parameters	147
Results and Discussion	147
o-Phenylenediamine electropolymerization	147
oPD-SPE characterization	150
Optimized detection of NAF at oPD-SPE	150
Interfering compounds and degradation study	152
Calibration plot	153
Real sample analysis	154
Conclusions	154
Final remarks	154

References	156
------------	-----

## **Chapter 6**

<b>Electrochemistry in milk</b>	<b>163</b>
---------------------------------	------------

Materials and methods	165
-----------------------	-----

Milk pretreatments evaluation	165
-------------------------------	-----

Results and Discussion	166
------------------------	-----

Electrochemical behaviour of ACN and ISO in 0.1 M PB pH 2 and whole milk	166
--	-----

Electrochemical behaviour of CFQ in ACN and ISO	168
---	-----

Simplified pre-treatment	169
--------------------------	-----

Electrochemistry in undiluted raw milk - Effect of chloride ions on $\beta$ -lactam antibiotics electrochemistry in buffer solutions	171
--	-----

Electrochemistry of $\beta$ -lactam antibiotics in raw milk and with addition of KNO <sub>3</sub>	175
---	-----

Conclusions	180
-------------	-----

References	182
------------	-----

<b>Conclusions and perspectives</b>	<b>186</b>
-------------------------------------	------------

<b>Appendix</b>	<b>192</b>
-----------------	------------

Classification of $\beta$ -lactam antibiotics	192
---	-----

Abstract	196
----------	-----

Samenvatting	198
--------------	-----

Academic curriculum vitae	201
---------------------------	-----

Acknowledgments	205
-----------------	-----

# Aim of the thesis

---

The presence of antibiotic residues, particularly  $\beta$ -lactams, in the food chain is a severe threat to the public health. These residues have several adverse effects and contribute to the increase of antimicrobial resistance (AMR). It is worth to notice that the occurrence of resistant strain of bacteria is regarded as one of the biggest threat to public health in the years to come. To fight and control AMR, international regulatory agencies have established maximum residues limits (MRLs) for the antibiotic residues in food commodities and animal tissues. The prevention strategies require frequent, large-scale monitoring plans to be performed on-site using selective, sensitive and reliable analytical tools. The current screening methods, mostly based on microbial growth inhibition assays, lack in selectivity and are prone to false positive and negative results. The aim of the present thesis is to develop a new class of analytical tools, which can be employed in the on-site monitoring of  $\beta$ -lactam antibiotics at their MRLs level in milk. The proposed approach is based on the electrochemical behaviour of these antibiotics, the so called electrochemical fingerprint. To attain better selectivity and sensitivity, we combine this electrochemical fingerprint identification with electrode modifiers, namely aptamers and polymers. The proposed modified electrodes are evaluated in term of analytical performances taking into account the cost, user-friendliness and applicability on-site along with recyclability and eco-friendliness. The final goal is to use these bio(mimetic) sensors for on-site milk analysis performed by non-specialists.



# General outline

---

The dire previsions of the World Health Organization on the so-called “post-antibiotic era”, with the continuous and global rise of anti-microbial resistance (AMR), spurs the research community to find better ways to fight this threat by implementing vast-scale prevention strategies and cautious use of antimicrobial drugs. In light of this severe threat to human health many attempts have been made to develop efficient methods to detect antibiotic residues in different streams. Electrochemistry offers an inviting approach for on-site and fast monitoring. In this thesis, the need of reliable analytical approaches for monitoring plans will be addressed exploiting electrochemistry coupled with novel bio(mimetic) recognition elements, specifically aptamers and polymers. The proposed strategies were developed keeping in mind the final application of selective and sensitive determination of  $\beta$ -lactam residues in milk at their respective Maximum Residues Limits (MRLs), established by the European Union.

**Chapter 1** presents an overview on  $\beta$ -lactam antibiotics, their mode of action and the insurgence of AMR especially in the context of food and feed safety, with a focus on the current analytical problems faced by producers and authorities. A review on sensing strategies based on (bio)mimetic electrode modifiers will be presented, along with the state of the art on the electrochemistry of  $\beta$ -lactam antibiotics.

In **Chapter 2** a novel methodology for the identification of antibiotics residue by means of their electrochemical fingerprint will be outlined. The limits and the potential of this approach will be highlighted. The study of the electrochemistry of nafcillin and of the isoxazolyl penicillin group will be reported in detail.

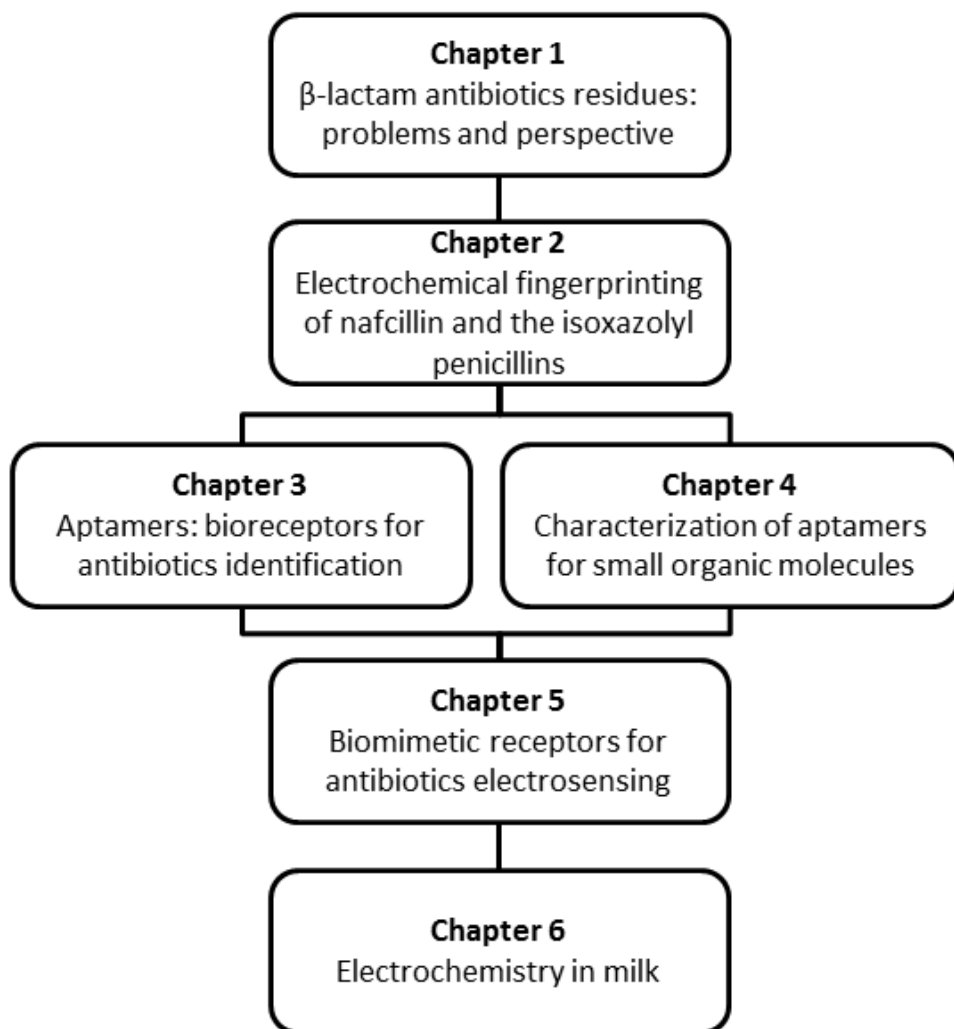
**Chapter 3** will be devoted to aptamers as bio recognition elements and their selection strategies, with a focus on small organic molecules detection. The available aptamers for  $\beta$ -lactam antibiotics will be critically reviewed and the results of the SELEX procedures for nafcillin and cephalexin, two antibiotics difficult to detect with the current screening test, will be presented. Two protocols for aptamer selection will be compared: the traditional FluMag SELEX procedure and a variation based on graphene oxide.

The goal of **Chapter 4** is to shed light on the characterization approaches of aptamers for small organic molecules. The state of the art will be outlined and an example of a robust and reliable characterization protocol will be presented, stressing the importance of the awareness on aptamer binding mechanism studies. The case of AMP17, an aptamer for ampicillin, will show how poor our understanding is of the affinity and binding mechanism for these kind of receptors and the need for a re-evaluation of some critical parameters, especially if those aptamers are needed for ultra-sensitive analytical applications.

**Chapter 5** will show an approach for  $\beta$ -lactam residues electroensing at electrodes modified through the electropolymerization of (in silico selected) monomers. Two case studies will be presented: i) the development of a conductive molecular imprinted polymer for the detection of cefquinome and ii) the modification of the electrode surface with electropolymerized o-phenylenediamine for the analysis of nafcillin. These approaches benefit from a deeper understanding of the interaction between the monomer and its target, obtained by rational monomer design. The proposed protocols are very promising for technology transfer.

**Chapter 6** will focus on the efforts devoted to the detection of  $\beta$ -lactam antibiotics in raw milk. After an overview of the composition of the milk matrix, two strategies to promote the electrochemical oxidation of  $\beta$ -lactams on graphite screen printed electrodes will be presented. A simplified pre-treatment based on solvent addition (isopropanol or acetonitrile) will be optimized along with the study of the antibiotics electrochemistry in raw undiluted milk based on the addition of high concentration of supporting electrolyte.

The **Conclusions and perspectives** section will give the reader an outlook on possible future directions, underlining what has been achieved and what still needs to be done to fully exploit the joint action between electrochemistry and bio(mimetic) receptors for  $\beta$ -lactam analysis in milk.



### ***List of abbreviations***

<sup>1</sup>H-NMR – Nuclear magnetic resonance  
2E1N - 2-ethoxy-1-naphtoic acid  
3CMC - 3-(2-chlorophenyl)-5-methyl-4-isoxazolecarboxylic acid  
4-ABA – 4-aminobenzoic acid  
6-APA - 6-aminopenicilloic acid  
7-ACA - 7-aminocephalosporanic acid  
7-ADCA - 7- aminodeacetoxycephalosporanic acid  
ACN – Acetonitrile  
AMP – Ampicillin  
AMR – Antimicrobial resistance  
AMX – Amoxicillin  
ANI - Aniline  
AuNPs- Gold nanoparticles  
BDD – Boron doped diamond  
BRB – Britton-Robinson buffer  
CAP – Chloramphenicol  
CE – Capillary electrophoresis  
CFP – Cefpirome  
CFQ – Cefquinome  
CFU – Ceftiofur  
CFX – Cefalexin  
CLX – Cloxacillin  
CV – Cyclic voltammetry  
DCLX – Dicloxacillin  
DPV – Differential pulse voltammetry  
DSD – Double step detection  
dsDNA – double stranded DNA  
ECP – Electronically conductive polymer  
EDC - 1-Etil-3-(3-dimetilaminopropil)carbodiimide  
EIS – Electrochemical impedance spectroscopy  
ET – Electron transfer  
FCLX – Flucloxacillin  
FIA – Flow injection analysis  
GC – Glassy carbon  
GO – Graphene oxide

G-SPE – Graphite screen printed electrode  
IF – Imprinting factor  
ISO – Isopropanol  
ISOXA – Isoxazolyl penicillins  
ITC – Isothermal titration calorimetry  
 $K_d$  – Binding constant  
LC-QTOFMS - liquid chromatography coupled with quadrupole time of flight mass spectrometry  
LOD – Limit of detection  
LSV –Linear sweep voltammetry  
MES - 2-(N-morpholino)ethanesulfonic acid  
MIP – Molecularly imprinted polymer  
MRL – Maximum residue limits  
MS – Mass spectrometry  
MWCNTs – Multi walled carbon nanotubes  
NAF – Nafcillin  
nESI-MS – Native electron spray ionization mass spectrometry  
NHS - N-hydroxysuccinimide  
NIP – Non imprinted polymer  
OCP – Open circuit potential  
oPD – o-phenylenediamine  
OXA – Oxacillin  
PB – Phosphate buffer  
PBP – Penicillin-binding protein  
PBS – Phosphate buffer saline  
PCR – Polymerase chain reaction  
PEN V – Penicillin V  
PENG – Penicillin G  
Rct – Charge transfer resistance  
SC – Side chain  
SCE – Saturated calomel electrode  
SELEX – Systematic evolution of ligands by exponential enrichment  
SEM – Scanning electron microscopy  
SPE – Solid phase extraction  
SPR – Surface plasmon resonance  
SSC – Saline sodium citrate buffer

SSD – Single step detection  
ssDNA – single stranded DNA  
SWV – Square wave voltammetry

# $\beta$ -lactam antibiotics residues: an introduction

---

$\beta$ -lactam antibiotics are a class of broad-spectrum antimicrobials, all with a  $\beta$ -lactam ring in their molecular structure. These include penicillin derivatives (penams), cephalosporins (cephems), monobactams and carbapenems.  $\beta$ -lactam antibiotics are indicated for the prevention and treatment of bacterial infections caused by both Gram-positive and Gram-negative bacteria and can be used in human and animal medicine. This section will give a brief overview on their structure and classification, their use in medicine and the mechanism of anti-microbial resistance.

## Structure and classification of $\beta$ -lactams antibiotics

Penicillins and cephalosporins are the two most used classes of antimicrobial drugs nowadays [1–3] and are indicated as critically important antibiotics both for human [4] and veterinary medicine [5]. These drugs are bactericidal and act on the synthesis of the peptidoglycan layer of bacterial cell walls and cell wall structural integrity. The bactericidal activity of all  $\beta$ -lactam antibiotics derives mainly from the four-membered  $\beta$ -lactam ring (Fig. 1.1) as they interfere with the final transpeptidation step and competitively inhibit crosslinking of peptidoglycans [6]. Penicillins, such as penicillin G, penicillin V, amoxicillin, nafcillin, and ampicillin, are used for the treatment of Gram-positive infections and may be used alone or in preparations that include beta-lactamase inhibitors, such as clavulanic acid, tazobactam, and sulbactam, for treatment of penicillin-resistant organisms (see also Table A1). As shown in Table A2, several generations (first through fifth) of cephalosporin antibiotics have been developed and are widely prescribed with an increasingly broader spectrum of action against both Gram-negative and Gram-positive organisms. First-generation cephalosporins (e.g., cefazolin) are predominantly active against Gram-positive bacteria, while following generations have increased activity against Gram-negative bacteria, with a slight decrease in the efficiency against Gram-positive as trade-off.

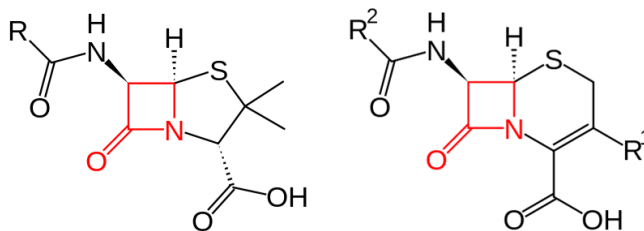


**Fig. 1.1** Core structure of penicillins (left) and cephalosporins (right) with the  $\beta$ -lactam ring in red.

Others  $\beta$ -lactam antibiotics, namely penem, carbapenem and monobactam (Table A3) are employed for specific therapeutic purposes: for example monobactams are active only against aerobic Gram-negative bacteria, such as *Pseudomonas* [7] while carbapenems are considered the last line of defence against bacteria that developed multi-drug resistance (MDR) [8].

The abuse and misuse of  $\beta$ -lactam antibiotics, and antimicrobials in general, is cause of great concern worldwide. Residues in the environment and in the food chain may cause allergic reactions in hypertensive individuals, interfere with fermentation processes, but most importantly, increase antimicrobial resistance (AMR) [9]. According to the World Health Organization (WHO), only in Europe each year about 25 000 patients die from infections caused by AMR [10]. In this frame, preventive strategies, such as large monitoring plans, are of paramount importance to fight the insurgence of AMR along with the development and commercialization of new and effective antibiotics.

The European Commission strictly regulates the levels of antibiotic residues in food and feed products. In the European Commission Regulation 37/2010, a Maximum Residue Limit (MRL) has been attributed to each antimicrobial drug in different matrixes, such as meat and milk [11]. Milk contamination with antibiotic residues is a relevant problem, not only for the obvious contribution to the AMR insurgence but also for the huge economic losses for dairy industries and farmers.

Penicillins and cephalosporins MRL values in bovine milk (Table 1.1) are in the range between 4 and 125  $\mu\text{g}/\text{kg}$  (or ppb) and in most cases their marker residues correspond to the entire antibiotic (with exception of ceftiofur and cephapirin).



**Table 1.1.** Maximum residue limits (MRLs, Commission Regulation (EU) No 37/2010 and amendments) of penicillins and cephalosporin in bovine milk.

Group	Pharmacologically active substance	Marker residues	MRL ( $\mu\text{g}/\text{kg}$ )
Penicillins	benzylpenicillin	benzylpenicillin	4
	ampicillin	ampicillin	4
	amoxicillin	amoxicillin	4
	oxacillin	oxacillin	30
	cloxacillin	cloxacillin	30
	dicloxacillin	dicloxacillin	30
	nafcillin	nafcillin	30
	penethamate	benzylpenicillin	4
Cephalosporins		sum of all residues retaining the $\beta$ -lactam structure expressed as desfuroylceftiofur	100
	ceftiofur		
	cefquinome	cefquinome	20
	cefazolin	cefazolin	50
	cephapirin	sum of cephapirin & desacetylcephapirin	60
	cefacetrile	cefacetrile	125
	cefoperazone	cefoperazone	50
	cefalexin	cefalexin	100
cefalonium	cefalonium	20	

## Use of antimicrobials in dairy industries

Antimicrobial drugs are used, since their discovery, in the daily practice of dairy industries and farms, not only for therapeutic and prophylactic purpose but also as growth promoters. Among the various classes of antibiotics, penicillins and tetracyclines cover more than 50% of the total antibiotics consumption worldwide with polypeptides, macrolides and sulphonamides accounting for around 20% (Fig. 1.2). The other classes of  $\beta$ -lactam antibiotics are less frequently used, with cephalosporins only reaching 0.9% of the total consumption.

## Chapter 1 - $\beta$ -lactam antibiotics residues: an introduction

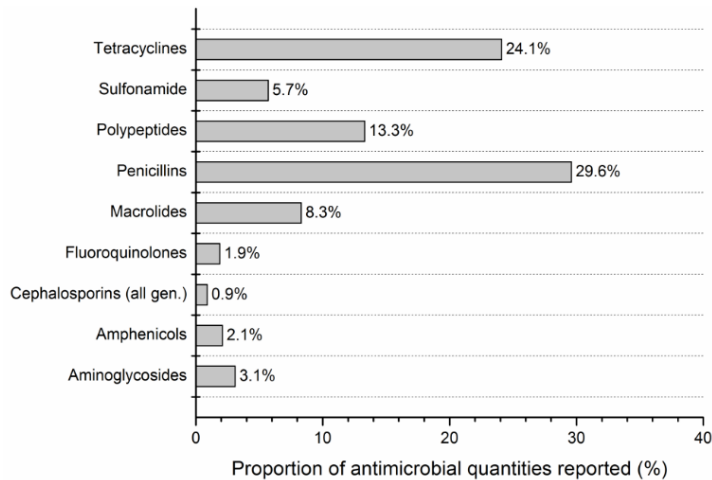


**Fig. 1.2** Proportion of antimicrobial quantities (by antimicrobial class) reported for use in animals worldwide from 2013-2016 (data from [3]).

In Europe, the situation is similar to the rest of the world, with tetracyclines (more than 40%) and penicillins (20%) leading the consumption. Cephalosporins account for only 0.7%, which can be explained by the fact that they are only used in specific cases as extra-label drugs, when other treatments are ineffective [12], while tetracyclines and penicillins have a broad spectrum of action.

The majority of  $\beta$ -lactam antibiotics are used in the dairy industry to treat the most common diseases of cows like mastitis, lameness, respiratory disease and gastrointestinal disorders [13]. Mastitis is the most common disease in lactating dairy cattle [12], and can be caused by intramammary infections, trauma, or chemical agents. It consists of an inflammation of the mammary gland and udder tissue that occurs as immune response to bacterial infections. Milk quality is negatively impacted by an increase in somatic cell count (SCC) and both clinical and subclinical mastitis can impact milk production and quality [14]. There are also prophylactic uses of antimicrobials, such as dry cow therapy [15] and treatments to prevent dairy calves disease like diarrhoea or pneumonia [16]. Routine practices vary worldwide based on cultural and legislative differences related to food safety, access to drugs, and different modes of dairy production.

## Mechanisms of resistance

$\beta$ -lactam antibiotics exert their antimicrobial effect by covalently binding to bacterial penicillin-binding proteins (PBPs) which are diverse enzymes (transpeptidases or carboxypeptidases) involved in bacterial cell wall synthesis and are situated in the cytoplasmic membrane of the bacteria. When antibiotics bind to PBPs, bacterial cell wall synthesis is impaired due to cell wall lysis, disruption of cell shape, and inhibition of cell division which eventually causes death. However, to exert their antibacterial action, these drugs must diffuse through the bacterial cell wall to bind with PBPs and the antibiotic must resist enzymatic degradation.

Resistance to beta-lactam antibiotics occurs through different mechanisms: the modification of PBPs structure that leads to a reduced binding affinity for the antibiotic, the alteration of porins that decrease the ability of the antibiotic to diffuse through bacterial cell wall (Fig. 1.3) and the action of beta-lactamases enzymes that inactivate the antibiotic by hydrolysis of beta-lactam ring [17,18]. Resistance to beta-lactam antibiotics due to PBP modification is either related to mutations of genes encoding PBPs or through acquisition of supplementary new genes that encode new PBPs with low or no affinity for beta-lactam antibiotics.

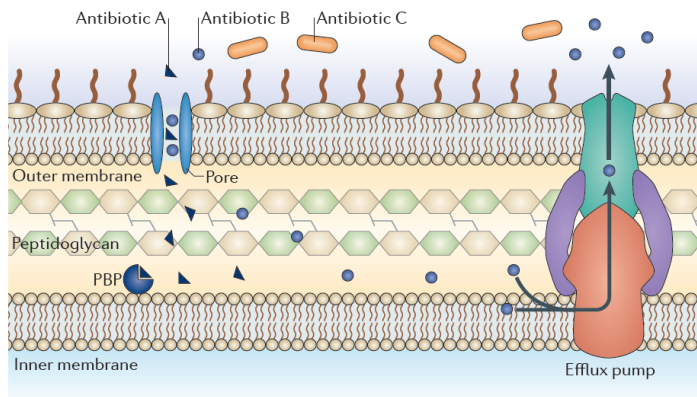


**Fig. 1.3** The figure shows an overview of resistance mechanisms. The example shown is of  $\beta$ -lactam antibiotics targeting a penicillin-binding protein (PBP). Antibiotic A can enter the cell via a porin protein, reach its target and inhibit peptidoglycan synthesis. Antibiotic B can also enter the cell via a porin, but unlike antibiotic A, it is efficiently removed by efflux. Antibiotic C cannot cross the outer membrane and so is unable to access the target PBP (from ref. [17]).

Gram-negative bacteria surround themselves with an additional outer membrane which acts as a barrier for antibiotics to diffuse through the membrane with subsequent binding with PBPs. Usually antibiotics and nutrients diffuse through the

protein channels on the cell membrane known as “porins.” During antibiotic resistance, these porin channels are altered thus reducing diffusion of antibiotics in the bacterial cell. However, the most common mechanism of  $\beta$ -lactam resistance is the production of  $\beta$ -lactamases by resistant bacteria [19]. The fast development of these resistance mechanisms has led from one side to the continuous need of new antibiotics and from the other side to the need of preventing bacteria exposure to antibiotics in the environment. Thus novel sensing and biosensing strategies are needed to address this growing societal and environmental issue.

### **Current analytical methods for $\beta$ -lactam antibiotics<sup>1</sup>**

Developing on-site analytical tools to monitor  $\beta$ -lactam residues in milk is a great challenge. Commonly used screening tests and novel (bio)sensor approaches will be now discussed and compared, underlining the limitations of currently employed analytical methods and the challenges that new concepts still face before implementation in the field.

Milk undergoes several tests during the different stages of collection and processing to assure its quality and safety. The methods for the detection of antibiotic residues can be divided into two categories: screening tests [20,21] and confirmatory methods [22,23]. In general, screening tests allow checking whether a sample contains antibiotic residues and provides mostly a yes/no type of answer and are, by design, geared towards the total antimicrobial residues content without discriminating between different antibiotics with different MRL values. In case of a positive result, it is essential to perform further analysis using confirmatory methods for an accurate identification and quantification of the residues.

Confirmatory methods consist mostly of chromatography-based techniques coupled with mass spectrometry [24–26], however the application of these methods is limited by their cost and time-consumption, by complicated sample pretreatments and by the need of specialized personnel. In an attempt to overcome such limitations, in the last decades, research mainly focused on qualitative, fast and cheap microbial inhibition tests. These have been optimized and thoroughly validated over the years [27,28].

---

<sup>1</sup> Partially based on F. Bottari, R. Blust, K. De Wael, *Bio(inspired) strategies for the electro-sensing of  $\beta$ -lactam antibiotics*, *Current Opinion in Electrochemistry*, 10, 2018, 136-142.

Microbial inhibition assays are based on spores of specific bacteria, sensitive to particular antibiotics, placed on agar gel containing nutrients for bacterial growth and a pH indicator [29]. After addition of milk to the test, it is incubated at the appropriate temperature to allow the growth of the bacteria on the agar gel. In the absence of antibiotic residues, the bacterial proliferation can be detected visually either by the change of opacity of the agar medium or by the colour change of the pH indicator, resulting from the production of acid metabolites. In the presence of antibiotic residues (or any other inhibitors such as somatic cells), the growth is suppressed and there are no observable changes of colour [30]. The main advantages of these tests are their low cost, ease of use, and broad selectivity toward different antibiotics, which are attractive qualities for large monitoring plans. Nevertheless, the bacterial strains used in these tests should be constantly monitored to ensure that they have not become resistant to the antimicrobials. The interpretation of the outcomes is often subjective and false negative or positive results are common [31,32].



**Fig. 1.4** Example of microbial inhibition tests, commercially known as Delvotest and CowSide II On the left: the main steps needed to perform a Delvotest. On the right: the complete kit of CowSide II (from company websites).

Apart from microbial inhibition tests, numerous screening tests based either on immunoassay or enzymatic reactions are available [33–35]. Most of them are receptor based assays. Since receptors are designed to bind only the active substances, the receptor technology has a higher accuracy in the detection of antibiotics. Receptor screening methods, such as radio receptor assay, colloidal gold receptor assay, enzyme colorimetry, enzyme labelling assay and biosensor assay,

have been established for the detection of specific classes of antibiotics such as  $\beta$ -lactams, sulphonamides and tetracyclines [36].

In radio receptor assays, target molecules labelled with radioisotopes ( $^{14}\text{C}$  and  $^3\text{H}$ ) compete with the ones in the milk sample to bind a specific site. Then, their binding rate is measured by a scintillation counter and expressed in term of target concentration. These assays are recognized standard screening tests, currently used in China under the commercial names of CHARM I ( $\beta$ -lactams in milk) and II ( $\beta$ -lactams, tetracyclines, sulphonamides, aminoglycosides, chloramphenicol, novobiocin, and macrolides in milk, meat, seafood, honey, etc.) [37–39]. Although these tests have good performances, radioisotopes are not the best candidates for developing in-situ, cheap tests. CHARM kits require trained operators, present a complex waste-disposal protocols and, not less important, are more expensive than microbial inhibition tests.

A receptor assay that does not present major pollution problems and has fast responses is the colloidal gold receptor assay, where the receptor proteins are labelled with coloured colloidal gold particles. The sample is added to the colloidal gold test strips and after five minutes of interaction, two red bands will appear; if the bands are weaker than the control, the result is positive, otherwise it is negative [40]. Even if these assays can detect 15  $\beta$ -lactams antibiotics in milk samples at MRL levels and are commercialized in Europe (Beta Star and Twin Sensor BT) and USA (Charm Rosa MRL), they present similar limits to the microbial tests: they provide simple quantifications with yes/no answer and are prone to interference.

A detection strategy based on colour change is the enzymatic colorimetric assay. The detection of antibiotic residues is performed by measuring the degree of inactivation of the DD-carboxypeptidase by  $\beta$ -lactams which causes a chain reaction, revealed by a redox indicator [41]. Enzyme-labelling receptor assay (ELRA) avoids the problem of interfering compounds by exploiting the specific interaction of a receptor-ligand and enzyme labelling technique, showing principles similar to Enzyme-Linked Immunosorbent Assay (ELISA) [42–44]. The enzyme labels are very selective and less expensive than radioisotopes but the protein stability is poor and a large scale technological transfer for in-situ monitoring has not been achieved.

### **Sensors and biosensors**

Several relevant examples of (bio)sensors for the analytical determination of  $\beta$ -lactams in food and feed have been reported in the last decades. Optical

biosensors are, along with electrochemical ones, the most commonly used both for research and commercial applications [45,46]. Surface plasmon resonance (SPR) has also been employed in several analytical configurations for the analysis of  $\beta$ -lactam antibiotics. In 2001 Gaudin *et al.* [47] reported an optical immunosensor based on SPR for ampicillin detection. They showed a different specificity of the chosen antibody against the intact and degraded form of the drug and compared enzymatic and chemical digestion to improve the sensitivity of the assay against the open ring structure. Another example of SPR immunosensor for ampicillin was reported by Tomassetti *et al.* [48] where they combined anti-ampicillin antibodies with SPR detection coupled with a flow system, attaining fast quantification times (below 30 minutes) with good selectivity against other antibiotics of the same class. Penicillin G (PENG) is another antibiotic that was detected with an immuno-SPR biosensor [49]; it used a competitive assay between PENG free in solution and conjugated with BSA, which was deposited on the sensor chip surface.

Other molecular recognition layers were used for antibiotics determination *via* SPR: Gustavsson *et al.* [50] combined enzymatic digestion with antibody recognition, for the by-products of the enzymatic reaction, to detect PENG in buffer and raw milk. Penicillin binding protein was also employed as capturing agent in a displacement assay for determination of benzylpenicillin, ampicillin, amoxicillin, cloxacillin, cephalixin and cefoperazone [51]. Still based on optical readout, chemiluminescent biosensors for  $\beta$ -lactams identification have attracted considerable attention in the past years. The detection event is based on the oxidation of the antibiotics, by means of oxidizing agents, in strong alkaline solutions. The hydrolysis of the lactam ring produces hydroxyl and superoxide radicals which in turn react with the luminophore, producing the chemiluminescent signal [52,53]. Several oxidizing agents were employed, namely  $\text{KO}_2$  [54],  $\text{KIO}_4$  [52,53],  $\text{KMnO}_4$  [55],  $\text{K}_3\text{Fe}(\text{CN})_6$  [56] and thiosemicarbazide [57]. The proposed methods attained good performances in term of limits of detection, even if the selectivity was still an issue. More recent examples combine the chemiluminescent detection with chip technology to attain simultaneous multi-analyte identification: Kloth *et al.* [58] reported a microarray immunochip based on chemiluminescence detection for the simultaneous quantification of 13 different antibiotics. Also nanomaterials have been employed as signal enhancer for the traditional luminol- $\text{H}_2\text{O}_2$  chemiluminescence reaction, *e.g.*, cupric oxide nanoparticles have been used for the determination of amoxicillin and cefazolin [59].

## Chapter 1 - $\beta$ -lactam antibiotics residues: an introduction

A luminescence based sensor was also proposed based on the bioluminescence of living organisms. An *Escherichia coli* strain, modified to host a plasmid gene (pBlaLux1) encoding the production of luciferase from *Photobacterium luminescens* [60], was used as whole cell biosensor to detect the presence of  $\beta$ -lactam antibiotics. Combining the antibiotics-induced bioluminescence of the mutated strain with a pattern recognition algorithm allowed to selectively detect several different antibiotics, both penicillins and cephalosporins [61].

Biosensors based on fluorescence have also been developed for antibiotic residues detection in raw milk. Bacigalupo *et al.* [62] formulated a fluoroimmunoassay for quantitative determination of ampicillin in cow milk samples with different fat contents. The fluorescent marker used was a goat anti-rabbit IgG conjugated with a chelating molecule complexed with  $\text{Eu}^{3+}$ . One of the very few examples of analytical quantification of carbapenems is also based on fluorescent detection [63] with meropenem (MP) and ertapenem (EP) being detected in pharmaceutical formulations. The method is based on the chelation of MP with  $\text{Tb}^{3+}$  and EP with  $\text{Zr}^{4+}$  in buffered organic medium at pH 4.0 to produce fluorescent chelates with zero and second-derivative synchronous fluorescence spectroscopy.

$\beta$ -lactam antibiotics have a very small mass compared to other analytical targets and thus are difficult to detect with mass-sensitive transducers [46], nevertheless a few examples of such biosensors have been reported in literature. Gruhl and Länge devised a surface acoustic wave (SAW) biosensor for PENG in milk [64]. The authors used a binding inhibition assay to overcome the mass limitation of the antibiotic, quantifying the free paratopes of the monoclonal anti-penicillin antibodies attached to the chip surface.

### **Electrochemical biosensors**

In the group of biosensors, electrochemical biosensing represents a promising strategy to monitor  $\beta$ -lactam residues combining a fast and easy-to-use analytical platform with integrated highly selective bio-recognition elements. In this section, the most recent findings in the field of electrochemical biosensing targeting  $\beta$ -lactam antibiotics and via the use of different molecular (bio)recognition elements will be presented.

#### **Antibodies**

Despite the huge amount of antibodies available on the market today, only a few have been raised against  $\beta$ -lactam antibiotics [65]. The main challenge, as



with other small molecules, lies in the poor immunogenicity of the compounds and the need to couple them with carrier proteins to elicit an immune response in animals. Despite this limitation, some anti-penicillin and anti-cephalosporin antibodies, both monoclonal and polyclonal, are available on the market, and have been used for a variety of biosensing applications [46]. However, the reported cross-reactivity with different types of antibiotics makes them unsuitable for the selective detection of single  $\beta$ -lactams. Recently, electrochemical immunosensors have been reported: Merola *et al.* [66] developed two competitive assays based on the immobilization of the molecular recognition layers on an Immobilon membrane, with amperometric readout following the activity of an enzymatic label, horse radish peroxidase (HRP). They achieved a limit of detection (LOD) in the low nanomolar range ( $10^{-10}$  M), also in real samples. Even if the class-selectivity is good, the antibodies also recognize other penicillins as well as some cephalosporins. The same research group lately proposed an improved strategy in which the immobilized PENG was conjugated to Bovine Serum Albumin (BSA), exploiting the already investigated competitive assay [67], with a slightly better selectivity. Li *et al.* [68] exploited a mouse anti PENG antibody to develop an impedimetric sensor, based on a bilayer lipid membrane modified with gold nanoparticles (AuNPs), to promote the immobilization of the antibodies. They report an increase in sensitivity due to the presence of nanoparticles, reaching a LOD of  $2.7 \times 10^{-4}$  ng/L. They tested the interference effect of two other antibiotics, ampicillin and streptomycin, obtaining also good recovery for real milk samples. Karaseva *et al.* [69] tested both monoclonal and polyclonal antibodies against PENG and AMP in a piezoelectric based sensor, immobilizing an antibiotic-protein conjugate on the surface of a polypyrrole modified electrode. They tested the sensors in different kinds of real samples with good recovery rates (>90%).

The intrinsic characteristic of the antibodies (stability, cost, ease of use) may limit the feasibility of a selective immunosensor for on-site screening even if good results were achieved in terms of real sample analysis and LOD [70].

### Enzymes

$\beta$ -Lactamase are bacterial enzymes which represent the most important mechanism of AMR. These enzymes, also called penicillinases, catalyse the hydrolysis of the lactam ring, the core structure of every  $\beta$ -lactam antibiotic, inactivating the drug [71]. The hydrolysis, operated by  $\beta$ -lactamases, involves

proton exchange that can be monitored by following the pH changes associated with the enzymatic reaction.

The most common electrochemical readout systems are amperometry and potentiometry; Wu *et al.* [72] used a pH indicator, hematein, to monitor the change of  $H^+$  concentration. The amperometric signal was given by the reduction of hematein to hematoxylin and the enzyme, in this case, was immobilized on graphene nanosheets modified with ionic liquids. Sotomajor and co-workers [73] used a cysteine SAM-modified gold electrode to immobilize a Class B penicillinase enzyme, followed by chronoamperometric detection of the pH changes in solutions upon addition of PENG. The same authors have exploited cobalt phthalocyanine as an electron mediator, with lower LOD ( $7.9 \times 10^{-8}$  M) and a wide linear range from  $2.6 \times 10^{-7}$  to  $6.6 \times 10^{-7}$  M [74]. As far as potentiometric detection is concerned, the group of Ismail used a potentiometric titration approach with different immobilization layers such as poly-vinyl alcohol [75] and polypyrrole [76] or the combination of both [77] together with glutaraldehyde and BSA. However, while useful for pharmaceutical formulations, milk sample analysis proved to be problematic and the reported LOD (3  $\mu$ M) is rather high.

All the above mentioned methods, while very sensitive in certain configurations, completely lack selectivity towards different  $\beta$ -lactams antibiotics, hindering their use in real samples.

### Proteins

The main antimicrobial activity of  $\beta$ -lactams antibiotics is expressed by the inhibition of the bacterial cell wall synthesis. The core structure of the antibiotics mimics the substrate of PBPs, that catalyse the polymerization of the glycan strands to form peptidoglycan [78]. Since this interaction is very specific and efficient ( $20 M^{-1} s^{-1}$  for benzylpenicillin) it was explored as a molecular recognition layer for antibiotic biosensing. In the last years, the group of Pingarron proposed two different assays exploiting a recombinant PBPs from *Streptococcus pneumoniae* R6. Firstly, they immobilized PBP on  $Co^{2+}$ -tetradentate nitrilotriacetic acid-modified screen printed electrodes [79], in a second approach they employed paramagnetic beads coated with the complex His-Tag-Isolation [80] (Fig. 1.5). Quantification of the binding event was performed with a competitive assay between the antibiotic residues and a HRP-labelled tracer. The use of magnetic beads allows better control in the washing and incubation steps and the total analysis time is around 30 minutes. These assays recognize specifically the active form of the antibiotics, an

issue rarely considered in the antibiotics biosensors literature. The LOD is well below the MRL values (0.7 and 0.9 ng/ml respectively) and the recovery rate from a real milk samples is satisfying (> 98%). The short shelf-life ( $\leq 10$  days) and the rather time consuming protocol to obtain the recombinant PBP, coupled with the lack of specificity, are possible drawbacks for future commercialization of this strategy.

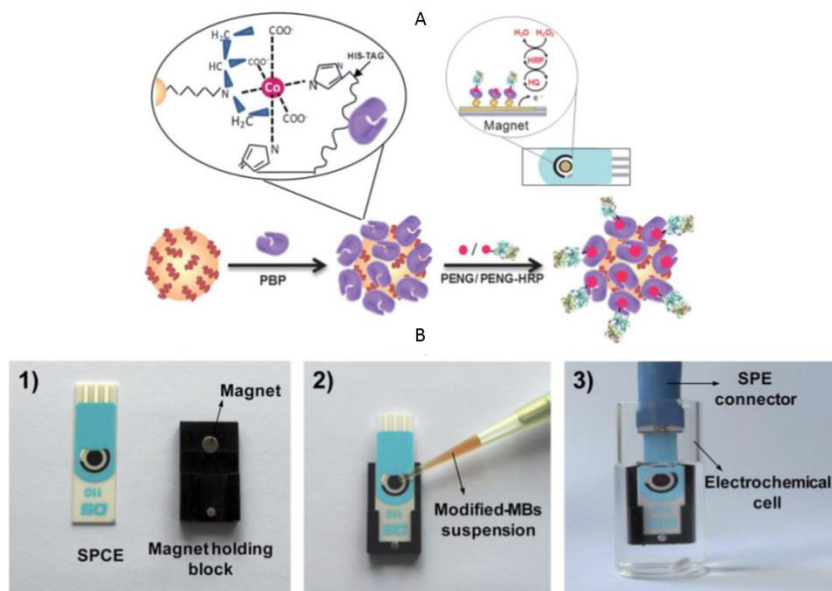


**Fig. 1.5** (A) Schematic display of the steps involved in the  $\beta$ -lactam antibiotics affinity magnetosensor developed. (B) Picture showing the SPCE and the homemade magnet holding block (1), the deposition of the modified MBs on the SPCE assembled on the magnet holding block (2) and the assembled SPCE-magnet holding block immersed in the electrochemical cell used for the amperometric measurements (3).

## Aptamers

Aptamers are short strands of DNA or RNA that recognize, with high specificity, the target against which they were selected. Regarded as one of the main innovations in the field of biomimetic materials, aptamers have attracted a lot of attention in recent years, especially for therapeutic applications and drug-delivery [81,82]. They are obtained by SELEX (Systematic Evolution of Ligand by Exponential Enrichment) [83] and their application in electroanalysis have been extensively reviewed [30–32 and references therein].

Like antibodies, it is challenging to select aptamers against small molecules [87–89], and there are still very few aptamers available for  $\beta$ -lactams. Song *et al.* [90] were the first to obtain aptamers against ampicillin (AMP4, AMP17 and AMP18). AMP17

was used by Li *et al.* [91] to develop a dual recycling amplification strategy for ampicillin detection (Fig. 1.6). The sensor used AMP17 inserted in a tailor-made oligonucleotide probe, labelled with methylene blue that reacts with Klenow Fragment (KF) polymerase and T7 exonuclease. A similar architecture was used by Huang *et al.* [92] in a quadratic recycling amplification strategy again with a phi29 polymerase and a nicking endonuclease *Nt.A/wI*. The figures of merit of both sensors are remarkable with a LOD well below the MRL for ampicillin (4 pM for the dual amplification and 1.09 pM for the quadratic amplification). However the inherent complexity of the analytical approach does not simplify the transition to a possible commercial application. The same aptamer was used by Lou *et al.* [41] for a signalling-probe displacement sensor: it presented a very good LOD (10 pM) and linear dynamic range (100 pM - 1 mM) and also the interference effect of other antibiotics is minimal.

The group of Lai [42,43] used thiolated AMP18, labelled with methylene blue, to develop two ampicillin aptasensors based on a *signal-on* approach. The conformational change of the aptamer upon binding to ampicillin decreases the distance between the redox probe and the electrode surface, increasing the electron transfer rate, recorded using alternate current voltammetry. In the first work [42] they convincingly addressed a fundamental issue for real world application, the reusability of the sensor. The authors showed that the sensor could be regenerated, up to four times, with a simple washing in water. The sensor, however, does not have the required characteristic in terms of LOD (1  $\mu$ M) and linear dynamic range (5-5000  $\mu$ M) for antibiotic analysis in real food samples. The same authors, in a follow-up work [43], improved the proposed strategy by adding a displacement probe to increase the distance of the redox mediator and the electrode surface, and thus a gain in signal upon binding with the target. In this way the authors achieved a LOD (30 nM) and a linear dynamic range (0.2-15000  $\mu$ M) useful for antibiotics detection in real samples. Unfortunately, the presence of the sacrificial displacement probe does not allow anymore the regeneration of the modified electrode.

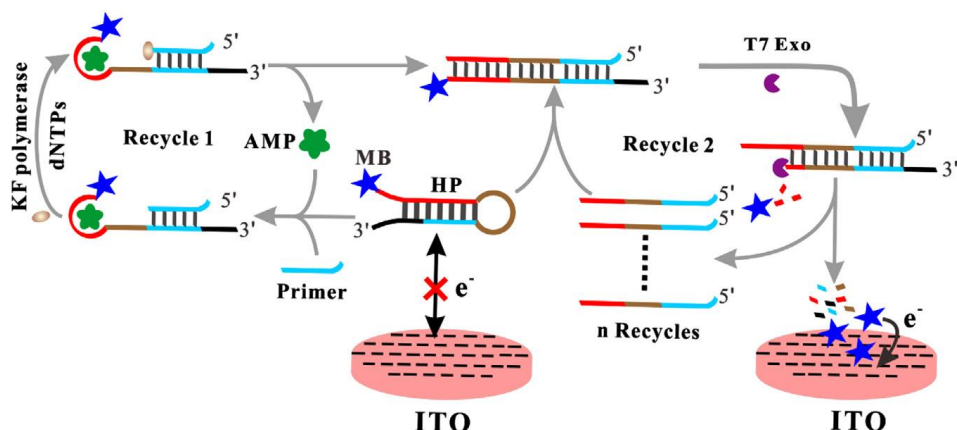


**Fig. 1.6** Principle of target-induced and T7 exonuclease-aided recycling amplification homogeneous electrochemical strategy for highly sensitive detection of AMP.

### Molecularly imprinted polymers

Along with aptamers, molecularly imprinted polymers (MIPs) have attracted a lot of attention in recent years for electroanalytical applications. These biomimetic materials are mostly used as a pre-concentration or extraction step for other analytical techniques, like chromatography [96,97] and different kinds of electrochemical biosensors [98]. Several strategies are used to synthesize MIPs, such as photo polymerization [99], free radical polymerization and electropolymerization [100] with different configurations like surface or bulk imprinting [101] or the realization of nanoparticles imprinted polymers [102]. Electropolymerization and radical polymerization are the most commonly used for biosensing purposes. In the field of  $\beta$ -lactam sensing, Yang *et al.* [103] proposed a sensor based on glassy carbon electrode modified with a gold network doped with an ionic liquid ( $[\text{BMIN}][\text{BF}_4]$ ) coupled with porous Pt nanoparticles and carboxyl graphene. The imprinted polymer is then electrodeposited on this composite by cyclic voltammetry (CV) using *o*-phenylenediamine as a functional monomer. The chosen target is cefotaxime, a third-generation cephalosporin used in human medicine and, illegally, for food preservation and processing. The sensor shows a good linear range and detection limit below the MRL value for cefotaxime. Lutfi Yola *et al.* developed a MIP-based electrochemical sensor for cefixime, using pyrrole as electroactive monomer [104]; they modified a glassy carbon electrode with Fe-Au nanoparticles and 2-aminoethanethiol-modified multiwalled carbon nanotubes for the electropolymerization of the MIP obtaining a very low LOD ( $2.2 \times 10^{-11}$  M).

Regarding the bulk polymerization approach, the group of Malekzadeh reported two different sensors for the detection of cefixime [105] and ceftazidime [106]. They used a glassy carbon electrode, functionalized with carboxyl-modified multiwalled carbon nanotubes and Ag dendrites, to attach the template molecule to the electrode surface. Afterwards they performed a bulk polymerization using acrylamide as a functional monomer, N,N-methylenebisacrylamide as a cross-linker and ammonium persulphate as polymerization initiator. They exploit the peculiar electrochemical signal of the target itself for the detection via anodic stripping differential pulse voltammetry. The LODs reported are remarkable, 0.5 nM for ceftazidime and 1 nM for cefixime, a very good reproducibility (1.8% and 3.7%, respectively) and a good recovery rate for real samples (>98%).

Another recent application of bulk polymerization is the creation of nanoparticulate molecularly imprinted polymers or nanoMIPs. This new kind of mimetic polymers should overcome many of the limitations of traditional MIPs obtained by bulk polymerization, such as residual template molecules, high binding site heterogeneity and difficult synthetic protocols [107,108]. Karaseva *et al.* [109] used nanoMIPs to develop a piezoelectric sensor for PENG and AMP detection. They deposit the synthesized nanoparticles by spin coating on a 10 MHz quartz resonator, covered with a thin layer of gold, and used the obtained sensor for a direct detection assay, monitoring the change in the resonance frequency before and after the addition of the target molecules. The selectivity study showed that, while the nanoMIPs are very good in discriminating between the target and other structurally different antibiotics (namely cefotaxime and streptomycin), the cross reactivity is quite high for closely related structures (up to 45 % for AMP from the PENG nanoMIPs). Regardless these limitations, the LOD is below the MRL value, 0.04  $\mu\text{g}/\text{mL}$  for PENG and 0.09  $\mu\text{g}/\text{mL}$  for AMP, but within a narrow linear range (0.1 – 1  $\mu\text{g}/\text{mL}$ ).

Given these examples, it is clear that the MIP approach could be a feasible alternative for  $\beta$ -lactam detection, especially for third and fourth generation antibiotics. These compounds present many different functional groups and thus more possible anchoring points for the functional monomer to interact with. For less substituted antibiotics, like first and second-generations, particular care should be devoted in the evaluation of interferences, taking into account more structurally related antibiotics before claiming selectivity and specificity of the proposed imprinted polymers. The detection of first and second generation  $\beta$ -lactams is of

particular interest since they are still the most used antibiotics both in human and veterinary medicine.

### **Photoelectrochemistry-based strategies**

In the last few years, photoelectrochemistry has been proven as an innovative strategy to detect many important compounds [110] and recently, De Wael *et al.* [111] reported a sensor, based on Zn-phthalocyanine photosensitizers, to detect phenolic antibiotics such as amoxicillin at low concentration (LOD=20 nM).

Robust, perfluorinated molecular photosensitizers, chemically resistant yet reactive, have been shown as proof-of-principle molecules mimicking enzymes for sensitive electrochemical (bio)sensing applications, while favourably enhancing the useful feature of the enzymatic detection mechanism, namely the catalytic formation of an easily detectable product and redox cycling. This approach can be seen as a feasible sensitive alternative for the direct detection of phenol-containing antimicrobial drugs.

### **Comparison of different analytical strategy for antibiotic residues**

Electrochemical biosensors have many advantages over traditional screening tests such as microbial growth inhibition assays, in term of sensitivity and selectivity, allowing single compound detection instead of simple yes or no answers. For on-site analysis, biosensors have the potential of reducing analysis times from hours to less than a minute, improving the efficacy of the monitoring plans. The data collected with these analytical tools will also greatly reduce the number of samples that has to be taken to the lab and analysed with confirmatory methods, cutting costs and decision time between the identification of the contamination and the possible contingency plan. Looking at the environmental impact of these different methods, electrochemical biosensors can be considered the best option, and while much work still needs to be done in this regard to obtain fully degradable and biocompatible biosensors, there is a growing interest in developing electrodes based on renewable source and eco-friendly electrode modifiers, based on waste or renewable natural materials [112].

**Table 1.3** Comparison of different analytical methods for  $\beta$ -lactam antibiotic residues identification.

	<b>Confirmatory Methods</b>	<b>Screening tests</b>		<b>Electrochemical biosensors</b>
	<i>HPLC/Uv-Vis or MS</i>	<i>Microbial assay</i>	<i>Receptor assay</i>	
<b>Sensitivity</b>	nM to pM	Yes/no answer	Yes/no answer	$\mu$ M to pM
<b>Selectivity</b>	Class and single compound selectivity	None	Class selectivity	Class and single compound selectivity
<b>Analysis time</b>	hours	hours	minutes to hours	less than a minute
<b>Price per analysis</b>	200-300 €	>5 €	~ 10 €	>10 €
<b>Environmental impact</b>	High	High	High to low	Low

Currently available screening test present some environmental problems, related for example to some of the labels used for amplification, as in the case of the Charm test kit that use radio isotopes [37,39]. Even the microbial growth inhibition assay produce several waste materials, both inorganic and organic. The use of large quantities of solvent and plastic consumables is also a problem of the more traditional confirmatory methods, which increases their environmental impact [113].

### **A new scenario: the electrochemical fingerprint for the identification of antibiotics residues**

The electroanalytical determination of antibiotics,  $\beta$ -lactams in particular, is not entirely unexplored. In the past, several papers reported the use of the oxidation or reduction signals of these drugs for their identification in a variety of real matrices. However, the reports conflict with each other's, giving different interpretation to



the same electrochemical peaks or presenting completely different behaviour for the same antibiotics. Thus, up to now, the electrochemical fingerprint of these antibiotics was never really investigated, neither molecular proof of their oxidation or reduction mechanism was given. A literature survey showed the contradictions and the deficiencies in the study of  $\beta$ -lactams antibiotics electrochemistry up to now. However, a combination between electrochemical data and mass spectrometry is instrumental to identify the oxidation mechanism as well as the degradation pathways and understand the best conditions for the electrochemical detection of these drugs.

### Cephalosporins

Reports on the electroactivity of cephalosporin antibiotics and the resulting analytical applications can be divided into two main groups: i) direct polarographic or voltammetric activity of cephalosporins [114–117] and ii) polarography, voltammetry or amperometry of the degradation products of cephalosporins after acidic, neutral or alkaline hydrolysis or UV photolysis [119–120]. The majority of the works reported the electroreduction of cephalosporins at rather low potential (around -1 V vs Ag/AgCl) in acidic medium (2-4), but already acknowledging the influence of the different side chains [121] on the peak position and intensity. Few articles dealt with the oxidation of cephalosporins at solid electrodes, often coupled with chromatographic separation, and the utilization of the anodic response for their identification [116,120–124]. Some oxidation peaks were correlated to the presence of different electroactive side chains. For example, the oxidation of the aminothiazole group and the functional group contained in the C7 side-chain of some cephalosporins (e.g. ceftizoxime, cefmenoxime, ceftazidime and ceftriaxone) were reported to enable the amperometric detection of said drugs [54-56], even with slightly worse performances than reduction signals [122]. More recently, two studies have appeared on the electrochemical behaviour of cephalosporins as a class [125-126].

In 2017, Feier *et al.* [125] reported on the electrochemistry of several cephalosporins antibiotics at bare boron doped diamond (BDD) electrode. They studied the oxidation signals of cephalalexin, ceftriazone, cefotazime, cefaclor, cefuroxime and ceftazidime in 0.2 M acetate buffer (pH 4.5) between +1 V and +2 V vs Ag/AgCl; this was possible due to the very wide potential window of boron doped diamond (BDD) electrodes in aqueous media (see Fig. 1.7) .

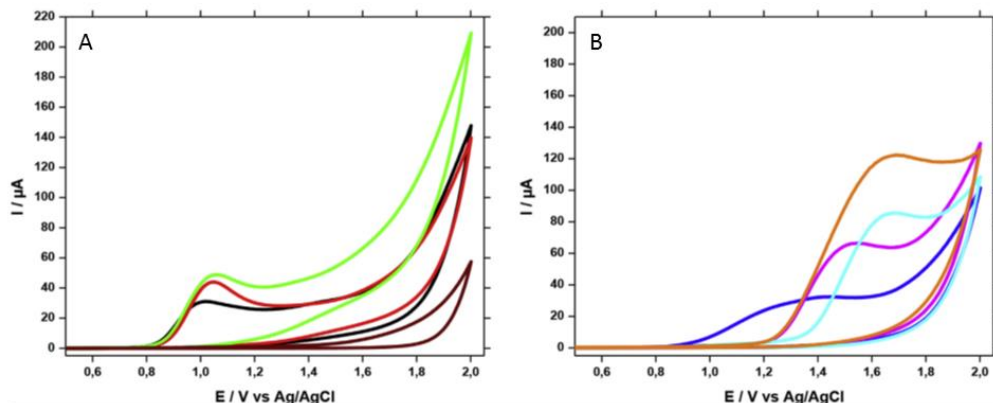


**Fig. 1.7** CVs at BDD electrode for 5 mM of (A) ceftriaxone (black), cefotaxime (red), ceftazidime (green) and (B) cefadroxil (blue), cefuroxime (pink), cefaclor (light blue), cephalixin (orange) (from [125]).

All antibiotics showed an irreversible oxidation peak at rather high potentials, but with differences in peak position and height. Feier *et al.* identified these peak as the oxidation of sulphide to sulfoxide on the  $\beta$ -lactam core structure. The authors stated that the different side chains present on each cephalosporin influenced both the peak potentials and the current intensities: these differences were related to the steric accessibility of the electroactive centre and to the possible adsorption onto the electrode surface. Cephalixin was used as a model molecule to develop a quantification strategy based on its oxidation signal with differential pulse voltammetry and flow injection analysis. Several problems of interferences between the tested cephalosporins were reported. Cephalixin oxidation peak strongly decreased in presence of ceftriaxone, cefotaxime, ceftazidime and it was not possible to separate the peaks for the binary mixture of cephalixin with cefuroxime or cefadroxil. Nonetheless, they addressed the comparative electrochemical study of cephalosporins as a class, suggesting a possible explanation for the different electrochemical behaviours, without however, giving any other molecular proof of the proposed mechanism.

Also Slegers *et al.* reported [126] the electrochemical fingerprint of several cephalosporins on graphite screen printed electrodes. The study was articulated to prove what is the real contribution to the electrochemical oxidation of the various side chains and core structure of the antibiotics. The electrochemical oxidation of six different antibiotics at two different pHs (2 and 7) was investigated and a liquid chromatography-mass spectrometry (LC-MS/MS) study of the oxidation products

was carried out to verify the mechanism. They compared the two main intermediates – 7-aminodeacetoxycephalosporanic acid (7-ADCA) and 7-aminocephalosporanic acid (7-ACA) – with cephalosporins containing only one side chain (cephalexin and cefacetrile) and two other presenting side chain in the C3 and C7 position (cefquinome and cefadroxil).

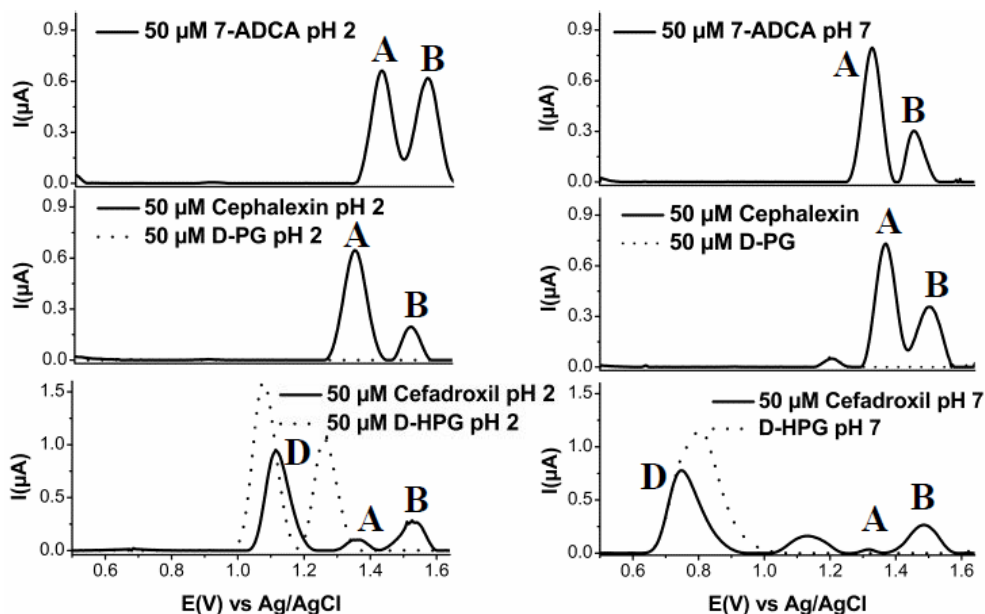


**Fig. 1.8** Baseline-corrected square-wave voltammetric responses (vs. Ag/AgCl) of 50  $\mu$ M solutions of 7 ADCA-based cephalosporins (solid) and their respective sidechains (dotted) at bare carbon screen-printed electrodes in 0.1 M phosphate buffer pH 2 (left) and pH 7 (right) (from [126]).

Each cephalosporin showed one or two oxidation peaks at high potential (around +1.4/1.5 V vs. Ag/AgCl) related to the oxidation of the core structure (peaks A and B in Fig. 1.8). By comparison of antibiotics with different side chains, it was possible to observe additional signals in the presence of different electroactive side chains. For example, in Fig. 1.8, the side chain of cephalexin, D-2-phenylglycine (D-PG), does not show any oxidation peak at both pHs (dotted lines in the middle panels), while D-(-)-4-hydroxyphenylglycine (D-HPG) showed oxidation signals at +0.75 V (peak D) which overlaps with the corresponding peak of the full antibiotics (full line in the bottom panels). From these findings, it was possible to envision the simultaneous detection of several cephalosporins by comparison of the peak position of the pure compounds with binary and ternary mixtures. As shown in Fig. 1.9, it was possible

to identify cephalixin, cefadroxil and cefquinome simultaneously.

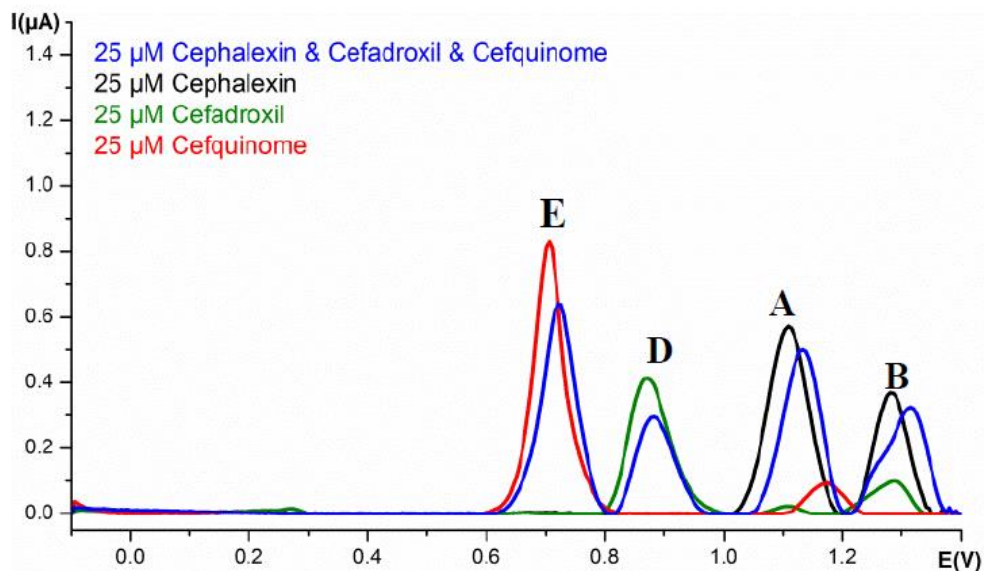


**Fig. 1.9** Baseline-corrected square-wave voltammetric responses (vs. int. ref.) of 25  $\mu\text{M}$  triple mixtures of cephalosporins at bare carbon screen-printed electrodes in 0.1 M phosphate buffer pH 2 (from [126]).

Having proved that some of the fingerprint signals of cephalosporins are related to the direct oxidation of the side chains, the authors undertook a mass spectrometry (MS) study of the oxidation products to verify the sulphoxide formation hypothesis, taken for granted up to now [127,128]. The MS analysis of oxidation products of cephalixin and cefacetriple suggested a novel electrochemical-chemical-electrochemical (ECE) oxidation pathway for the 7-ADCA based cephalosporins (Fig. 1.10). After a first electrochemical decarboxylation step (E), the addition of water as a chemical step (C) follows as an intermediate step leading to further oxidation into the keto analogue (E) and, in the case of cephalixin, it forms oxidation product 1 (P1). The two proposed oxidation mechanisms cannot be fully verified for now as no standards of these products are available on the market. Based on the LC-MS/MS measurements it was not possible to distinguish between the nucleophilic attack of water happening at the C2- position (Fig. 1.10A) or the C4-position (Fig. 1.10B).

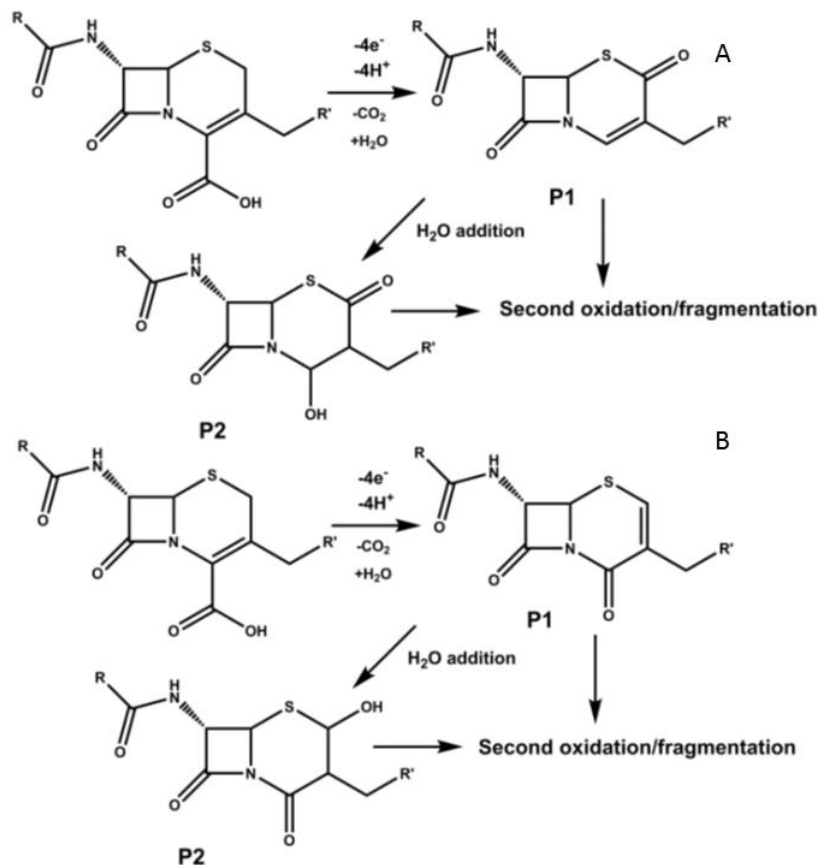
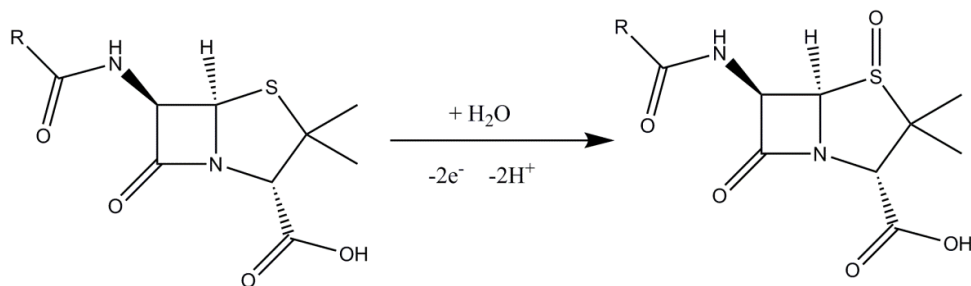


Fig. 1.10 Proposed electrochemical oxidation of cephalosporins (from [126]).

For the first time, molecular proof of the oxidation mechanism of cephalosporins was given, disproving the sulfoxide hypothesis and posing the ground work of an electrochemical strategy for identification and quantification of such antibiotics.

## Penicillins

Penicillin antibiotics electrochemistry was studied in the past mainly on gold and platinum electrodes with a variety of techniques [116,129,130], mainly in mild acid conditions (pH 4-6). This predilection for gold electrodes was in part due to the proposed oxidation mechanism for the penicillin core structure (Fig. 1.11). The oxidation should happen on the sulphur atom in the 5 position, with addition of water, leading to the corresponding sulfoxide, in a 2 electron 2 proton process. Gold interaction with the sulphur group and subsequent sulfoxide formation is the most accepted oxidation pathway.



**Fig. 1.11** Proposed oxidation mechanism for the penicillin core structure.

There are also examples of other electrode materials, mainly composite ones like carbon paste electrode [131,132], glassy carbon electrode modified with polyglutamic acid [133] or with multiwalled carbon nanotubes [134]. More recently the use of BDD seems to have caught the attention of researchers and several reports on the electrochemistry of penicillin have been published [127,128,135].

Among the latest, Feier *et al.* [127] reported the electrochemical study of five different penicillins, at bare BDD electrodes, in their native state and after basic and acid degradation. Oxacillin, penicillin V, penicillin G, ampicillin and amoxicillin all showed an oxidation peak at relatively high potential (between +1.6 V and +1.8 V vs. Ag/AgCl) again correlated to the sulphoxide formation on the 5 position of the  $\beta$ -lactam core structure. After both acid and basic degradation of the considered antibiotics, the electrochemical fingerprint changed sensibly with shifts in peak potentials and intensities. The authors claimed that these changes were due to the formation of degradation products, namely penicilloic acid, penicillamine and penilloaldehyde, which underwent different oxidation mechanisms, however they did not formulate any hypothesis related to the oxidation mechanisms. The simultaneous analysis of these penicillins proved to be difficult and the authors optimized only the detection of oxacillin via DPV and FIA, which still presented a rather high LOD (0.1 mM). Even if it was proven that it is possible to detect penicillins by means of their electrochemistry, the oxidation mechanism and the different contributions to the electrochemical fingerprint were not yet elucidated.

## Chapter 1 - $\beta$ -lactam antibiotics residues: an introduction

### References

- [1] European Centre for Disease Prevention and Control, Surveillance of Antimicrobial consumption in Europe. Annual Epidemiological Report for 2016, (2016).
- [2] ECDC, Antimicrobial resistance (AMR) reporting protocol 2017: European Antimicrobial Resistance Surveillance Network (EARS-Net) surveillance data for 2016., (2017).
- [3] W. organisation for animal Health, OIE Annual report on antimicrobial agents intended for use in animals, (2017) 123.
- [4] World Health Organization, Critically Important Antimicrobials for Human Medicine, (2017) 1–38.
- [5] W.O. for A. Health, OIE list of antimicrobial agents of veterinary importance, (2015).
- [6] W. Vollmer, D. Blanot, M.A. De Pedro, Peptidoglycan structure and architecture, *FEMS Microbiol. Rev.* 32 (2008) 149–167.
- [7] Y. Doi, H.F. Chambers, 22 - Other  $\beta$ -Lactam Antibiotics, in: J.E. Bennett, R. Dolin, M.J.B.T.-M. Blaser Douglas, and Bennett's Principles and Practice of Infectious Diseases (Eighth Edition) (Eds.), Mand. Douglas, Bennett's Princ. Pract. Infect. Dis. (Eighth Ed.), Philadelphia, 2015: pp. 293-297.e2.
- [8] T.G. Slama, Clinical review: balancing the therapeutic, safety, and economic issues underlying effective antipseudomonal carbapenem use, *Crit. Care.* 12 (2008) 233.
- [9] World Health Organization, Global Action Plan on Antimicrobial Resistance, 2015.
- [10] W.H.O. (WHO), Global action plan on antimicrobial resistance, WHO Press. (2015) 1–28.
- [11] E. Commission, Commission Regulation (EU) 37/2010, (2010).
- [12] J. Barlow, Mastitis Therapy and Antimicrobial Susceptibility: a Multispecies Review with a Focus on Antibiotic Treatment of Mastitis in Dairy Cattle, *J. Mammary Gland Biol. Neoplasia.* 16 (2011) 383–407.
- [13] S.W. Page, P. Gautier, Use of antimicrobial agents in livestock, *Rev. Sci. Tech. l'OIE.* 31 (2012) 145–188.
- [14] T.J.G.M. Lam, B.H.P. van den Borne, J. Jansen, K. Huijps, J.C.L. van Veersen, G. van Schaik, H. Hogeveen, Improving bovine udder health: A national mastitis control program in the Netherlands, *J. Dairy Sci.* 96 (2013) 1301–1311.
- [15] A.G. Zwald, P.L. Ruegg, J.B. Kaneene, L.D. Warnick, S.J. Wells, C. Fossler, L.W. Halbert, Management Practices and Reported Antimicrobial Usage on Conventional

## Chapter 1 - $\beta$ -lactam antibiotics residues: an introduction

and Organic Dairy Farms<sup>1</sup>, *J. Dairy Sci.* 87 (2004) 191–201.

- [16] S.A. McEwen, P.J. Fedorka-Cray, Antimicrobial Use and Resistance in Animals, *Clin. Infect. Dis.* 34 (2002) S93–S106.
- [17] J.M.A. Blair, M.A. Webber, A.J. Baylay, D.O. Ogbolu, L.J. V Piddock, Molecular mechanisms of antibiotic resistance, *Nat. Rev. Microbiol.* 13 (2015) 42–51.
- [18] S.M. Drawz, R.A. Bonomo, Three decades of  $\beta$ -lactamase inhibitors, *Clin. Microbiol. Rev.* 23 (2010) 160–201.
- [19] J.D.D. Pitout, C.C. Sanders, W.E. Sanders, Antimicrobial Resistance with Focus on  $\beta$ -Lactam Resistance in Gram-Negative Bacilli, *Am. J. Med.* 103 (1997) 51–59.
- [20] L. Kantiani, M. Farré, D. Barceló, D. Barceló, Analytical methodologies for the detection of  $\beta$ -lactam antibiotics in milk and feed samples, *TrAC - Trends Anal. Chem.* 28 (2009) 729–744.
- [21] R. Chafer-Pericas, Consuelo, Maquieira, Angel, Puchades, Fast screening methods to detect antibiotic residues in food samples, *Trends Trends Anal. Chem.* 29 (2010) 1038–1049.
- [22] M. Gaugain-Juhel, B. Delépine, S. Gautier, M.P. Fourmond, V. Gaudin, D. Hurtaud-Pessel, E. Verdon, P. Sanders, Validation of a liquid chromatography-tandem mass spectrometry screening method to monitor 58 antibiotics in milk: a qualitative approach, *Food Addit. Contam. Part A.* 26 (2009) 1459–1471.
- [23] M. Di Rocco, M. Moloney, T. O’Beirne, S. Earley, B. Berendsen, A. Furey, M. Danaher, Development and validation of a quantitative confirmatory method for 30  $\beta$ -lactam antibiotics in bovine muscle using liquid chromatography coupled to tandem mass spectrometry, *J. Chromatogr. A.* 1500 (2017) 121–135.
- [24] A. Junza, R. Amatya, D. Barrón, J. Barbosa, Comparative study of the LC–MS/MS and UPLC–MS/MS for the multi-residue analysis of quinolones, penicillins and cephalosporins in cow milk, and validation according to the regulation 2002/657/EC, *J. Chromatogr. B.* 879 (2011) 2601–2610.
- [25] R.W. Han, N. Zheng, Z.N. Yu, J. Wang, X.M. Xu, X.Y. Qu, S.L. Li, Y.D. Zhang, J.Q. Wang, Simultaneous determination of 38 veterinary antibiotic residues in raw milk by UPLC–MS/MS, *Food Chem.* 181 (2015) 119–126.
- [26] A. Junza, N. Dorival-García, A. Zafra-Gómez, D. Barrón, O. Ballesteros, J. Barbosa, A. Navalón, Multiclass method for the determination of quinolones and beta-lactams , in raw cow milk using dispersive liquid – liquid microextraction and ultra high performance liquid chromatography – tandem mass spectrometry, *J. Chromatogr. A.* 1356 (2014) 10–22.
- [27] D. Scannella, P. Neaves, K. Keedy, C. Bell, An evaluation of the Delvo X-Press  $\beta$ L test



## Chapter 1 - $\beta$ -lactam antibiotics residues: an introduction

for detecting  $\beta$ -lactams in ex-farm raw milks, *Int. Dairy J.* 7 (1997) 93–96.

- [28] J. Eric Hillerton, B.I. Halley, P. Neaves, M.D. Rose, Detection of Antimicrobial Substances in Individual Cow and Quarter Milk Samples Using Delvotest Microbial Inhibitor Tests, *J. Dairy Sci.* 82 (1999) 704–711.
- [29] M.A.-T. Tumini Melisa A4 - Nagel, Orlando A4 - Molina, Maria Pilar A4 - Althaus, Rafael, Microbiological assay with *Bacillus licheniformis* for the easy detection of quinolones in milk, *Int. Dairy J.* v. 64 (2017) 9-13–2017 v.64.
- [30] J.R. Bishop, A.B. Bodine, G.D. O'Dell, J.J. Janzen, Quantitative Assay for Antibiotics Used Commonly in Treatment of Bovine Infections<sup>1</sup>, *J. Dairy Sci.* 68 (1985) 3031–3036.
- [31] Å. Carlsson, L. Björck, K. Persson, Lactoferrin and Lysozyme in Milk During Acute Mastitis and Their Inhibitory Effect in Delvotest P, *J. Dairy Sci.* 72 (1989) 3166–3175.
- [32] J.H. Kang, J.H. Jin, F. Kondo, False-Positive Outcome and Drug Residue in Milk Samples Over Withdrawal Times, *J. Dairy Sci.* 88 (2010) 908–913.
- [33] F. Xu, K. Ren, Y. Yang, J. Guo, G. Ma, Y. Liu, Y. Lu, X. Li, Immunoassay of chemical contaminants in milk: A review, *J. Integr. Agric.* 14 (2015) 2282–2295.
- [34] Y.-F. Li, Y.-M. Sun, R.C. Beier, H.-T. Lei, S. Gee, B.D. Hammock, H. Wang, Z. Wang, X. Sun, Y.-D. Shen, J.-Y. Yang, Z.-L. Xu, Immunochemical techniques for multianalyte analysis of chemical residues in food and the environment: A review, *TrAC Trends Anal. Chem.* 88 (2017) 25–40.
- [35] M. Carlier, V. Stove, S.C. Wallis, J.J. De Waele, A.G. Verstraete, J. Lipman, J.A. Roberts, Assays for therapeutic drug monitoring of  $\beta$ -lactam antibiotics: A structured review, *Int. J. Antimicrob. Agents.* 46 (2015) 367–375.
- [36] S. Ahmed, J. Ning, G. Cheng, I. Ahmad, J. Li, L. Mingyue, W. Qu, M. Iqbal, M.A.B. Shabbir, Z. Yuan, Receptor-based screening assays for the detection of antibiotics residues – A review, *Talanta.* 166 (2017) 176–186.
- [37] M.C. Beltrán, T. Romero, R.L. Althaus, M.P. Molina, Evaluation of the Charm maximum residue limit  $\beta$ -lactam and tetracycline test for the detection of antibiotics in ewe and goat milk, *J. Dairy Sci.* 96 (2013) 2737–2745.
- [38] R. Salter, S. Holmes, D. Legg, J. Coble, B. George, Hog Charm II Tetracycline Test Screening Results Compared with a Liquid Chromatography Tandem Mass Spectrometry 10- $\mu$ g/kg Method, *J. Food Prot.* 75 (2012) 405–407.
- [39] T. Romero, S. Van Weyenberg, M.P. Molina, W. Reybroeck, Detection of antibiotics in goats' milk: Comparison of different commercial microbial inhibitor tests developed for the testing of cows' milk, *Int. Dairy J.* 62 (2016) 39–42.

## Chapter 1 - $\beta$ -lactam antibiotics residues: an introduction

- [40] Y. Chen, Y. Wang, L. Liu, X. Wu, L. Xu, H. Kuang, A. Li, C. Xu, A gold immunochromatographic assay for the rapid and simultaneous detection of fifteen  $\beta$ -lactams, *Nanoscale*. 7 (2015) 16381–16388.
- [41] R. Žvirauskienė, J. Šalomskienė, An evaluation of different microbial and rapid tests for determining inhibitors in milk, *Food Control*. 18 (2007) 541–547.
- [42] J. Lamar, M. Petz, Development of a receptor-based microplate assay for the detection of beta-lactam antibiotics in different food matrices, *Anal. Chim. Acta*. 586 (2007) 296–303.
- [43] X. Liang, Z. Wang, C. Wang, K. Wen, T. Mi, J. Zhang, S. Zhang, A proof-of-concept receptor-based assay for sulfonamides, *Anal. Biochem*. 438 (2013) 110–116.
- [44] L. Wang, Y. Zhang, X. Gao, Z. Duan, S. Wang, Determination of Chloramphenicol Residues in Milk by Enzyme-Linked Immunosorbent Assay: Improvement by Biotin–Streptavidin-Amplified System, *J. Agric. Food Chem*. 58 (2010) 3265–3270.
- [45] J. Kuncová-Kallio, S. Auer, A. Spehar, J.H. Qu, D. Spasic, J. Lammertyn, CHAPTER 11 Optical and Acoustic Label-free Instrumentation for Molecular Detection with a Focus on Food, in: *Rapid Antibody-Based Technol. Food Anal.*, The Royal Society of Chemistry, 2019: pp. 223–255.
- [46] V. Gaudin, Advances in biosensor development for the screening of antibiotic residues in food products of animal origin – A comprehensive review, *Biosens. Bioelectron*. 90 (2017) 363–377.
- [47] V. Gaudin, J. Fontaine, P. Maris, Screening of penicillin residues in milk by a surface plasmon resonance-based biosensor assay: Comparison of chemical and enzymatic sample pre-treatment, *Anal. Chim. Acta*. 436 (2001) 191–198.
- [48] M. Tomassetti, G. Conta, L. Campanella, G. Favero, G. Sanzò, F. Mazzei, R. Antiochia, A flow SPR immunosensor based on a sandwich direct method, *Biosensors*. 6 (2016) 1–13.
- [49] A. Pennacchio, A. Varriale, M.G. Esposito, A. Scala, V.M. Marzullo, M. Staiano, S. D’Auria, A rapid and sensitive assay for the detection of benzylpenicillin (PenG) in milk, *PLoS One*. 10 (2015) 1–10.
- [50] E. Gustavsson, J. Degelaen, P. Bjurling, Å. Sternesjö, Determination of  $\beta$ -Lactams in Milk Using a Surface Plasmon Resonance-Based Biosensor, *J. Agric. Food Chem*. 52 (2004) 2791–2796.
- [51] G. Cacciatore, M. Petz, S. Rachid, R. Hakenbeck, A.A. Bergwerff, Development of an optical biosensor assay for detection of  $\beta$ -lactam antibiotics in milk using the penicillin-binding protein 2x\*, *Anal. Chim. Acta*. 520 (2004) 105–115.
- [52] H. Yao, Y. Tang, Y. Li, Y. Sun, Flow Injection Chemiluminescence Determination of

## Chapter 1 - $\beta$ -lactam antibiotics residues: an introduction

Cephalosporin Antibiotics by Their Enhancing Effects on Luminol-Potassium Periodate System, *Anal. Lett.* 36 (2003) 2975–2983.

- [53] Y. Li, Y. Tang, H. Yao, J. Fu, Determination of ampicillin and amoxicillin by flow injection chemiluminescence method based on their enhancing effects on the luminol-periodate reaction, *Luminescence*. 18 (2003) 313–317.
- [54] J. Sun, S.G. Schulman, J.H. Perrin, Chemiluminescence of  $\beta$ -lactam antibiotics following oxidation by potassium superoxide, *Anal. Chim. Acta.* 338 (1997) 1–2.
- [55] Y. Li, J. Lu, Chemiluminescence flow-injection analysis of  $\beta$ -lactam antibiotics using the luminol-permanganate reaction, *Luminescence*. 21 (2006) 251–255.
- [56] W. Liu, Z. Zhang, Z. Liu, Determination of  $\beta$ -lactam antibiotics in milk using micro-flow chemiluminescence system with on-line solid phase extraction, *Anal. Chim. Acta.* 592 (2007) 187–192.
- [57] M.H. Sorouraddin, M. Iranifam, A. Imani-Nabiyyi, Study of the enhancement of a new chemiluminescence reaction and its application to determination of  $\beta$ -lactam antibiotics, *Luminescence*. 24 (2009) 102–107.
- [58] K. Kloth, M. Rye-Johnsen, A. Didier, R. Dietrich, E. Märtlbauer, R. Niessner, M. Seidel, A regenerable immunochip for the rapid determination of 13 different antibiotics in raw milk, *Analyst*. 134 (2009) 1433–1439.
- [59] M. Iranifam, M. Khabbaz Kharamah, Cupric oxide nanoparticles-enhanced chemiluminescence method for measurement of  $\beta$ -lactam antibiotics, *Luminescence*. 30 (2015) 625–630.
- [60] S.J. Valtonen, J.S. Kurittu, M.T. Karp, A luminescent *Escherichia coli* biosensor for the high throughput detection of  $\beta$ -lactams, *J. Biomol. Screen.* 7 (2002) 127–134.
- [61] O.P. Smolander, A.S. Ribeiro, O. Yli-Harja, M. Karp, Identification of  $\beta$ -lactam antibiotics using bioluminescent *Escherichia coli* and a support vector machine classifier algorithm, *Sensors Actuators, B Chem.* 141 (2009) 604–609.
- [62] M.A. Bacigalupo, G. Meroni, F. Secundo, R. Lelli, Time-resolved fluoroimmunoassay for quantitative determination of ampicillin in cow milk samples with different fat contents, *Talanta*. 77 (2008) 126–130.
- [63] E.S. Elzanfaly, R.M. Youssif, N.N. Salama, A.S. Fayed, H.A.M. Hendawy, M.Y. Salem, Zero and second-derivative synchronous fluorescence spectroscopy for the quantification of two non-classical  $\beta$ -lactams in pharmaceutical vials: Application to stability studies, *Luminescence*. 32 (2017) 1517–1527.
- [64] F.J. Gruhl, K. Länge, Surface Acoustic Wave (SAW) Biosensor for Rapid and Label-Free Detection of Penicillin G in Milk, *Food Anal. Methods*. 7 (2014) 430–437.

## Chapter 1 - $\beta$ -lactam antibiotics residues: an introduction

- [65] A. Bremus, R. Dietrich, L. Dettmar, E. Usleber, E. Märtlbauer, A broadly applicable approach to prepare monoclonal anti-cephalosporin antibodies for immunochemical residue determination in milk, *Anal. Bioanal. Chem.* 403 (2012) 503–515.
- [66] G. Merola, E. Martini, M. Tomassetti, L. Campanella, New immunosensor for Beta-lactam antibiotics determination in river waste waters, *Sensors Actuators B. Chem.* 199 (2014) 301–313.
- [67] G. Merola, E. Martini, M. Tomassetti, L. Campanella, Simple and suitable immunosensor for Beta-lactam antibiotics analysis in real matrixes: Milk, serum, urine, *J. Pharm. Biomed. Anal.* 106 (2015) 186–196.
- [68] H. Li, B. Xu, D. Wang, Y. Zhou, H. Zhang, W. Xia, S. Xu, Y. Li, Immunosensor for trace penicillin G detection in milk based on supported bilayer lipid membrane modified with gold nanoparticles, *J. Biotechnol.* 203 (2015) 97–103.
- [69] N.A. Karaseva, T.N. Ermolaeva, Piezoelectric immunosensors for the detection of individual antibiotics and the total content of penicillin antibiotics in foodstuffs, *Talanta.* 120 (2014) 312–317.
- [70] A. Chen, S. Yang, Replacing antibodies with aptamers in lateral flow immunoassay, *Biosens. Bioelectron.* 71 (2015) 230–242.
- [71] M. Babic, A.M. Hujer, R.A. Bonomo, What 's new in antibiotic resistance ? Focus on beta-lactamases, *Drug Resist. Updat.* 9 (2006) 142–156.
- [72] Y. Wu, L. Tang, L. Huang, Z. Han, J. Wang, H. Pan, A low detection limit penicillin biosensor based on single graphene nanosheets preadsorbed with hematein / ionic liquids / penicillinase, *Mater. Sci. Eng. C.* 39 (2014) 92–99.
- [73] L. Moreira, W.F.A. Callera, M.D.P.T. Sotomayor, P.R. Bueno, Penicillinase-based amperometric biosensor for penicillin G, *Electrochem. Commun.* 38 (2014) 131–133.
- [74] M. Thiago, M. V Foguel, L.M. Gonc, P.T. Sotomayor, Beta-Lactamase-based biosensor for the electrochemical determination of benzylpenicillin in milk, *Sensors Actuators B. Chem.* 210 (2015) 254–258.
- [75] F. Ismail, S.B. Adeloju, The Use of Poly (Vinyl Alcohol ) to Cross-link Penicillinase for the Fabrication of a Penicillin Potentiometric Biosensor, *Electroanalysis.* 26 (2014) 2701–2709.
- [76] F. Ismail, S.B. Adeloju, A.N. Moline, Fabrication of a Single Layer and Bilayer Potentiometric Biosensors for Penicillin by Galvanostatic Entrapment of Penicillinase into Polypyrrole Films, *Electroanalysis.* (2014) 2607–2618.
- [77] F. Ismail, S.B. Adeloju, Comparison of Single Layer and Bilayer Biosensors Based on Crosslinking of Penicillinase for Potentiometric Detection of Penicillin in Milk and Antibiotics, *Electroanalysis.* 27 (2015) 1523–1531.

## Chapter 1 - $\beta$ -lactam antibiotics residues: an introduction

- [78] E. Sauvage, M. Terrak, J.A. Ayala, P. Charlier, The penicillin-binding proteins : structure and role in peptidoglycan biosynthesis, *Fems Microbiol. Rev.* 32 (2008) 234–258.
- [79] F. Conzuelo, S. Campuzano, P. Mart, M. Esteban-torres, B. De Rivas, A.J. Reviejo, R. Mun, J.M. Pingarro, Integrated Amperometric Affinity Biosensors Using Co<sup>2+</sup> – Tetradentate Nitrotriacetic Acid Modified Disposable Carbon Electrodes: Application to the Determination of  $\beta$  - Lactam Antibiotics, *Anal. Chem.* 85 (2013) 3246–3254.
- [80] M. Gamella, S. Campuzano, F. Conzuelo, M. Esteban-torres, B. De Rivas, An amperometric affinity penicillin-binding protein magnetosensor for the detection of  $\beta$ -lactam antibiotics in milk, *Analyst.* 138 (2013) 2013–2022.
- [81] K. Chen, B. Liu, B. Yu, W. Zhong, Y. Lu, J. Zhang, J. Liao, Advances in the development of aptamer drug conjugates for targeted drug delivery, *Wires Nanomed Nanobiotechnol.* 9 (2017) 1–15.
- [82] S. Catuogno, C.L. Esposito, V. De Franciscis, Aptamer-Mediated Targeted Delivery of Therapeutics : An Update, *Pharmaceuticals.* 9 (2016).
- [83] R. Stoltenburg, C. Reinemann, B. Strehlitz, SELEX — A (r)evolutionary method to generate high-affinity nucleic acid ligands, *Biomol. Eng.* 24 (2007) 381–403.
- [84] J. Liu, D. Melissa, F.C. Macazo, L.R. Schoukroun-barnes, R.J. White, The Current and Future Role of Aptamers in Electroanalysis, *J. Electrochem. Soc.* 161 (2014) H301–H313.
- [85] H. Malekzad, A. Jouyban, M. Hasanzadeh, Ensuring food safety using aptamer based assays : Electroanalytical approach, *Trends Anal. Chem.* 94 (2017) 77–94.
- [86] Y. Xu, G. Cheng, P. He, Y. Fang, A Review : Electrochemical Aptasensors with Various Detection Strategies, *Electroanalysis.* 21 (2009) 1251–1259.
- [87] R. Stoltenburg, N. Nikolaus, B. Strehlitz, Capture-SELEX : Selection of DNA Aptamers for Aminoglycoside Antibiotics, *Journa Anal. Methods Chemistry.* 2012 (2012).
- [88] N. Nikolaus, B. Strehlitz, DNA-Aptamers Binding Aminoglycoside Antibiotics, *Sensors.* 14 (2014) 3737–3755.
- [89] F. Pfeiffer, G. Mayer, D. Lafontaine, G. Göttingen, K.A. White, G. Mayer, Selection and Biosensor Application of Aptamers for Small Molecules, *Front. Chem.* 4 (2016) 1–21.
- [90] K. Song, E. Jeong, W. Jeon, M. Cho, C. Ban, Aptasensor for ampicillin using gold nanoparticle based dual fluorescence – colorimetric methods, *Anal. Bioanal. Chem.* 402 (2012) 2153–2161.

## Chapter 1 - $\beta$ -lactam antibiotics residues: an introduction

- [91] X. Wang, S. Dong, P. Gai, R. Duan, F. Li, Highly sensitive homogeneous electrochemical aptasensor for antibiotic residues detection based on dual recycling amplification strategy, *Biosens. Bioelectron.* 82 (2016) 49–54.
- [92] H. Wang, Y. Wang, S. Liu, J. Yu, W. Xu, Y. Guo, J. Huang, Target–aptamer binding triggered quadratic recycling amplification for highly specific and ultrasensitive detection of antibiotics at the attomole level, *Chem. Commun.* 51 (2015) 8377–8380.
- [93] Z. Yang, X. Ding, Q. Guo, Y. Wang, Z. Lu, H. Ou, Z. Luo, X. Lou, Second generation of signaling-probe displacement electrochemical aptasensor for detection of picomolar ampicillin and sulfadimethoxine, *Sensors Actuators B. Chem.* 253 (2017) 1129–1136.
- [94] Z. Yu, R.Y. Lai, A reagentless and reusable electrochemical aptamer-based sensor for rapid detection of ampicillin in complex samples, *Talanta.* 176 (2018) 619–624.
- [95] Z. Yu, A.L. Sutlief, R.Y. Lai, Towards the development of a sensitive and selective electrochemical aptamer-based ampicillin sensor, *Sensors Actuators B. Chem.* 258 (2018) 722–729.
- [96] A.N. Baeza, J.L. Urraca, R. Chamorro, G. Orellana, M. Castellari, Multiresidue analysis of cephalosporin antibiotics in bovine milk based on molecularly imprinted polymer extraction followed by liquid chromatography-tandem mass spectrometry, *J. Chromatogr. A.* 1474 (2016) 121–129.
- [97] J.L. Urraca, R. Chamorro-mendiluce, G. Orellana, M.C. Moreno-bondi, Molecularly imprinted polymer beads for clean-up and preconcentration of  $\beta$ -lactamase-resistant penicillins in milk, *Anal. Bioanal. Chem.* 408 (2016) 1843–1854.
- [98] R. Gui, H. Jin, H. Guo, Z. Wang, Biosensors and Bioelectronics Recent advances and future prospects in molecularly imprinted polymers-based electrochemical biosensors, *Biosens. Bioelectron.* 100 (2018) 56–70.
- [99] Y. Fuchs, O. Soppera, K. Haupt, Photopolymerization and photostructuring of molecularly imprinted polymers for sensor applications—A review, *Analytica Chimica Acta* 717 (2012) 7–20.
- [100] M. Włoch, J. Datta, Chapter Two - Synthesis and polymerisation techniques of molecularly imprinted polymers, Editor(s): M. Marć, *Comprehensive Analytical Chemistry*, Elsevier, 86, (2019) 17–40
- [101] G. Erturk, B. Mattiasson, Molecular imprinting techniques used for the preparation of biosensors, *Sensors*, 17, (2017) 288.
- [102] H. Zhang, Molecularly Imprinted Nanoparticles for Biomedical Applications. *Adv. Mater.* (2019), 1806328.
- [103] G. Yang, F. Zhao, B. Zeng, Electrochemical determination of cefotaxime based on a

## Chapter 1 - $\beta$ -lactam antibiotics residues: an introduction

- three-dimensional molecularly imprinted film sensor, *Biosens. Bioelectron.* 53 (2014) 447–452.
- [104] M. Lüt, T. Eren, N. Atar, Molecularly imprinted electrochemical biosensor based on Fe @ Au nanoparticles involved in 2-aminoethanethiol functionalized multi-walled carbon nanotubes for sensitive determination of cefexime in human plasma, *Biosens. Bioelectron.* 60 (2014) 277–285.
- [105] N. Karimian, M.B. Gholivand, G. Malekzadeh, Cefixime detection by a novel electrochemical sensor based on glassy carbon electrode modified with surface imprinted polymer / multiwall carbon nanotubes, *J. Electroanal. Chem.* 771 (2016) 64–72.
- [106] M. Torkashvand, M.B. Gholivand, G. Malekzadeh, Construction of a new electrochemical sensor based on molecular imprinting recognition sites on multiwall carbon nanotube surface for analysis of ceftazidime in real samples, *Sensors Actuators B. Chem.* 231 (2016) 759–767.
- [107] I.E. Tothill, M.J. Abdin, Nano Molecular Imprinted Polymers (NanoMIPs) for Food Diagnostics and Sensor, in: R. Prasad, V. Kumar, M. Kumar (Eds.), *Nanotechnol. Food Environ. Paradig.*, Springer Singapore, Singapore, 2017: pp. 131–151.
- [108] F. Canfarotta, A. Poma, A. Guerreiro, S. Piletsky, Solid-phase synthesis of molecularly imprinted nanoparticles, *Nat. Protoc.* 11 (2016) 443.
- [109] N. Karaseva, T. Ermolaeva, B. Mizaikoff, Piezoelectric sensors using molecularly imprinted nanospheres for the detection of antibiotics, *Sensors Actuators B. Chem.* 225 (2016) 199–208.
- [110] W. Zhao, J. Xu, H. Chen, Photoelectrochemical bioanalysis : the state of the art, *Chem. Soc. Rev.* 44 (2015) 729–741.
- [111] S.M.G. & K.D.W. Stanislav Trashin, Vanoushe Rahemi, Karpagavalli Ramji, Liselotte Neven, Singlet oxygen-based electroensing by molecular photosensitizers, *Nat. Commun.* 8 (2017) 1–10.
- [112] G. Moro, F. Bottari, J. Van Loon, E. Du Bois, K. De Wael, L. M. Moretto, Disposable electrodes from waste materials and renewable sources for (bio)electroanalytical applications, *Biosens. Bioelectr.* 146 (2019) 111758.
- [113] Y. Gaber, U. Törnvall, M. A. Kumar, M. Ali Amine, R. Hatti-Kaula, HPLC-EAT (Environmental Assessment Tool): A tool for profiling safety, health and environmental impacts of liquid chromatography methods, *Green Chem.* 13 (2011), 2021-2025.
- [114] D.A. Hall, D.M. Berry, C.J. Schneider, The electrochemistry of cephalosporin C derivatives: Part II. Cephalothin, sodium salt, *J. Electroanal. Chem. Interfacial Electrochem.* 80 (1977) 155–170.

## Chapter 1 - $\beta$ -lactam antibiotics residues: an introduction

- [115] B. Ogorevc, V. Hudnik, S. Gomišček, Polarographic analysis of some cephalosporin antibiotics, *Fresenius' Zeitschrift Für Anal. Chemie.* 330 (1988) 59–64.
- [116] E. Bishop, W. Hussein, Electroanalytical studies of antibacterial and diuretic drugs at rotating disc electrodes of gold and platinum, *Analyst.* 109 (1984) 913–921.
- [117] E. Muñoz, L. Camacho, J.L. Avila, F. García-Blanco, Cyclic and linear sweep voltammetry of cefazolin and cefmetazole: Electroanalytical applications, *Analyst.* 114 (1989) 1611–1615.
- [118] J.A. Squella, L.J. Nuñez-Vergara, E.M. Gonzalez, Polarographic analysis of cephalixin, *J. Pharm. Sci.* 67 (1978) 1466–1467.
- [119] L.J. Nuñez-Vergara, J.A. Squella, M.M. Silva, Polarography of an acidic degradation product from cephalixin, *Talanta.* 29 (1982) 137–138.
- [120] A.G. Fogg, N.M. Fayad, Differential pulse polarographic study of the degradation of ampicillin, *Anal. Chim. Acta.* 113 (1980) 91–96.
- [121] B. Ogorevc, S. Gomišček, Electrochemical analysis of cephalosporin antibiotics, *J. Pharm. Biomed. Anal.* 9 (1991) 225–236.
- [122] A. Ivaska, F. Nordström, Determination of some cephalosporins by differential pulse polarography and linear scan voltammetry, *Anal. Chim. Acta.* 146 (1983) 87–95.
- [123] H. Fabre, M.D. Blanchin, U. Tjaden, High-performance liquid chromatography with anodic amperometric detection for the determination of cefotaxime and its metabolites, *Analyst.* 111 (1986) 1281–1284.
- [124] M.D. Blanchin, W.T. Kok, H. Fabre, New detection modes for the determination of cephalosporins and their decomposition products, *Chromatographia.* 24 (1987) 625–627.
- [125] B. Feier, A. Gui, C. Cristea, R. Săndulescu, Electrochemical determination of cephalosporins using a bare boron-doped diamond electrode, *Anal. Chim. Acta.* 976 (2017) 25–34.
- [126] N. Slegers, A.L.N. van Nuijs, M. van den Berg, K. De Wael, Cephalosporin Antibiotics: Electrochemical Fingerprints and Core Structure Reactions Investigated by LC–MS/MS, *Anal. Chem.* 91 (2019) 2035–2041.
- [127] B. Feier, I. Ionel, C. Cristea, R. Sandulescu, Electrochemical behaviour of several penicillins at high potential, *New J. Chem.* 41 (2017) 12947–12955.
- [128] L. Svorc, J. Sochr, M. Rievaj, P. Tomcik, D. Bustin, Voltammetric determination of penicillin V in pharmaceutical formulations and human urine using a boron-doped diamond electrode, *Bioelectrochemistry.* 88 (2012) 36–41.



## Chapter 1 - $\beta$ -lactam antibiotics residues: an introduction

- [129] L. Koprowski, E. Kirchmann, L.E. Welch, The electrochemical oxidation of penicillins on gold electrodes, *Electroanalysis*. 5 (1993) 473–482.
- [130] P. Norouzi, M.R. Ganjali, T. Alizadeh, P. Daneshgar, Fast Fourier continuous cyclic voltammetry at gold ultramicroelectrode in flowing solution for determination of ultra trace amounts of Penicillin G, *Electroanalysis*. 18 (2006) 947–954.
- [131] B. Uslu, Y. Biryol, Voltammetric determination of amoxicillin using a poly(N-vinyl imidazole) modified carbon paste electrode, *J. Pharm. Biomed. Anal.* 20 (1999) 591–598.
- [132] M.F. Bergamini, M.F.S. Teixeira, E.R. Dockal, N. Bocchi, É.T.G. Cavalheiro, Evaluation of Different Voltammetric Techniques in the Determination of Amoxicillin Using a Carbon Paste Electrode Modified with [N, N-ethylene bis (salicylideneaminato)] oxovanadium (IV), *J. Electrochem. Soc.* 153 (2006) 94–98.
- [133] D.P. Santos, M.F. Bergamini, M.V.B. Zanoni, Voltammetric sensor for amoxicillin determination in human urine using polyglutamic acid/glutaraldehyde film, *Sensors Actuators, B Chem.* 133 (2008) 398–403.
- [134] B. Rezaei, S. Damiri, Electrochemistry and adsorptive stripping voltammetric determination of amoxicillin on a multiwalled carbon nanotubes modified glassy carbon electrode, *Electroanalysis*. 21 (2009) 1577–1586.
- [135] L. Svorc, J. Sochr, P. Tomcik, M. Rievaj, D. Bustin, Simultaneous determination of paracetamol and penicillin v by square-wave voltammetry at a bare boron-doped diamond electrode, *Electrochim. Acta.* 68 (2012) 227–234.



# Electrochemical fingerprinting of nafcillin and isoxazolyl penicillins

---

The electrochemical characterization of five different penicillins was performed at bare graphite screen printed electrodes (G-SPE), combining electrochemistry and mass spectrometry data. The possibility to elucidate their electrochemical fingerprint and to use these findings for the optimization of electrochemical sensing strategies was investigated. We tried to unravel the oxidation and degradation mechanisms of these antibiotics, finding the best experimental conditions for their electrochemical detection.

Nafcillin (NAF, (2*S*,5*R*,6*R*)-6-[(2-ethoxynaphthalene-1-carbonyl)amino]-3,3-dimethyl-7-oxo-4-thia-1-azabicyclo[3.2.0]heptane-2-carboxylic acid) is a narrow spectrum  $\beta$ -lactam antibiotic [1] of the penicillin class (Fig. 2.1A). As a  $\beta$ -lactamase-resistant penicillin, it is used to treat infections caused by gram-positive bacteria, in particular species of staphylococci that are resistant to other penicillins [2]. Although NAF is generally well tolerated, with few side effects, it has been reported to have a potential for associated hepatotoxicity and acute interstitial nephritis [3,4]. NAF is also used in intramammary formulations for the treatment of mastitis and its prevention in cows [5]. Its antimicrobial activity is related to the 6-aminopenicilloic acid core structure (6-APA) (Fig. 2.1B), common to all penicillins, which inhibits the penicillin-binding proteins (PBPs) blocking the transpeptidation step and consequently the synthesis of the bacterial cell wall. NAF is the only penicillin having the 2-ethoxy-1-naphthoic acid side chain (2E1N) (Fig. 2.1C) which has a two-fold effect: on one hand it modifies the steric hindrance of the molecule, reducing the affinity for the active site of  $\beta$ -lactamase, and on the other it increases moderately the acid resistance, making the oral administration of the drug possible [6].

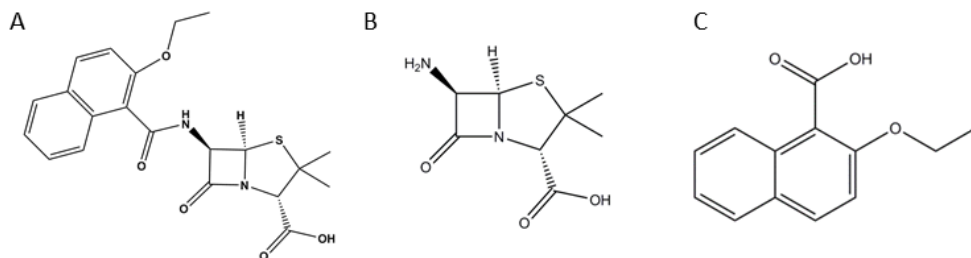


**Fig. 2.1** Chemical structure of nafcillin (A), 6-aminopenicilloic acid (B) and 2-ethoxy-1-naphthoic acid.

Semisynthetic penicillins have been synthesized in the past to improve various characteristics like oral adsorption or resistance to  $\beta$ -lactamase digestion. This is the case of the isoxazolyl penicillins (ISOXA), firstly obtained in the 1960's [7–9] (Fig. 2.2). The isoxazolyl moiety improves the oral adsorption; moreover, the bulky side chain hinder  $\beta$ -lactamase binding, improving the resistance of these antibiotics to enzymatic digestion [6]. Adding different heteroatoms (i.e. Cl and F) to the side chain improves the plasma levels of the drugs after oral administration, especially for dicloxacillin (DCLX) and flucloxacillin (FCLX) [10,11]. This effect is linked to the lipophilic character of the side chain which promotes the penetration in the lipid membrane of the gut walls [6]. The isoxazolyl moiety slightly improves the acid resistance of the antibiotics, making them suitable for oral administration [12,13], increasing their half-life in blood plasma.

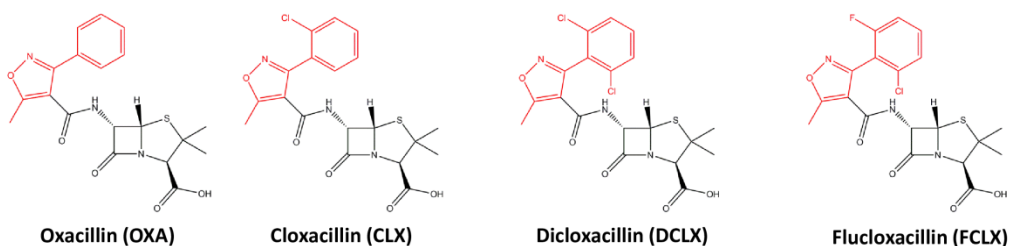


**Fig. 2.2** Chemical structure of ISOXA penicillins, with the side chain containing the isoxazole ring in red.

In veterinary medicine, ISOXA penicillins are used to treat both acute [14] and subclinical mastitis caused by *Staphylococci* strains, also in combination with other extra-label antibiotics [15]. Relatively few example of analytical methods for ISOXA penicillins have been reported [16–21], and none based on their electrochemistry; thus a direct electrochemical detection strategy for this class of penicillins is highly desirable.

The electrochemistry of NAF and ISOXA penicillins were investigated on G-SPE electrodes and their behaviour in different pH was evaluated and correlated with MS data on their degradation, to understand whether it is possible to use their electrochemical fingerprint for the quantification of the pharmacologically active marker residues, used to calculate the MRLs value in milk.

### Materials and methods

#### Reagents and materials

Nafcillin sodium salt (NAF), oxacillin sodium salt (OXA), cloxacillin sodium salt (CLX), dicloxacillin sodium salt monohydrate (DCLX) and flucloxacillin sodium salt (FCLX) were purchased from Sigma Aldrich Ltd (Belgium). G-SPE, composed of a graphite working electrode (diameter = 3 mm), a graphite counter electrode and silver pseudo reference electrode, were purchased from Italsens (Palmsens BV, The Netherlands). All potentials are referred to the pseudo Ag internal reference electrode, which is -200 mV in respect to saturated calomel electrode (SCE). All the other reagents were of analytical grade and used as received. All aqueous solutions were prepared using MilliQ water ( $R > 18 \text{ M}\Omega\text{cm}$ ).

#### Instrumentation

Electrochemical measurements (CV, SWV) were carried out using an Autolab potentiostat/galvanostat (PGSTAT 302N, ECOCHEMIE, the Netherlands) controlled by NOVA 1.1 software. UV-Vis spectra were acquired between 200 and 500 nm with a NanoPhotometer N60 (Implen) operated by NanoPhotometer NPOS software. CV curves were recorded between +0.3 and +1.4 V at 50 mV/s. SWV curves were recorded between +0.3 and +1.4 V, 1 mV step potential, 25 mV amplitude, 10 Hz frequency. All results obtained by SWV are presented after baseline correction using the mathematical algorithm "Moving average" (peak width = 1) contained within NOVA 1.1 software, to improve the visualization and identification of the peaks over the baseline. All data elaboration was done with Origin 8.0 software (OriginLab). Chromatograms and mass spectra were recorded using LC coupled to a QTOF-MS mass spectrometer with electrospray ionization (ESI) operating in positive mode. The apparatus consisted of a 1290 Infinity LC (Agilent Technologies, Wilmington, DE, USA) connected to a 6530 Accurate-Mass QTOF MS (Agilent Technologies) with a heated-ESI source (JetStream ESI). Chromatographic separation was performed on a Kinetex Biphenyl column (100 × 2.1 mm, 2.6  $\mu\text{m}$ ), at room temperature, using a mobile phase composed of 0.04% of formic acid in

ultrapure water (A) and acetonitrile/ultrapure water (80/20, v/v) with 0.04% formic acid (B), in gradient. The flow rate and the injection volume were set at 0.3 mL/min and 1  $\mu$ L, respectively. The QTOF-MS instrument was operated in the 2 GHz (extended dynamic range) mode, which provides a full width at half maximum (FWHM) resolution of approximately 4700 at  $m/z$  118 and 10,000 at  $m/z$  922. Positive polarity ESI mode was used under the following specific conditions: gas temperature 300 °C; gas flow 8 L/min; nebulizer pressure 40 psi; sheath gas temperature 350 °C; sheath gas flow 11 L/min. Capillary and fragmentor voltages were set to 4000 V and 135 V, respectively. The ions selected for recalibrating the mass axis, ensuring the mass accuracy throughout the run, were  $m/z$  121.0508 and 922.0097. The QTOFMS was acquiring from  $m/z$  50 to 1000 in MS mode. Data-dependent acquisition mode (auto-MS/MS) was applied using two different collision energies (10 eV and 20 eV) for the fragmentation of the selected parent ions. The maximum number of precursors per MS cycle was set to four with minimal abundance of 2500 counts. In addition, precursor ions were excluded after every spectrum and released after 0.2 min.

## Results and discussion

### Nafcillin

Fig. 2.3A shows the CV of 1 mM of NAF in 0.1 M citrate-phosphate buffer pH 6. NAF presents an intense peak at +1.1 V, ascribed to an irreversible oxidation process. The analysis of the peak current at different scan rates (Fig. 2.3B), between 10 and 200 mV/s, showed a linear relationship between the peak current and the square root of the scan rate (Fig. 2.3C), characteristic for diffusion controlled processes. Moreover, the slope of the linear relationship between the Log of peak currents and the Log of scan rates (Fig. 2.3D) is 0.55, which is very close to the value expected (0.5) for a diffusive behavior [22].

## Chapter 2 - Electrochemical fingerprinting of nafcillin and isoxazolyl penicillins

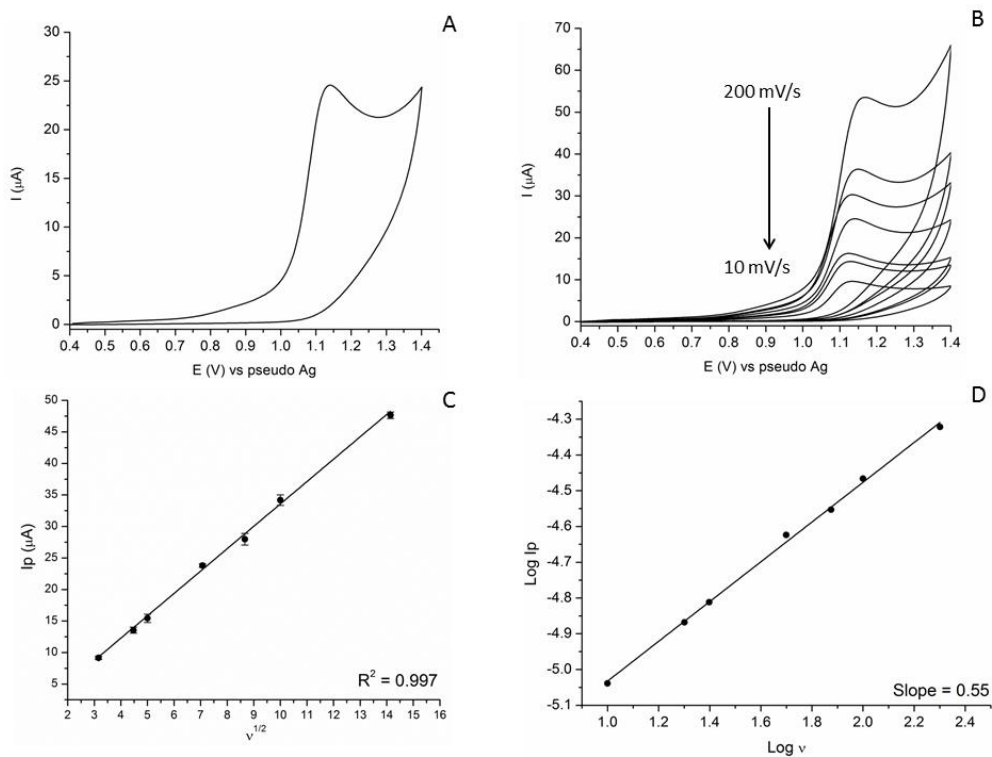


**Fig. 2.3** A) CV of 1 mM NAF in 0.1 M citrate phosphate buffer pH 6 at G-SPE at 50 mV/s; B) Scan rate study of 1 mM of NAF in 0.1 M citrate phosphate buffer pH 6 at G-SPE; C) Plot of  $I_p$  vs square root of scan rate; SD calculated for  $n=3$ ; D) Plot of  $\text{Log } I_p$  vs  $\text{Log } v$ .

The electrochemical oxidation of NAF is also dependent on the pH: the peak intensity for the oxidation of 100 μM of NAF increases by decreasing the pH (Fig. 2.4A) reaching a maximum at pH 4. At more acidic pH (2-3), NAF becomes unstable and prone to degradation. The degradation processes are evident below pH 4 as the solution turned immediately cloudy below that pH value.

The electrochemistry of the 2E1N side chain as sole compound was also investigated to better understand the functional groups involved in the oxidation process of NAF. In Fig. 2.4B, the comparison of the oxidation signals of 100 μM NAF (black line) and 100 μM 2E1N (grey line) evidences a difference in the peak potential: while NAF oxidation occurs at +1.1 V, 2E1N shows a more intense oxidation peak at +0.9 V.

## Chapter 2 - Electrochemical fingerprinting of nafcillin and isoxazolyl penicillins

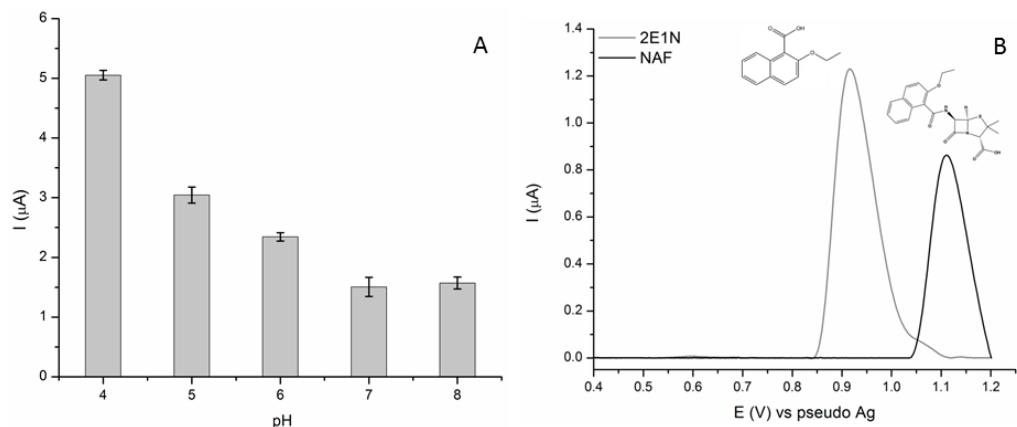


**Fig. 2.4** A) Peak intensity for the oxidation of 100  $\mu\text{M}$  of NAF at different pHs (from 4 to 8) in 0.1 M BRB, SD calculated for  $n=3$ ; B) SWVs of 100  $\mu\text{M}$  NAF (black line) and 2E1N (grey line) at G-SPE in 0.1 M BRB pH4.

These results suggest that NAF oxidation may not involve only the side chain but also the penicillin core structure, which shifts the potential towards more positive values. To verify this hypothesis, a degradation study of NAF and 2E1N was performed; alkaline degradations were performed in 100  $\mu\text{M}$  solutions of NAF and 2E1N to identify the degradation products. The pH of the solution was adjusted to 12 and SWVs were acquired at different time points (0, 1 h, 3 h, 24 h).

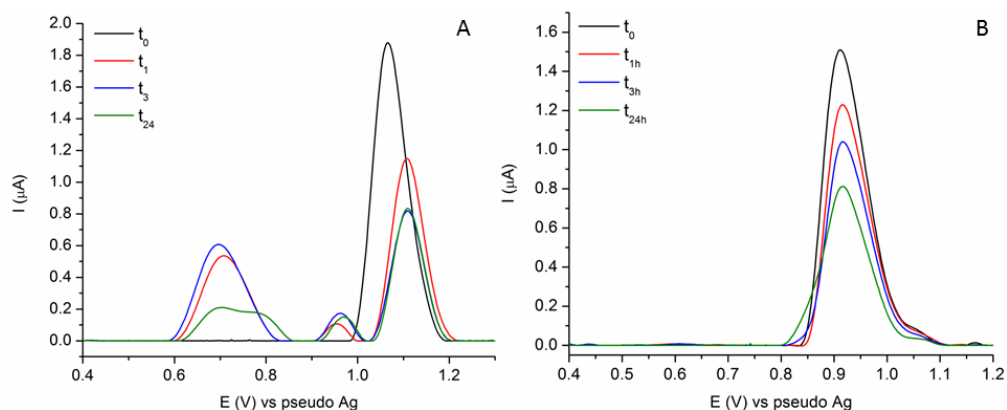


**Fig. 2.5** SWVs at G-SPE of 100  $\mu\text{M}$  NAF (A) and 2E1N (B) at different basic degradation times in 0.1 M BRB pH4.

After only 1 h of alkaline degradation, the electrochemical response of NAF is affected by the degradation process. The NAF peak at +1.1 V decreases and two new peaks appear, a broad peak at +0.6 V and another smaller one at +0.9 V (red



curve in Fig. 2.5A). Comparing the response of the degraded solution of 2E1N with that of the degraded NAF, it was possible to see that no shift in peak position nor appearance of new peaks occurs for 2E1N, only a decrease in peak intensities, up to 24 h of degradation (Fig. 2.5B). Thus, it was possible to conclude that NAF oxidation signal is not only related to the oxidation of the 2E1N side chain. The small peak at +0.9 V (Fig. 2.5 A) can be ascribed to 2E1N molecules free in solution, but the major degradation involves the core penicillin structure. It is known that the  $\beta$ -lactam ring of penicillins undergoes hydrolysis in basic environments [23,24], losing their antimicrobial activity.

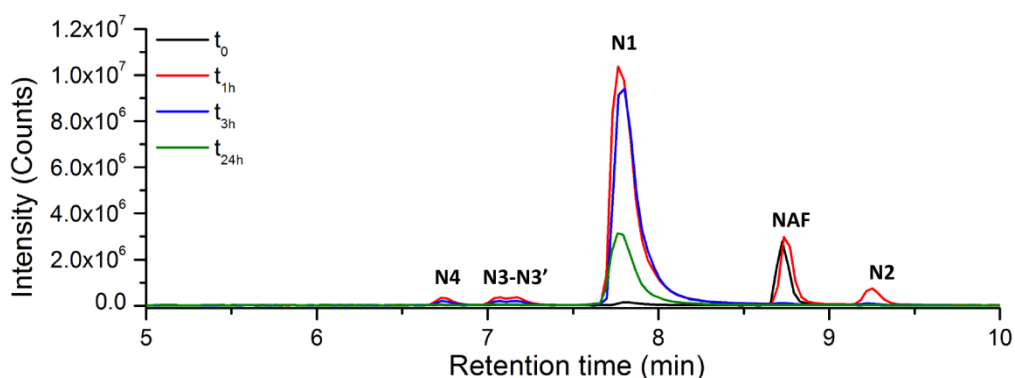


**Fig. 2.6** Extracted ion chromatogram of 20 ng/ $\mu$ L solutions nafcillin (black line), directly injected alkaline degraded samples after 1 h (red line), 3 h (blue line) and 24 h (green line).

To verify the hypothesis that the change in the electrochemical fingerprint of NAF is related to the degradation of the core penicillin structure, mass spectrometry analysis of the degraded solutions at different time was performed with liquid chromatography coupled with quadrupole time of flight mass spectrometry (LC-QTOFMS). The degraded samples were diluted to approximately 20 ng/ $\mu$ L with ultrapure water and injected in the LC-QTOFMS system. The obtained chromatograms are compared to a 20 ng/ $\mu$ L standard of NAF (black line in Fig. 2.6). In the first hour of degradation (red line in Fig. 2.6), four main degradation products were identified as product 1 (N1) at 7.77 min ( $m/z$  433.1460,  $C_{21}H_{24}N_2O_6S$ ), product 2 (N2) at 9.25 min ( $m/z$  415.1316,  $C_{21}H_{22}N_2O_5S$ ), product 3 (N3 and N3') at 7.00 and 7.14 min ( $m/z$  415.1316,  $C_{21}H_{22}N_2O_5S$ ) and product 4 (N4) at 6.75 min ( $m/z$  415.1316,  $C_{21}H_{22}N_2O_5S$ ) when compared to NAF at 8.73 min ( $m/z$  415.1316,  $C_{21}H_{22}N_2O_5S$ ) (black line in Fig. 2.6). As expected, the mass difference between NAF and product N1 corresponds to the loss of  $H_2O$ . Therefore, it is possible to relate the

main product N1 to the hydrolysis of the  $\beta$ -lactam ring (Fig. 2.7). After 3 h the signal of N2 slightly decreased; after 24 h this decrease in intensity progresses further which reveals that the formed products further degraded to other products that could not be observed in the LC-QTOF-MS analysis. Likewise the signal of the remaining intact NAF decreased drastically after three hours of degradation and is completely absent in the 24 h spectra.

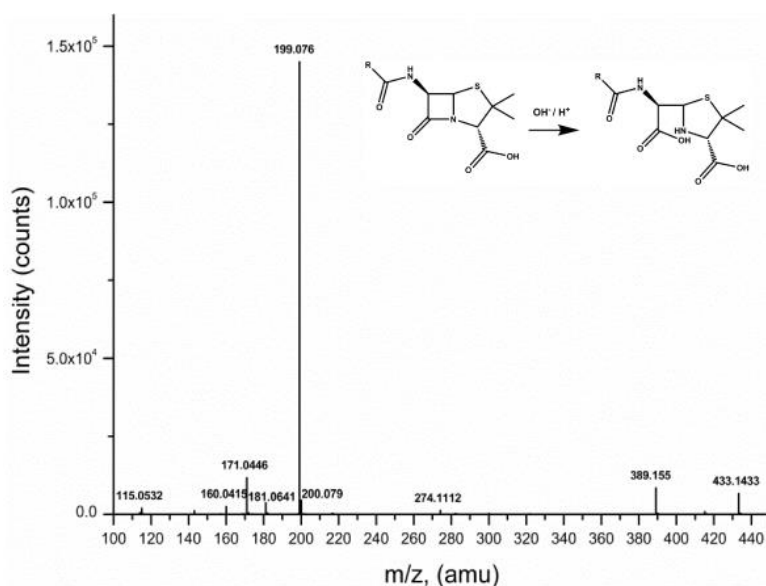


**Fig. 2.7** MS/MS spectra of product N1 at 7.77 min ( $m/z$  433.1460,  $\text{C}_{21}\text{H}_{24}\text{N}_2\text{O}_6\text{S}$ ). Inset: hydrolysis of the  $\beta$ -lactam ring.

These observations confirmed that the oxidation peak of NAF at +1.1 V is due to the oxidation of the side chain conjugated with the core penicillin structure and not only to the oxidation of the 2E1N alone. Looking at the SWVs response it was possible to distinguish between the pharmacologically active form of NAF and its degraded products, since there is a change in their electrochemical fingerprint. It is worth reminding that MRL value for antibiotics in food and feed products are calculated on the intact form of the drug only, thus direct electrochemical detection of NAF shows an intrinsic selectivity in this regard.

### Isoxazolyl penicillins

The electrochemistry of this class of penicillins was investigated on bare G-SPE in 0.1 M PB pH 2. In Fig. 2.8A, the SWVs for the oxidation of 500  $\mu\text{M}$  of each ISOXA penicillins are presented. A peak at positive potentials (+1.3 V) accounts for

the oxidation of the penicillin core structure while another oxidation peak around +0.6 V is related to the side chain oxidation. This was confirmed by examining the oxidation behaviour of the side chain alone. In Fig. 2.8B, the SWV of 100  $\mu\text{M}$  of CLX side chain (3-(2-chlorophenyl)-5-methyl-4-isoxazolecarboxylic acid – 3CMC) is shown, indicating an irreversible oxidation peak at +0.6 V, same as the corresponding peak of CLX (red curve in Fig. 2.8A).

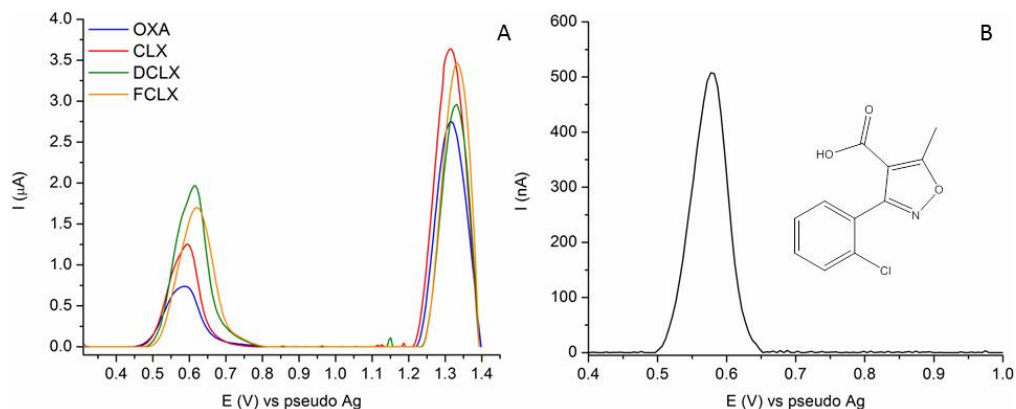


**Fig. 2.8** A) SWVs for 500  $\mu\text{M}$  of OXA (blue), CLX (red), DCLX (green) and FCLX (orange) in 0.1M PB pH 2 on G-SPE; B) SWVs for 100  $\mu\text{M}$  of 3CMC in 0.1M PB pH 2 on G-SPE.

While the peak at +1.3 V is common to all the penicillins, the oxidation signal at +0.6 V could be used for the quantification of the total content of isoxazoyl penicillins, but not for the identification of the single compounds. The pH study of ISOXA penicillins shows that lower pH results in higher peak intensities for the oxidation of the side chain at +0.6 V (see Fig. 2.9), as already seen for NAF. The results have to be considered as a general trend indication since no errors are reported. For pH values higher than 5, however, the oxidation peak at + 0.6 V is not visible anymore.

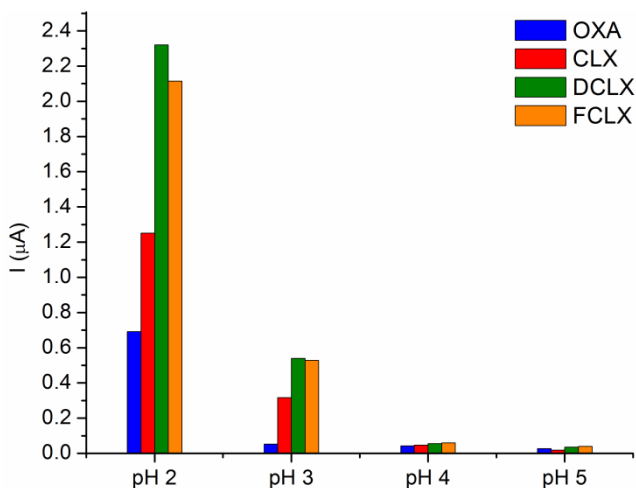


**Fig. 2.9** pH study for the oxidation peak at +0.6 V for 500  $\mu\text{M}$  of OXA (blue), CLX (red), DCLX (green) and FCLX (orange) on G-SPE.

The poor stability of the diluted solution of ISOXA penicillin in lower pH values (2-3) supports our observation. Immediately upon dilution, the solution turns cloudy as already seen for NAF. To verify the possible changes in the electrochemical fingerprint under acidic conditions, an acid degradation study was performed. A 500  $\mu\text{M}$  solution of each ISOXA penicillins was prepared in 0.1 M  $\text{H}_2\text{SO}_4$  (c.a. pH 1) and UV-Vis and SWVs analysis were performed at different degradation time (0, 15 min, 30 min, 2 h, 6 h, 16 h, 24 h).

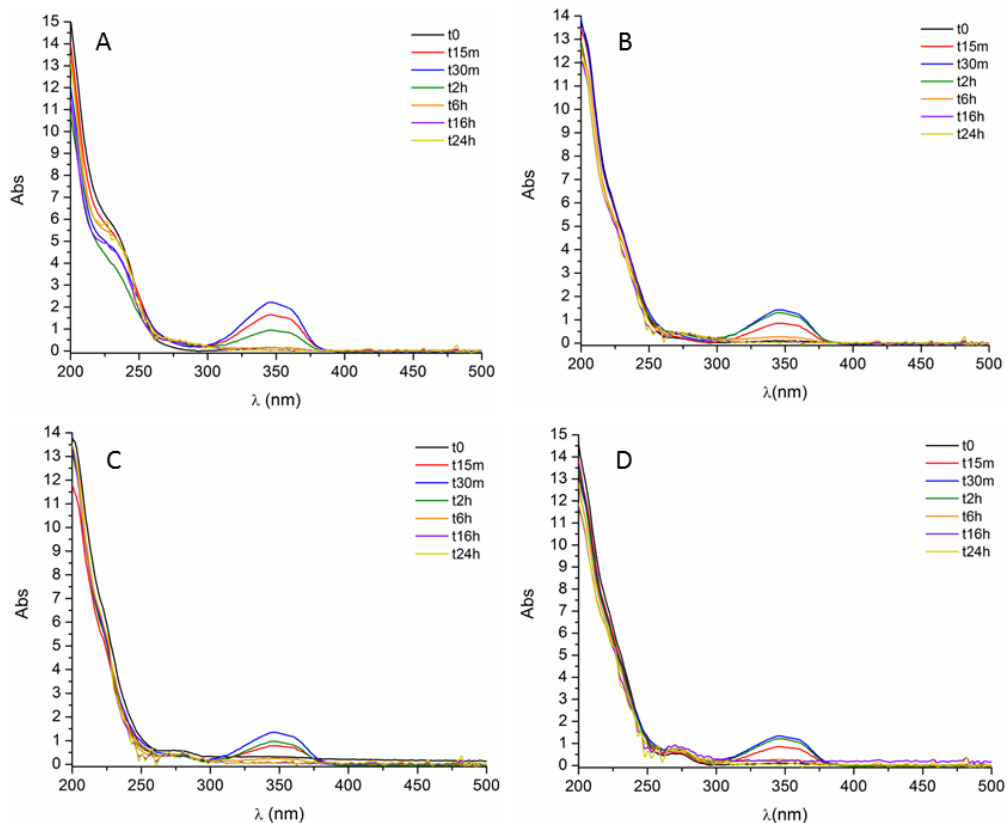


**Fig. 2.10** Uv-Vis spectra of 500 μM solution of ISOXA penicillin at different degradation time: A) oxacillin; B) cloxacillin; C) dicloxacillin; D) flucoxacillin.

Preliminary tests had shown that the degradation of the ISOXA penicillin is very fast (within minutes), thus more analyses were performed for shorter degradation times. Indeed, looking at the UV-Vis spectra in Fig. 2.10, it is possible to observe the appearance of a broad band at 350 nm for very short degradation time. The trend is the same for all four antibiotics: the band appears at 15 min, increase in intensity for 30 min and start decreasing at 2 h to completely disappear at longer degradation times. The UV-Vis spectra did not present any other interesting feature apart from a band at 225 nm for OXA, which remains more or less constant over time. The appearance of this degradation product could also be seen in the SWVs for different degradation times.

## Chapter 2 - Electrochemical fingerprinting of nafcillin and isoxazolyl penicillins

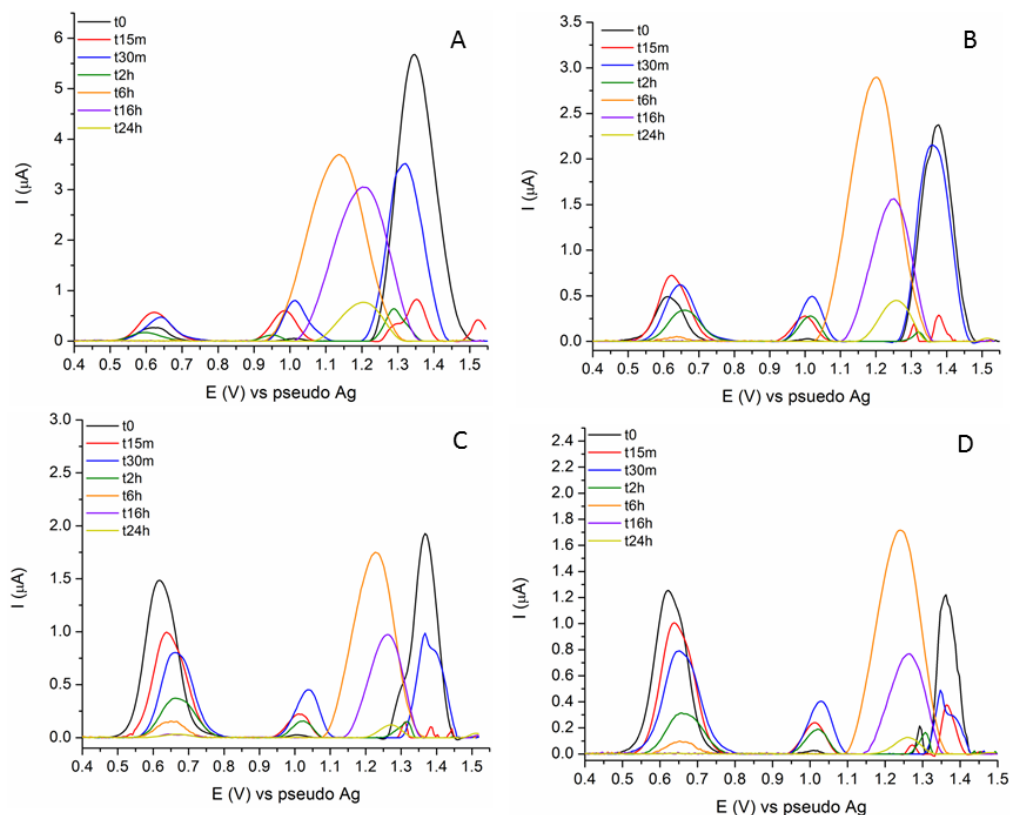


**Fig. 2.11** SWVs of 500  $\mu\text{M}$  solution of ISOXA penicillin at different degradation time: A) OXA; B) CLX; C) DCLX; D) FCLX. SWV parameters: Freq 10 Hz, amplitude 25 mV, step potential 5 mV.

Looking at Fig. 2.11A and B, the peak of the side chain at +0.6 V increase slightly at 15 min degradation time for both OXA and CLX (red curves), decreasing in intensity after with increasing degradation time. For DCLX and FCXL instead the oxidation peak at +0.6 V decreases steadily increasing degradation times before disappearing completely after 16h. Therefore, also the side chains themselves undergo degradation, suppressing their electrochemistry. Starting from 15 min of degradation, a new oxidation peak appears at *c.a.* +1.0 V. It reaches a maximum intensity at 30min and then disappearing for degradation times longer than 2h. This peak seems to follow the same trend of the UV-Vis band at 350 nm (see Fig. 2.10) leading to the hypothesis that both signals are due to the same product. The peak of the core structure at *c.a.* +1.3/1.4 V shows significant changes compared to the native solution: after a decrease in intensity for shorter degradation times (15 min, 30 min, 2 h) it shifts to less positive potential (+1.25 V) for 6 h and 16 h, reaching a minimum in intensity for 24 h degradation. The modification of the oxidation peak

of the core structure is probably related to the opening of the  $\beta$ -lactam ring and thus the inactivation of the antibiotic. To verify this assumption, DCLX was subjected to LC-QTOF-MS analysis. The sample corresponding to 30 min of degradation was diluted to 20 ng/ $\mu$ L with ultrapure water and injected directly in the LC-QTOF. The obtained chromatograms were then compared to a 20 ng/ $\mu$ L standard of DCLX (Fig. 2.12).

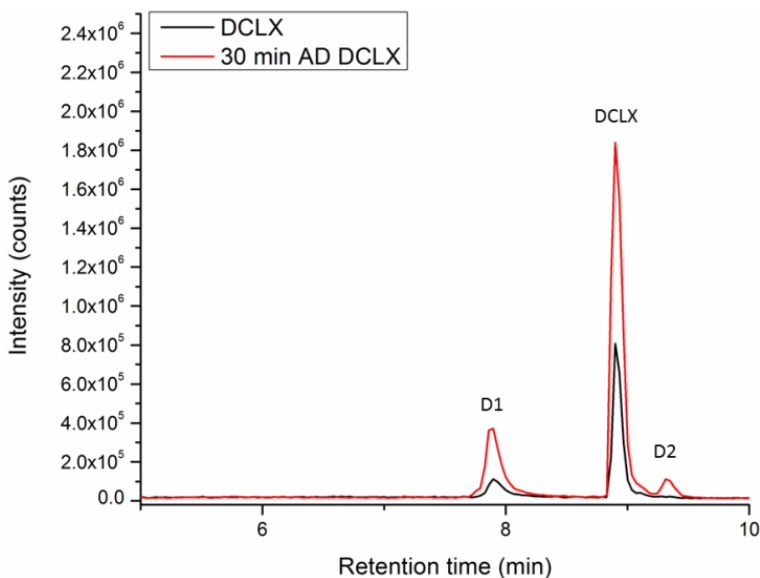


**Fig. 2.12** Extracted ion chromatogram of 20 ng/ $\mu$ L solutions dicloxacillin (black), directly injected and acid (red) degraded after 30 min.

Two degradation products of DCLX were identified: product D1 at 7.84 min ( $m/z$  488.0444,  $C_{19}H_{19}Cl_2N_3O_6S$ ) and product D2 at 9.22 min ( $m/z$  470.0339,  $C_{19}H_{17}Cl_2N_3O_5S$ ). The black line in Fig. 2.12 represents pure DCLX at 8.81 min ( $m/z$  470.0339,  $C_{19}H_{17}Cl_2N_3O_5S$ ). The degradation product D1 is partially present in the standard solution (black line) probably due to degradation of the stock solution. However the peak grows in intensity for degraded DCLX and another degradation products appears (D2), not present in the standard solution. Again, the difference in mass between the intact DCLX and its main degradation product (D1) is exactly the weight of  $H_2O$  which results from the hydrolysis of the  $\beta$ -lactam ring, rendering DCLX in an inactive form. Product D2 could be probably related to the UV-Vis active product, but no standards are available to identify it.

## Conclusions

The feasibility of a direct detection strategy for NAF and the ISOXA penicillins has been evidenced, thanks to the in-depth understanding of their electrochemical fingerprint and degradation pattern. NAF and the ISOXA penicillins can be detected electrochemically exploiting the oxidation signal of their side chains. While the electrochemical fingerprint of NAF is unique, all the ISOXA penicillins showed similar electrochemical behaviour. Thus, it is possible to achieve class selectivity but identification on single compound level is not feasible, explained by the fact that all the ISOXA penicillins share the same electrochemical fingerprint, with one oxidation peak for the side chain at +0.6 V and one for the core structure at +1.3 V. However, given the difference in the heteroatom present on the ISOXA side chains (Cl, F) it is possible to envision signal amplification strategies that could differentiate the electrochemical fingerprint of some ISOXA penicillins from the others, based on nanomaterials or other selective electrode modifiers. The data about the degradation of ISOXA penicillins showed that low pH values are not useful since this type of penicillins degrades in this medium. Therefore, the expected electrochemical signals cannot be related to the intact form of the antibiotics. Again, it is worth reminding that MRLs values are calculated on the pharmacologically active form of the drugs, and the analysis in acid pH may give rise to an underestimation of the concentration. To fully exploit the electrochemical fingerprint of the ISOXA penicillins, the pH of the analysis buffer should not be strongly acid, and signal amplification strategies have to be devised to increase the very low oxidation signal intensity of the side chains. The combination of MS and electrochemistry was fundamental to identify the best experimental conditions in terms of pH, to avoid possible misinterpretation of the data regarding the difference between the pharmacologically active form of the antibiotics and their degradation products.



## Chapter 2 - Electrochemical fingerprinting of nafcillin and isoxazolyl penicillins

### References

- [1] D.L. Palmer, S.B. Pett, B.F. Akl, Bacterial wound colonization after broad-spectrum versus narrow-spectrum antibiotics, *Ann. Thorac. Surg.* 59 (1995) 626–631.
- [2] A.K. Tan, A.L. Fink, Identification of the site of covalent attachment of nafcillin, a reversible suicide inhibitor of beta-lactamase, *Biochem. J.* 281 (1992) 191 LP – 196.
- [3] T. Hoppes, M. Prikis, A. Segal, Four cases of nafcillin-associated acute interstitial nephritis in one institution, *Nat. Clin. Pract. Nephrol.* 3 (2007) 456.
- [4] C.B. Whitman, M.J. Wike, Possible case of nafcillin-induced acute interstitial nephritis, *Am. J. Heal. Pharm.* 69 (2012) 1049–1053.
- [5] S.W. Page, P. Gautier, Use of antimicrobial agents in livestock, *Rev. Sci. Tech. l'OIE.* 31 (2012) 145–188.
- [6] J.H.C. Nayler, Structure-Activity Relationships of Semisynthetic Penicillins, *Proc. R. Soc. London B.* 179 (1971) 357–367.
- [7] F.P. Doyle, A.A.W. Long, J.H.C. Nayler, E.R. Stove, New Penicillins Stable towards Both Acid and Penicillinase, *Nature.* 192 (1961) 1183–1184.
- [8] J.C. Hanson, A.A.W. Long, J.H.C. Nayler, E.R. Stove, 1120. Derivatives of 6-aminopenicillanic acid. Part VIII. Further analogues of 3-O-chlorophenyl-5-methyl-4-isoxazolylpenicillin, *J. Chem. Soc.* (1965) 5976–5983.
- [9] J.C. Hanson, J.H.C. Nayler, T. Taylor, P.H. Gore, 1121. Derivatives of 6-aminopenicillanic acid. Part IX. 2,4-di- and 2,4,5-tri-substituted-3-furylpenicillins, *J. Chem. Soc.* (1965) 5984–5988.
- [10] G.P. Bodey, C. Vallejos, D. Stewart, Flucloxacillin: A new semisynthetic isoxazolyl penicillin, *Clin. Pharmacol. Ther.* 13 (1972) 512–515.
- [11] R. Sutherland, E.A.P. Croydon, G.N. Rolinson, Flucloxacillin, a New Isoxazolyl Penicillin, Compared with Oxacillin, Cloxacillin, and Dicloxacillin, *Br. Med. J.* 4 (1970) 455–460.
- [12] N.G. Donskaya, V.L. Lapidus, G.S. Libinson, P.S. Braginskaya, Stability of Dicloxacillin in Aqueous solution, *Pharm. Chem. J.* 10 (1976) 108–111.
- [13] A.P. Kondrat'eva, V.P. Bruns, Stability of Penicillins in Aqueous Solutions. I. Oxacillin and Phenoxymethylpenicillin, *Pharm. Chem. J.* 1 (1967) 696–701.
- [14] W.T. Davis, D.C. Maplesden, R.P. Natzke, W.N. Philpot, Sodium cloxacillin for treatment of mastitis in lactating cows, *J. Dairy Sci.* (1975).
- [15] R.S. Rossi, A.F. Amarante, S.T. Guerra, G.S. Latosinski, B.F. Rossi, V.L.M. Rall, J.C. de

## Chapter 2 - Electrochemical fingerprinting of nafcillin and isoxazolyl penicillins

- F. Pantoja, Efficacy of cefquinome and a combination of cloxacillin and ampicillin for treatment of dairy cows with *Streptococcus agalactiae* subclinical mastitis, *PLoS One*. 14 (2019) e0216091.
- [16] E. Usleber, M. Lorber, M. Straka, G. Terplan, E. Märtlbauer, Enzyme immunoassay for the detection of isoxazolyl penicillin antibiotics in milk, *Analyst*. 119 (1994) 2765–2768.
- [17] E.G. Kulapina, V. V. Baraguzina, O.I. Kulapina, Ion-selective sensors for determining ampicillin and oxacillin in biological fluids and pharmaceuticals, *Pharm. Chem. J.* 40 (2006) 171–174.
- [18] W. Yu, Y. Chen, M. Knauer, R. Dietrich, E. Märtlbauer, X. Jiang, Microfluidic Chip-Based Immunoassay for Reliable Detection of Cloxacillin in Poultry, *Food Anal. Methods*. 9 (2016) 3163–3169.
- [19] Y. Chen, Y. Wang, L. Liu, X. Wu, L. Xu, H. Kuang, A. Li, C. Xu, A gold immunochromatographic assay for the rapid and simultaneous detection of fifteen  $\beta$ -lactams, *Nanoscale*. 7 (2015) 16381–16388.
- [20] Y. Hu, Z. Zhang, H. Zhang, L. Luo, S. Yao, A sensitive and selective sensor-coated molecularly imprinted sol-gel film incorporating  $\beta$ -cyclodextrin-multi-walled carbon nanotubes and cobalt nanoparticles-chitosan for oxacillin determination, *Surf. Interface Anal.* 44 (2012) 334–341.
- [21] E.G. Kulapina, S. V. Snesarev, Potentiometric sensors based on organic ion exchangers of tetraalkylammonium and silver complexes with ampicillin, oxacillin, and cefazolin, *J. Anal. Chem.* 67 (2012) 163–167.
- [22] D.K. Gosser, *Cyclic voltammetry : simulation and analysis of reaction mechanisms*, New York (N.Y.) : VCH, 1993.
- [23] A.D. Deshpande, K.G. Baheti, N.R. Chatterjee, Degradation of  $\beta$ -lactam antibiotics, *Curr. Sci.* 87 (2004) 1684–1695.
- [24] M. Grover, M. Gulati, B. Singh, S. Singh, Correlation of Penicillin Structure with Rate Constants for Basic Hydrolysis, *Pharm. Pharmacol. Commun.* 6 (2010) 355–363.



# Aptamers: bioreceptors for antibiotics identification

---

Aptamers are DNA, or RNA, strands that bind a specific target molecule. Developed for the first time in the nineties of last century, they opened up new avenues of research in many different fields, from drug delivery, over therapeutics to analytical applications. Especially, ssDNA aptamers for small organic molecules, such as antibiotics, might represent the turning point for medical and environmental analysis.

In this chapter, an overview of the selection strategies used to obtain such bio recognition elements will be presented, with the focus on the aptamers currently available for  $\beta$ -lactam antibiotics. The second part will be devoted to the selection of new aptamers for nafcillin and cephalexin. A comparison of the performances of the traditional Flu-Mag SELEX with a novel variation based on Graphene Oxide will be shown.

Since their discovery, aptamers were considered a leap forward in many analytical and biomedical applications. The single stranded DNA, or RNA, sequences offer considerable advantages over traditional molecular biorecognition elements such as antibodies or enzymes, including stability over a wider range of temperatures and pHs, ease of synthesis and modification, lower production costs and longer shelf-life [1]. They can be selected against almost every possible analytical target, such as proteins, carbohydrates, enzymes, cells, bacteria and small organic molecules [2]. RNA and DNA aptamers have been reported in literature for therapeutic and drug-delivery studies [3,4], as well as for analytical purposes [5,6]. Additionally, a wide range of SELEX approaches (such as Capture-SELEX, Cell-SELEX and Capillary SELEX [7–13]) were described in literature since 1990.

## **Aptamers: selection strategies**

Methodologies to select specific oligonucleotide sequences with strong affinity for a given target from a large pool of random fragments were first reported in the end of last century, independently, by Ellington and Szostak [14] and Tuerk and Gold [15]. In those pivotal papers, the authors used RNA libraries to select aptamers

against a bacteriophage T4 DNA polymerase [14] and two organic dyes, Cibacron Blue 3G-A and Reactive Blue 4 [15]. The second example shows how, since the very beginning, small molecules were considered a suitable target for selection. From that point onwards aptamer selection strategies bloomed and the application of this new technology covered almost every possible analytical target. Aptamers, DNA or RNA, were selected in the following years against proteins [16], small molecules [17], ions [18], cells [19] and even viruses [20].

The protocol to obtain aptamers is generally called SELEX which is the acronym for Systematic Evolution of Ligand by Exponential Enrichment. It is a *Systematic Evolution* because the random mutation of the oligonucleotides upon subsequent cycles of selection play a big part in promoting the diversity of the original pool of fragments. It is also considered *Exponential* since from a very large starting library ( $\sim 10^8$  different sequences) it is possible to obtain a very narrow distribution of similar binding sequence (between 1 and 10 groups of sequence with high consensus regions). A general scheme of a traditional SELEX protocol is reported in Fig. 3.1: the initial library of random ssDNA or ssRNA is mixed with the desired target, usually immobilized on a solid surface. The sequences that recognize the target will bind to it and all the remaining strands are discarded. The bound oligonucleotides will be recovered and amplified to obtain another starting library with higher affinity for the target; subsequently another round of selection will be performed using this enriched pool.

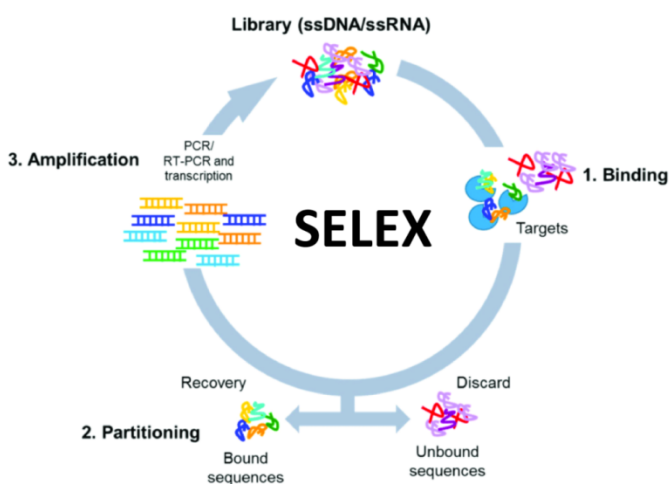
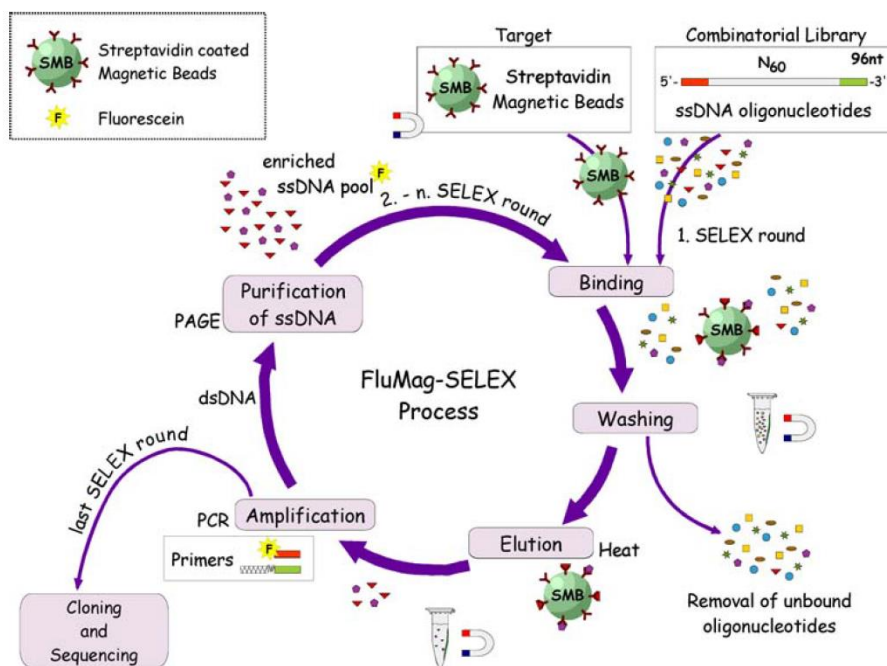


Fig. 3.1 Systematic Evolution of Ligands by Exponential Enrichments (SELEX) general scheme.

This basic scheme has been adapted in many different variations over the years to address several technological issues. One of the most commonly used variant was developed in 2005 by Stoltenburg *et al.* [21]. This protocol, called FluMag SELEX (Fig. 3.2), combines the immobilization of the target on magnetic beads with the use of fluorescent labels for DNA quantification. The immobilization on magnetic beads allows easy handling, use of very small amounts of target, rapid and efficient separation of bound and unbound fractions, and more stringent washing steps. The selected strands are labelled with fluorescein, thus enabling their quantification in further rounds and the monitoring of the enrichment of target-specific aptamers. This strategy has become the gold standard for many different applications and it is one of the most commonly used [22].



**Fig. 3.2** Schematic representation of the fluorescence-monitored in-vitro selection procedure, the so-called FluMag-SELEX, for generating DNA aptamers for specific target molecules immobilized on magnetic beads (from ref [21]).

### Capture-SELEX

As far as the selection of aptamers for small molecules (less than 1000 atomic mass units) is concerned, one of the main problems is the immobilization of the target. Due to their small size, the functional groups, and therefore the possible interaction

points between the target and the aptamer, are much more limited. In most cases, one of the functional groups is used for the immobilization, further decreasing the amount of possible interactions with the ssDNA strands. The selection of aptamers against immobilized targets may also lead to inconsistent results when the intended analytical application has to happen in solution [23,24]. Trying to overcome this problem, in 2012 Stoltenburg *et al.*, developed a strategy called Capture-SELEX [25], depicted in Fig. 3.3. In this new protocol, instead of immobilizing the small target molecule, a special library is anchored to the magnetic beads using a capture oligo, which can hybridize with a docking sequence present in the random region of the library. This strategy, that can be seen as an evolution of the FluMag Selex [21], overcomes the drawbacks usually linked to the immobilization of the target: as a proof-of-concept the author selected aptamers against an aminoglycoside antibiotic, kanamycin A.

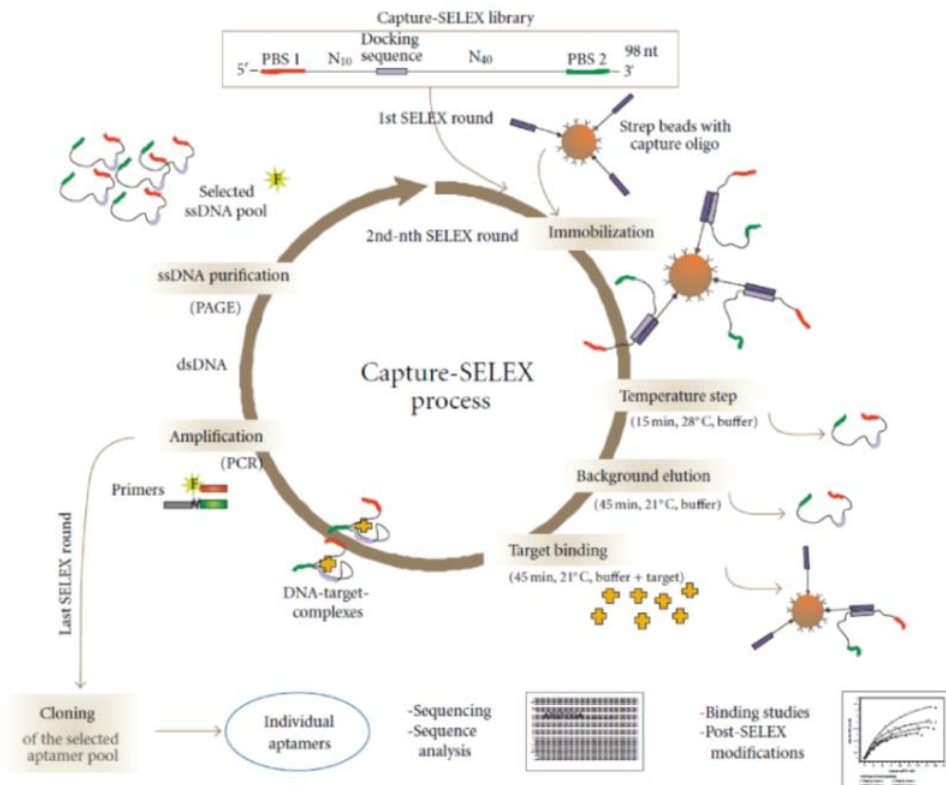
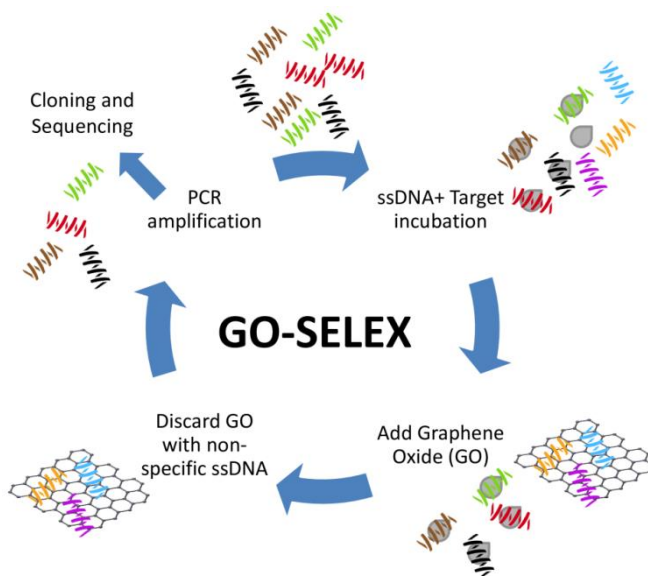


Fig. 3.3 Capture-SELEX general scheme (from ref. [26]).

*Graphene oxide SELEX*

Another kind of selection strategy which has been gathering attention in the last years is based on the interaction of ssDNA with graphene oxide (Fig. 3.4). The so called Graphene Oxide (GO) SELEX takes advantage of the  $\pi$ - $\pi$  stacking interactions between the graphene oxide sheets and the ssDNA in solution [27]. The dsDNA adsorption on GO is very weak due to the shielding of nucleobases by the phosphate backbone, while ssDNA binds much strongly on GO. The kinetics of adsorption and desorption of ssDNA on GO is well studied [28]. The desorption of ssDNAs from GO can occur through two mechanisms: the hybridization with a complementary sequence or the conformational change induced by the interaction with proteins or small molecules [29–31]. This event can be used as partitioning strategy for the aptamer selection. One of the main advantages of this selection strategy, apart from the straightforwardness, is the fact that neither the target nor the ssDNA library need to be immobilized on a solid support. This allows the maximum freedom of conformational change upon binding and the availability of all functional groups present on the target molecules [32].



**Fig. 3.4** Graphene oxide (GO) SELEX general scheme.

Two main configurations have been developed so far: the GO can be used to collect the unbound ssDNA left in solution after a selection round (see Fig. 3.4) or the pre adsorbed library can be subsequently incubated with the target, allowing the



specific strands to separate from the surface and be recovered [33]. Both configurations of this selection strategy were already successfully applied to the selection of small molecules aptamer such as antibiotics [30,31].

In the last decades, several other selection strategies were developed to include different targets or to streamline the whole process. Technological improvement have been achieved with Capillary Electrophoresis SELEX [34,35] or Microfluidic SELEX [36–38]. These approaches combined the advantages of capillary electrophoresis in a self-contained device, which requires very small sample volume (c.a. 50  $\mu$ L) [39] and sometimes it is integrated with a PCR amplification system [9] allowing very high-throughput and shorter duration for each selection round (> 60 min). Another selection strategy for whole cell was developed in the early 2000's – Cell-SELEX [40,41]. This protocol was originally used to select aptamers against cancer cell lines. The advantages are manifold; the selected aptamers will recognize the compounds present on the cell outer wall in their native biological state [19]. The aptamers obtained with this protocol can also be used for disease biomarkers identifications and targeted therapeutics. The great diversity of possible recognitions sites on the cell surface will reduce the chance of poor selectivity of the obtained aptamers [42,43].

Other protocols, collected under the umbrella term of Non-SELEX selections, have been reported in the past, even if they are not yet commonly applied and remain more proof-of-concept studies [7,44–46].

**Table 3.1** Comparison of different aptamer selection strategies.

<b>Selection strategy</b>	<b>Immobilization</b>		<b>Advantages</b>	<b>Disadvantages</b>	<b>Possible targets</b>
	<i>Target</i>	<i>Library</i>			
<b>SELEX</b>	X		Easy to perform	Hard to adapt and very time consuming	Mostly protein and large molecules
<b>Flu-Mag SELEX</b>	X		Easy sample handling, versatile	Linked to the chemistry of the target and the possibility of fluorescent labelling	Mostly protein and large molecules
<b>Capture-SELEX</b>		X	Specific for small molecules	Higher cost and complexity	Small molecules
<b>GO-SELEX</b>			Rapid and requiring less reagents	Need to optimize the protocol for each specific target and applications	All, limited by specific interaction target-GO

Considering the most used selection strategies, summarized in Table 3.1, one could evaluate the best approach for the intended target. While traditional SELEX is still the most commonly used, it presents various drawbacks (such as immobilization to solid support or need to use radiolabelled reagents to follow the recovery procedures) especially for small molecule targets such as antibiotics. Moreover, it is very time consuming and hard to adapt. FluMag and Capture SELEX are better suited to select aptamers for small organic molecules and present several advantages. The immobilization of the target or the library on magnetic beads allows easy sample handling and washing step, speeding up the procedure considerably. The need for specific reagents and coupling step may, however, hamper the wide accessibility of these protocols and require additional optimization studies. GO-SELEX, on the other hand, is an immobilization free selection protocol which is particularly appealing for aptamer selection for small molecules, it is fast and easy to perform, but again needs careful optimization for each new analytical target, especially to assure that the interactions between the GO and the target are minimal. Thus, we decided to test first of all the traditional Flu-Mag SELEX, thanks to its versatility and the fact that it was already successfully employed in the past. Capture SELEX, while especially suited for small molecule aptamers, was not considered since it requires time consuming optimization, from the design of the library and the specific primers to the more complex ssDNA recovery after PCR, which has to maintain the library structure intact. We focused on GO-SELEX because it is relatively easy to perform, does not require any immobilization step and could present aspects of novelty.

### **Aptamers for $\beta$ -lactam antibiotics: the state of the art**

The first example of aptamers for  $\beta$ -lactam antibiotics was reported in 2012 by Song *et al.* [47]: they selected three sequences (AMP4, AMP17, AMP18) for ampicillin and used them in a colorimetric gold nanoparticles (AuNPs) assay. The authors claim that the aptamer sequences bind to the side chain of AMP, assuring good selectivity against other antibiotics, with binding affinities in the low nanomolar range (*c.a.* 10 nM). Said aptamer sequences were used in the following years in a variety of biosensing configurations, mainly for electrochemical biosensors, with very good performances also in real sample analysis (Table 3.2 presents a complete overview).

## Chapter 3 – Aptamers: bioreceptors for antibiotics identification

**Table 3.2** Summary of analytical parameters of biosensors based on AMP aptamers, (ACV = alternate current voltammetry, SWV = square wave voltammetry).

Analytical approach	Aptamer	Linear range	LOD	Selectivity	Real samples	Ref.
Dual colorimetric detection with AuNPs	AMP4 AMP17 AMP18	0.1 to 140 nM	0.1 nM	Amoxicillin Benzyl penicillin	Milk	[47]
Microfluidic impedimetric biosensor	AMP17	10 pM to 1 $\mu$ M	10 pM	non-specific ssDNA sequence	Milk	[48, 49]
Electrochemical aptasensor based on quadratic recycling amplification	AMP17	5 pM to 10 nM	1.09 pM	Amoxicillin Benzyl penicillin Penicillin	Milk	[50]
Electrochemical aptasensor based on dual recycling amplification	AMP17	0.2 to 40 nM	4 pM	Amoxicillin Benzyl penicillin Penicillin Lincomycin	Milk	[51]
Signaling probe displacement electrochemical aptasensor	AMP17	100 pM to 1 mM	10 pM	Kanamycin A Tetracycline Streptomycin Sulfadimethoxine	no	[52]
Fluorescent AuNPs aptasensors with nicking enzyme	AMP17	0.1 to 100 nM	0.07 nM	Amoxicillin Benzylpenicillin Sulfadimethoxine Chloramphenicol	River water	[53]
Probe displacement electrochemical aptasensor	AMP18	0.2 to 15000 $\mu$ M	30 nM	Levofloxacin Amoxicillin Trimethoprim Sulfamethoxazole Nitrofurantoin	Urine Tap water Milk Saliva	[54]
Reusable signal-off electrochemical aptasensor	AMP18	5 to 5000 $\mu$ M (ACV) 100 to 5000 $\mu$ M (SWV)	1 $\mu$ M (ACV) 30 $\mu$ M (SWV)	Levofloxacin Amoxicillin Trimethoprim Sulfamethoxazole Nitrofurantoin	Milk Saliva Calf serum	[55]
Electrochemical-SPR aptasensor	AMP4	2.5 to 1000 $\mu$ M	1 $\mu$ M	Penicillin G Penicillin V Oxacillin Cephalexin	River water	[56]
Metal-organic framework impedimetric biosensor	AMP18	0.001 to 2000 pg/ml	$0.2 \cdot 10^{-3}$ pg/ml	Doxorubicin Trombamycin Streptomycin Kanamycin Penicillin Cefazolin	Serum River water Milk	[57]

## Chapter 3 – Aptamers: bioreceptors for antibiotics identification

<b>Electrochemical aptasensor with endonuclease digestion amplification</b>	AMP17	0.1-100 nM	32 pM	Chloramphenicol Florfenicol Thiamphenicol Tobramycin Streptomycin Tetracycline Kanamycin Oxytetracycline Amoxicillin Penicillin Lincomycin Melamine	Milk Tap water	[58]
<b>Metal-organic framework AuNPs (MOF) colorimetric sensing platform</b>	AMP17	50-100 nM	13 nM	Chloramphenicol Sulfadimidine Kanamycin Oxytetracycline Tetracycline	no	[59]
<b>Metal-organic framework impedimetric aptasensor</b>	AMP18	0.01 pg/ml–2 ng/ml	6 fg/ml	Tetracycline Kanamycin Tobramycin , Na <sup>+</sup> , K <sup>+</sup> , Streptomycin Oxytetracycline	Diluted human serum	[60]
<b>Ladder-shaped DNA based electrochemical aptasensor</b>	AMP17	7 pM–100 nM	1 pM	Amoxicillin Levofloxacin Chloramphenicol Kanamycin Tetracycline	Milk	[61]
<b>Dual AuNPs colorimetric assay</b>	AMP17	1-600 nM 1-400 nM	0.1 nM 0.5 nM	Amoxicillin Penicillin Lincomycin Benzylpenicillin	Milk	[62]
<b>Exonuclease III-powered DNA walking machine electrochemical aptasensor</b>	AMP17	1 pM – 10 nM	0.7 pM	Kanamycin Chloramphenicol Oxytetracycline Terramycin Carbenicillin	Milk	[63]
<b>DNase I-assisted cyclic enzymatic signal amplification graphene oxide aptasensor</b>	AMP17	10 ng/ml – 500 ng/ml	2.4 ng/ml	Chloramphenicol Penicillin Carbenicillin Amoxicillin	Milk	[64]

More recently, two other research groups selected aptamers against PENG. Lee *et al.* [30] obtained an aptamer (BBA1) for PENG via reduced

graphene oxide (rGO) SELEX and the performance of the aptamer was evaluated with fluorescence quenching experiments. BBA1 showed a binding constant ( $K_d$ ) of 383 nM and good selectivity against other antibiotics, both  $\beta$ -lactams and from other families. However, the aptamer showed a significant cross-reactivity with ampicillin (almost 80%), which somehow limits its applicability in real samples. Another example of aptamer for PENG was reported in 2017 by Paniel *et al.* [65].

The authors used a Capture-SELEX approach and devised an electrochemical impedance spectroscopy biosensor for quantification of PENG in buffer and real food samples. The aptamer performances were evaluated with affinity chromatography on Sepharose gel cartridges and the best candidate (P8) was used for the construction of the impedimetric biosensor. The proposed biosensor has a wide linear range (0.4 to 1000 µg/L) and a LOD of 0.17 µg/L, below the MRL value for PENG in milk (4 µg/L). This sequence shows a relevant cross-reactivity with ampicillin and amoxicillin, like the BBA1.

An aptamer for the cephalosporin antibiotic cefquinome (CFQ) was reported by Wang *et al.* [66]: it was selected using traditional Flu-Mag SELEX and used in a magnetic nanoparticles based fluorescent assay. The best candidate sequence (W1) showed a  $K_d$  of 40 nM, obtained by fluorescent titration, and the developed biosensor had a good linear range (0.5 to 150 ng/ml) with a LOD (0.09 ng/ml) useful for real sample analysis. The detection strategy was tested in spiked milk samples with good recovery (more than 95%) and low cross reactivity against other cephalosporins, namely cefpirome and cefixime.

Apart from AMP aptamers, all the above mentioned sequences were used and characterized only by the original research group that selected them. Moreover, the lack of aptamer sequences for  $\beta$ -lactam antibiotics, compared to other antimicrobial drugs families, severely limits the possibilities of  $\beta$ -lactam aptasensing for commercial applications today.

### **Flu-Mag SELEX for nafcillin and cephalixin**

The selection of aptamers specific for NAF and CFX was first considered because of the problems in detecting these antibiotics with traditional screening tests [67,68]. The Flu-Mag SELEX protocol employed here was adapted from [69–71], developed in Sphere research group for other small organic molecules, such as ergot alkaloids [71] or polychlorobiphenyls (PCBs) [70].

## **Materials and methods**

### **Flu Mag SELEX**

#### **Reagents**

The 80bp random library (5'-AGC-AGC-ACA-GAG-GTC-AGA-TGN-NNN-NNN-NNN-NNN-NNN-NNN-NNN-NNN-NNN-NNN-CCT-ATG-CGT-GCT-ACC-GTG-

AA-3'), the forward (5'-AGC-AGC-ACA-GAG-GTC-AGA-TG-3') and biotinylated reverse primer (5'-TTC-ACG-GTA-GCA-CGC-ATA-GG-3'), used for PCR amplification, were all purchased from Eurogentec (Belgium). Dynabeads® M-270 Amine and Dynabeads™ M-280 Streptavidin, 10 bp DNA Ladder (10 to 300 bp) were obtained from Invitrogen (Thermo Fischer, Belgium). GelRed™ Nucleic Acid Gel Stain, 10000X in water, was from Biotium (USA). Binding buffer (BB) made with 100 mM NaCl, 20 mM Tris-HCl, 2 mM MgCl<sub>2</sub>, 5 mM KCl, 1 mM CaCl<sub>2</sub>, 0.02 Tween 20, pH 7.6; elution buffer (EB) made with 40 mM Tris-HCl, 10 mM EDTA, 3.5 M urea, 0.02% Tween 20, pH 8.0; 2x binding-cum-washing buffer made with 10 mM Tris-HCl (pH 7.5), 1 mM EDTA, 2 M NaCl; 1x Saline sodium citrate buffer pH 7 (SSC) made with 30 mM Na<sub>3</sub>C<sub>6</sub>H<sub>5</sub>O<sub>7</sub>, 300 mM NaCl were used for the SELEX protocol. Nuclease-Free Water was obtained from Invitrogen (Thermo Fischer, Belgium). All other reagents were analytical grade and used as received. All solution were prepared in MilliQ water.

### **Instrumentation**

The ssDNA PCR amplification was performed on a Biometra Thermocycler T-Gradient ThermoBlock from Biometra (Germany); agarose gel electrophoresis was carried out with Mupid-One Advance electrophoresis system (Eurogentec, Belgium) and the gel visualized with a FastGene UV Transilluminator (Nippon Genetics, Japan). A centrifuge 5427 R from Eppendorf (Belgium) was used. UV-Vis spectra were acquired with a NanoPhotometer N60 (Implen) operated by NanoPhotometer NPOS software. All the electrochemical measurements were performed on G-SPE (Italsens, Italy) with an Autolab potentiostat (302N) controlled by NOVA 1.11 software.

### **SELEX protocol**

#### ***Immobilization of antibiotics onto magnetic beads***

The amine coated magnetic Dynabeads were washed with 0.1 M MES with 0.5 M NaCl pH 6. The target antibiotic was dissolved in the same buffer to a concentration of 5 mg/ml and added to the beads. A solution of 10 mg EDC and 15 mg NHS per mL in cold deionized water was prepared, immediately before use. A 10 µL aliquot of EDC/NHS solution for each mg of target used was added. The solution was incubated for two hours at room temperature with slow tilt rotation. Hydroxylamine-HCl was then added to a final concentration of 10 mM to quench the reaction, and incubate for 15 min at room temperature with slow tilt rotation. Finally, the coated beads were washed with 0.1 M PBS with 0.5% BSA, 0.01% Tween®-20 and re-suspended in the same buffer.

### *Selection round*

A homogeneous suspension of the target-coated beads was obtained by vortexing for approximately one minute. Before each SELEX round, the beads were washed eight times with binding buffer (BB) and finally re-suspended in 100  $\mu\text{L}$  of BB. For the first round of SELEX, 36  $\mu\text{g}$  of DNA library were added to 400  $\mu\text{L}$  of BB. Before its application in the binding reaction, the ssDNA library was denatured (unfolded) in BB at 90  $^{\circ}\text{C}$  for 10 min, immediately cooled at 4  $^{\circ}\text{C}$  for 15 min, followed by a five minutes incubation at room temperature (RT). The resulting ssDNA solution was added to the target-coated beads solution and incubated at RT for 30 min with tilting and rotation. The unbound oligonucleotides were removed by five washing steps using 500  $\mu\text{L}$  BB each time. The bound oligonucleotides were eluted from the target-coated magnetic beads, by incubating the target-DNA complex in 100  $\mu\text{L}$  elution buffer (EB) at 80  $^{\circ}\text{C}$  for 10 min with gentle shaking, followed by magnetic separation of beads and ssDNA recovery. This step was repeated four times.

### *Ethanol precipitation of ssDNA*

A 1/10<sup>th</sup> volume of 3 M sodium acetate and three volumes of 100% ice-cold ethanol were added to the DNA solution. The solution was then incubated at  $-80^{\circ}\text{C}$  for one h to ensure complete precipitation of the ssDNA and then centrifuged at 16000 g for 15 min at 4  $^{\circ}\text{C}$  to pellet the ssDNA precipitate. The supernatant was discarded leaving approximately 50  $\mu\text{L}$  at the bottom of the vial. The ssDNA pellet was washed two times in 70% ice-cold ethanol. After a short centrifugation step the supernatant was discarded leaving approximately 50  $\mu\text{L}$  of solution. The remaining solution was dried under a gentle stream of nitrogen and the resulting DNA pellet was re-suspended in nuclease-free water. Finally, the DNA concentration was measured with the Nanodrop.

### *PCR*

In addition to  $\sim 50$  ng of DNA template, PCR mixtures contained 10 mM KCl, 10 mM  $(\text{NH}_4)_2\text{SO}_4$ , 20 mM Tris-HCl (pH 8.8), 2 mM  $\text{MgSO}_4$ , 0.1% Triton X-100, 1 mM of each deoxyribonucleotide triphosphate (dNTP), 1  $\mu\text{M}$  of each primer (forward and biotinylated reverse primer), and 0.025 unit/ $\mu\text{L}$  Taq DNA polymerase. The total volume of the PCR reaction mixture was 50  $\mu\text{L}$ . The PCR cycle is reported in Table 3.3.

**Table 3.3** PCR cycles parameter.

Temp ( $^{\circ}\text{C}$ )	Time
94	6 min

<b>94</b>	<b>30 s</b>	} 20 times
<b>55</b>	<b>20 s</b>	
<b>72</b>	<b>20 s</b>	
94	3 min	
55	20 s	
72	2 min	
4	hold	

The PCR products were checked with agarose gel electrophoresis: 10  $\mu$ L of PCR product was loaded onto a 2 % agarose gel plus 0.01 % of GelRed nucleic acid stain and electrophoresis was carried out at 10 V/cm for 45 min in 1 X Tris-acetate EDTA. The PCR products were then purified by the MinElute PCR purification Kit (QIAGEN, Belgium) and re-suspended in nuclease-free water.

#### *dsDNA strand separation*

The dsDNA were immobilized on streptavidin coated magnetic Dynabeads. The beads were first washed three times with 1x binding-cum-washing (B&W) buffer, then suspended in 2x B&W buffer to a final concentration of 5  $\mu$ g/ $\mu$ L. An equal volume of the biotinylated dsDNA in nuclease free water was added to dilute the 2x B&W Buffer, diluting NaCl from 2 M to 1 M for optimal binding. The beads were incubated for 25 min at room temperature using gentle rotation to allow the binding between streptavidin and biotinylated dsDNA strands. The coated beads were washed two times with 1x B&W buffer and re-suspended in the appropriate solution for denaturation (NaOH or SCC, see below).

#### *NaOH denaturation*

The beads were suspended in 0.15 M NaOH and held at 37 °C for 5 min to separate the strands. The solution was then recovered and neutralized with equal amount of 0.15 M acetic acid, while the beads were separated using a magnet. The ssDNA was again precipitated with the ethanol precipitation protocol.

#### *SSC denaturation*

The coated beads were washed with 50  $\mu$ L of 1x saline sodium citrate buffer (SSC), then re-suspended in 25  $\mu$ L of the same buffer. The beads were incubated at 95 °C for five minutes, then immediately cooled on ice. The beads were separated with a magnet and the supernatant recovered. The process was repeated three times. The pooled supernatants were put on a magnet to remove all the left-over beads and transferred in a new tube. The obtained ssDNA was precipitated with the ethanol precipitation protocol.





NAF. Thus, it was concluded that NAF is on the surface of the beads and in the first washing step part of the antibiotics is released in solution.

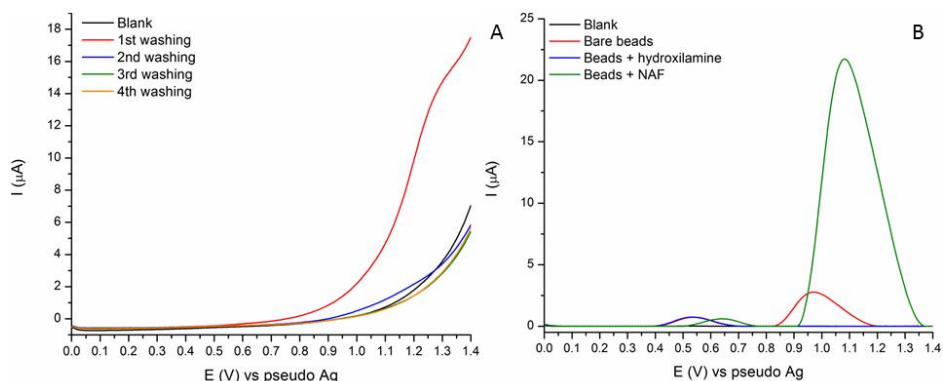


**Fig. 3.5** A) SWVs of four washing solutions for immobilization of 5 mg/ml of NAF on amine coated magnetic beads; B) SWVs (baseline corrected) of blank 0.1 MES pH 6 (black), bare amine coated magnetic beads (red), beads coated with hydroxylamine (blue) and beads coated with NAF (green).

By building a calibration plot for NAF (Fig. 3.6A and B) in the immobilization buffer (0.1 M MES pH 6) it was possible to re-calculate the concentration of NAF present in the first washing solution and indirectly the amount of NAF immobilized on the beads. In the starting solution of NAF,  $12.06 \pm 0.06 \mu\text{mol}$  of antibiotics are present. From the oxidation peak current present in the first washing solution (red curve in Fig. 3.5A), the amount of NAF in solution resulted to be about  $0.03 \pm 0.04 \mu\text{mol}$ . From this estimation it was possible to conclude that with the proposed immobilization protocol more than 99% of the target antibiotic is immobilized onto the beads.

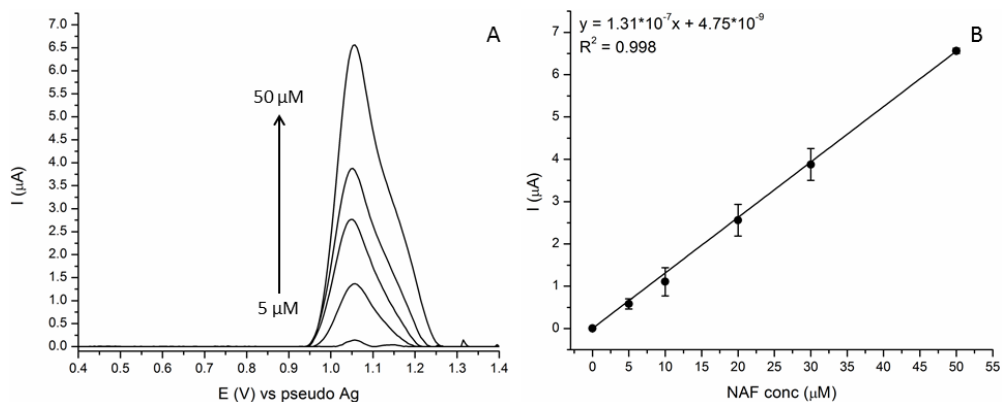


**Fig. 3.6** A) SWVs of NAF in 0.1 M MES pH 6 at different concentration (from 5 to 50  $\mu$ M); B) calibration plot for NAF in 0.1 M MES pH 6. SD calculated on n=3.

### ssDNA recovery optimization

Two different strategies for the separation of the dsDNA strands after PCR amplification were tested. The biotinylated dsDNA was attached to streptavidin coated magnetic beads and either NaOH or SCC denaturation protocols were employed (details in Materials and Methods). The ssDNA recovery was calculated from a starting dsDNA pool of 1  $\mu$ M. Each protocol was used on freshly prepared beads and the recovery was calculated on triplicate measurements. The NaOH denaturation gave an average recovery of  $37 \pm 14\%$ : the original protocol considered only one step, thus the yield is relatively low and most of the dsDNA is still hybridized. The SCC protocol instead showed a recovery rate of  $54 \pm 20\%$  for the first round only.

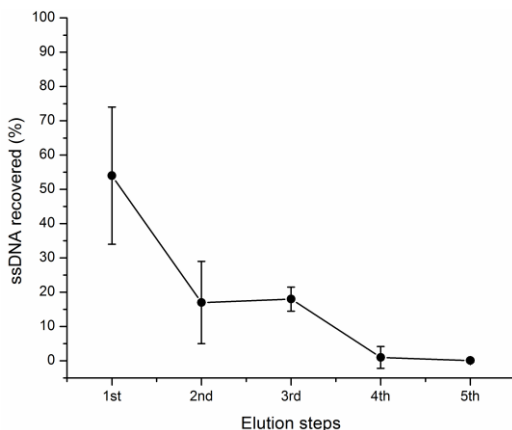


**Fig. 3.7** ssDNA recovery for each elution step for the SSC protocol. SD calculated on n=3.

Considering the small volume of buffer required (25  $\mu$ L) and the short denaturation time (5 min), it is possible to perform multiple denaturation steps and then pool the resulting ssDNA. Fig. 3.7 presents the relative recovery rate for an increasing number of elution steps in SSC. The highest amount of ssDNA is obtained in the first step (54 %). However, in the second and third step it is still possible to recover around 15 % of the original dsDNA on the beads. From the fourth step onwards the recovery is minimal (~1%). Thus SSC denaturation was used in the subsequent SELEX procedure, with three elution steps.

### PCR amplification

After each round of selection, the recovered ssDNA was amplified with PCR and analysed using agarose gel electrophoresis, to verify the length of the PCR products. The PCR parameters employed were previously optimized to obtain products of the correct length [70,71]. The dsDNA was checked with agarose gel electrophoresis after each amplification cycle (details in Materials and Methods). Fig. 3.8 shows the stained gel under UV illumination for the first round of selection for both NAF and CFX SELEX procedures.

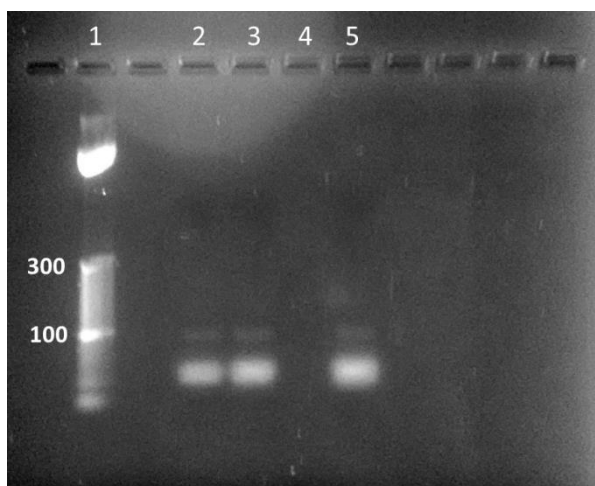


**Fig. 3.8** Agarose gel electrophoresis of PCR products; 1) 10 bp DNA ladder, 2) PCR products for 1<sup>st</sup> round of SELEX for NAF, 3) PCR products for 1<sup>st</sup> round of SELEX for CFX, 4) Negative control (without ssDNA template), 5) original 80 bp ssDNA library.

The obtained dsDNA have the correct length (80 bp) for both NAF (line 2) and CFX (line 3) recovered DNA. The negative control (line 4) shows no bands confirming the specificity of the results. Also the positive control, only with the 80 bp ssDNA random library, shows only a band at the corresponding height of 80 for the DNA ladder. Therefore, it can be concluded that the PCR amplification protocol is correct and the resulting dsDNA can be used for subsequent rounds of selection.

### SELEX recovery rates

SELEX for NAF aptamers was carried on for a total of 10 rounds; after the first round a negative selection with beads covered only with hydroxylamine was performed to remove non-specific binding sequences. After the fourth round, a counter selection was performed with beads covered with ampicillin (AMP) to remove the sequences that might bind to the core penicillin structure and improve the selectivity of the

aptamer. The selection protocol for CFX was carried out for seven rounds with the negative selection taking place after the second round.

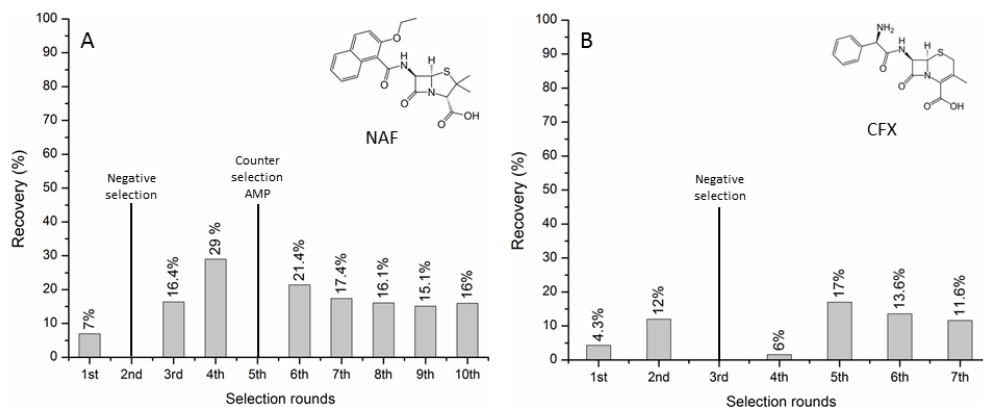


**Fig. 3.9** A) Recovery for the SELEX protocol for NAF aptamer; B) Recovery for SELEX protocol for CFX aptamer.

The amount of ssDNA recovered after each round, obtained from the UV-Vis spectra of the ssDNA solution, was used to calculate the yield of the selection round (*i.e.*  $(ssDNA_{after}/ssDNA_{before}) * 100$ ). The yield is used as an indicator for the enrichment of the library in strong binders for the target. The selection procedure is considered complete when the recovery for subsequent rounds achieves a high yield (80-90%) and remains constant, indicating a ssDNA pool rich in strong binders. Looking at the results of the Flu-Mag SELEX protocols for NAF and CFX (Fig. 3.9) it is possible to see that the recovery remains very low up to the 10<sup>th</sup> round for NAF and the 7<sup>th</sup> for CFX. The amount of ssDNA recovered (15-16% for NAF and 12-13% for CFX) is constant over the last rounds but remains very low, suggesting the non-specific nature of the recovered pool of fragments.

Several explanations can be proposed to justify the low yields obtained. First of all the immobilization of the target on the magnetic beads, while efficient, reduces the possible interaction points between the ssDNA and the target. The side chains of the two antibiotics should be exposed to the solution on the beads surface and thus allowing the interaction on this specific site. However, the difference in size between the long ssDNA fragments (80bp) and the small molecules target will make the specific folding of the prospective aptamers on the beads surface difficult. The interactions taking place between the strands and the side chains were probably not strong enough to sustain the subsequent washing steps and the recovered ssDNA showed a poor affinity. Another reason could be linked to the strands

separation after PCR amplification. The protocol employed (SSC denaturation) gave good results in terms of recovery rate, but some of the dsDNA was still hybridized after three elution step (see Fig. 3.7). Moreover, some complementary strands might have been released in solution, thus giving a wrong estimation of the actual concentration of ssDNA recovered. All this factors together probably concurred to the final result, suggesting that the proposed adapted FluMag SELEX is not suited for selection of  $\beta$ -lactam antibiotics aptamers.

### **Modified GO-SELEX**

After having concluded that immobilization of the target might be one of the main reasons of the poor performances of FluMag SELEX for NAF and CFX, we looked at alternative selection strategies in which neither the target antibiotic nor the library needs to be immobilized on a solid support. One of the more recently developed SELEX strategies, based on GO, was considered [27,31,33].

As already reported above, GO-SELEX is based on the interactions between the GO functional groups and the nucleotides of ssDNA. Said interaction was carefully studied in recent years [28] and used also as a sensing strategy for different targets [29,64,72]. GO binds more strongly to unfolded ssDNA than to dsDNA or well folded ssDNA [73,74] in a process that is reversible for complementary strands or molecules that induce a conformational change [75], making this specificity useful to separate folded sequences from non-specific ones. Moreover the binding is driven by a mix of  $\pi$ - $\pi$  stacking interactions and hydrogen bonds [75,76]. The ssDNA first binds the oxidized groups present on the GO and then change conformation to promote the stacking of the aromatic rings of the nucleobase with those of the graphene surface. All these interactions can be controlled by varying several parameters. For instance the length of the ssDNA directly influences the kinetics of binding, with longer sequences showing slower adsorption kinetics [72]; also the ionic strength and the pH have a deep influence on the efficiency of binding [28].

The already developed GO-SELEX protocols use the graphene-ssDNA interaction mainly to separate the bound and unbound sequences in solution, without the need to immobilize any reagents. However, they still use PCR amplification and dsDNA strand separation recovery to obtain the enriched pool for subsequent selection rounds. The possibility to use instead this interaction as both partitioning system and driving force of the selection has been investigated. The idea behind is to tune the stringency of the selection rounds by varying the buffer composition, in terms

of pH, salt types and concentrations. By increasing the selection pressure upon subsequent rounds, it may be possible to enrich the ssDNA pool, removing weak or non-specific binding sequences. At each round the amount of ssDNA recovered will be lower until reaching a plateau. All the ssDNA left will bind more strongly to the target than to the GO, even in the most stringent buffer conditions (see Figure 3.10).

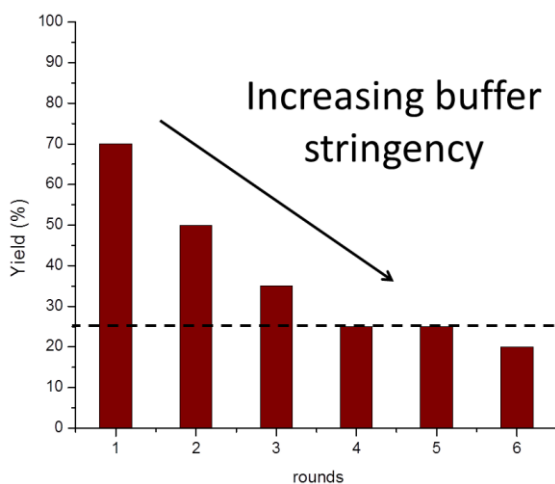


**Fig. 3.10** Expected yields trend for the modified GO-SELEX.

The ssDNA recovered from the last round will be cloned and sequenced and the obtained aptamers will be characterized with the usual methods. This selection strategy promise to be faster and simpler than other GO-SELEX variants, once the critical parameters have been identified. Thus, the preliminary study will be focused on the optimization of the ssDNA-GO interaction and the clear determination of the parameters influencing it. The effect of pH and the concentration of NaCl and MgCl<sub>2</sub> will be assessed, and compared also in presence of the target antibiotic, NAF, to verify whether its presence influences the efficiency of binding and the stringency of the procedure.

#### **ssDNA-GO ratio optimization**

To avoid the need of PCR amplification, it is possible to tune the stringency of the SELEX rounds by varying the affinity of the interaction GO-ssDNA. First, the critical ratio between GO and ssDNA concentration, which is the concentration of GO necessary to adsorb all the ssDNA in solution, has to be determined at a given buffer composition [27]. This loading experiment was performed with an initial

concentration of 5  $\mu\text{M}$  (c.a. 22  $\mu\text{g}$ ) of 80 bp ssDNA random library. The concentration of GO tested varied from 0 to 0.5 mg/ml, from the starting stock solution of 2 mg/ml; increasing amounts of GO were added to different aliquots of ssDNA library and incubated at RT under shaking for 1 h. The solution was then centrifuged for 30 min at 13000 rpm and the supernatant recovered.

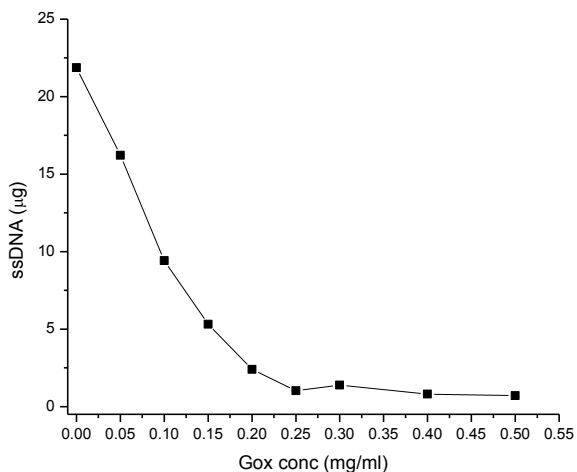


**Fig. 3.11** Ratio of adsorbed ssDNA for different GO concentration in 20 mM Tris buffer pH 7, 50 mM NaCl, 1 mM  $\text{MgCl}_2$ .

The results shown in Fig. 3.11 are reported in terms of  $\mu\text{g}$  of ssDNA left in solution and calculated by UV-Vis spectroscopy. The ssDNA concentration left in solution decreases steadily upon increasing the GO concentration reaching a minimum for 0.25 mg/ml. The ssDNA left in solution for higher GO concentration is negligible, thus 0.25 mg/ml was considered the critical concentration, which correspond to a 3:1 ratio in respect to the ssDNA. This GO:ssDNA ratio was used in all the subsequent experiments and the buffer composition was taken as an upper limit for tuning the stringency of the interaction.

#### **Influence of salts concentration on the ssDNA-GO interaction**

The concentration of salts, namely NaCl and  $\text{MgCl}_2$ , was reported to be one of the main parameters that could influence the GO-ssDNA interaction. For this reason increasing concentrations of both salts were tested in 20 mM Tris pH 7 to verify their influence on the adsorption trend of ssDNA.

With NaCl (Fig. 3.12) it is possible to see an increase in the amount of ssDNA adsorbed at increasing concentrations of salt. Starting from 30% of the initial ssDNA in pure Tris buffer, the addition of 10 mM NaCl results in a 7% increase in the



amount of adsorbed ssDNA. Going to higher concentration the strength of the interaction increase even further, reaching a maximum of 73% for 100 mM NaCl.

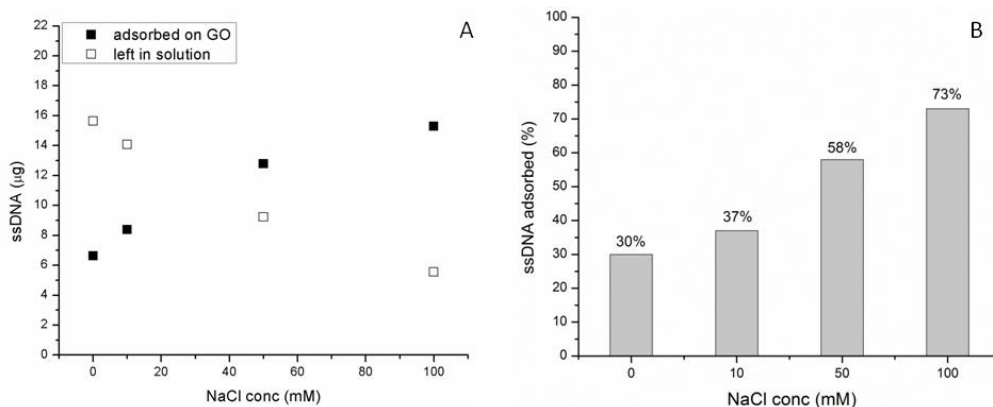


**Fig. 3.12** Ratio of adsorbed ssDNA on 0.25 mg/ml GO for increasing concentration of NaCl (0, 10, 50, 100 mM) in 20 mM Tris buffer pH 7.

The effect of increasing concentration of  $MgCl_2$  is even more intense (Fig. 3.13). Just with 0.5 mM of  $MgCl_2$  added the amount of adsorbed ssDNA is close to 95% and remain more or less constant for higher concentrations. This behaviour can be expected since divalent metal ions, such as  $Mg^{2+}$ , are much more effective in shielding the charges of negative molecules in comparison to monovalent ions [77]. Given the excess of  $MgCl_2$  in respect to the concentration the ssDNA (5 µM) the binding is almost quantitative in respect to the amount of phosphate linkages present [78].

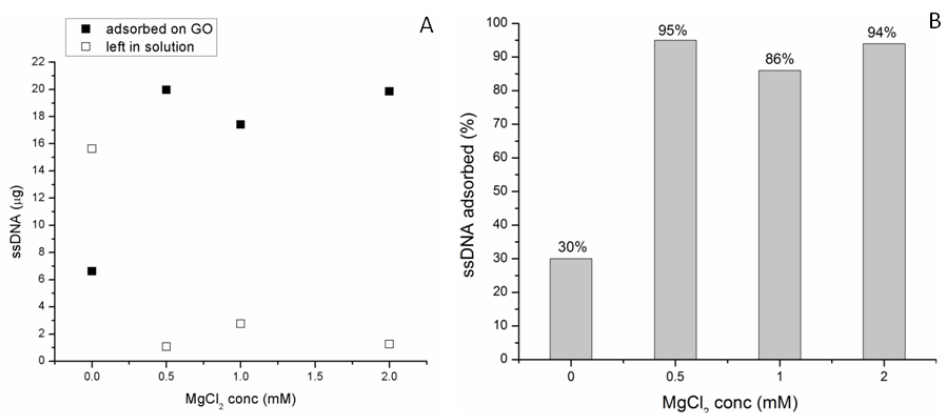


**Fig. 3.13** Ratio of adsorbed ssDNA on 0.25 mg/ml GO for increasing concentration of  $MgCl_2$  (0, 0.5, 1, 2 mM) in 20 mM Tris buffer pH 7.

While NaCl concentration changes give more granularity to the binding interaction, and it is thus possible to finely tune the affinity GO-ssDNA, MgCl<sub>2</sub> can be used in the final rounds of selection to achieve maximum stringency in the given condition.

### Influence of buffer pH on the ssDNA-GO interaction

Another critical parameter for the ssDNA-GO interaction is the pH of the selection buffer. While most of the SELEX protocols reported before employ buffers around physiological pH (6-7.5), this somewhat limits the application of aptamers for analytical purposes. The selection buffer is usually the one also used for the experimental protocol and the aptamer performances are heavily impaired when not operating in these conditions [79,80]. Thus, performing aptamer selection in different buffer conditions or pH, *e.g.* best suited for electrochemistry, is an appealing alternative, and has been explored within this preliminary optimization study.

Different buffer composition, in a range of pH between 2 and 7, have been tested, including acid pH values due to the fact that  $\beta$ -lactam antibiotics present better electrochemistry in lower pHs [81,82]. The same adsorption test protocol employed for the salts was applied to 20 mM solutions of different buffers. The results, reported in Fig. 3.14, show that the amount of ssDNA adsorbed for intermediate pH values (5, 6 and 7) is relatively small (around 10-20% on average), while pHs 2 and 4 show an opposite behaviour. The amount of ssDNA adsorbed at pH 2 is more than 90% while for pH 4 is close to zero, without added salts.

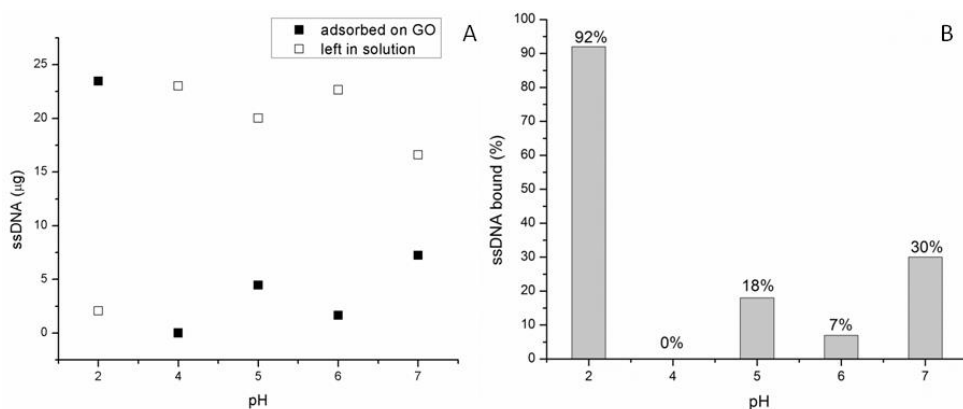


**Fig. 3.14** Ratio of adsorbed ssDNA on 0.25 mg/ml GO for different pHs: 2 (PB), 4 (BRB), 5 (AB), 6 (MES) and 7 (Tris).

This behaviour can be explained by the pH effect on the carboxylic acid groups present on the GO surface. Since the  $pK_a$  of these groups is close to 4 [83,84], at pH 4 GO has a mostly neutral net charge, while at pH 2 presents a positive charge. The positive charge of the GO surface will attract more strongly the negatively charged ssDNA backbone, while at pH 4 hydrogen bonding, which is one of the main driving force of the interaction, will be minimal and thus no ssDNA will be adsorbed on the GO. Another effect to take into account is that the hydrophilic interactions will also be less intense as the surface is less polar. While a buffer at pH 4 is ideal to develop a GO based selection strategy, in pH 2 no control of the GO-ssDNA interaction can be achieved. Since pH 4 is optimal for the electrochemical detection of NAF [82], it is particularly suited to test this approach for aptamer selection for  $\beta$ -lactam antibiotics. The interaction between GO and ssDNA in pH 4 will be only driven by the concentration of salts (NaCl or  $MgCl_2$ ) as in the pure buffer there is no interaction.

### **NAF GO-SELEX: optimization of the binding buffer**

To verify the feasibility of GO-SELEX for a NAF aptamer at pH 4 (20 mM Britton Robinson buffer), the study of the influence of the salts concentration was repeated, following the same protocol as before. Looking at the NaCl concentration effect (Fig. 3.15A and C) a large increase of ssDNA adsorbed is achieved already at 10 mM (c.a. 70 %) and going towards complete saturation for higher concentration. The same trend can be observed for  $MgCl_2$  (Fig. 3.15B and D) where, as seen before, at 0.5 mM concentration the ssDNA adsorbed is almost 90% of the starting solution.

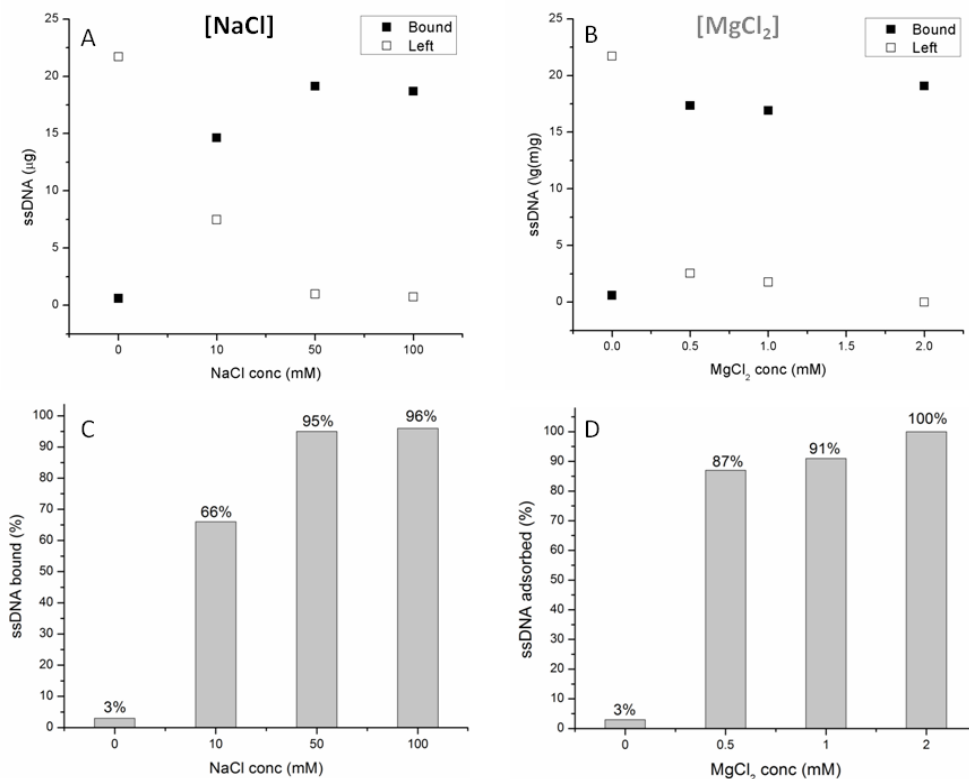


**Fig. 3.15** Ratio of adsorbed ssDNA on 0.25 mg/ml GO in 20 mM BRB pH 4 for different concentration of NaCl (A and C) and MgCl<sub>2</sub> (B and D).

As was discussed before, a higher control of the GO/ssDNA is achievable tuning the NaCl concentration, so the adsorption experiments at pH 4 were repeated in a broader range of NaCl concentrations. Fig. 3.16 shows the percentage recoveries of ssDNA for different NaCl concentrations. The amount of adsorbed ssDNA grows steadily from 19% for 1 mM to almost 100 % for 50 mM. Using these results as a guideline, it is possible to hypothesize the progression of the binding buffers necessary for a GO-SELEX protocol. Increasing stringency will be achieved by increasing the NaCl concentration up to 50 mM, and performing the last round with 1mM added MgCl<sub>2</sub> to confirm the affinity of the remaining ssDNA for the target molecules.

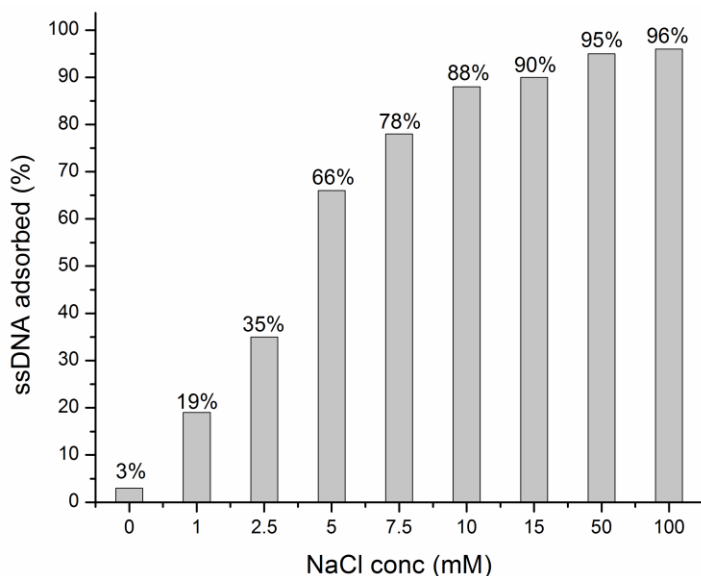


**Fig. 3.16** Ratio of adsorbed ssDNA on 0.25 mg/ml GO in 20 mM BRB pH 4 for different concentration of NaCl (from 0 to 100 mM).

To assess whether the presence of the target antibiotics influences somehow the GO-ssDNA interaction in different buffer compositions, another set of adsorption experiments was performed with an equimolar concentration of NAF (5  $\mu$ M) in respect to the ssDNA. Table 3.4 reports on the composition of the binding buffers tested and the percentage recovery of ssDNA after GO adsorption, with and without NAF in solution. Mean values and SD were calculated on three independent experiments.

**Table 3.4** Recovery of ssDNA in different buffer composition with and without NAF. SD calculated on n=3.

20 mM BRB pH4	Recovery without NAF (%)	Recovery with NAF (%)
+1 mM NaCl	20 $\pm$ 2	44 $\pm$ 3
+2.5 mM NaCl	35 $\pm$ 2	55 $\pm$ 2
+ 5 mM NaCl	66 $\pm$ 2	68 $\pm$ 3
+ 10 mM NaCl	84 $\pm$ 4	88 $\pm$ 4
+ 50 mM NaCl	95 $\pm$ 3	96 $\pm$ 2
+ 50 mM NaCl, + 1 mM MgCl <sub>2</sub>	95 $\pm$ 2	97 $\pm$ 3

Looking at the recovery rates for the experiments with NAF it is evident that the recovery increases in presence of the target antibiotics. A difference of c.a. 25 % is obtained, comparing the recovery of the first round with and without antibiotic. The

presence of NAF in solution affects the interaction between GO and ssDNA, and it can be assumed that part of the pool is left in solution because it is interacting with NAF. By increasing the stringency of the selection buffer, this difference became smaller but always significant. This can be seen as an indication of the feasibility of the proposed strategy. Indeed the fact that the ssDNA is still present in solution even for the most stringent buffer compositions could mean that the interaction between NAF and the library is strong enough to overcome the interaction with the GO.

### **Conclusions**

The feasibility of a PCR-free selection strategy for aptamers based on GO was verified in this study. The influence of salt concentration and pH was assessed in respect to the interaction strength between GO and ssDNA. NaCl concentration can finely tune the binding efficiency of this interaction, while MgCl<sub>2</sub> was proven to dramatically increase the ssDNA adsorption, even for low concentrations (low mM). The influence of pH was also addressed, revealing that the functional groups present on the graphene surface radically influence the interaction at different pHs, allowing to perform the selection in conditions best suited for downstream applications.

The feasibility of the new strategy for the selection of NAF aptamers in pH 4 was investigated. The proposed strategy is appealing because it does not need the immobilization of the small molecules target or the library. Moreover it is possible to perform the selection in the best buffer for downstream application, in this case 0.1 M BRB pH4 was chosen, the optimal buffer for the electrochemical detection of NAF. Notwithstanding the encouraging preliminary results, much work still needs to be done, on the one hand to independently verify the effect of other possible targets on the ssDNA-GO interaction and on the other hand to carry on the characterization of the obtained pool of fragments, to understand whether the selected aptamers show improved performance compared to traditionally selected ones.

## Chapter 3 – Aptamers: bioreceptors for antibiotics identification

### References

- [1] A. Chen, S. Yang, Replacing antibodies with aptamers in lateral flow immunoassay, *Biosens. Bioelectron.* 71 (2015) 230–242.
- [2] J. Yan, H. Xiong, S. Cai, N. Wen, Q. He, Y. Liu, D. Peng, Z. Liu, Advances in aptamer screening technologies, *Talanta.* 200 (2019) 124–144.
- [3] C. Ke, L. Bo, Y. Bo, Z. Wen, L. Yi, Z. Jiani, L. Jie, L. Jun, P. Ying, Q. Liping, Z. Liqin, L. Huixia, T. Weihong, Advances in the development of aptamer drug conjugates for targeted drug delivery, *Wiley Interdiscip. Rev. Nanomedicine Nanobiotechnology.* 9 (2016) e1438.
- [4] S. Catuogno, C.L. Esposito, V. de Franciscis, Aptamer-mediated targeted delivery of therapeutics: an update, *Pharmaceuticals.* 9 (2016) 69.
- [5] X. Ying, C. Guifang, H. Pingang, F. Yuzhi, A review: electrochemical aptasensors with various detection strategies, *Electroanalysis.* 21 (2009) 1251–1259.
- [6] H. Malekzad, A. Jouyban, M. Hasanzadeh, Ensuring food safety using aptamer based assays : Electroanalytical approach, *Trends Anal. Chem.* 94 (2017) 77–94.
- [7] M. Berezovski, M. Musheev, A. Drabovich, S.N. Krylov, Non-SELEX Selection of Aptamers, *J. Am. Chem. Soc.* 128 (2006) 1410–1411.
- [8] C.J. Colin, R. Peter, E.A. D., Automated RNA Selection, *Biotechnol. Prog.* 14 (2008) 845–850.
- [9] C.-J. Huang, H.-I. Lin, S.-C. Shiesh, G.-B. Lee, Integrated microfluidic system for rapid screening of CRP aptamers utilizing systematic evolution of ligands by exponential enrichment (SELEX), *Biosens. Bioelectron.* 25 (2010) 1761–1766.
- [10] S. Li, H. Li, X. Yang, W. Wang, A. Huang, J. Li, X. Qin, F. Li, G. Lu, H. Ding, X. Su, L. Hou, W. Xia, M. Shi, H. Zhang, Q. Zhao, J. Dong, X. Ge, L. Sun, C. Bai, C. Wang, X. Shen, T. Fang, F. Wang, H. Zhang, N. Shao, Vasorin is a potential serum biomarker and drug target of hepatocarcinoma screened by subtractive-EMSA-SELEX to clinic patient serum, *Oncotarget.* 6 (2015) 10045–10059.
- [11] S.D. Mendonsa, M.T. Bowser, In Vitro Selection of High-Affinity DNA Ligands for Human IgE Using Capillary Electrophoresis, *Anal. Chem.* 76 (2004) 5387–5392.
- [12] K. Sefah, D. Shangguan, X. Xiong, M.B. O’Donoghue, W. Tan, Development of DNA aptamers using Cell-SELEX, *Nat. Protoc.* 5 (2010) 1169.
- [13] R. Stoltenburg, C. Reinemann, B. Strehlitz, FluMag-SELEX as an advantageous method for DNA aptamer selection, *Anal. Bioanal. Chem.* 383 (2005) 83–91.
- [14] A.D. Ellington, J.W. Szostak, In vitro selection of RNA molecules that bind specific

### Chapter 3 – Aptamers: bioreceptors for antibiotics identification

- ligands, *Nature*. 346 (1990) 818.
- [15] C. Tuerk, L. Gold, Systematic evolution of ligands by exponential enrichment: RNA ligands to bacteriophage T4 DNA polymerase, *Science* (80- ). 249 (1990) 505 LP – 510.
- [16] C. Tuerk, S. MacDougal, L. Gold, RNA pseudoknots that inhibit human immunodeficiency virus type 1 reverse transcriptase, *Proc. Natl. Acad. Sci.* 89 (1992) 6988 LP – 6992.
- [17] R.D. Jenison, S.C. Gill, A. Pardi, B. Polisky, High-resolution molecular discrimination by RNA, *Science* (80- ). 263 (1994) 1425 LP – 1429.
- [18] H.P. Hofmann, S. Limmer, V. Hornung, M. Sprinzl, Ni<sup>2+</sup>-binding RNA motifs with an asymmetric purine-rich internal loop and a G-A base pair, *RNA*. 3 (1997) 1289–1300.
- [19] G. Mayer, M.-S.L. Ahmed, A. Dolf, E. Endl, P.A. Knolle, M. Famulok, Fluorescence-activated cell sorting for aptamer SELEX with cell mixtures, *Nat. Protoc.* 5 (2010) 1993.
- [20] G.M. London, B.M. Mayosi, M. Khati, Isolation and characterization of 2'-F-RNA aptamers against whole HIV-1 subtype C envelope pseudovirus, *Biochem. Biophys. Res. Commun.* 456 (2015) 428–433.
- [21] R. Stoltenburg, C. Reinemann, B. Strehlitz, FluMag-SELEX as an advantageous method for DNA aptamer selection, *Anal. Bioanal. Chem.* 383 (2005) 83–91.
- [22] M. McKeague, E.M. McConnell, J. Cruz-Toledo, E.D. Bernard, A. Pach, E. Mastronardi, X. Zhang, M. Beking, T. Francis, A. Giamberardino, A. Cabecinha, A. Ruscito, R. Aranda-Rodriguez, M. Dumontier, M.C. DeRosa, Analysis of in vitro aptamer selection parameters, *J. Mol. Evol.* 81 (2015) 150–161.
- [23] C. Wilson, J.W. Szostak, Isolation of a fluorophore-specific DNA aptamer with weak redox activity, *Chem. Biol.* 5 (1998) 609–617.
- [24] C. Mannironi, A. Di Nardo, P. Fruscoloni, G.P. Tocchini-Valentini, In Vitro Selection of Dopamine RNA Ligands, *Biochemistry*. 36 (1997) 9726–9734.
- [25] R. Stoltenburg, N. Nikolaus, B. Strehlitz, Capture-SELEX : Selection of DNA Aptamers for Aminoglycoside Antibiotics, *Journa Anal. Methods Cehmistry*. 2012 (2012).
- [26] R. Stoltenburg, N. Nikolaus, B. Strehlitz, Capture-SELEX: Selection of DNA aptamers for aminoglycoside antibiotics, *J. Anal. Methods Chem.* 1 (2012).
- [27] J.W. Park, R. Tatavarty, D.W. Kim, H.T. Jung, M.B. Gu, Immobilization-free screening of aptamers assisted by graphene oxide, *Chem. Commun.* 48 (2012) 2071–2073.
- [28] M. Wu, R. Kempaiah, P.J.J. Huang, V. Maheshwari, J. Liu, Adsorption and desorption



### Chapter 3 – Aptamers: bioreceptors for antibiotics identification

of DNA on graphene oxide studied by fluorescently labeled oligonucleotides, *Langmuir*. 27 (2011) 2731–2738.

- [29] J. Zhang, Z. Li, S. Zhao, Y. Lu, Size-dependent modulation of graphene oxide–aptamer interactions for an amplified fluorescence-based detection of aflatoxin B1 with a tunable dynamic range, *Analyst*. 141 (2016) 4029–4034.
- [30] A.Y. Lee, N.R. Ha, I.P. Jung, S.H. Kim, A.R. Kim, M.Y. Yoon, Development of a ssDNA aptamer for detection of residual benzylpenicillin, *Anal. Biochem*. 531 (2017) 1–7.
- [31] Y. Zhang, Y. You, Z. Xia, X. Han, Y. Tian, N. Zhou, Graphene oxide-based selection and identification of ofloxacin-specific single-stranded DNA aptamers, *RSC Adv*. 6 (2016) 99540–99545.
- [32] H. Gu, N. Duan, S. Wu, L. Hao, Y. Xia, X. Ma, Z. Wang, Graphene oxide-assisted non-immobilized SELEX of okadaic acid aptamer and the analytical application of aptasensor, *Sci. Rep*. 6 (2016) 1–9.
- [33] V.T. Nguyen, Y.S. Kwon, J.H. Kim, M.B. Gu, Multiple GO-SELEX for efficient screening of flexible aptamers, *Chem. Commun*. 50 (2014) 10513–10516.
- [34] S.D. Mendonsa, M.T. Bowser, In vitro selection of high-affinity DNA ligands for human IgE using capillary electrophoresis, *Anal. Chem*. 76 (2004) 5387–5392.
- [35] S.D. Mendonsa, M.T. Bowser, In Vitro Evolution of Functional DNA Using Capillary Electrophoresis, *J. Am. Chem. Soc*. 126 (2004) 20–21.
- [36] G. Hybarger, J. Bynum, R.F. Williams, J.J. Valdes, J.P. Chambers, A microfluidic SELEX prototype, *Anal. Bioanal. Chem*. 384 (2006) 191–198.
- [37] R.K. Mosing, M.T. Bowser, Microfluidic selection and applications of aptamers, *J. Sep. Sci*. 30 (2007) 1420–1426.
- [38] X. Lou, J. Qian, Y. Xiao, L. Viel, A.E. Gerdon, E.T. Lagally, P. Atzberger, T.M. Tarasow, A.J. Heeger, H.T. Soh, Micromagnetic selection of aptamers in microfluidic channels, *Proc. Natl. Acad. Sci*. 106 (2009) 2989–2994.
- [39] L.A. Fraser, Y.W. Cheung, A.B. Kinghorn, W. Guo, S.C.C. Shiu, C. Jinata, M. Liu, S. Bhuyan, L. Nan, H.C. Shum, J.A. Tanner, Microfluidic Technology for Nucleic Acid Aptamer Evolution and Application, *Adv. Biosyst*. 3 (2019) 1–16.
- [40] D. Shangguan, Y. Li, Z. Tang, Z.C. Cao, H.W. Chen, P. Mallikaratchy, K. Sefah, C.J. Yang, W. Tan, Aptamers evolved from live cells as effective molecular probes for cancer study, *Proc. Natl. Acad. Sci*. 103 (2006) 11838 LP – 11843.
- [41] Z. Tang, D. Shangguan, K. Wang, H. Shi, K. Sefah, P. Mallikaratchy, H.W. Chen, Y. Li, W. Tan, Selection of Aptamers for Molecular Recognition and Characterization of Cancer Cells, *Anal. Chem*. 79 (2007) 4900–4907.

### Chapter 3 – Aptamers: bioreceptors for antibiotics identification

- [42] X. Pang, C. Cui, S. Wan, Y. Jiang, L. Zhang, L. Xia, L. Li, X. Li, W. Tan, Bioapplications of cell-SELEX-generated aptamers in cancer diagnostics, therapeutics, theranostics and biomarker discovery: A comprehensive review, *Cancers (Basel)*. 10 (2018).
- [43] H. Kaur, Recent developments in cell-SELEX technology for aptamer selection, *Biochim. Biophys. Acta - Gen. Subj.* 1862 (2018) 2323–2329.
- [44] M. V Berezovski, M.U. Musheev, A.P. Drabovich, J. V Jitkova, S.N. Krylov, Non-SELEX: Selection of aptamers without intermediate amplification of candidate oligonucleotides, *Nat. Protoc.* 1 (2006) 1359–1369.
- [45] L.H. Lauridsen, H.A. Shamaileh, S.L. Edwards, E. Taran, R.N. Veedu, Rapid one-step selection method for generating nucleic acid aptamers: Development of a DNA Aptamer against  $\alpha$ -bungarotoxin, *PLoS One.* 7 (2012) 1–6.
- [46] S. Arnold, G. Pampalakis, K. Kantiotou, D. Silva, C. Cortez, S. Missailidis, G. Sotiropoulou, One round of SELEX for the generation of DNA aptamers directed against KLK6, in: *Biol. Chem.*, 2012: pp. 343–353.
- [47] K. Song, E. Jeong, W. Jeon, M. Cho, C. Ban, Aptasensor for ampicillin using gold nanoparticle based dual fluorescence – colorimetric methods, *Anal. Bioanal. Chem.* 402 (2012) 2153–2161.
- [48] J. Dapra, L.H. Lauridsen, A.T. Nielsen, N. Rozlosnik, Comparative study on aptamers as recognition elements for antibiotics in a label-free all-polymer biosensor, *Biosens. Bioelectron.* 43 (2013) 315–320.
- [49] G. Rosati, J. Daprà, S. Cherré, N. Rozlosnik, Performance Improvement by Layout Designs of Conductive Polymer Microelectrode Based Impedimetric Biosensors, *Electroanalysis.* 26 (2014) 1400–1408.
- [50] H. Wang, Y. Wang, S. Liu, J. Yu, W. Xu, Y. Guo, J. Huang, Target–aptamer binding triggered quadratic recycling amplification for highly specific and ultrasensitive detection of antibiotics at the attomole level, *Chem. Commun.* 51 (2015) 8377–8380.
- [51] X. Wang, S. Dong, P. Gai, R. Duan, F. Li, Highly sensitive homogeneous electrochemical aptasensor for antibiotic residues detection based on dual recycling amplification strategy, *Biosens. Bioelectron.* 82 (2016) 49–54.
- [52] Z. Yang, X. Ding, Q. Guo, Y. Wang, Z. Lu, H. Ou, Z. Luo, X. Lou, Second generation of signaling-probe displacement electrochemical aptasensor for detection of picomolar ampicillin and sulfadimethoxine, *Sensors Actuators B. Chem.* 253 (2017) 1129–1136.
- [53] Z. Luo, Y. Wang, X. Lu, J. Chen, F. Wei, Z. Huang, C. Zhou, Y. Duan, Fluorescent aptasensor for antibiotic detection using magnetic bead composites coated with gold nanoparticles and a nicking enzyme, *Anal. Chim. Acta.* 984 (2017) 177–184.

### Chapter 3 – Aptamers: bioreceptors for antibiotics identification

- [54] Z. Yu, A.L. Sutlief, R.Y. Lai, Towards the development of a sensitive and selective electrochemical aptamer-based ampicillin sensor, *Sensors Actuators B. Chem.* 258 (2018) 722–729.
- [55] Z. Yu, R.Y. Lai, A reagentless and reusable electrochemical aptamer-based sensor for rapid detection of ampicillin in complex samples, *Talanta*. 176 (2018) 619–624.
- [56] A. Blidar, B. Feier, M. Tertis, R. Galatus, C. Cristea, Electrochemical surface plasmon resonance (EC-SPR) aptasensor for ampicillin detection, *Anal. Bioanal. Chem.* 411 (2019) 1053–1065.
- [57] X. Liu, M. Hu, M. Wang, Y. Song, N. Zhou, L. He, Z. Zhang, Novel nanoarchitecture of Co-MOF-on-TPN-COF hybrid: Ultralowly sensitive bioplatform of electrochemical aptasensor toward ampicillin, *Biosens. Bioelectron.* 123 (2019) 59–68.
- [58] T. Wang, H. Yin, Y. Zhang, L. Wang, Y. Du, Y. Zhuge, S. Ai, Electrochemical aptasensor for ampicillin detection based on the protective effect of aptamer-antibiotic conjugate towards DpnII and Exo III digestion, *Talanta*. 197 (2019) 42–48.
- [59] J. Li, C. Yu, Y. Wu, Y. Zhu, J. Xu, Y. Wang, H. Wang, M. Guo, F. Li, Novel sensing platform based on gold nanoparticle-aptamer and Fe-metal-organic framework for multiple antibiotic detection and signal amplification, *Environ. Int.* 125 (2019) 135–141.
- [60] M. Wang, M. Hu, J. Liu, C. Guo, D. Peng, Q. Jia, L. He, Z. Zhang, M. Du, Covalent organic framework-based electrochemical aptasensors for the ultrasensitive detection of antibiotics, *Biosens. Bioelectron.* 132 (2019) 8–16.
- [61] S.M. Taghdisi, N.M. Danesh, M.A. Nameghi, M. Ramezani, M. Alibolandi, K. Abnous, An electrochemical sensing platform based on ladder-shaped DNA structure and label-free aptamer for ultrasensitive detection of ampicillin, *Biosens. Bioelectron.* 133 (2019) 230–235.
- [62] O.H. Shayesteh, R. Ghavami, Two colorimetric ampicillin sensing schemes based on the interaction of aptamers with gold nanoparticles, *Microchim. Acta.* 186 (2019) 485.
- [63] R. Zhang, Y. Wang, X. Qu, S. Li, Y. Zhao, S. Liu, J. Huang, Exonuclease III-powered DNA Walking Machine for Label-free and Ultrasensitive Electrochemical Sensing of Antibiotic, *Sensors Actuators B Chem.* 297 (2019) 126771.
- [64] H. Youn, K. Lee, J. Her, J. Jeon, J. Mok, J. So, S. Shin, C. Ban, Aptasensor for multiplex detection of antibiotics based on FRET strategy combined with aptamer/graphene oxide complex, *Sci. Rep.* 9 (2019) 7659.
- [65] N. Paniel, G. Istamboulié, A. Triki, C. Lozano, L. Barthelmebs, T. Nougier, Selection of DNA aptamers against penicillin G using Capture-SELEX for the development of an impedimetric sensor, *Talanta*. 162 (2017) 232–240.

### Chapter 3 – Aptamers: bioreceptors for antibiotics identification

- [66] L. Wang, C. Wang, H. Li, Selection of DNA aptamers and establishment of an effective aptasensor for highly sensitive detection of cefquinome residues in milk, *Analyst*. 143 (2018) 3202–3208.
- [67] W. Reybroeck, S. Ooghe, H.F. De Brabander, E. Daeseleire, Validation of the Charm MRL-3 for fast screening of beta-lactam antibiotics in raw milk, *J. AOAC Int.* 94 (2011) 373–382.
- [68] C. Bion, A. Beck-Henzelin, Y. Qu, G. Pizzocri, E. Buffoli, Analysis of 27 antibiotic residues in raw cow's milk and milk-based products - validation of Delvotest® T, *Food Addit. Contam. Part A.* (2015).
- [69] J. Mehta, B. Van Dorst, E. Rouah-Martin, W. Herrebout, M.L. Scippo, R. Blust, J. Robbens, In vitro selection and characterization of DNA aptamers recognizing chloramphenicol, *J. Biotechnol.* 155 (2011) 361–369.
- [70] E. Rouah-Martin, W. Herrebout, B. Van Dorst, J. Robbens, B. Maes, J. Mehta, R. Blust, F. Dardenne, M.-L. Scippo, Selection and Characterization of PCB-Binding DNA Aptamers, *Anal. Chem.* 84 (2011) 1669–1676.
- [71] E. Rouah-Martin, J. Mehta, B. Van Dorst, S. De Saeger, P. Dubruel, U.W.B. Maes, F. Lemiere, E. Goormaghtigh, D. Daems, W. Herrebout, F. Van Hove, R. Blust, J. Robbens, Aptamer-Based Molecular Recognition of Lysergamine, Metergoline and Small Ergot Alkaloids, *Int. J. Mol. Sci.* . 13 (2012).
- [72] S. He, B. Song, D. Li, C. Zhu, W. Qi, Y. Wen, L. Wang, S. Song, H. Fang, C. Fan, A graphene nanoprobe for rapid, sensitive, and multicolor fluorescent DNA analysis, *Adv. Funct. Mater.* 20 (2010) 453–459.
- [73] Z. Liu, J.T. Robinson, X. Sun, H. Dai, PEGylated Nanographene Oxide for Delivery of Water-Insoluble Cancer Drugs, *J. Am. Chem. Soc.* 130 (2008) 10876–10877.
- [74] L. Lin, Y. Liu, X. Zhao, J. Li, Sensitive and Rapid Screening of T4 Polynucleotide Kinase Activity and Inhibition Based on Coupled Exonuclease Reaction and Graphene Oxide Platform, *Anal. Chem.* 83 (2011) 8396–8402.
- [75] Z. Xu, X. Lei, Y. Tu, Z.J. Tan, B. Song, H. Fang, Dynamic Cooperation of Hydrogen Binding and  $\pi$  Stacking in ssDNA Adsorption on Graphene Oxide, *Chem. - A Eur. J.* 23 (2017) 13100–13104.
- [76] S. Gowtham, R.H. Scheicher, R. Ahuja, R. Pandey, S.P. Karna, Physisorption of nucleobases on graphene: Density-functional calculations, *Phys. Rev. B - Condens. Matter Mater. Phys.* 76 (2007) 2–5.
- [77] S. Liu, K. Ghosh, M. Muthukumar, Polyelectrolyte solutions with added salt: A simulation study, *J. Chem. Phys.* 119 (2003) 1813–1823.
- [78] E. Rowatt, R.J.P. Williams, The binding of polyamines and magnesium to DNA, *J.*

### Chapter 3 – Aptamers: bioreceptors for antibiotics identification

Inorg. Biochem. 46 (1992) 87–97.

- [79] P. Baaske, C.J. Wienken, P. Reineck, S. Duhr, D. Braun, Optical thermophoresis for quantifying the buffer dependence of aptamer binding, *Angew. Chemie - Int. Ed.* 49 (2010) 2238–2241.
- [80] E.J. Cho, J.R. Collett, A.E. Szafranska, A.D. Ellington, Optimization of aptamer microarray technology for multiple protein targets, *Anal. Chim. Acta.* 564 (2006) 82–90.
- [81] N. Slegers, A.L.N. Van Nuijs, M. Van Den Berg, K. De Wael, Cephalosporin Antibiotics: Electrochemical Fingerprints and Core Structure Reactions Investigated by LC-MS/MS, *Anal. Chem.* 91 (2019) 2035–2041.
- [82] F. Bottari, G. Moro, N. Slegers, A. Florea, T. Cowen, S. Piletsky, A.L.N. van Nuijs, K. De Wael, Electropolymerized o-phenylenediamine on Graphite Promoting the Electrochemical Detection of Nafcillin, *Electroanalysis*, (2019).
- [83] L.A. Langley, D.E. Villanueva, D.H. Fairbrother, Quantification of surface oxides on carbonaceous materials, *Chem. Mater.* 18 (2006) 169–178.
- [84] J. Ederer, P. Janoš, P. Ecorchard, V. Štengl, Z. Bělčická, M. Šťastný, O. Pop-Georgievski, V. Dohnal, Quantitative determination of acidic groups in functionalized graphene by direct titration, *React. Funct. Polym.* 103 (2016) 44–53.



# Characterization of aptamers for small organic molecules<sup>2</sup>

---

In this chapter, we compared different analytical methodologies to validate or disprove the binding capabilities of aptamer sequences. This was prompted by the lack of a universally accepted and robust quality control protocol for the characterization of aptamer performances coupled with the observation of independent yet inconsistent data sets in the literature. As an example, we chose three aptamers for ampicillin, a  $\beta$ -lactam antibiotic, used as biorecognition elements in several detection strategies described in the literature, and one well characterized aptamer for cocaine/quinine binding (MN4). Application of a well-known colorimetric assay based on aggregation of AuNPs yielded conflicting results with respect to the original report. Therefore, ampicillin binding was evaluated in solution using Isothermal Titration Calorimetry (ITC), native nano-Electrospray Ionization Mass spectrometry (native nESI-MS) and <sup>1</sup>H-Nuclear Magnetic Resonance spectroscopy (<sup>1</sup>H-NMR). By coupling the thermodynamic data obtained with ITC with the structural information on the binding event given by native nESI-MS and <sup>1</sup>H-NMR we could verify that none of the ampicillin aptamers show any specific binding with their intended target. The effect of AuNPs on the binding event was studied by both ITC and <sup>1</sup>H-NMR, again without providing positive evidence of ampicillin binding. The results clearly indicate the need for a multi-faceted analytical approach, to unequivocally establish the actual detection potential and performance of aptamers aimed at small organic molecules.

New aptamers are typically characterized using affinity binding assays such as equilibrium dialysis, ultrafiltration, affinity chromatography with magnetic beads or fluorescence based tests [1,2]. These assays are relatively cheap, easy to perform and do not require particular equipment. However, these practical advantages are offset by the fact that affinity constants measured using two or more of these assays on the same system of interest can vary considerably, up to several orders of

---

<sup>2</sup> Based on F. Bottari, E. Daems, A.M. de Vries, P. Van Wielendaele, S. Trashin, R. Blust, F. Sobott, J. C. Martins, A. Madder, K. De Wael, *Do aptamers always bind? The need for a multi-faceted analytical approach when demonstrating binding affinity between aptamer and low molecular weight compounds*, in preparation.

magnitude. This casts considerable doubt on the reliability of aptamer performances reported from these assays, and two or more assays should at least be combined and assessed for their similarity [1].

Instrumental analytical techniques, such as Surface Plasmon Resonance (SPR) [3] or Capillary Electrophoresis (CE) [4], can be also used for affinity characterization. For example, SPR measurements are highly accurate, providing both quantitative and reproducible results, however, the need to immobilize the aptamer (or the target) on the sensor chips can influence the affinity or even the binding mechanism [5,6]. Indeed, the addition of linkers, spacers or labels to the aptamer sequences for immobilization and sensing purposes, may perturb the recognition event to an extent that is currently unknown since a systematic comparison has not yet been presented. Lastly, CE is well suited to characterize aptamer interaction with large molecules (such as proteins and enzymes) but is not easily applicable to small molecule [2]. Small molecules, however, represent the largest class of environmental contaminants, and their determination/quantification is of the utmost importance in many different analytical fields.

### **A multi-faceted approach to study aptamer affinity**

Robust and reliable characterization protocols are of the utmost importance for analytical application of aptamers, and especially for those developed against small molecules (<1000 atomic mass unit) such as pesticides, drugs or antibiotics (<1000 atomic mass unit).

Selecting aptamers against small molecules is challenging and often leads to a very poor yield of the SELEX protocol [7]. Unfortunately, most of these aptamers present a lower affinity towards their targets than to control target groups such as proteins or cells [1,7]. Additionally, very few aptamers for small molecules were extensively characterized and their affinity validated. The few exceptions, such as cocaine-binding aptamers [8], have become the gold standard to test new analytical approaches and to undertake mechanistic and theoretical studies. On average, novel aptamers for small organic molecules are only characterized by the research group that select them in the first place and are used uncritically afterwards in other applications by different researchers.

Caution towards (the affinity of) the aptamers in each new application (with different experimental settings) has considerably diminished over time and is



almost always taken for granted. Given the observation of inconsistent data sets in literature, it is clear that a better validation of the selected aptamer sequences is needed.

To address this need, a multi-analytical characterization protocol was designed focusing on the ampicillin aptamer, already reviewed in Chapter 2. In 2012, Song *et al.* [9] selected three different aptamer sequences for ampicillin (AMP4, AMP17 and AMP18) and used them in a colorimetric assay. Their detection strategy was based on aggregation of AuNPs and enable to monitor the antibiotic in the low nanomolar range, both in buffer solution and in milk samples. The colorimetric approach was also used to calculate the  $K_d$  values. This was the very first example of aptamers against a  $\beta$ -lactam antibiotic described in literature. More specifically, the authors reported that their selected aptamers were capable of recognizing the side chain of ampicillin (1-phenylethylamine), assuring a high selectivity against structurally related compounds.

In the last eight years, these aptamers have been applied by other research groups around the world, in different analytical approaches and sensor configurations (see Table 3.1 for a complete overview). The latter include mostly electrochemical transduction, with very good results both in terms of figures of merit and real sample analysis [10]. The affinity constant, the selectivity and the specificity reported in the original paper were always taken for granted, and not further investigated.

Therefore, we undertook a systematic study of the ampicillin aptamer binding interactions, using different state-of-the-art analytical techniques which do not require immobilization: ITC, native nESI-MS and  $^1\text{H-NMR}$ . These techniques were previously used for aptamer characterization [11–14], but rarely combined although they provide complementary results. ITC gives information about the dissociation constant ( $K_d$ ), thermodynamics, and stoichiometry of the interaction [13,15,16]. Native nESI-MS provides information about the stoichiometry (provided that the affinity is in the low  $\mu\text{M}$  to nM range), and allows identification and characterization of individual species. Moreover, multiple species, which are *e.g.* co-existing in equilibrium, can be detected separately rather than as an average or a selected, prominent state [14,17,18]. Solution state  $^1\text{H-NMR}$  reveals the behaviour of compounds on a molecular level and allows delineating the location of the intermolecular interaction surface involved in the aptamer-target interactions [19–22]. By combining ITC, native nESI-MS and  $^1\text{H-NMR}$  it is possible to obtain a

complete overview of the binding affinity, selectivity and mechanism between aptamers and small molecule targets without immobilizing them to a substrate [14,21–23].

The combination of these three analytical techniques can validate or disprove, beyond reasonable doubt, the binding affinity and mechanism of interaction between aptamer sequences and small organic molecules.

## Materials and Methods

### Aptamers and reagents

Ampicillin aptamers (AMP4, AMP17 and AMP18), MN4 (quinine/cocaine binding) aptamer and a random ssDNA sequence (N36) were all purchased from Eurogentec (Belgium). Table 4.1 presents the specifications of the different sequences. AMP, NAF, quinine hydrochloride dihydrate and ammonium acetate solution (7.5 M) were obtained from Sigma Aldrich. CFX and chloramphenicol (CAP) were obtained from TCI (Europe). All other chemicals were reagent grade and used without further purification. MilliQ water was obtained with a Millipore Milli-Q Academic system.

**Table 4.1.** Acronym, sequence, length and  $K_d$  of the ampicillin aptamers (AMP4, AMP17 and AMP18), MN4 (quinine/cocaine binding) aptamer and random ssDNA sequence (N36) used in the study.

Acronym	Sequence	Length (bp)	$K_d$ (nM)
AMP4	5'-CAC-GGC-ATG-GTG- GGC-GTC-GTG-3'	21	9.4
AMP17	5' GCG-GGC-GGT-TGT-ATA- GCG-G-3'	19	13.4
AMP18	5'-TTA-GTT-GGG-GTT-CAG- TTG-G-3'	19	9.8
MN4	5'-GGC-GAC-AAG-GAA- AAT-CCT-TCA-ACG-AAG- TGG-GTC-GCC-3'	36	100*
N36	5'-NNN-NNN-NNN-NNN- NNN-NNN-NNN-NNN-NNN- NNN-NNN-NNN-3'	36	-

\* $K_d$  value of binding with quinine.

### AuNPs synthesis

Gold nanoparticles were prepared according to Storhoff *et al.* [24]. All glassware was cleaned in aqua regia (3 parts HCl, 1 part HNO<sub>3</sub>), rinsed with MilliQ, and then oven dried prior to use. An aqueous solution of 1 mM HAuCl<sub>4</sub> was brought to boiling under stirring, and then 10 mL of a 38.8 mM trisodium citrate (Na<sub>3</sub>C<sub>6</sub>H<sub>5</sub>O<sub>7</sub>) solution was added quickly, which resulted in a color change from pale yellow to deep red.

After the color change, the solution was left to boil for additional 15 min and then allowed to cool down to room temperature. The resulting NPs were filtrated under vacuum to remove aggregates and impurities. The size and concentration of the nanoparticles was estimated according to Haiss *et al.* [25]. AuNPs with a diameter of 13 nm and a concentration of 20.4 nM were obtained.

### **AuNPs colorimetric assay**

The colorimetric AuNPs assay was performed according to Song *et al.* [9]. A solution of AuNPs ( $\approx 4$  nM) was incubated with 100 nM of the selected ampicillin aptamers in 10 mM phosphate buffer (PB) pH 8 for 1 h with tilting and rotation. A 100 nM solution of the chosen target in 10 mM PB pH 8 was then added to the vial and incubated for 1 h. Subsequently, 100 mM of NaCl was added to the solution to promote the eventual aggregation of the nanoparticles and the color change (from red to purple) linked to the binding event. UV-Vis spectra were recorded after each step. The results were reported in terms of the ratio between the absorbance at 520 and 620 nm ( $A_{520}/A_{620}$ ). UV-Vis spectra were acquired between 400 and 800 nm with a Cary100 Conc spectrophotometer (Agilent Technologies) operated by Cary Win UV 4.20 software and with a NanoPhotometer N60 (Implen) operated by NanoPhotometer NPOS software.

### **ITC protocol**

ITC experiments were performed on a MicroCal PEAQ-ITC instrument (Malvern Panalytical) operated by MicroCal PEAQ-ITC control software. Data analysis was performed with the MicroCal PEAQ-ITC Analysis software. Since many different parameters have been tested, Table 4.2 shows a summary of these. The reference cell was filled with degassed ultrapure water. The aptamer solutions were always put in the sample cell, after two minutes of pre-equilibration time with the assay buffer. The target solution was administered with the injection syringe. The instrument temperature was set to the run temperature before loading and kept constant during the complete run. In order to determine the dilution heats, control titrations were performed consisting of injection of the ligand into the sample cell filled only with buffer. Thermograms for the binding of MN4 and quinine were analyzed using the 'one set of sites' binding model, by including the corresponding control titration.

### **ITC with AuNPs**

Prior to the ITC experiments, AuNPs were dialyzed overnight against MilliQ water with a dialysis cellulose membrane (avg. flat width 10 mm, Sigma Aldrich). ITC

measurements were performed at 25 °C, with 26 injections of 1.5 µL of 1 mM ampicillin solution, with 1 µM of AMP17 and 4 nM of AuNPs in the cell. Different titrations were performed without aptamers and without nanoparticles, to assess the heat exchange contribution of all interactions.

### **Native nESI-MS protocol**

Prior to native MS analysis, the aptamers were buffer exchanged into either MilliQ water or 150 mM aqueous ammonium acetate (pH 6.8) using Micro-Biospin P-6 columns (Bio-rad Laboratories, USA) in order to desalt the samples and to provide a volatile electrospray buffer of appropriate ionic strength. Solutions of 5 µM or 10 µM aptamers with a five-fold excess of ampicillin or quinine were prepared for binding to the AMP17 or MN4 aptamers respectively, and 3 µL of each sample was injected into the mass spectrometer using in-house prepared, gold-coated borosilicate nano-electrospray ionization (nano-ESI) emitters. The experiments were performed on a Synapt G2 HDMS (Waters, Manchester, UK) in positive ionization mode using careful tuning to maintain fragile noncovalent interactions during ionization and inside the instrument. Experiments were performed in sensitivity and mobility mode. The spray capillary voltage ranged between 1.4-1.5 kV and the sampling cone voltage was 25-50 V. The trap and transfer collision energy were set at 5 V and 0 V, respectively, and the trap DC bias was fixed to 35 V. The IMS wave velocity was set to 800 m/s and the IMS wave height to 35 V. Gas pressures were 2.57 mbar and  $2.16 \times 10^{-3}$  mbar for the backing and source gas, respectively. All data was analyzed using MassLynx 4.1 (Waters).

### **<sup>1</sup>H-NMR protocol**

Nuclear magnetic resonance spectra were recorded at 25 or 5 °C on a Bruker Avance II spectrometer operating at a <sup>1</sup>H frequency of 700.13 MHz, under Topspin 3.1p17 and using a 5 mm triple channel Prodigy N<sub>2</sub>-cryocooled probe with a Z-gradient of 6.56 G/mm. Standard pulse sequences from the Bruker library were used throughout. Samples for reference spectra consisted of 550 µL of 1 mM solutions of AMP17 and ampicillin in D<sub>2</sub>O, buffered at pH 7 using aliquots of acid or base (DCl or NaOD). All 1D <sup>1</sup>H spectra were recorded using a spectral width of 20 ppm and consisted of 128 to 256 scans of 64K TD points each preceded by a 2.0 s relaxation delay. Processing consisted of one order zero-filling prior to multiplication and Fourier transformation. Chemical shifts are referenced against internal DSS (4,4-dimethyl-4-silapentane-1-sulfonic acid). An additional experiment involved <sup>1</sup>H-<sup>13</sup>C HMBC for assignment of the ampicillin resonances. Titrations were

performed by adding aliquots from a solution containing 8 mM ampicillin and 0.4 mM AMP17, to a 0.4 mM solution of AMP17, thus keeping the AMP17 concentration constant throughout the titration. Final aptamer:ampicillin ratios varied from 1:0 to 1:10. Additionally, PFG-NMR was performed to detect aptamer-ligand interactions by monitoring the diffusion coefficient of the ampicillin resonances.

**Table 4.2** Instrumental and analytical parameters of the ITC experiments.

Total number of injections:	13-19-25	Stirring speed: 750 rpm	
Cell temperature:	20-25-30-37-40 °C	Injection volume:	1-2-3 µL
Reference power:	2-5-10 µcal/s	Spacing:	150 s
Initial delay:	180 s		
Aptamers	AMP4 AMP17 AMP18 MN4	Molar ratios	1/2 1/5 1/10
Targets	Ampicillin Cephalexin Quinine	Aptamer conc. range	5 to 25 µM
		Target conc. range	50 µM to 1 mM
Buffers	0.1 M Phosphate buffer, 100 mM NaCl 10 mM Phosphate buffer, 100 mM NaCl 0.1 M Tris buffer, 5 mM KCl 10 mM Tris Buffer, 5 mM KCl	Annealing <sup>1</sup>	Yes/No
pHs	2-5-6-7-7.4-7.6-8	Sonication <sup>2</sup>	Yes/No

<sup>1</sup>Annealing [26] = 3 min at 90 °C, followed by 1 min at 4°C, then 1 min at RT before injection;

<sup>2</sup>Sonication = all solutions were sonicated in an ultrasonic bath for 10 min to remove air bubbles.

## Results and Discussion

### Colorimetric AuNPs assay

To test the specificity of the aptamers, the colorimetric AuNPs assay employed by Song *et al.* was repeated. In this type of assay, ssDNA is first adsorbed on the gold surface to protect the nanoparticles against aggregation in the presence of an electrolyte [27,28]. Upon addition of a target with affinity for the aptamer, the

aptamer folds to allow binding and dissociates from the nanoparticle surface. As a result, the nanoparticles are no longer stabilized in solution and aggregation or even precipitation occurs upon increasing the salt concentration [29]. This aggregation/precipitation phenomenon results in a colour change which serves as proxy to identify the original binding event. An explicative scheme of the assay is depicted in Fig. 4.1. Colorimetric assays based on citrate capped AuNPs are widely used as an analytical tool to investigate aptamer-target interactions [29,30]. It supposedly provides a fast approach to test aptamer performances and binding capabilities. The assay used by Song *et al.* was replicated to allow direct comparison with the original results. Along with AMP, CFX was tested since it has the same side-chain as AMP, for which, according to the conclusion of the original article, the aptamer should be selective. Two other antibiotics for which no affinity is expected, NAF and CAP, were also tested. In addition, a random ssDNA sequence (N36) was tested in similar conditions.

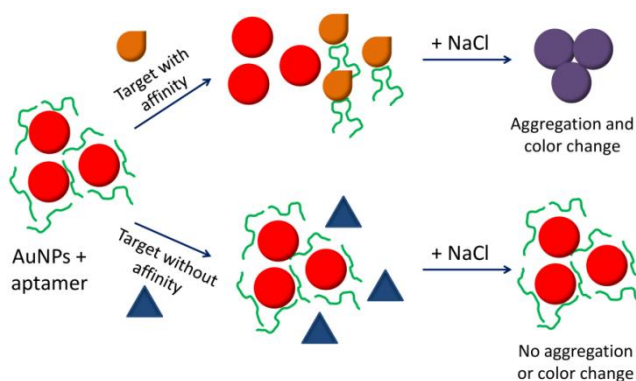


**Fig. 4.1** Schematic representation of the colorimetric AuNPs assay.

The results for the colorimetric test are reported in terms of the ratio between the absorbance of the UV-Vis band at 520 and 620 nm respectively. The band at 520 nm corresponds to the amount of dispersed particles while the one at 620 nm corresponds to that of aggregated particles. This aggregation of AuNPs is typically monitored by a decrease in the  $A_{520}/A_{620}$  ratio (Fig. 4.2) which is considered more reliable and sensitive than the change in individual absorbance alone [30]. In the original paper, a ratio of 2 is reported as a threshold between positive (binding, ratio <2) and negative (non-binding, ratio >2) results. According to the authors, only the assays for the reported aptamer sequences and ampicillin showed an  $A_{520}/A_{620}$  ratio below 2, with AMP17 demonstrating the best performances.

We first repeated the measurements with AMP17. The histogram in Fig. 4.3 shows that the ratio for all the considered combinations (including NAF and CAP for which no binding is expected) is lower than 2, so all have to be considered as positive results, according to the original protocol. It was observed that for AMP and CFX the  $A_{520}/A_{620}$  ratio is lower than the ratio obtained with NAF and CAP.

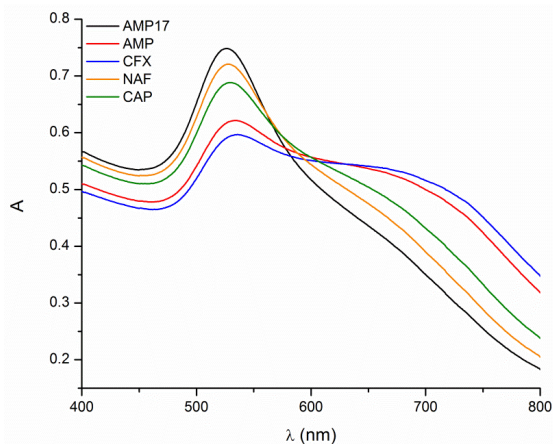


**Fig. 4.2** UV Vis spectra for the AuNPs solutions with AMP17 in the absence of an antibiotic (black) and with 100 nM of various antibiotics in the presence of 100 mM NaCl: AMP (red), CFX (blue), NAF (orange) and CAP (green).

These results present the same trend reported by Song *et al.*, as the aptamer should specifically recognize the side chain of ampicillin and cephalixin. For this reason, a more efficient binding can be expected for those two targets, explaining the lowest value for the ratio. However, the standard deviations of triplicate measurements are relatively large. The differences in  $A_{520}/A_{620}$  between targets remains small and below the threshold value of 2 in all cases. These results are not entirely consistent with the ones reported before and prompted us to investigate the interaction via other techniques to establish whether the effect seen with the AuNPs assay is linked (or not) to the binding event.

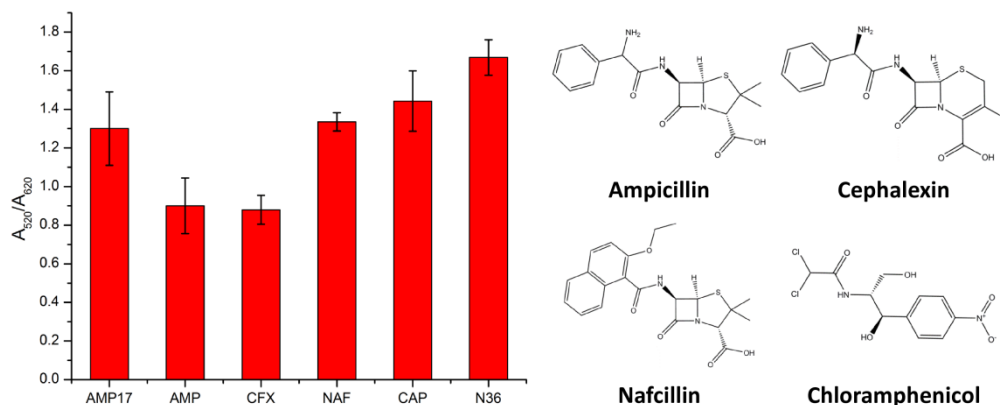


**Fig. 4.3** Absorbance ratio ( $A_{520}/A_{620}$ ) for the AuNPs solutions with 100 nM of AMP17 in the absence of an antibiotic (AMP17) and with 100 nM of various antibiotics in the presence of 100 mM NaCl: ampicillin (AMP), cephalixin (CFX), nafcillin (NAF) and chloramphenicol (CAP); Negative control with a random 36 bp ssDNA sequence (N36) in the presence of 100 nM ampicillin and 100 mM NaCl. Inset: structures of ampicillin, cephalixin, nafcillin and chloramphenicol. SD calculated on  $n=3$ .

### Aptamer binding in solution

Since the AuNP assay can be considered a label and immobilization-free assay, other techniques which do not involve labelling and immobilization were selected to characterize the behaviour of the aptamer in the same conditions. ITC measurements were carried out whilst varying different parameters such as buffer composition, pH and ligand to aptamer molar ratio. First of all, the titration was performed in the conditions reported for the original AuNPs assay, *i.e.* 10 mM phosphate buffer pH 8 with the AMP17 aptamer in a concentration of 5  $\mu$ M titrated with 50  $\mu$ M of AMP. Given the reported  $K_d$  value (13.4 nM), the thermogram should show a clear exothermic binding trend. However, no heat exchange that could be linked to specific binding was observed, even when changing the aptamer (AMP4 and AMP18 were also tested) as can be seen in Fig. 4.4A.

Trying to understand if the buffer composition could influence the affinity of the aptamers for ampicillin, we varied several parameters: the ionic strength by adding NaCl and KCl and using Tris instead of phosphate buffer. Also the possible effect of the pH on the interaction between ampicillin and the aptamer was taken into consideration. Since AMP is a zwitterion, with pKa of 3.2 and 7.4 [31] several buffers with pHs above and below the pKa of ampicillin were tested (see Table 4.2 for a complete overview). However, none of the considered combinations allowed to observe a response characteristic of binding.



Fig. 4.4 shows two sets of thermograms comparing different aptamers (Fig. 4.4A) and different buffers (Fig. 4.4B), where the only visible heat exchange is related to the injection heat. As the binding heat exchanged may be smaller than expected and therefore not easily detected by ITC protocol, native nESI-MS experiments were performed to further investigate the aptamer-ampicillin interaction. Fig. 4.4C shows the mass spectrum of the aptamer before and after addition of the ligand at a 1:5 aptamer:ampicillin ratio. The aptamer is detected at charge states 4+ ( $m/z = 1486.2$ ) and 3+ ( $m/z = 1981.3$ ) with some non-specifically bound sodium ions. Sodium ions are a rather common contamination in MS due to impurities of the chemicals and solvents used or they can also originate from the borosilicate needles used for nESI. For a 1:1 binding stoichiometry, the aptamer-ampicillin complex should occur at  $m/z = 1573.5$  and  $m/z = 2097.4$  for the 4+ and 3+ charge state respectively. However, no high-intensity peaks are visible at these  $m/z$  values (dotted lines in Fig. 4.3C). Assuming specific binding of ampicillin to the aptamer taking place according to the previously reported  $K_d$  of 13.4 nM [9], these peaks should be present with high intensity. A small, broad peak at the theoretical value for the 4+ complex is most likely due to non-specific binding or very weak interactions. Thus, similar to the performed ITC experiments, the nESI-MS results do not support the occurrence of a specific aptamer-target complex under the conditions used. The absence of the complex might be due to the fact that only complexes with a  $K_d$  in the low  $\mu\text{M}$  to nM range can be observed using native nESI-MS, which means that complexation can still occur in the high  $\mu\text{M}$  to mM range [18].

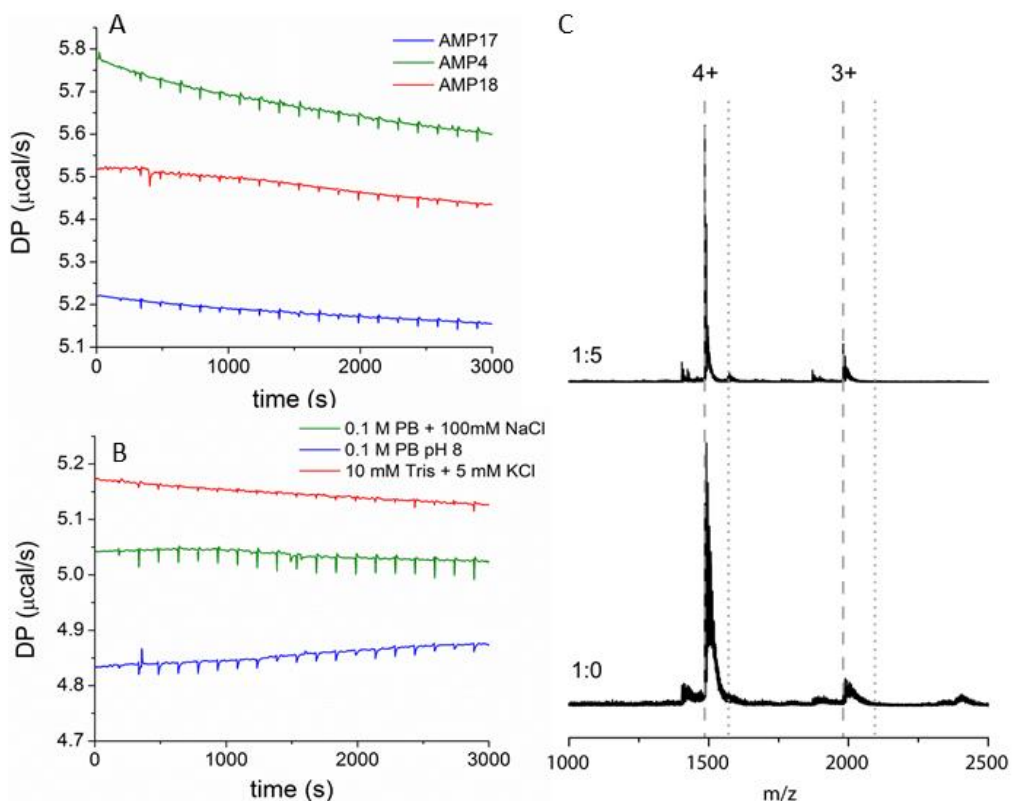


**Fig. 4.4** Different thermograms for the (absent) interaction of ampicillin aptamers with their target (ampicillin); A) AMP17 (blue), AMP4 (green), AMP18 (red) in 10 mM PB pH 8 at 25 °C; B) AMP17 at 25 °C in 0.1 M PB pH 8 with 100 mM NaCl (green), 0.1 M PB pH 8 (blue), 0.1 M Tris buffer pH 7.4 with 5 mM KCl (red); C) Native nESI-MS of the ampicillin-binding aptamer AMP17 without ampicillin and with ampicillin incubated at a 1:5 aptamer:ampicillin ratio in 150 mM ammonium acetate buffer pH 6.8. Theoretical  $m/z$ -values of the apo form (dashed lines) and the 1:1 stoichiometry of the complex (dotted lines) are indicated for the 4+ and 3+ charge state.

To investigate the possibility of a lower affinity complexation, we turned to  $^1\text{H-NMR}$  spectroscopy, as this allows to monitor specific intermolecular interactions with  $K_d$  values well into the mM range. Typically, the presence of a specific interaction may be inferred by monitoring the changes in the  $^1\text{H-NMR}$  fingerprint as the target is titrated into a solution of the aptamer [32,33]. A low affinity interaction will typically manifest itself through the presence of a set of resonances for each species with concentration dependent chemical shifts due to fast exchange conditions on the NMR timescale [33,34]. In favourable cases, monitoring these enables  $K_d$  determination. Alternatively, chemical exchange may be slow on the NMR time scale, leading to a separate set of resonances for the free and complexed species in

solution and immediately indicate the presence of complex formation. The titration of a 0.4 mM solution of the AMP17 aptamer with ampicillin up to a ten-fold excess of the latter is shown in Fig. 4.4A. Given that the  $K_d$  value reported before for AMP17 [9] is in the nM range, this should lead to full complexation and clear perturbations of the  $^1\text{H}$ -NMR spectra. While the full assignment of all resonances in the spectra is not required for monitoring purposes, the resonances of ampicillin could be completely assigned, while only partial assignment of the aptamer sequence was obtained.

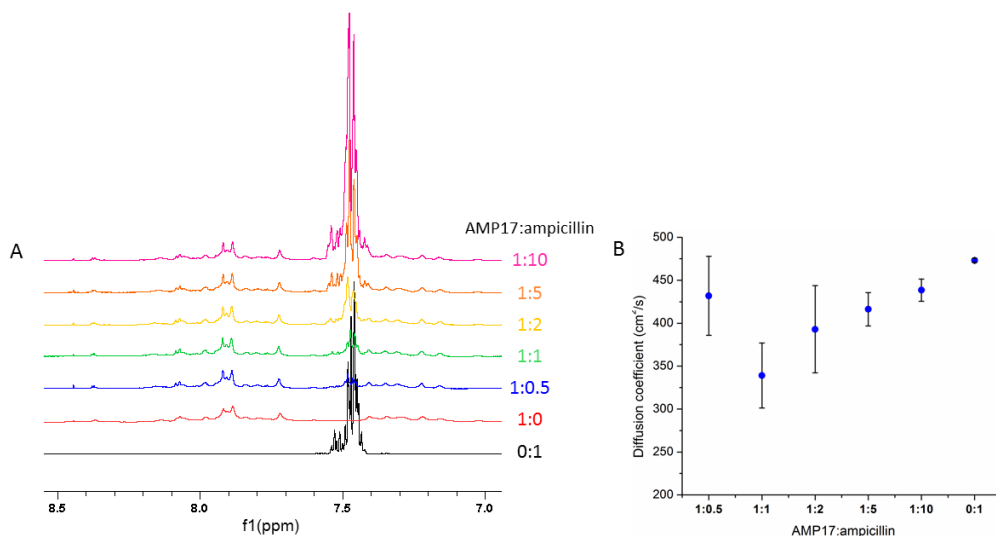


**Fig. 4.5** Impact of the titration of ampicillin in the presence of the AMP17 aptamer monitored by  $^1\text{H}$ -NMR spectroscopy. A) Stacked plot of the 1D  $^1\text{H}$ -NMR spectra of (from bottom to top) pure ampicillin (black), AMP17 (red) and mixtures of AMP17:ampicillin with ratios varying from 1:0.5 to 1:10. A concentration of 0.4 mM AMP17 was used throughout. SD calculated on  $n=6$ .

As can be seen from Fig. 4.5A, each spectrum recorded when titrating ampicillin to the AMP17 solution leads to a single set of resonances for each species, with constant chemical shifts that are in all cases completely identical to those of the individual species in the pure solutions, suggesting lack of interaction. In literature, several examples exist of aptamer-NMR studies where changes that occur in the imino region of the aptamer, including the appearance of additional imino signals, are used as a sensitive indicator of binding and associated with changes in tertiary structure upon binding [35–37]. Here again, no change can be seen and line-widths also appear unaffected, all indicative of a lack of interaction (Fig. 4.6).

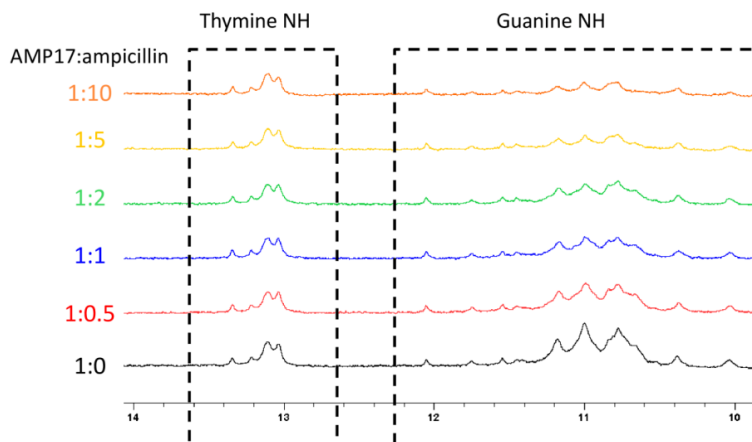


**Fig. 4.6** Overlay of the imino region of the AMP17 aptamer during titration with ampicillin, ratios are indicated (0.4 mM AMP17, H<sub>2</sub>O/D<sub>2</sub>O 90:10, pH 7, 700 MHz).

Finally, the same conclusion follows from monitoring the molecular translational diffusion coefficients of the aptamer and the ampicillin target using pulsed-field-gradient (PFG) NMR spectroscopy. Assuming rapid exchange on the diffusion time-scale [33] and depending on whether ampicillin is mostly complexed or free in solution as the ampicillin to aptamer ratio increases, the self-diffusion coefficient will increase, reflecting the changing balance between bound and free state. However, within error, the self-diffusion coefficients remain constant, and similar to that of the pure solutions, during the whole titration (Fig. 4.5B). To conclude, all NMR data indicates the absence of complexation in the mM concentration range and therefore, any aptamer to target affinity must lie well above the mM  $K_d$  range. We venture to state that this is the final independent indication that the aptamer does not bind to the target. Together with the lack of any interaction from ITC and native nESI-MS we must conclude that there are no grounds to believe that complexation occurs within the low nM to high mM range.

#### Characterization of MN4 aptamer binding with quinine

All the results presented thus far evidence the lack of any binding between AMP17 and its target ampicillin. To validate our approach with a positive control, the same set of experiments was performed with another aptamer, MN4: this cocaine-binding aptamer is one of the most studied and well-characterized for analytical applications and it also strongly binds quinine [26,38], as evidenced by a lower  $K_d$  value (c.a. 100 nM compared to 5.5  $\mu$ M for cocaine), bringing it close to the value reported for the ampicillin binding aptamers (nM range). Therefore, the quinine/MN4 system

provides a suitable positive control for the combined analytical approach. The native nESI-MS experiments performed in a 1:5 MN4:quinine ratio clearly demonstrate the binding of MN4 aptamer. In Fig. 4.7A, the MN4 is detected at charge states 6+ ( $m/z = 1855.7$ ), 5+ ( $m/z = 2226.7$ ) and 4+ ( $m/z = 2783.1$ ) with some non-specifically bound sodium. After addition of the ligand, new peaks that correspond to the 6+ ( $m/z = 1909.8$ ), 5+ ( $m/z = 2291.6$ ) and 4+ ( $m/z = 2864.2$ ) charge state of the complex are present. Moreover, the thermogram for the titration of MN4 aptamer with quinine in 0.1 M Tris buffer pH 7.4 with 5 mM KCl (Fig. 4.7B) shows clear evidence of an exothermic binding process (Fig. 4.7C) from which it is possible to calculate a  $K_d$  of  $171 \pm 45$  nM ( $n = 3$ ). This value is close to the one previously reported in the literature ( $\sim 100 \pm 40$  nM) using ITC [23].  $^1\text{H-NMR}$  for the cocaine-binding aptamer was already extensively reported before and the tertiary structure of the aptamer and binding mechanism were already validated [37,39]. Thus, we conclude that our combined analytical methodology is not failing to detect the ampicillin:AMP17 interaction.

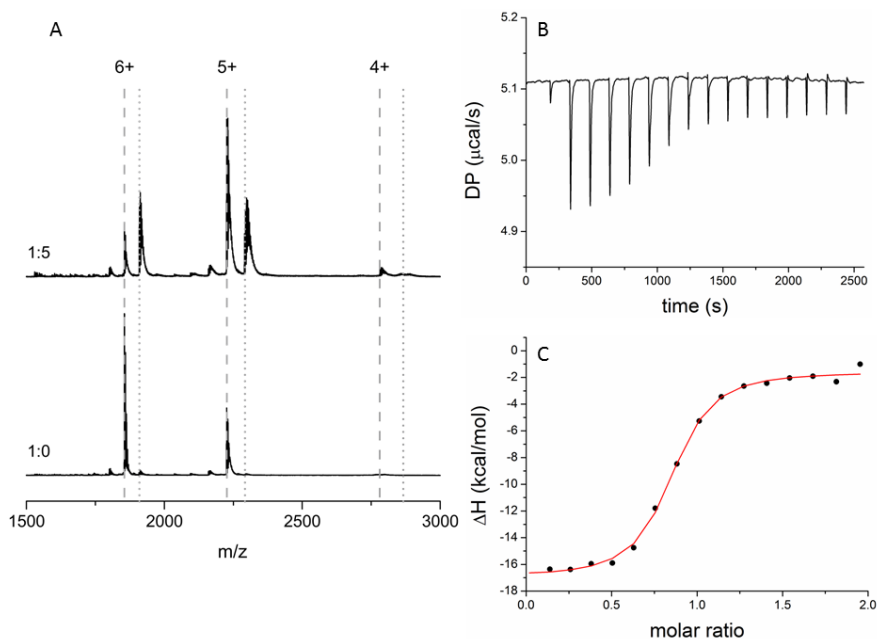


**Fig. 4.7** A) Native nESI-MS of the MN4 aptamer with and without quinine incubated at a 1:5 aptamer:quinine ratio in 150 mM ammonium acetate (pH 6.8). Theoretical peaks of the apo form (dashed lines) and complex (dotted lines) are indicated for the 6+, 5+ and 4+ charge state, B) Thermogram for the titration of 5  $\mu\text{M}$  of MN4 aptamer with 50  $\mu\text{M}$  of quinine in 0.1 M Tris buffer pH 7.4 with 5 mM KCl, C) Binding curve of titration for MN4 and quinine, the red line represent the fitting with the 'one set of binding sites' model.

**Effect of AuNPs on ampicillin-binding aptamers**

To explain the discrepancy between our findings and the results reported by Song *et al.*, one could hypothesize a beneficial effect of the AuNPs on the binding event between AMP17 and target, even if such an effect on the binding between aptamer and target was never reported before. This hypothesis was explicitly considered as many different interactions are known to take place between DNA and AuNPs [27]. To test this hypothesis, ITC titrations were performed with AuNPs and aptamers using the same AuNPs concentration (4 nM) as reported by Song *et al.* [40,41]. Two titrations were performed to assess all possible heat exchange contributions: the first one with AuNPs, AMP17 and the ampicillin target, the second one with AuNPs and ampicillin but without the AMP17 aptamer.

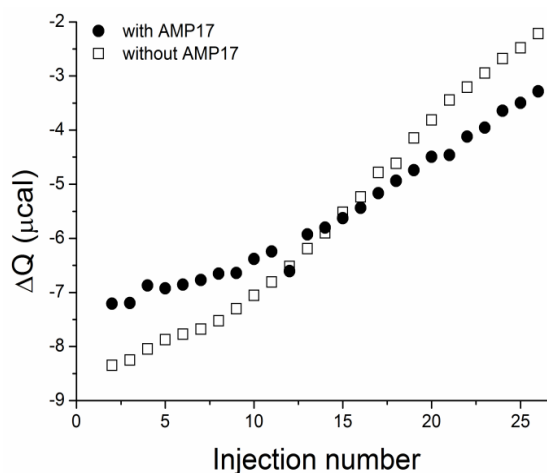


**Fig. 4.8**  $\Delta Q$  for each injection for the titration with AMP 17 aptamer (full dots) and without AMP17 aptamer (empty squares) in the ITC cell.

Fig. 4.8 illustrates the heat generated ( $\Delta Q$ ) at each injection for the titration of the AMP17/AuNPs solution with ampicillin (full dots) compared to the titration with only ampicillin and AuNPs (empty squares). The graph shows that the detected heat exchange mainly stems from the interaction of the antibiotic with the AuNPs, while AMP17 does not contribute to the generated heat. This indicates that ampicillin has a strong affinity for the AuNPs. Native nESI-MS experiments could not be performed due to the presence of the AuNPs which cannot be transferred to the gas-phase. Therefore the absence of a specific interaction between AMP17 and its target ampicillin, in the presence of AuNPs, was verified again using  $^1\text{H-NMR}$ .

The spectra of the aptamer with and without nanoparticles (Fig. 4.9A) shows no relevant differences apart from a slight broadening of the peaks; also the titration with ampicillin (Fig. 4.9B) does not indicate binding between AMP17 aptamer and the target in presence of AuNPs. As observed before, when considering the diffusion coefficient measurements for the antibiotic in the absence of AuNPs (see Fig. 4.5B), and also when titrating ampicillin into AMP17 in the presence of AuNPs, the values remain constant, within experimental error, associated with 6 repeated measurements for ampicillin (Fig. 4.9C). All these data reaffirm the absence of binding between the aptamer and ampicillin even in the presence of AuNPs in solution.

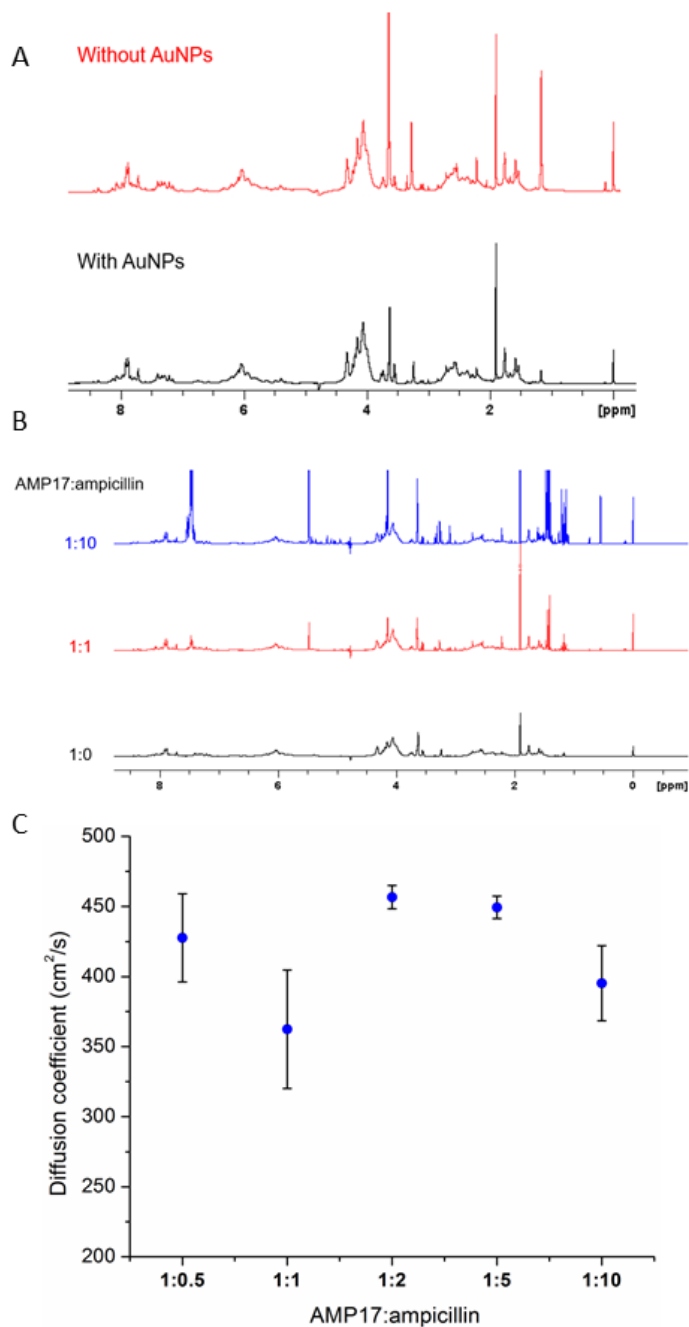


**Fig. 4.9** A) Overlay of 1D  $^1\text{H}$  spectra of AMP17 with (black) and without (red) AuNPs; B) Overlay of the titration experiment, AMP17:ampicillin ratios are indicated, in the presence of AuNPs; C) Diffusion coefficient of ampicillin upon titration into a solution of AMP17 in presence of AuNPs. SD calculated on  $n=6$ .



## Conclusions

In line with the increasing awareness within the aptamer community, we clearly illustrated the need to address and validate the aptamer-target interaction using a multi-faceted analytical approach before “applying” aptamer sequences in other studies. More specifically, researchers should avoid relying exclusively on fast and easy-to-perform assays as analytical approaches to validate binding affinity since the risk to misinterpret the real performance of a specific aptamer is particularly high. For the majority of data collected in this way, the exact experimental conditions play a critical role and are often not entirely clear from the description of the work, thus difficult to replicate or adapt to a different analytical application. Therefore, extrapolating the performances of a given aptamer sequence to different experimental conditions may lead to conflicting or poorly reproducible results. Here, we offer a validation strategy to verify the performance and improve the reliability of aptamers for analytical applications. As for the aptamers used in the present study the question is still open; without completely ruling out the possibility that they indeed bind ampicillin, it is obvious that their binding mechanism is poorly understood or superficially evaluated. This need for critical evaluation of aptamer performances was firmly identified and discussed on the occasion of the Aptamers 2019 meeting in Oxford, UK. Guidelines for standardization in aptamer selection, characterization and application are slowly finding their way into the interdisciplinary oriented aptamer community. With the present study we aim to contribute to these endeavours and provide the research community with the tools to adopt a robust analytical multi-faceted approach to validate aptamer-target interactions prior to applying them.

**References**

- [1] M. McKeague, A. De Girolamo, S. Valenzano, M. Pascale, A. Ruscito, R. Velu, N.R. Frost, K. Hill, M. Smith, E.M. Mcconnell, M.C. Derosa, Comprehensive analytical comparison of strategies used for small molecule aptamer evaluation, *Anal. Chem.* 87 (2015) 8608–8612.
- [2] A. Ruscito, M.C. DeRosa, Small-Molecule Binding Aptamers: Selection Strategies, Characterization, and Applications, *Front. Chem.* 4 (2016) 14.
- [3] A.L. Chang, M. McKeague, J.C. Liang, C.D. Smolke, Kinetic and equilibrium binding characterization of aptamers to small molecules using a label-free, sensitive, and scalable platform, *Anal. Chem.* 86 (2014) 3273–3278.
- [4] M. Gong, I. Nikcevic, K.R. Wehmeyer, P.A. Limbach, W.R. Heineman, Protein-aptamer binding studies using microchip affinity capillary electrophoresis, *Electrophoresis.* 29 (2008) 1415–1422.
- [5] S. Amaya-González, L. López-López, R. Miranda-Castro, N. De-los-Santos-Álvarez, A.J. Miranda-Ordieres, M.J. Lobo-Castañón, Affinity of aptamers binding 33-mer gliadin peptide and gluten proteins: Influence of immobilization and labeling tags, *Anal. Chim. Acta.* 873 (2015) 63–70.
- [6] T. Hianik, V. Ostatná, M. Sonlajtnerova, I. Grman, Influence of ionic strength, pH and aptamer configuration for binding affinity to thrombin, *Bioelectrochemistry.* 70 (2007) 127–133.
- [7] A. Ruscito, M.C. DeRosa, Small-molecule binding aptamers: selection strategies, characterization, and applications, *Front. Chem.* 4 (2016) 14.
- [8] M.N. Stojanovic, P. de Prada, D.W. Landry, Fluorescent sensors based on aptamer self-assembly, *J. Am. Chem. Soc.* 122 (2000) 11547–11548.
- [9] K. Song, E. Jeong, W. Jeon, M. Cho, C. Ban, Aptasensor for ampicillin using gold nanoparticle based dual fluorescence – colorimetric methods, *Anal. Bioanal. Chem.* 402 (2012) 2153–2161.
- [10] F. Bottari, R. Blust, K. De Wael, Bio(inspired) strategies for the electro-sensing of  $\beta$ -lactam antibiotics, *Curr. Opin. Electrochem.* 10 (2018) 136–142.
- [11] B. Gulbakan, Oligonucleotide aptamers: emerging affinity probes for bioanalytical mass spectrometry and biomarker discovery, *Anal. Methods.* 7 (2015) 7416–7430.
- [12] T. Sakamoto, NMR study of aptamers, *Aptamers.* 1 (2017) 13–18.
- [13] T. Sakamoto, E. Ennifar, Y. Nakamura, Thermodynamic study of aptamers binding to their target proteins, *Biochimie.* 145 (2018) 91–97.
- [14] B. Gülbakan, K. Barylyuk, P. Schneider, M. Pillong, G. Schneider, R. Zenobi, Native electrospray ionization mass spectrometry reveals multiple facets of aptamer–ligand interactions: from mechanism to binding constants, *J. Am. Chem. Soc.* 140 (2018) 7486–7497.

## Chapter 4 – Characterization of aptamers for small organics molecules

- [15] M. Vogel, B. Suess, Label-Free Determination of the Dissociation Constant of Small Molecule-Aptamer Interaction by Isothermal Titration Calorimetry BT - Nucleic Acid Aptamers: Selection, Characterization, and Application, in: G. Mayer (Ed.), Springer New York, New York, NY, 2016: pp. 113–125.
- [16] S. Cai, J. Yan, H. Xiong, Y. Liu, D. Peng, Z. Liu, Investigations on the interface of nucleic acid aptamers and binding targets, *Analyst*. 143 (2018) 5317–5338.
- [17] F. Balthasart, J. Plavec, V. Gabelica, Ammonium ion binding to DNG G-quadruplexes: Do electrospray mass spectra faithfully reflect the solution-phase species?, *J. Am. Soc. Mass Spectrom.* 24 (2013) 1–8.
- [18] B.E. Elisabetta, P. Carlo, The emerging role of native mass spectrometry in characterizing the structure and dynamics of macromolecular complexes, *Protein Sci.* 24 (2015) 1176–1192.
- [19] M. Kouchakdjian, B.F.L. Li, P.F. Swann, D.J. Patel, Pyrimidine · pyrimidine base-pair mismatches in DNA: A nuclear magnetic resonance study of T · T pairing at neutral pH and C · C pairing at acidic pH in dodecanucleotide duplexes, *J. Mol. Biol.* 202 (1988) 139–155.
- [20] P. Schultze, R.F. Macaya, J. Feigon, Three-dimensional solution structure of the thrombin-binding DNA aptamer d(GGTTGGTGGTTGG), *J. Mol. Biol.* 235 (1994) 1532–1547.
- [21] T. Dieckmann, E. Suzuki, G.K. Nakamura, J. Feigon, Solution structure of an ATP-binding RNA aptamer reveals a novel fold., *RNA*. 2 (1996) 628–640.
- [22] M.A.D. Neves, O. Reinstein, P.E. Johnson, Defining a stem length-dependent binding mechanism for the cocaine-binding aptamer. A combined NMR and calorimetry study, *Biochemistry*. 49 (2010) 8478–8487.
- [23] S. Slavkovic, M. Altunisik, O. Reinstein, P.E. Johnson, Structure-affinity relationship of the cocaine-binding aptamer with quinine derivatives, *Bioorganic Med. Chem.* 23 (2015) 2593–2597.
- [24] J.J. Storhoff, R. Elghanian, R.C. Mucic, C.A. Mirkin, R.L. Letsinger, One-pot colorimetric differentiation of polynucleotides with single base imperfections using gold nanoparticle probes, *J. Am. Chem. Soc.* 7863 (1998) 1959–1964.
- [25] W. Haiss, N.T.K. Thanh, J. Aveyard, D.G. Fernig, Determination of size and concentration of gold nanoparticles from UV–Vis spectra, *Anal. Chem.* 79 (2007) 4215–4221.
- [26] S. Slavkovic, M. Altunisik, O. Reinstein, P.E. Johnson, Structure–affinity relationship of the cocaine-binding aptamer with quinine derivatives, *Bioorg. Med. Chem.* 23 (2015) 2593–2597.
- [27] J.M. Carnerero, A. Jimenez-Ruiz, P.M. Castillo, R. Prado-Gotor, Covalent and non-covalent DNA–gold-nanoparticle interactions: New avenues of research, *ChemPhysChem*. 18 (2017) 17–33.

## Chapter 4 – Characterization of aptamers for small organics molecules

- [28] X. Zhang, M.R. Servos, J. Liu, Surface science of DNA adsorption onto citrate-capped gold nanoparticles, *Langmuir*. 28 (2012) 3896–3902.
- [29] S.C.B. Gopinath, T. Lakshmi Priya, K. Awazu, Colorimetric detection of controlled assembly and disassembly of aptamers on unmodified gold nanoparticles, *Biosens. Bioelectron.* 51 (2014) 115–123.
- [30] W. Zhao, M.A. Brook, Y. Li, Design of gold nanoparticle-based colorimetric biosensing assays, *ChemBioChem*. 9 (2008) 2363–2371.
- [31] IARC. Monographs on the Evaluation of the Carcinogenic Risk of Chemicals to Humans. Geneva: World Health Organization, International Agency for Research on Cancer, 1972-PRESENT., (1990) V50.
- [32] T.D.W. Claridge, High-resolution NMR techniques in organic chemistry, ed. J.E.B., Elsevier, 2009.
- [33] B. Fritzing, I. Moreels, P. Lommens, R. Koole, Z. Hens, J.C. Martins, In Situ Observation of Rapid Ligand Exchange in Colloidal Nanocrystal Suspensions Using Transfer NOE Nuclear Magnetic Resonance Spectroscopy, *J. Am. Chem. Soc.* 131 (2009) 3024–3032.
- [34] A.D. Bain, Chemical exchange in NMR, *Prog. Nucl. Magn. Reson. Spectrosc.* 43 (2003) 63–103.
- [35] P.A. Mirau, J.E. Smith, J.L. Chávez, J.A. Hagen, N. Kelley-Loughnane, R. Naik, Structured DNA aptamer interactions with gold nanoparticles, *Langmuir*. 34 (2018) 2139–2146.
- [36] S.A. Robertson, K. Harada, A.D. Frankel, D.E. Wemmer, Structure determination and binding kinetics of a DNA aptamer–argininamide complex, *Biochemistry*. 39 (2000) 946–954.
- [37] Z.R. Churcher, M.A.D. Neves, H.N. Hunter, P.E. Johnson, Comparison of the free and ligand-bound imino hydrogen exchange rates for the cocaine-binding aptamer, *J. Biomol. NMR*. 68 (2017) 33–39.
- [38] M.A.D. Neves, S. Slavkovic, Z.R. Churcher, P.E. Johnson, Salt-mediated two-site ligand binding by the cocaine-binding aptamer, *Nucleic Acids Res.* 45 (2017) 1041–1048.
- [39] O. Reinstein, M. Yoo, C. Han, T. Palmo, S.A. Beckham, M.C.J. Wilce, P.E. Johnson, Quinine binding by the cocaine-binding aptamer. thermodynamic and hydrodynamic analysis of high-affinity binding of an off-target ligand, *Biochemistry*. 52 (2013) 8652–8662.
- [40] A. Gourishankar, S. Shukla, K.N. Ganesh, M. Sastry, Isothermal titration calorimetry studies on the binding of DNA bases and PNA base monomers to gold nanoparticles, *J. Am. Chem. Soc.* 126 (2004) 13186–13187.
- [41] H. Joshi, P.S. Shirude, V. Bansal, K.N. Ganesh, M. Sastry, Isothermal titration calorimetry studies on the binding of amino acids to gold nanoparticles, *J. Phys. Chem. B*. 108 (2004) 11535–11540.



# Biomimetic receptors for antibiotics electroensing

---

Biomimetic materials, such as MIPs, are promising electrode modifiers for the design of electrochemical sensors able to selectively detect numerous food and environmental contaminants [1–3] such as  $\beta$ -lactam antibiotics [4–6]. MIPs represent an appealing alternative to bioreceptors (enzymes, antibodies or proteins) thanks to their higher stability, low cost and easy preparation protocol [7]. The synthesis of MIPs is characterized by three main steps: (1) the formation of a pre-polymerization complex between the template, *i.e.*, the target molecule, and the functional monomers (*pre-arrangement step*), (2) the (electro)polymerization of the monomer and (3) the subsequent removal of the template (*extraction step*) that leads to the formation of target-specific cavities within the polymeric network. These cavities, complementary in size, shape and chemical functionalities with the template, selectively bind the target molecules, even in presence of structurally related compounds.

In recent years, the use of imprinted polymers for electroanalytical applications gathered considerable attention thanks to the versatility of these electrode modifiers [5,8]. Their combination with conductive nanomaterials such as carbon nanotubes, gold nanoparticles or graphene allows to greatly improve the sensitivity for electroactive targets [9,10] as well as non-electroactive ones [11]. The main advantages of imprinted polymers for analytical applications are related to their robustness, the possibility to reduce matrix interferences and the versatility of the possible analytical configurations [12,13]. Moreover, compared to traditional MIPs obtained by bulk polymerization, electropolymerized ones do not require an additional immobilization step, a factor that could limit the application in electroanalysis [14–16]. MIPs can be directly integrated with the transducer surface by electropolymerization of the monomer under potentiostatic or -dynamic conditions [17]. The variation of the electropolymerization conditions allows to adjust the rate of polymer nucleation and growth, the film thickness and morphology, which lead to specific electrochemical properties [18]. The properties of the final polymer mainly depend on the monomer concentration, the electropolymerization technique and the electrolyte and solvents used during the polymerization [19,20]. The possibility to obtain an electronically conductive

polymer (ECP) is of paramount importance for the detection of electroactive targets because the selectivity provided by the key-and-lock mechanism of the MIP cavities will be coupled with the specific electrochemical signal of the target leading to highly selective biomimetic sensors.

Another interesting possibility, is to use such electropolymerizable monomers as electrode modifiers, exploiting their intrinsic affinity for the target molecules. In this regard, substituted anilines provide an excellent stability of the film obtained and only require mild polymerization conditions [21]. These polymers are used in a variety of analytical applications and surface electrode modifications, most commonly to obtain MIPs [22–24] or as linkers for other modifiers, such as carbon nanomaterials [25], metal nanoparticles or biorecognition elements [26,27]. At present, only a few examples of the use of these polymers dedicated to the direct electrochemical detection of small molecules, due to the intrinsic affinity between target and polymer-modified electrode, have been published [28,29]. The selection of the monomer through computational tools can be fundamental in the development of modified sensors with enhanced affinity for targets. The possibility to *in-silico* simulate the interaction between the monomer and the target can assure the best performance of the obtained modified electrode [30,31]. The most investigated ECPs are based on pyrrole, 3-aminophenylboronic acid, phenol, thiophenol, aniline and derivatives [32]. Recently, carboxyl-substituted anilines, known as aminobenzoic acids (ABAs), and in particular 4-ABA, are giving promising results in sensing applications. 4-ABA has been previously employed in chemical sensors [33,34], biosensor platforms [35–38], anticorrosion coatings [39,40] and as a linker for polyoxometalates immobilization on glassy carbon electrodes [41]. Despite its numerous applications, the polymerization mechanism of 4-ABA remains unclear [42] and no extensive studies have been dedicated to map the film properties in different electropolymerization conditions (pH, buffer composition, monomer concentration, etc.).

The use of electropolymerizable conductive polymers as electrode modifiers for enhancing electrochemical detection has gathered increasing attention over the past decades [14,43,44]. The simplicity and reproducibility of the obtained modifications are assets in the field of sensor analysis. By combining screen printed electrodes, a portable potentiostat and a standardized modification protocol it becomes possible to apply these polymer-modified electrodes to real sample analysis by non-specialists.

The following section reports two examples of the proposed approaches: first the the development of a conductive MIP for CFQ and then an o-phenylenediamine (oPD) modified electrode for determination of NAF, both based on electropolymerizable monomers selected by rational monomer design.

## Material and Methods

### Reagents

CFQ, 4-ABA, NAF, o-phenylenediamine (oPD), AMX, PENG and AMP were purchased from Sigma-Aldrich Ltd (Belgium). 2-(2-aminothiazole-4-yl)-2-methoxyiminoacetic acid (SC), cefoperazone (CFP), CFX and ceftiofur (CFU) were obtained from TCI (Europe). Aniline (ANI) was obtained from Fluka (Belgium). 0.1 M PB solutions were prepared by mixing stock solutions of 0.1 M  $\text{NaH}_2\text{PO}_4$  and 0.1 M  $\text{Na}_2\text{HPO}_4$ , to obtain different pH values and 0.1 M of NaCl was added to obtain the corresponding saline buffer (PBS). To extend the pH range until 3 and 4, suitable amounts of phosphoric acid ( $\text{H}_3\text{PO}_4$ ) were added. The PB pH 2 was obtained from phosphoric acid. A 0.1 M  $\text{H}_2\text{SO}_4$  solution was used for the lowest pH value ( $\text{pH} \approx 1$ ). Britton Robinson buffer (BRB) was prepared with  $\text{CH}_3\text{COOH}$ ,  $\text{H}_3\text{BO}_3$  and  $\text{H}_3\text{PO}_4$  in equal concentrations (0.1 M) and the pH was adjusted with 0.1 M NaOH. All other reagents of analytical grade were used without further purification. All aqueous solutions were prepared using MilliQ water ( $\rho > 18 \text{ M}\Omega\text{cm}$ ).

### Rational monomer design

The computational modelling was performed as described by Piletsky et al. [45]. Briefly, a virtual library of electropolymerizable monomers ( $\approx 20$ ) was screened using the LEAPFROG™ algorithm (SYBYL® 7.3 software package, Tripos International, USA) to investigate their interaction with the template. Energy minimization was conducted to a minimum of  $0.001 \text{ kcal mol}^{-1} \text{ \AA}^{-1}$  gradient. The parameters of molecular mechanics were method Powell, force field Tripos and charges Gasteiger-Huckel.

### Electrochemical measurements

CV, SWV, EIS and LSV were carried out using an Autolab potentiostat/galvanostat (PGSTAT 302N, ECOCHEMIE, The Netherlands) controlled by NOVA 1.1 software. Bare G-SPEs and modified with multi-walled carbon nanotubes (MWCNT-G-SPEs) were purchased from DropSens (Metrohm, Belgium). They are composed of a graphite working electrode (3 mm diameter), a graphite counter electrode and a silver pseudo reference electrode. Except where otherwise stated, all the potentials



are referred to Ag pseudo reference (-200 mV compared to SCE). All results obtained by SWV are presented after baseline correction using the mathematical algorithm “Moving average” (peak width = 1) contained within NOVA 1.1 software, to improve the visualization and identification of the peaks over the baseline.

## **Conductive imprinted polymers for the direct electrochemical detection of cefquinome<sup>3</sup>**

A biomimetic sensor for CFQ was designed at MWCNTs-G-SPEs as a proof-of-concept for the creation of a sensor array for  $\beta$ -lactam antibiotics detection in milk. The detection strategy is based on the characteristic electrochemical fingerprint of the target antibiotic CFQ. A conductive electropolymerized MIP coupled with MWCNTs was found to be the optimal electrode modifier, able to provide an increased selectivity and sensitivity for CFQ detection. The design of CFQ-MIP was facilitated by the rational selection of the monomer, 4-ABA. The electropolymerization process of 4-ABA has not been fully elucidated yet; for this reason a thorough study and optimization of electropolymerization conditions was performed to obtain a conductive and stable poly(4-ABA) film. The modified electrodes were characterized by EIS, SEM and CV. CFQ-MIP were synthesized at MWCNT-G-SPEs by electropolymerization at pH $\approx$ 1 (0.1 M sulphuric acid) with a monomer:template ratio of 5:1. Two different analytical protocols were tested (single and double step detection) to minimize unspecific adsorptions and improve the sensitivity. Under optimal conditions, the lowest CFQ concentration detectable by SWV at the modified sensor was 50 nM in 0.1 M phosphate buffer pH 2.

## **Experimental section**

### **Reagents**

Stock solutions of 10 mM CFQ in MilliQ water were kept at 4 °C for up to three days. Standard working solutions of CFQ were obtained by dilution of the stock solutions with the suitable buffer. Stock solutions of 10 mM 4-ABA in 0.1 M PBS at pH 7 were prepared daily.

---

<sup>3</sup> Based on G. Moro, F. Bottari, N. Slegers, A. Florea, T. Cowen, L. M. Moretto, S. Piletsky, K. De Wael, *Conductive imprinted polymers for the direct electrochemical detection of  $\beta$ -lactam antibiotics: The case of cefquinome*, Sensors and Actuators B: Chemical, 297, 2019, 126786

### Rational monomer design

The library of electroactive monomers was ranked depending on the  $\Delta G$  calculated as the difference between the energy of each ligand-monomer complex and the corresponding energies of the free monomers and the free CFQ. Among the first five monomers that yielded the lowest  $\Delta G$  (reported in Table 5.1), 4-aminobenzoic acid (4-ABA) was selected ( $\Delta G = -104.081 \text{ kJ mol}^{-1}$ ).

**Table 5.1**  $\Delta G$  ranking of the monomers obtained by rational monomers design.

Monomer	$\Delta G$ (kcal/mol)
pyrrole-2-carboxylic acid	-144.143
pyrrolidine-2-carbohydrazide	-116.106
4-aminobenzoic acid	-104.081
o-phenylenediamine	-77.860
4-aminothiophenol	-64.994

### Electrochemical measurements

The following parameters were employed for the electropolymerization of 4-ABA by CV: -0.3 V to +1.2 V potential range,  $50 \text{ mV s}^{-1}$  scan rate with seven consecutive cycles. CVs used to investigate the CFQ electrochemical fingerprint and its C7 side chain (2-(2-aminothiazole-4-yl)-2-methoxyiminoacetic acid) were performed between 0.0 V and +1.5 V potential range,  $50 \text{ mV s}^{-1}$  scan rate, 0.1 M PB pH 2. To obtain SWVs of CFQ, the following parameters were used: +0.4 V and +1 V potential range, 5 mV step potential, 25 mV amplitude, 10 Hz frequency.

### Analytical protocol

For the single step detection (SSD), a drop of 100  $\mu\text{L}$  of PB solution spiked with different CFQ concentrations was left in contact with the electrode for 1 min before running a SWV. For the double step detection (DSD) 50  $\mu\text{L}$  of PB solution spiked with different CFQ concentrations were placed at the modified electrode for various timeframes (1-5 mins) (*step 1*). Afterwards, the drop was removed and the electrode surface was rinsed with 3 mL of MilliQ water and 100  $\mu\text{L}$  of 0.1 M PB pH 2 was placed at the electrode (*step 2*) before running a SWV.

### Electrode characterization

The modified electrodes were characterized by SEM and EIS. SEM images were acquired with a Field Emission Gun – Environmental Scanning Electron Microscope equipped with an Energy Dispersive X-Ray detector (FEI Quanta 250, USA). EIS measurements were carried out in 0.1 M PBS pH 7 with 2 mM  $[\text{Fe}(\text{CN})_6]^{3-/4-}$ , in the

frequency range between 100 kHz and 1 Hz, with 0.01 V amplitude and DC potential determined by open circuit potential (OCP).

## Results and discussion

### Cefquinome electrochemical behaviour

The electrochemical fingerprint of CFQ at G-SPEs (Fig. 5.1A) is characterized by two irreversible oxidation peaks at +0.7 V and +1.3 V. The peak at +1.3 V corresponds to the irreversible oxidation of the cephem nucleus, common to all cephalosporins, thus not useful for a selective identification of CFQ [46]. The oxidation peak at +0.7 V (red curve, Fig. 5.1A) can be ascribed to CFQ C7 side chain (SC) that is characteristic only of the more recent classes of cephalosporins such as the 3<sup>rd</sup> and 4<sup>th</sup> generations. Therefore, it is possible to base CFQ identification directly on the SC signal.

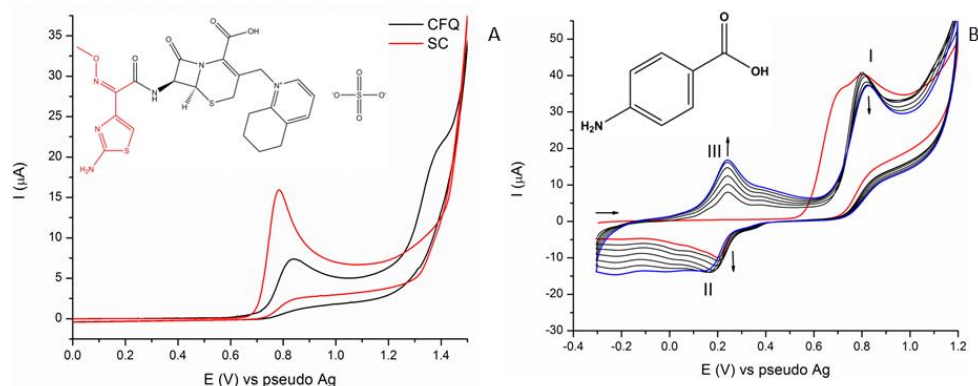


**Fig. 5.1** (A) CVs of individual solutions of 500  $\mu\text{M}$  CFQ and SC in 0.1 M PB pH2 at G-SPEs, 50  $\text{mVs}^{-1}$ ; inset: CFQ structure with SC in red; (B) CVs obtained for the electropolymerization of 1 mM 4-ABA in 0.1 M  $\text{H}_2\text{SO}_4$  at MWCNTs-G-SPE, 50  $\text{mVs}^{-1}$ . The arrows indicate the direction of the current increase/decrease as a function of the number of CV cycles from the first cycle (red) to the 7<sup>th</sup> (blue). Inset: 4-aminobenzoic acid structure.

### 4-ABA electropolymerization study

The cyclic voltammograms accounting for the electropolymerization of 4-ABA on MWNTs-G-SPE (Fig. 5.1B) are characterized by: the monomer region in which 4-ABA is irreversibly oxidized around +0.8 V, peak (I), leading to the formation of radical species (*activated monomers*) and the polymer region between -0.3 V and +0.4 V where the redox peaks (II and III) allow to follow the polymer growth [35].

In the first cycle (red line, Fig. 5.1B), the monomer peak was preceded by a shoulder at +0.7 V that could be ascribed to the adsorption of the neutral monomer at the electrode surface before its oxidation [47] or to the formation of different highly-

reactive radicals [35]. Increasing the number of cycles, leads to a decrease in the anodic peak current of the monomer (I), showing the progressive oxidation of the monomer at the electrode surface. The main polymer redox peaks showed an  $E_{pc}$  of +0.17 V (II) and an  $E_{pa}$  of +0.23 V (III) in the last voltammogram (blue line, Fig. 5.1B); both peaks (II and III) showed increasing currents upon increasing number of cycles. The constant increase of the polymer peak currents together with the decrease in the monomer peak current testifies the constant and surface controlled nature of the modification, while maintaining the electrode surface conductivity.

### Optimization of the pH

A pH study between 1 and 7 was performed to map the pH dependent behaviour of 4-ABA and to choose the optimal pH to obtain a conductive and stable modification (Fig. 5.2A-G). Analysis of the peak currents of the polymer showed that for pH 2 to 6 the polymer growth seems faster than at pH 1 and 7. At pH 2, 3 and 6 the polymer peaks (II and III in Fig. 5.1B) remained constant after five CV cycles. At pH 4 and 5 both peaks II and III started decreasing after three cycles with a clear overlap in both oxidation and reduction peaks (Fig. 5.2D and E). The pH influence was evident also considering the peak potential shifts: the polymer  $E_{pc}$  was +0.17 V at pH 7 and +0.55 V at pH 1 (see Fig. 5.2G and A). These observations were justified considering the amphoteric nature of 4-ABA whose functional groups can be protonated or deprotonated depending on the pH of the electrolyte ( $pK_{a1} = 2.38$ ,  $pK_{a2} = 4.85$  at 25 °C [48,49]). In the pH range 2 to 6, the heterogeneous forms of the functional groups could enhance the polymerization rate, while at pH 1 and 7 the monomers are completely protonated or deprotonated resulting in a slower, but monotonic polymer growth.

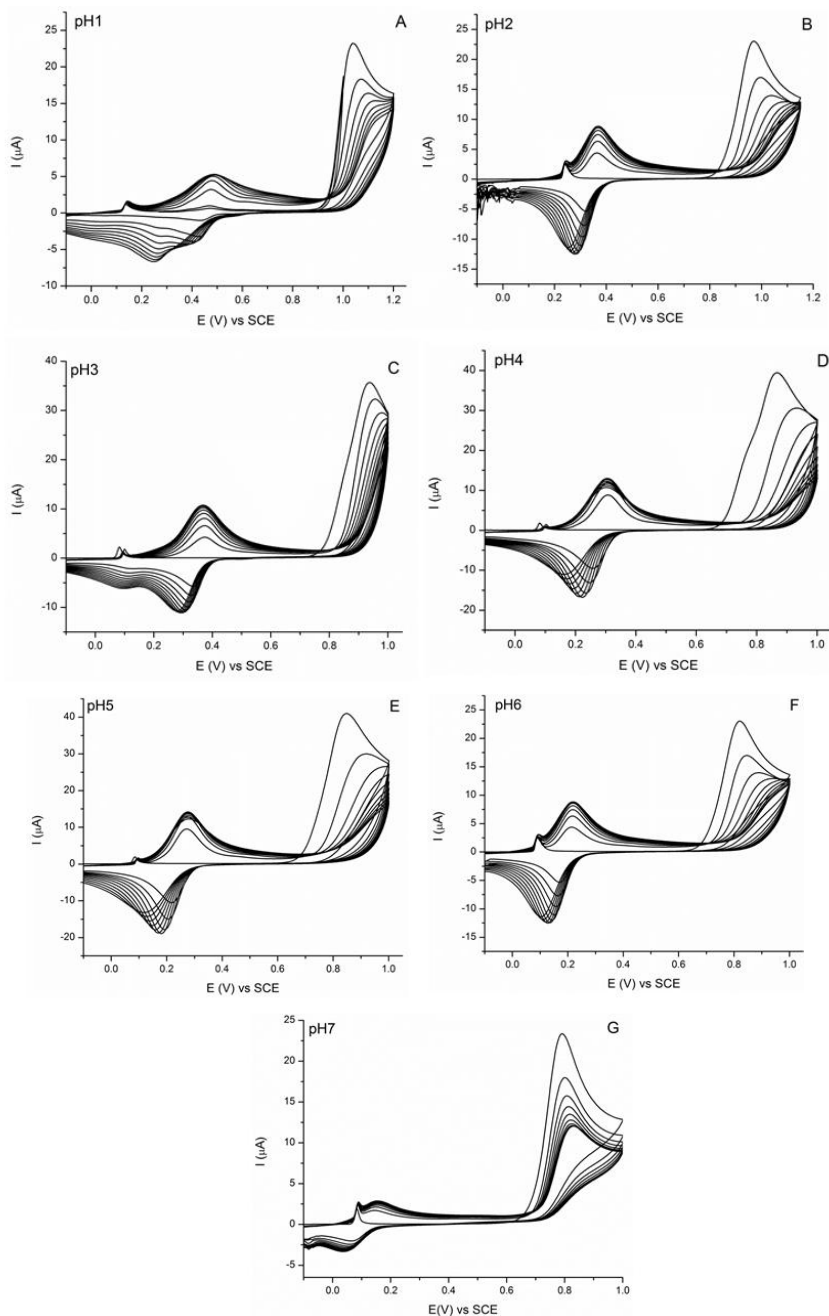


**Fig. 5.2** Electropolymerization of 4-ABA at different pH from 1 (A) to 7 (G); 10 cycles between -0.2 and +1 V for pH 7 to 3, between -0.2 and +1.2 V for pH 2 and 1, 50 mV/s. The spike at +0.1 V is due to the presence of Ag conductive paste on the graphite screen printed electrode.

Aiming to perform surface controlled polymerization, the relationship between the peak current and the number of cycles was accurately evaluated (see Fig. 5.3). Only at pH 1 and pH 7 the polymer showed a gradual growth resulting in an increased oxidation and reduction currents (peaks II and III in Fig. 5.1B) while in 2 to 6 pH range (with pH 5 shown in Fig. 5.3) a decrease in the same currents after the first few CV cycles suggests the formation of a thicker and less conductive layer. This behaviour is in agreement with many electropolymerization mechanisms reported for other electroactive monomers [50–52].

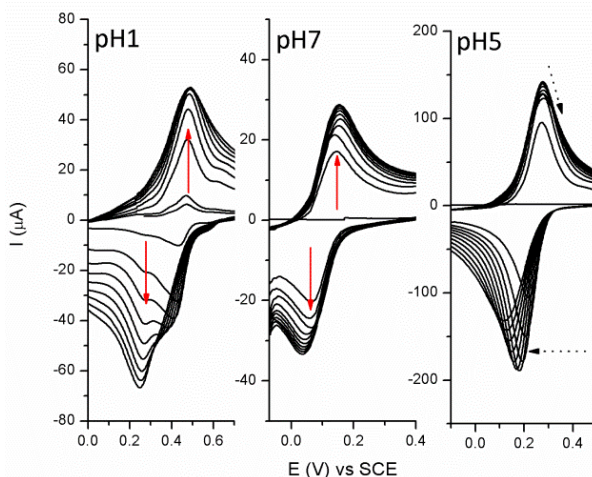


**Fig. 5.3** Focus on polymers  $I_{pa}$  and  $I_{pc}$  for the electropolymerization of 4-ABA (from left to right) at pH 1, 7, 5; 10 consecutive cycles of CV at  $50 \text{ mVs}^{-1}$  for 1 mM 4-ABA at G-SPE.

Despite the fast growth observed using pHs from 2 to 6, these pH values were discarded because of the difficulty in controlling the film electrochemical properties. The passivating effect, evident from the decrease of the current of the polymer peaks, was deemed not suitable to monitor the effect of other parameters (e.g. monomer:template ratio) on the conductivity of the obtained film. Differences in the peak current and potential of the polymers peaks can thus be used as an indication of the effect of the MIP protocol optimization on the obtained polymer. For the same reasons, both pH 1 and pH 7 were considered suitable for the present application and further tested in the following optimization study, expecting different responses because of the different ionic species involved during electropolymerization.

### Optimization of scan rate, monomer concentration and number of CV cycles

A literature survey allowed to identify the most commonly used parameters for scan rates, monomer concentrations and number of CV cycles [34,35]. These parameters were tested following an one-variable-at-a-time approach (OVAT), keeping constant the other two. The first criterion considered in the selection of the optimal value of a parameter was the consistency of the electropolymerization voltammograms with the standard presented in Fig. 5.1B, upon changing the investigated parameter. If no discernible differences in the voltammograms pattern were identified, the selected subset of parameters was further compared using the oxidation signal of 50  $\mu\text{M}$  CFQ to select the best value for each parameter.

The second selection criterion was based on the expected CFQ response (oxidation peak at +0.7 V vs pseudo Ag) and a sensible difference in its intensity ( $I_p$ ) between the bare and the 4-ABA modified electrode. Indeed, CFQ oxidation should be detectable in the presence of a stable conductive modification giving a less intense signal if compared to bare electrode. The decrease in signal can be used as an indication that the film formed on the surface is thick enough to host imprinted cavities while still maintaining good conductivity and allowing the ET with the antibiotic.

The first parameter studied was the scan rate: the literature [7,8] gives values of 50  $\text{mV s}^{-1}$  or 100  $\text{mV s}^{-1}$  for electropolymerization, thus these two values were tested at both pH (1 and 7). Scan rate of 50  $\text{mV s}^{-1}$  showed a evident difference between the bare and the modified electrode signal ( $I_p = 1.4 \mu\text{A}$  at G-SPE and an  $I_p = 0.8 \mu\text{A}$  at 4-ABA modified G-SPE, for 50  $\mu\text{M}$  CFQ) with a smaller STD. At 100  $\text{mV s}^{-1}$ , the peaks of the polymer in the electropolymerization CVs showed a behaviour similar to the one of intermediate pH values, with overlaps after a few cycles of electropolymerization. Thus, 50  $\text{mV s}^{-1}$  was chosen as the optimal scan rate value; indeed increasing the scan rate of the electropolymerization CVs has been proven to result in an increase in  $\Delta E_p$  of the polymer peak indicating a less reversible system [53].

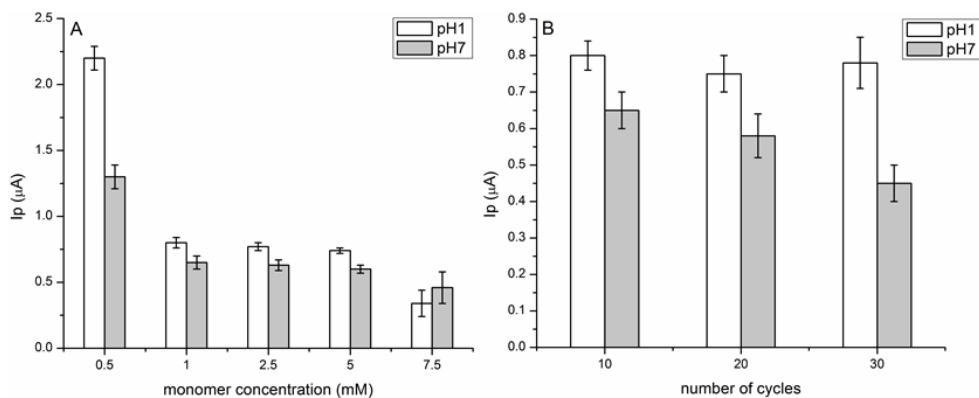


**Fig. 5.4** Comparison of peak currents of CFQ (50  $\mu\text{M}$ ) at G-SPEs modified with 4-ABA using: (A) different monomer concentrations or (B) different numbers of CV cycles during the electropolymerization. SD calculated on  $n=3$ .

Considering the monomer concentration, the tested values were: 0.5, 1, 2.5, 5 and 7.5 mM (see Fig. 5.4A). The performances of intermediate concentrations (1, 2.5, 5 mM) were found to be comparable with an associated error of 4% at pH 1 and 6% at pH 7 on average, while the lowest and highest monomer concentrations gave sensibly different responses. The films with 7.5 mM of 4-ABA provided signals with an intensity three times lower in comparison to intermediate monomer concentrations in acid conditions while at pH 7 a smaller difference was recorded ( $\approx 0.1 \mu\text{A}$ ). The results obtained for 0.5 mM were very similar to the ones recorded at bare electrodes suggesting that the films were probably too thin and inhomogeneous to form stable target-specific cavities. Thus, the 7.5 mM and the 0.5 mM were discarded and only the intermediate monomer concentrations were found to be suitable for these kind of modifications. Considering the two pHs, in all cases, pH 1 gave better results in terms of CFQ signal intensity and reproducibility. From the present study, the electropolymerization of 1 mM 4-ABA solution at pH 1 appeared to be the optimal combination to obtain a conductive film with a good balance between reproducibility and CFQ signal intensity.

Keeping 4-ABA concentration fixed at 1 mM and the scan rate at  $50 \text{ mV s}^{-1}$ , the electropolymerization was performed at 10, 20 and 30 consecutive CV cycles. For all the three values, a good agreement with the standard electropolymerization pattern in Fig. 5.1B and no significant differences in the SSD results (Fig. 5.4B) were found. Thus, the lower value, 10 cycles, was chosen to reduce the total protocol time.



The final optimal conditions for 4-ABA electropolymerization at G-SPEs were: 50 mV/s<sup>-1</sup> scan rate, 1 mM monomer concentration and 10 CV cycles.

### MWCNTs

After having optimized the main electropolymerization conditions and before the CFQ-MIP synthesis design, the possibility to integrate MWCNTs was evaluated. The voltammetric response of CFQ solutions at different concentrations was recorded at MWCNTs-G-SPEs. An increase in the faradic peak currents of 40% compared to the bare G-SPE was observed (see Fig. 5.5A). The lowest detectable concentration decreased from 0.5 to 0.1  $\mu$ M in 0.1 M PB pH 2 (Fig. 5.5B). Aiming to monitor nanomolar CFQ concentrations the improvement of the signal provided by these modifiers was considered fundamental.

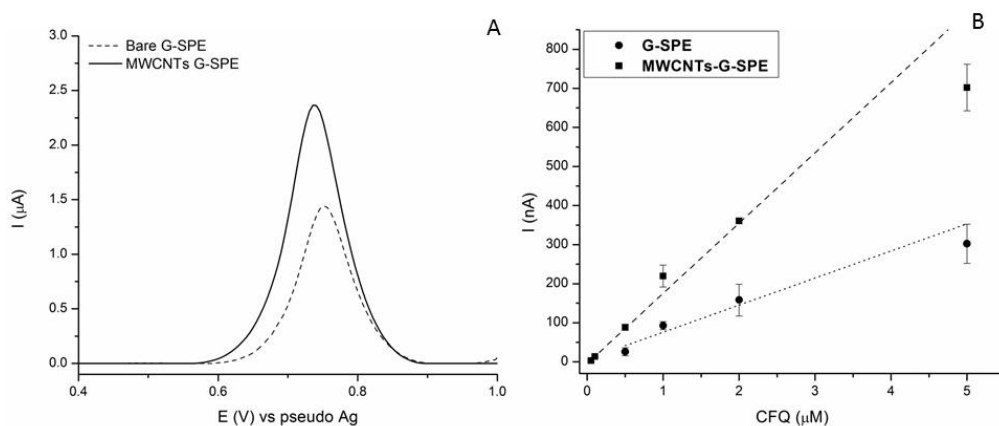


**Fig. 5.5** (A) SWV of 100  $\mu$ M CFQ in 0.1 M PB pH 2 on MWCNTs-G-SPEs (full line) and G-SPEs (dashed line), (B) Calibration curves for CFQ in 0.1 M PB pH 2 recorded by SWV on MWCNTs-G-SPEs (square) and G-SPEs (dots). SD calculated on n=3.

Switching from G-SPEs to the MWCNTs-G-SPEs, further tests of the electropolymerization conditions were needed. The number of CV cycles was reduced from 10 to 7. Indeed, after 7 CV cycles on MWCNTs-G-SPEs the redox peaks of the polymer showed an overlapping pattern similar to the result reported for intermediate pH value (2-6) for the study of 4-ABA electropolymerization. As already concluded, this overlap is indicative of a less conductive modification [51,54]. This behaviour could be ascribed to the improved conductivity and active area provided by the MWCNTs which promoted the growth of the polymer on the electrode.

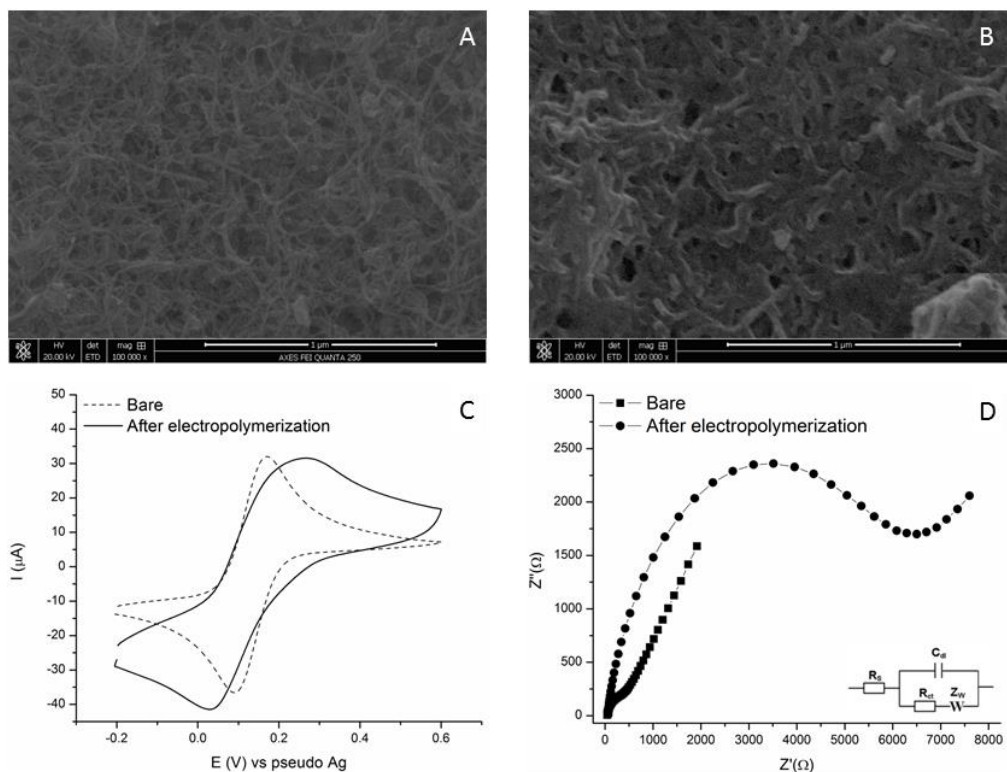


**Fig. 5.6** (A) SEM images of bare MWCNTs-G-SPEs and (B) 4-ABA-MWCNTs-G-SPEs; (C) CV of 2 mM  $[\text{Fe}(\text{CN})_6]^{3-/4-}$  in 0.1 PBS pH 7 for bare MWCNTs-SPE, 50  $\text{mVs}^{-1}$  (dashed line) and 4-ABA-MWCNTs-SPE (full line); (D) Nyquist plot for 2 mM  $[\text{Fe}(\text{CN})_6]^{3-/4-}$  in 0.1 PBS pH 7 at bare MWCNTs-G-SPEs (square) and 4-ABA-MWCNTs-SPE (dots), inset: Randles equivalent circuit used to fit the data.

The MWCNTs-G-SPEs modified with poly(4-ABA) were characterized by SEM analysis, CV and EIS. Comparing the SEM image of the bare (Fig. 5.6A) and 4-ABA modified electrodes (Fig. 5.6B) it is possible to observe that the MWCNTs are partially wrapped by a smooth polymer layer. CVs in presence of 2 mM  $[\text{Fe}(\text{CN})_6]^{3-/4-}$  confirmed that the deposition was successful and that the electrode surface is still conductive. The CV (full line in Fig. 5.6C) shows that, after the electropolymerization, the value for  $\Delta E_p$  increases ( $\sim 220$  mV) and the peaks are broader compared to the situation at the bare electrode (dashed line in Fig. 5.6C). In addition, the Nyquist plot in Fig. 5.6D indicates that the deposition was successful, registering an increase in the semi-circular area of the spectrum at higher frequencies, related to the charge transfer resistance on the electrode surface.

### CFQ-MIP synthesis protocol

To finalize the design of CFQ-MIP, two other important set of parameters were taken into account: the monomer:template ratio and the parameters for the extraction procedure, both in terms of solvent and extraction time. The optimal value for each parameter was selected by comparison of the performances of the film after the CFQ rebinding in terms of oxidation signal intensity and reproducibility. The rebinding of the target was performed by allowing a drop of the target solution in PB (50  $\mu$ M) in contact with the modified electrode for 2 min, before rinsing with MilliQ water to remove unspecific adsorbed species and finally running a SWV in a fresh microvolume (100  $\mu$ L) of 0.1 M PB pH 2 to detect the oxidation signal of CFQ. As a comparison, non-imprinted polymers (NIP) were also synthesized using the same protocol without the addition of the target template and used as a control to verify the success of the imprinting approach.

Concerning the monomer:template ratio, two values, 5:1 and 3:1, were studied. Preliminary tests suggested that at higher ratios (*e.g.*, 10:1) a lower number of cavities were created, while with lower ratios (1:1, 2:1) unstable modifications were obtained. Ratios of 5:1 and 3:1 gave stable modifications with a significant difference in MIP and NIP responses in terms of signal reproducibility. The results showed that the 3:1 ratio gave an average current intensity higher than the 5:1, but it was less reproducible with an error of 12% against the 6% of the 5:1. Reproducibility being a fundamental issue for the proposed modification, the monomer:template ratio 5:1 was chosen.

The effect of the template in the polymerization solution was also ascertained looking at the electropolymerization CVs for both MIP and NIP (electropolymerization patterns reported in Fig. 5.7). The voltammetric pattern is the same for both modified sensors, with the only difference being the absence of the shoulder at +0.7 V (see also Fig. 5.1B) in the first cycle for the MIP. Thus we may conclude that the presence of the template does not hinder the formation of the 4-ABA film on the electrode surface.

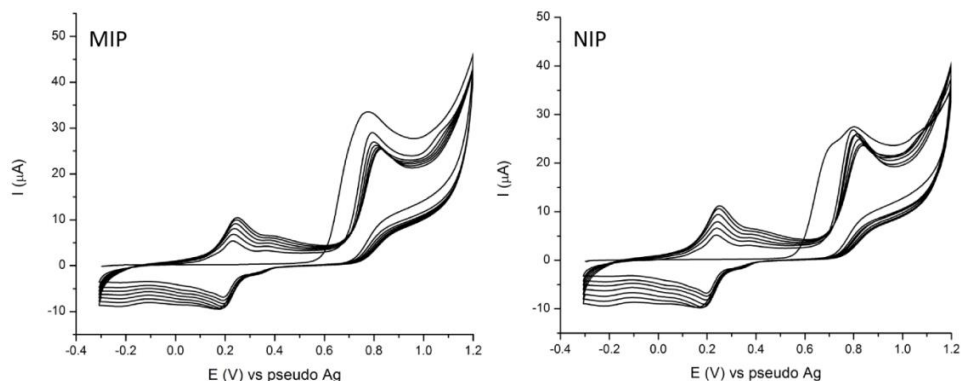


**Fig. 5.7** CVs electropolymerization pattern for MIP (left) and NIP (right).

The extraction step aims to remove the template without interfering with the architecture of the polymeric network and to allow the rebinding of the target. To design this step, warm ( $\sim 60^{\circ}\text{C}$ ) and RT MilliQ water, water:acetonitrile (4:1) and 0.1 M PB pH 12 were tested as extraction solvents with a fixed extraction time of 5 min. As shown in Fig. 5.8A, only the extraction in 0.1 M PB pH 12 assured a complete removal of the template. Using the other extraction solutions, CFQ remained partially entrapped as can be seen by the presence of its electrochemical signal after the extraction. Moreover, the 0.1 M PB pH 12 did not hamper the detection of the CFQ after the rebinding. The corresponding signal ( $0.84\ \mu\text{A}$ ) was higher than the one obtained with RT ( $0.68\ \mu\text{A}$ ) and warm MilliQ water ( $0.76\ \mu\text{A}$ ). In presence of water:acetonitrile (4:1), the increased signal observed was ascribed to the presence of template residues interacting with the solvent.

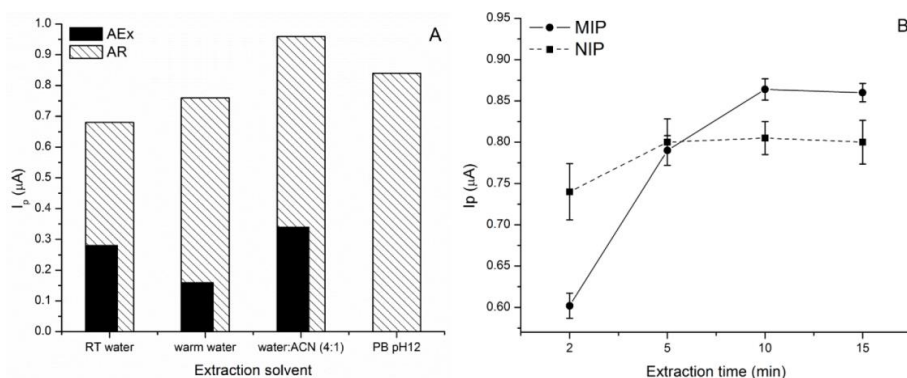


**Fig. 5.8** (A) Comparison of performances after rebinding of  $50\ \mu\text{M}$  CFQ in 0.1 M PB pH 2 using different extraction solvents for MIP AEx: after extraction, AR: after rebinding, extraction time 5 min; (B) Signal intensity of  $50\ \mu\text{M}$  of CFQ after rebinding with different incubation times for the extraction step with 0.1 M PB pH 12 for MIP and NIP. SD calculated on  $n=3$ .

Different extraction times ( $t_{\text{ex}}$  = 2, 5, 10, 15 min) were tested using 0.1 M PB pH 12 as extraction solution and the results were compared with the ones obtained on the corresponding NIP (see Fig. 5.8B) for the rebinding of 50  $\mu\text{M}$  of CFQ. At  $t_{\text{ex}}$  lower than 10 min, the CFQ signal was lower than expected because of an incomplete removal of the template. At  $t_{\text{ex}}$  higher than 10 min no difference was observable and the CFQ signal remained stable for longer extraction times. Thus, an extraction step of 10 min in 0.1 M PB pH 12 was chosen. Also the difference between MIP and NIP responses was evident for  $t_{\text{ex}}$  equal or higher than 10 min. This behaviour can be explained by the presence of the target-mimetic cavities on the MIP which are free to rebind the target, while for the NIP the signal is only due to non-specific adsorption on the polymeric network which is not influenced by the extraction step. To avoid shifts in the CFQ peak potential and poorly reproducible results (due to the presence of an unchecked pH in the MIP polymeric network), an additional conditioning step was performed after the extraction, consisting in the incubation of a 100  $\mu\text{L}$  drop of 0.1 M PB pH 2 at the modified electrode for 1 min.

The final CFQ-MIP synthesis protocol involved the following steps:

1. Pre-incubation of the electropolymerization solution of 1 mM 4-ABA and 0.2 mM CFQ in 0.1 M  $\text{H}_2\text{SO}_4$  pH 1 for 10 min.
2. Electropolymerization at the MWCNT-G-SPEs for 7 CV cycles, from -0.3 V to +1.2 V at  $50 \text{ mVs}^{-1}$ .
3. Rinse with 3 mL of MilliQ water and perform a 10 min template extraction with 100  $\mu\text{L}$  of 0.1 M PB pH 12.
4. The modified electrode is rinsed and incubated for 1 min with 100  $\mu\text{L}$  of 0.1 M PB pH 2 before the rebinding.

The modified electrodes were thus ready for the rebinding step.

### **Analytical protocol and calibration plot**

The performances of two different detection strategies, the SSD and the DSD described in Materials and Methods, were compared in order to find the most suitable analytical protocol. The two protocols were compared considering the differences between the MIP and the NIP responses. By applying SSD, this difference appears to be negligible for all tested concentrations and CFQ concentrations lower than 10  $\mu\text{M}$  were not detectable. On the contrary, using the DSD the signal intensity results were higher for MIP than NIP modified sensors. This difference became more relevant when nanomolar concentrations were considered, *i.e.* at 0.1  $\mu\text{M}$  the CFQ signal was only visible when using the MIP

modified electrodes. Thus, nanomolar CFQ concentrations ( $\leq 100$  nM) were detectable only using the MIP-MWCNT-G-SPEs coupled with a DSD. Moreover, this approach proved to be more reliable, by reducing the non-specific absorption on the polymer network and by increasing the response of the MIP for concentrations in the nanomolar range.

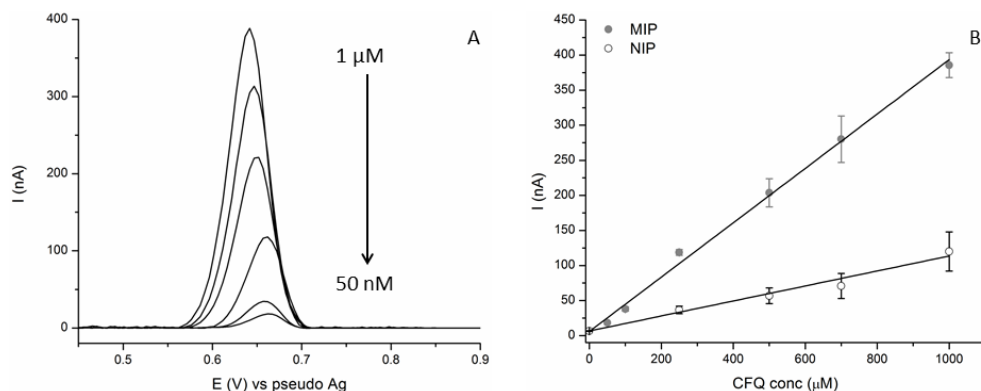


**Fig. 5.9** (A) SWVs of different concentrations (50, 100, 250, 500, 700 and 1000 nM) of CFQ on MIP-MWCNT-G-SPEs and (B) calibration plots obtained with DSD for MIP (full grey dots) and NIP (empty white dots). SD calculated on  $n=4$ .

With the DSD approach it was possible to obtain a calibration plot for CFQ between 50 nM and 1 μM (Fig. 5.9) in 0.1 M PB pH 2 and showing satisfying reproducibility (STD < 5% for 4 different electrodes). The corresponding calibration plot at the NIP modified electrode shows that it is not capable of detecting concentrations lower than 250 nM (Fig. 5.9B) while the imprinted sensor is capable of reaching lower concentrations. The imprinting factor (IF), calculated by dividing the slope of the linear fit of the MIP by the one of the NIP, is 3.5.

### Interference study

To test the selectivity of the proposed sensor towards CFQ, three other electroactive cephalosporins [55] – CFU, CFX and CFP – were analysed at MIP and NIP sensors using the DSD protocol and 1 μM spiked solutions. Special attention was paid to the response of CFU, a third generation cephalosporin that differs from CFQ only in the C3 side chain. It is worth reminding that CFU is the only other cephalosporin licensed for cattle treatment that has the same active side chain as CFQ.

As can be seen in Fig. 5.10, CFX and CFP gave no signal on both the MIP and the NIP at the oxidation potential of CFQ (+0.7 V). For CFU the response is the same for MIP and NIP (220 nA); which can be explained by non-specific interaction of the

antibiotic with the sensor. For CFQ, the signal for 1  $\mu\text{M}$  is higher on the MIP (380 nA) than the NIP (250 nA) with a lower associated error ( $\pm 17$  nA vs.  $\pm 70$  nA). The very high standard deviation on the NIP is due to the employed detection strategy (DSD): the rebinding step, performed removing the spiked solution from the electrode and placing a fresh drop of buffer, makes the subsequent detection on non-imprinted electrodes less reproducible. The cavities of the MIP selectively capture the antibiotics on the electrode surface, while the NIP signal is only due to non-specific interaction between the bulk polymer and the targets, which can vary significantly between different analysis.

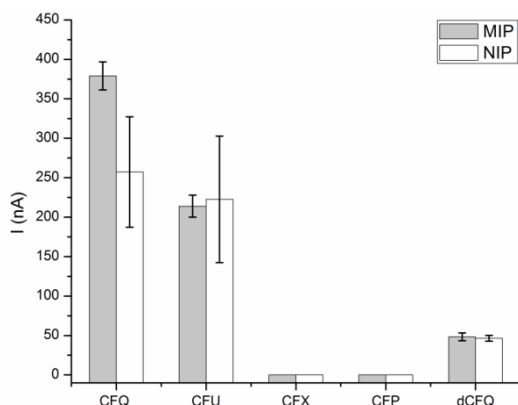


**Fig. 5.10** Interference study: response of 1  $\mu\text{M}$  of cefquinome (CFQ), ceftiofur (CFU), cephalexin (CFX), cefoperazone (CFP) and degraded CFQ (dCFQ) for MIP-MWCNTs-SPE and NIP-MWCNTs-SPE in 0.1 M PB pH2. SD calculated on n=3.

The proposed modification is also capable of distinguishing between the native and degraded form of CFQ. The signal for 1  $\mu\text{M}$  of CFQ after 24 h of basic degradation at pH 12 on MIP and NIP is almost the same ( $\sim 50$  nA). Thus for very small concentration (nM range) the signal for the degraded form is negligible and not detect at both MIP and NIP modified electrodes. It is worth reminding that the MRLs value are referred to pharmacologically active form of the antibiotics, so the proposed modified sensor shown better selectivity toward the native form of the antibiotic.

## Conclusions

The proposed MIP for CFQ illustrates the fact that an electronically conductive MIP using 4-ABA as functional monomer could be obtained. The electropolymerization at pH 1 was proven to be optimal to obtain conductive polymers and stable molecularly imprinted cavities. Moreover, CFQ identification can be based on the

signal of its C7 side chain; the specificity of the electrochemical signal combined with the selectivity of the MIP permitted to distinguish between closely related compounds and more important between intact and degraded forms of the antibiotic. The modified electrode already possesses the qualities required for a successful technological transfer and for on-site applications.



## Electropolymerized *o*-phenylenediamine on graphite promoting the electrochemical detection of nafcillin<sup>4</sup>

In this study we report the detection of NAF on a G-SPE modified with electropolymerized oPD, selected by rational design. Experimental parameters, such as monomer concentration, pH and number of electropolymerization cycles were optimized to obtain the highest amperometric current signal for target detection. NAF identification was based on the peak at +1.1 V, ascribed to the oxidation of its C7 side chain. With the optimized modification protocol, a two-fold increase in NAF signal could be obtained: the calibration plot in 0.1 M BRB pH 4 showed a LOD of 80 nM with a good sensitivity and reproducibility (RSD<5%).

### Experimental Section

#### Reagents

The oPD stock solution in MilliQ water (10 mM) was prepared fresh every day and stored in dark at 4 °C. Antibiotic stock solutions (10 mM) were prepared in MilliQ water and kept at 4 °C for maximum three days. River water was obtained from the Scheldt river in Antwerp. The water samples were first filtered through a disposable syringe filter with pore size 0.45 µm (Chromafil® AO-45/25), then diluted 1:10 in 0.1 M BRB pH 4 and spiked with 1 µM of NAF: the solution was analysed by SWV with the oPD-SPE electrode after five min accumulation time.

#### Rational monomer design

The monomers were ranked by relative binding energy and the most stable arrangement of each monomer-target complex was obtained. Among the monomers which gave the lowest binding energies with the target, *o*-phenylenediamine (oPD) was selected (-39.09 kJ mol<sup>-1</sup>) (Table 5.2).

---

<sup>4</sup> Based on F. Bottari, G. Moro, N. Slegers, A. Florea, T. Cowen, S. Piletsky, A. L. van Nuijs, and K. De Wael, *Electropolymerized o-phenylenediamine on Graphite Promoting the Electrochemical Detection of Nafcillin*, *Electroanalysis*, 2019

**Table 5.2.**  $\Delta G$  ranking of the monomers obtained by rational monomers design.

Monomer	$\Delta G$ (kcal/mol)
<i>o</i> -phenylenediamine	-39.09
proline	-38.10
aniline	-36.49
pyrrolidine-2-carbohydrazide	-35.69
4-aminobenzoic acid	-32.32

### Analytical parameters

Electropolymerization of oPD was performed by CV in 0.1 M H<sub>2</sub>SO<sub>4</sub> between -0.8 and +0.6 V with different number of cycles. CV and EIS characterization were carried out in 0.1 M KNO<sub>3</sub> with 2 mM [Fe(CN)<sub>6</sub>]<sup>3-/4-</sup>. Impedance spectra were recorded between 100 kHz and 1 Hz, with 0.01 V amplitude and DC potential of +0.2 V. SWVs at bare and oPD modified electrodes were performed between +0.4 and +1.3 V, 5 mV step potential, 25 mV amplitude, 10 Hz frequency. The SWVs for the calibration plot are reported after blank subtraction.

## Results and Discussion

### *o*-Phenylenediamine electropolymerization

The electropolymerization mechanism of oPD is well-studied [21] and it is known that the features of the resulting polymer can be strongly influenced by the electropolymerization conditions such as pH, electrolyte [51,56,57], potentials applied [58,59], duration of the polymerization and initial monomer concentration [60]. Looking at the voltammetric curves for the electropolymerization of 1 mM oPD in 0.1 M H<sub>2</sub>SO<sub>4</sub> (Fig. 5.11), a peak at +0.3 V, ascribed to the irreversible oxidation of the monomer to its corresponding radical cation, is observed. The peaks at -0.4 and -0.5 V are related to the oxidation and reduction of the polymer which is growing on the surface of the electrode, at each subsequent voltammetric scan (as previously shown by electrochemical quartz crystal microbalance – EQCM [51]). The electropolymerization proceeds through dimerization by radical coupling (head-to-head, head-to-tail, tail-to-tail). According to Losito *et al.* and Rothwell *et al.*, the obtained dimers can be further oxidized producing a linear chain polymer by subsequent addition or by cyclization, creating a ladder-like structure [57,61,62]. As can be seen in Fig. 5.11 the gradual increase in the peak currents supports the hypothesis that the polymer growth is controlled by the number of CV cycles [60].

For the application of direct electrochemical detection, it is of paramount importance to obtain a conductive polymer on the electrode.

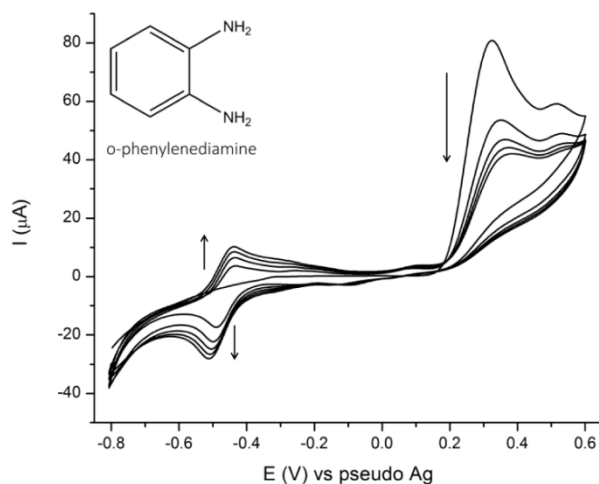


**Fig. 5.11** Electropolymerization (five CV cycles at  $100 \text{ mV s}^{-1}$ ) of 1 mM oPD on G-SPE in 0.1 M H<sub>2</sub>SO<sub>4</sub>. Inset: structure of o-phenylenediamine.

It was previously observed that in acidic solutions the oPD electropolymerization gives rise to porous and conductive films, while in neutral or basic conditions the film passivates the electrode surface [51,56,58]. Another factor that affects the performance of the electropolymerized layer is the composition and concentration of the monomer solution. Previous studies reported on the influence of the acid used on the polymerization rate and the solubility of the obtained dimers at the electrode surface. Moreover, it has been shown that for 0.1 M H<sub>2</sub>SO<sub>4</sub> the electropolymerization is more efficient even at shorter times [51] and the solubility of the dimers is minimal. So it is possible to obtain stable and conductive films even for very short electropolymerization periods. Regarding the dimers solubility, the small waves between -0.1 and +0.2 V (Fig. 5.11) can be ascribed to the oxidation and reduction of the dimers in solutions; they become much more evident increasing the monomer concentration or changing the type of acid in solution. After the electropolymerization, the solution turns slightly orange, with darker colour for higher concentrations; this phenomenon is due to the dimers released in solution from the electrode surface. However, in the selected conditions of this work these effects are minimal, assuring robust results. Additionally, the chosen potential window (from -0.8 to +0.6 V) was selected to obtain the fastest polymer

growth avoiding excessive over-oxidation of the obtained film in subsequent cycles [57–59].

### oPD-SPE characterization

Preliminary tests were performed to understand the influence of the length of the electropolymerization period on the electrode performance. The G-SPE were modified with a constant concentration of oPD (1 mM) for three different CV cycles length, namely three, five and seven cycles. The resulting modified electrodes were analysed by CV and EIS in a 2 mM  $[\text{Fe}(\text{CN})_6]^{3-/4-}$  solution with 0.1 M  $\text{KNO}_3$ . Fig. 5.12A illustrates that for three and five electropolymerization cycles the electron transfer (ET) of the redox probe at the electrode surface is unaffected by the modification, while for seven cycles the  $\Delta E_p$  increases with a concurrent decrease of both anodic and cathodic peak current.

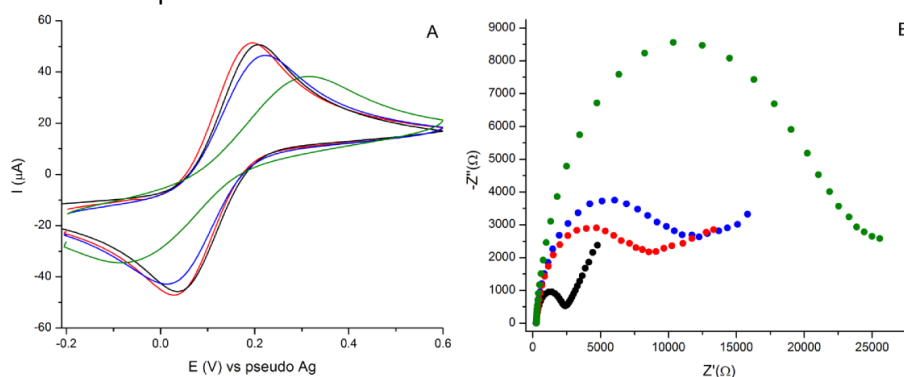


**Fig. 5.12** A) CVs of bare (black line) and oPD modified electrode at different cycles: three (red line), five (blue line) and seven (green line); B) Nyquist plots of bare (black dots) and modified electrode at different cycles: three (red dots), five (blue dots) and seven (green dots). Both set of measurements were performed in 0.1 M  $\text{KNO}_3$  with 2 mM  $[\text{Fe}(\text{CN})_6]^{3-/4-}$ .

This suggests that the modification obtained with seven cycles results in a less conductive film. These observations were confirmed by EIS; the Nyquist plot for the modified electrodes (Fig. 12B) shows an increase in the charge transfer resistance ( $R_{ct}$ ), with increasing number of cycles (from 1920  $\Omega$  for the bare to 7920  $\Omega$  for three cycles, 10540  $\Omega$  for five cycles and 21805  $\Omega$  for seven cycles). The  $R_{ct}$ , in this case, is linked to the presence of the polymer on the surface, which affects the interaction between the mediator in solution and the electrode. The difference between the bare electrode (black dots) and the modified electrodes after three (red dots) and five (blue dots) cycles confirms that the polymer is formed on the surface. However,

all the tested values of electropolymerization cycles (three, five, seven) were considered for further optimization to understand whether the slight loss in conductivity for the film obtained with seven cycles could be instead instrumental to obtain a better response for the modified sensor.

#### **Optimized detection of NAF at oPD-SPE**

The electropolymerization of oPD was studied and optimized in respect to NAF detection with a subset of analytical parameters, following an OVAT approach (one-factor-at-a-time). The number of electropolymerization cycles and the monomer concentration were optimized, with respect to the oxidation peak intensity of NAF and the stability of the polymer. All SWVs were recorded on the modified electrode after 5 min accumulation of the NAF solution in 0.1 M BRB pH 4. This accumulation step promotes the interaction between NAF and the polymer on the electrode surface. Comparing the faradic peak current of the oxidation peak for 20  $\mu\text{M}$  of NAF at different electropolymerization cycles (Fig. 5.13A), the highest current and the lowest error were obtained at five cycles. The fact that for seven cycles the signal (peak current) is much lower confirms the findings about the decrease in conductivity of the surfaces obtained with a higher number of electropolymerization cycles (see oPD-SPE characterization). Looking at the monomer concentration results, in Figure 5.13B, 5 mM of oPD seems the optimal choice, as it gives the highest peak intensity. However the SWV of the modified electrode in 0.1 M BRB pH 4 presented a broad peak around + 1.1 V that hinders the clear attribution of the NAF peak. So among the oPD concentrations 2 mM was selected. The final modification protocol encompasses the electropolymerization for 5 cycles of a 2 mM oPD solution in 0.1 M  $\text{H}_2\text{SO}_4$  and the subsequent analysis of NAF in 0.1 M BRB at pH 4, after 5 min of accumulation.

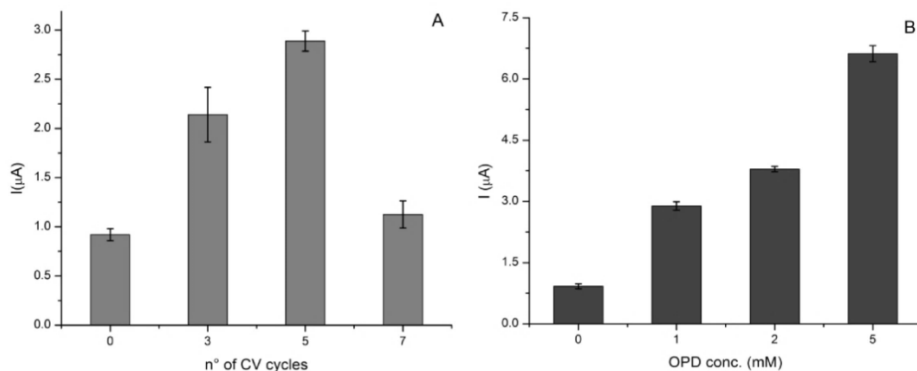


**Fig. 5.13** A) Optimization of electropolymerization cycles, 20  $\mu\text{M}$  NAF in 0.1 M BRB pH 4 with 1 mM oPD B) Optimization of oPD concentration, 20  $\mu\text{M}$  NAF in 0.1 M BRB pH 4, five electropolymerization cycles. SD calculated on  $n=3$ .

The electrochemical response of NAF on the modified electrode, following the optimized protocol, was further investigated. At the oPD modified electrodes, a current enhancing effect was observed by SWV, as shown in Fig. 5.14A. The oxidation peak current for 20  $\mu\text{M}$  of NAF at the oPD-SPE (red line) is 2 times higher than the one on the bare G-SPE (green line). A scan rate study (Fig. 5.14B) was performed with LSV; a linear increase in the peak currents with the scan rate was found and ascribed to the NAF adsorption at the modified electrodes confirming the interaction between NAF and oPD film, as predicted by rational monomer design.

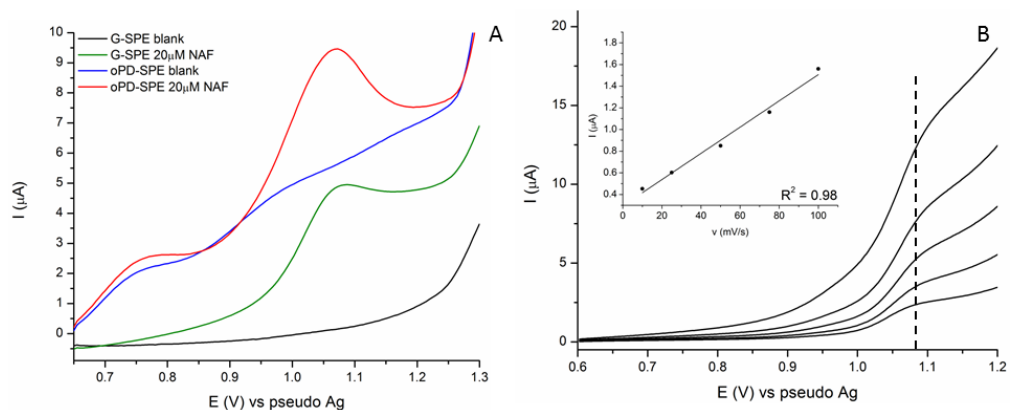


**Fig. 5.14** A) SWV of NAF at bare G-SPE (black line – blank; green line – 20  $\mu\text{M}$  NAF) and oPD-SPE (blue line – blank, red line – 20  $\mu\text{M}$  NAF); B) Scan rate study of 20  $\mu\text{M}$  NAF at oPD-SPE, inset: linear relation  $I_p$  vs  $v$ .

To test the specificity of the interaction between NAF and oPD, two other monomers were tested, namely aniline (ANI) and 4 amino benzoic acid (4-ABA) (see

also Table 5.2). Both monomers were electropolymerized on the surface of G-SPE in the same experimental conditions used for oPD. However the blank SWV response in buffer showed a significant oxidation process at the oxidation potential of NAF, +1.1 V, for both. Thus was not possible to distinguish the oxidation signal of NAF from the background, while for oPD the oxidation peak was clearly visible (see red curve in Fig. 5.14).

### **Interfering compounds and degradation study**

The selectivity of the proposed strategy was tested in respect to other commonly used penicillins, namely AMX, PENG and AMP. As can be seen from Fig. 5.15A, none of the penicillins present a resolved oxidation peak in the potential window of interest (between +0.4 V and +1.3 V). The oxidation of AMX phenolic side chain at +0.7 V is covered by the peaks of the polymer on the surface. The side chains of AMP and PENG are not electroactive and the only oxidation signal that could be present is the one of the core structure at higher potentials (+1.3/1.4 V) The signal of NAF at +1.1 V does not overlap with any other oxidation peaks and thus can be used for the selective identification of the antibiotic. Looking at the oxidation signal of NAF it is also possible to distinguish between the pharmacologically active form of the drug and its degradation products, as already seen in Chapter 2. To verify this hypothesis also on the oPD modified electrodes, alkaline degradation was performed on a 20  $\mu$ M solution of NAF to identify the fingerprint of the degradation products: the pH of the solution was adjusted to 12 and SWVs were acquired at different time points (Fig. 5.15B). After only 1 h of alkaline degradation, the electrochemical response of NAF is affected by the degradation process; apart from the sensible decrease of the NAF peak at +1.1 V, the appearance of a broad peak at +0.6 V is observed. This effect is due to the opening of the  $\beta$ -lactam ring, responsible for the antimicrobial activity (see also Chapter 2).

## Chapter 5 – Biomimetic receptors for antibiotics electroensing

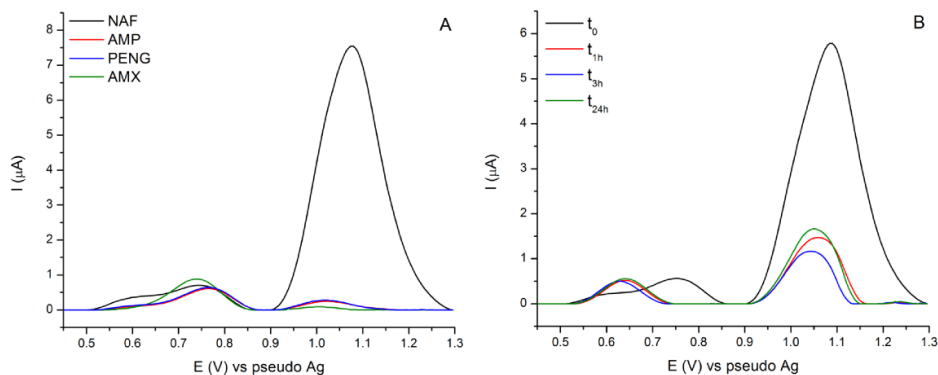


**Fig. 5.15** A) Comparison of the oxidation signals of different penicillins, SWVs of 100 μM of each antibiotics in 0.1 M BRB pH 4 at oPD-SPE; B) SWVs of 20 μM of NAF in 0.1 M BRB pH 4 at different alkaline degradation times (0-black line, 1h-red line, 3h-blue line, 24h-green line) at oPD-SPE.

### Calibration plot

A calibration plot was obtained at a modified oPD-SPE in the concentration range between 100 nM and 20 μM NAF in 0.1 M BRB pH 4 with an  $R^2$  of 0.999 and 80 nM LOD ( $3\sigma_b/m$ ). Comparing the calibration plot obtained at the bare electrode (Fig. 5.16A and B) it is possible to observe an improvement in the sensitivity, going from a LOD of 2 μM at the bare electrode to 80 nM obtained at the modified electrode.

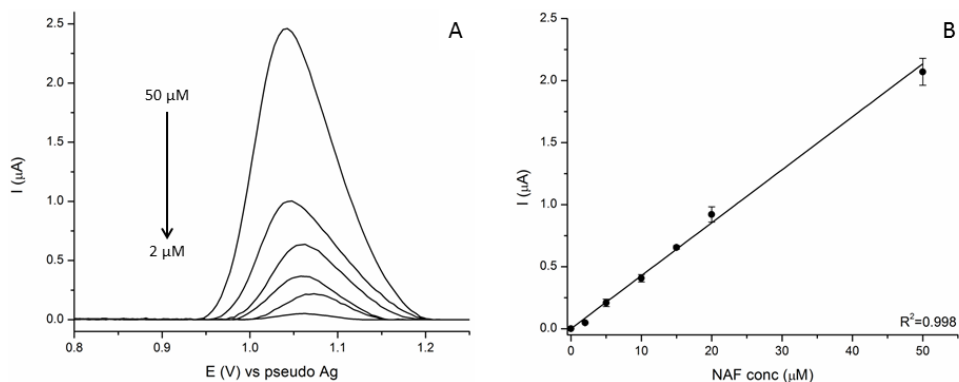


**Fig. 5.16** SWVs (A) and calibration plot (B) for NAF at bare G-SPE in 0.1 M BRB pH4. SD calculated on  $n=3$ .

The linear range is wider at the bare electrode but the modified electrode can reach nanomolar concentration which is the range of antibiotics residue in the food chain and environment. As can be seen from Fig. 5.17A, a saturation behaviour is recorded for concentrations higher than 10 μM; this can be explained by the saturation of the functional group of the polymer present on the surface, able to



interact with the target. In Fig. 5.17B the SWVs, after moving average baseline correction, are shown for the concentrations from 100 nM to 10  $\mu$ M.

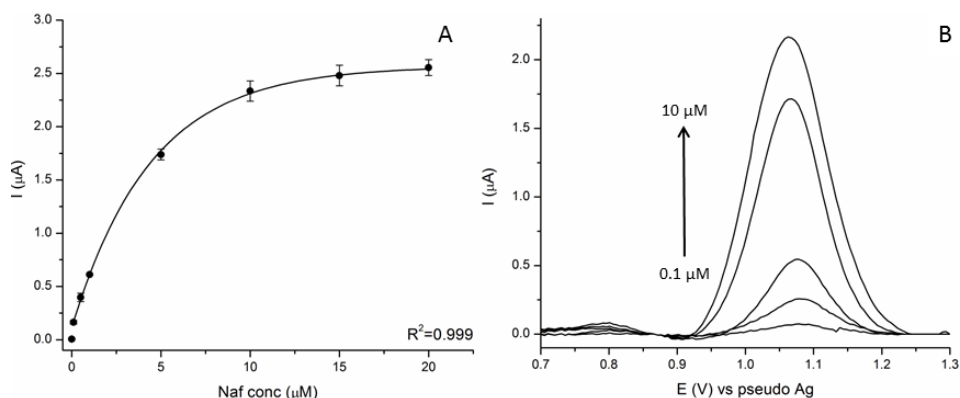


**Fig. 5.17** A) Calibration plot for oPD-SPE; B) SWVs for different concentrations (0.1, 0.5, 1, 5, 10  $\mu$ M) of NAF in 0.1 M BRB pH4 at OPD-SPE. SD calculated on  $n=3$ . Polynomial fit:  $y=a-b \cdot c^x$ .

### Real sample analysis

The modified electrode was tested also in river water sample spiked with 1  $\mu$ M NAF. Sample preparation is reported in Materials and Reagents. The recovery was in the order of 95% with an RSD of 3% on three repeated measurements. The proposed modification is thus suitable for real environmental sample analysis with little sample pretreatment.

### Conclusions

The modification of G-SPE with electropolymerized oPD increased the sensitivity for the electrochemical detection of NAF down to nM level (MRLs range). Moreover the sensor is capable of distinguishing between the active and degraded form of the antibiotic. The selective identification of the target NAF is assured by the oxidation peak of the C7 side chain, as it not overlaps with other penicillin oxidations. The presented modification protocol is rapid, robust and versatile, promising for commercial application and proven to be applicable to real sample analysis.

### Final remarks

Substituted anilines have been employed in the fabrication of polymer modified sensors thanks to the synergy between rational monomer design and electropolymerization experimental optimization. The protocol followed for 4-ABA

based C-MIP was developed to be a blueprint to tackle similar sensor optimizations and the results obtained can be used in different fields, from energy storage application to protective coatings. The direct detection at polymer modified electrode, as in the case of NAF at oPD-SPE, is another inviting approach that, while might lack in selectivity for different targets, proved to be robust and easy to perform on a larger scale. These kind of polymer modified electrodes can be easily integrated in an array for the multi-sensing of different antimicrobial residues at the same time. The proposed strategies combine disposable and low cost screen printed electrodes with robust modification protocols, easy to up-scale for commercial applications. The use of polymers modified electrodes seems the most promising alternative for on-site electrochemical monitoring of antibiotic residues.

**References**

- [1] S. Ansari, Application of magnetic molecularly imprinted polymer as a versatile and highly selective tool in food and environmental analysis: Recent developments and trends, *TrAC - Trends Anal. Chem.* 90 (2017) 89–106.
- [2] S. Boulanouar, S. Mezzache, A. Combès, V. Pichon, Molecularly imprinted polymers for the determination of organophosphorus pesticides in complex samples, *Talanta*. 176 (2018) 465–478.
- [3] N. Karimian, A.M. Stortini, L.M. Moretto, C. Costantino, S. Bogialli, P. Ugo, Electrochemosensor for Trace Analysis of Perfluorooctanesulfonate in Water Based on a Molecularly Imprinted Poly(o-phenylenediamine) Polymer, *ACS Sensors*. 3 (2018) 1291–1298.
- [4] J.O. Mahony, K. Nolan, M.R. Smyth, B. Mizaikoff, Molecularly imprinted polymers—potential and challenges in analytical chemistry, *Anal. Chim. Acta*. 534 (2005) 31–39.
- [5] O.S. Ahmad, T.S. Bedwell, C. Esen, A. Garcia-Cruz, S.A. Piletsky, Molecularly Imprinted Polymers in Electrochemical and Optical Sensors, *Trends Biotechnol.* 37 (2019) 294–309.
- [6] C. Chen, J. Luo, C. Li, M. Ma, W. Yu, J. Shen, Z. Wang, Molecularly Imprinted Polymer as an Antibody Substitution in Pseudo-immunoassays for Chemical Contaminants in Food and Environmental Samples, *J. Agric. Food Chem.* 66 (2018) 2561–2571.
- [7] G. Yang, F. Zhao, Molecularly imprinted polymer grown on multiwalled carbon nanotube surface for the sensitive electrochemical determination of amoxicillin, *Electrochim. Acta*. 174 (2015) 33–40.
- [8] F.W. Scheller, X. Zhang, A. Yarman, U. Wollenberger, R.E. Gyurcsányi, Molecularly imprinted polymer-based electrochemical sensors for biopolymers, *Curr. Opin. Electrochem.* 14 (2019) 53–59.
- [9] A.A. Lahcen, A. Amine, Recent Advances in Electrochemical Sensors Based on Molecularly Imprinted Polymers and Nanomaterials, *Electroanalysis*. 31 (2019) 188–201.
- [10] B. Yang, C. Fu, J. Li, G. Xu, Frontiers in highly sensitive molecularly imprinted electrochemical sensors: Challenges and strategies, *TrAC - Trends Anal. Chem.* 105 (2018) 52–67.
- [11] G. Moro, K. De Wael, L.M. Moretto, Challenges in the electrochemical (bio)sensing of non-electroactive food and environmental contaminants, *Curr. Opin. Electrochem.* (2019).
- [12] A. Martín-Esteban, Recent molecularly imprinted polymer-based sample preparation techniques in environmental analysis, *Trends Environ. Anal. Chem.* 9 (2016) 8–14.

## Chapter 5 – Biomimetic receptors for antibiotics electroensing

- [13] A. Speltini, A. Scalabrini, F. Maraschi, M. Sturini, A. Profumo, Newest applications of molecularly imprinted polymers for extraction of contaminants from environmental and food matrices: A review, *Anal. Chim. Acta.* 974 (2017) 1–26.
- [14] R. Gui, H. Jin, H. Guo, Z. Wang, Recent advances and future prospects in molecularly imprinted polymers-based electrochemical biosensors, *Biosens. Bioelectron.* 100 (2018) 56–70.
- [15] N. Alizadeh, A. Salimi, Ultrasensitive Bioaffinity Electrochemical Sensors: Advances and New Perspectives, *Electroanalysis.* 30 (2018) 2803–2840.
- [16] P. Yáñez-Sedeño, S. Campuzano, J.M. Pingarrón, Electrochemical sensors based on magnetic molecularly imprinted polymers: A review, *Anal. Chim. Acta.* 960 (2017) 1–17.
- [17] C. Malitesta, E. Mazzotta, R.A. Picca, A. Poma, I. Chianella, S.A. Piletsky, MIP sensors - The electrochemical approach, *Anal. Bioanal. Chem.* 402 (2012) 1827–1846.
- [18] E.V. Piletska, A.R. Guerreiro, M.J. Whitcombe, S.A. Piletsky, Influence of the polymerization conditions on the performance of molecularly imprinted polymers, *Macromolecules.* 42 (2009).
- [19] J. Heinze, Electronically Conducting Polymers, *Top. Curr. Chem.* . 152 (1990) 1–47.
- [20] M.H. Naveen, N.G. Gurudatt, Y.B. Shim, Applications of conducting polymer composites to electrochemical sensors: A review, *Appl. Mater. Today.* 9 (2017) 419–433.
- [21] X. Li, M. Huang, W. Duan, Y. Yang, Novel Multifunctional Polymers from Aromatic Diamines by Oxidative Polymerizations, *Chem. Rev.* 102 (2002) 2925–3030.
- [22] W. Song, Y. Chen, J. Xu, X. Yang, D.B. Tian, Dopamine sensor based on molecularly imprinted electrosynthesized polymers, *J Solid State Electrochem.* 14 (2010) 1909–1914.
- [23] N. Karimian, M. Vagin, M. Hossein, A. Zavar, M. Chamsaz, A.P.F. Turner, A. Tiwari, An ultrasensitive molecularly-imprinted human cardiac troponin sensor, *Biosens. Bioelectron.* 50 (2013) 492–498.
- [24] N. Karimian, A.M. Stortini, L.M. Moretto, C. Costantino, S. Bogialli, P. Ugo, Electrochemosensor for Trace Analysis of Perfluorooctanesulfonate in Water Based on a Molecularly Imprinted Poly( *o* -phenylenediamine) Polymer, *ACS Sensors.* (2018) accsensors.8b00154.
- [25] S. Han, B. Li, Z. Song, S. Pan, Z. Zhang, H. Yao, S. Zhu, G. Xu, A kanamycin sensor based on an electrosynthesized molecularly imprinted poly-*o*-phenylenediamine film on a single-walled carbon nanohorn modified glassy carbon electrode, *Analyst.* 142 (2017) 218–223.

## Chapter 5 – Biomimetic receptors for antibiotics electroensing

- [26] K.L. Baker, F.B. Bolger, J.P. Lowry, A microelectrochemical biosensor for real-time in vivo monitoring of brain extracellular choline, *Analyst*. 140 (2015) 3738–3745.
- [27] A. Khan, S.A. Ghani, Multienzyme microbiosensor based on electropolymerized o-phenylenediamine for simultaneous in vitro determination of acetylcholine and choline, *Biosens. Bioelectron.* 31 (2012) 433–438.
- [28] A. Florea, T. Cowen, S. Piletsky, K. De Wael, Polymer platforms for selective detection of cocaine in street samples adulterated with levamisole, *Talanta*. 186 (2018) 362–367.
- [29] J. Wang, M. Wang, J. Guan, C. Wang, G. Wang, Construction of a non-enzymatic sensor based on the poly(o-phenylenediamine)/Ag-NPs composites for detecting glucose in blood, *Mater. Sci. Eng. C*. 71 (2017) 844–851.
- [30] F. Bates, M.C. Cela-Pérez, K. Karim, S. Piletsky, J.M. López-Vilariño, Virtual Screening of Receptor Sites for Molecularly Imprinted Polymers, *Macromol. Biosci.* 16 (2016) 1170–1174.
- [31] T. Cowen, K. Karim, S. Piletsky, Computational approaches in the design of synthetic receptors – A review, *Anal. Chim. Acta*. 936 (2016) 62–74.
- [32] X.G. Li, M.R. Huang, W. Duan, Y.L. Yang, Novel multifunctional polymers from aromatic diamines by oxidative polymerizations, *Chem. Rev.* 102 (2002) 2925–3030.
- [33] J.G. Pacheco, P. Rebelo, F. Cagide, L.M. Gonçalves, F. Borges, J.A. Rodrigues, C. Delerue-Matos, Electrochemical sensing of the thyroid hormone thyronamine (TOAM) via molecular imprinted polymers (MIPs), *Talanta*. 194 (2019) 689–696.
- [34] F. Lopes, J.G. Pacheco, P. Rebelo, C. Delerue-Matos, Molecularly imprinted electrochemical sensor prepared on a screen printed carbon electrode for naloxone detection, *Sensors Actuators, B Chem.* 243 (2017) 745–752.
- [35] L.F. Ferreira, C.C. Santos, F.S. da Cruz, R.A.M.S. Correa, R.M. Verly, L.M. Da Silva, Preparation, characterization, and application in biosensors of functionalized platforms with poly(4-aminobenzoic acid), *J. Mater. Sci.* 50 (2015) 1103–1116.
- [36] F. Ma, Y. Chen, Y. Zhu, J. Liu, Electrogenerated chemiluminescence biosensor for detection of mercury (II) ion via target-triggered manipulation of DNA three-way junctions, *Talanta*. 194 (2019) 114–118.
- [37] M. Shamsipur, L. Samandari, A. (Arman) Taherpour, A. Pashabadi, Sub-femtomolar detection of HIV-1 gene using DNA immobilized on composite platform reinforced by a conductive polymer sandwiched between two nanostructured layers: A solid signal-amplification strategy, *Anal. Chim. Acta*. 1055 (2019) 7–16.
- [38] S. Guerrero, L. Agúí, P. Yáñez-Sedeño, J.M. Pingarrón, Oxidative grafting vs. monolayers self-assembling on gold surface for the preparation of electrochemical

## Chapter 5 – Biomimetic receptors for antibiotics electrosensing

- immunosensors. Application to the determination of peptide YY, *Talanta*. 193 (2019) 139–145.
- [39] L. Adamczyk, A. Pietrusiak, H. Bala, Corrosion resistance of stainless steel covered by 4-aminobenzoic acid films, *Cent. Eur. J. Chem.* 10 (2012) 1657–1668.
- [40] A. Yadav, R. Kumar, H.K. Choudhary, B. Sahoo, Graphene-oxide coating for corrosion protection of iron particles in saline water, *Carbon N. Y.* 140 (2018) 477–487.
- [41] J. Liu, L. Cheng, B. Liu, S. Dong, Covalent modification of a glassy carbon surface by 4-aminobenzoic acid and its application in fabrication of a polyoxometalates-consisting monolayer and multilayer films, *Langmuir*. 16 (2000) 7471–7476.
- [42] C. Thiemann, C.M.A. Brett, Electrosynthesis and properties of conducting polymers derived from aminobenzoic acids and from aminobenzoic acids and aniline, *Synth. Met.* 123 (2001) 1–9.
- [43] M.H. Naveen, N.G. Gurudatt, Y.B. Shim, Applications of conducting polymer composites to electrochemical sensors: A review, *Appl. Mater. Today*. 9 (2017) 419–433.
- [44] J.G. Ibanez, M.E. Rincón, S. Gutierrez-Granados, M. Chahma, O.A. Jaramillo-Quintero, B.A. Frontana-Urbe, Conducting Polymers in the Fields of Energy, Environmental Remediation, and Chemical–Chiral Sensors, *Chem. Rev.* 118 (2018) 4731–4816.
- [45] F. Yañez, I. Chianella, S.A. Piletsky, A. Concheiro, C. Alvarez-Lorenzo, Computational modeling and molecular imprinting for the development of acrylic polymers with high affinity for bile salts, *Anal. Chim. Acta.* 659 (2010) 178–185.
- [46] N. Slegers, A.L.N. van Nuijs, M. van den Berg, K. De Wael, Cephalosporin Antibiotics: Electrochemical Fingerprints and Core Structure Reactions Investigated by LC-MSMS, *Anal. Chem.* (2019).
- [47] G. Camurri, P. Ferrarini, R. Giovanardi, R. Benassi, C. Fontanesi, Modelling of the initial stages of the electropolymerization mechanism of o-phenylenediamine, *J. Electroanal. Chem.* 585 (2005) 181–190.
- [48] G. Kortum, *Dissociation Constants of Organic Acids in Aqueous Solution*, International Union of Pure and Applied Chemistry, 1961.
- [49] E.P. Serjeant, B. Dempsey, *Ionization constants of organic acids in aqueous solution.*, (1979) 321.
- [50] D. Vanossi, L. Pigani, R. Seeber, P. Ferrarini, P. Baraldi, C. Fontanesi, Electropolymerization of ortho-phenylenediamine . Structural characterisation of the resulting polymer film and its interfacial capacitive behaviour, *J. Electroanal. Chem.* 710 (2013) 22–28.

## Chapter 5 – Biomimetic receptors for antibiotics electroensing

- [51] H. Dai, Q. Wu, S. Sun, K. Shiu, Electrochemical quartz crystal microbalance studies on the electropolymerization processes of ortho -phenylenediamine in sulfuric acid solutions, *J. Electroanal. Chem.* 456 (1998) 47–59.
- [52] M. Zhou, J. Heinze, Electropolymerization of Pyrrole and Electrochemical Study of Polypyrrole. 2. Influence of Acidity on the Formation of Polypyrrole and the Multipathway Mechanism, *J. Phys. Chem. B.* 103 (1999) 8443–8450.
- [53] M. Babaiee, M. Pakshir, B. Hashemi, Effects of potentiodynamic electropolymerization parameters on electrochemical properties and morphology of fabricated PANI nanofiber/graphite electrode, *Synth. Met.* 199 (2015) 110–120.
- [54] M. Zhou, J. Heinze, Electropolymerization of Pyrrole and Electrochemical Study of Polypyrrole. 2. Influence of Acidity on the Formation of Polypyrrole and the Multipathway Mechanism, *J. Phys. Chem. B.* 103 (2002) 8443–8450.
- [55] N. Slegers, A.L.N. Van Nuijs, M. Van Den Berg, K. De Wael, Cephalosporin Antibiotics: Electrochemical Fingerprints and Core Structure Reactions Investigated by LC-MS/MS, *Anal. Chem.* 91 (2019) 2035–2041.
- [56] B.-X. Ye, W.-M. Zhang, X.-Y. Zhou, Electrochemical characteristics of poly(o-phenylenediamine) film electrodes in phosphatic solution, *Chinese J. Chem.* 15 (2010) 343–352.
- [57] I. Losito, F. Palmisano, P.G. Zamboni, o-Phenylenediamine Electropolymerization by Cyclic Voltammetry Combined with Electrospray Ionization-Ion Trap Mass Spectrometry, *Anal. Chem.* 75 (2003) 4988–4995.
- [58] S.A. Rothwell, C.P. McMahon, R.D.O. Neill, Effects of polymerization potential on the permselectivity of poly (o-phenylenediamine) coatings deposited on Pt – Ir electrodes for biosensor applications, *Electrochim. Acta.* 55 (2010) 1051–1060.
- [59] S.A. Rothwell, R.D.O. Neill, Effects of applied potential on the mass of non-conducting poly(ortho-phenylenediamine) electro-deposited on EQCM electrodes: comparison with biosensor selectivity parameters, *Phys. Chem. Chem. Phys. PCCP.* 13 (2011) 5413–5421.
- [60] D. Vanossi, L. Pigani, R. Seeber, P. Ferrarini, P. Baraldi, C. Fontanesi, Electropolymerization of ortho-phenylenediamine. Structural characterisation of the resulting polymer film and its interfacial capacitive behaviour, *J. Electroanal. Chem.* 710 (2013) 22–28.
- [61] C. Barbero, J.J. Silber, L. Sereno, Formation of a novel electroactive film by electropolymerization of ortho-aminophenol: Study of its chemical structure and formation mechanism. Electropolymerization of analogous compounds, *J. Electroanal. Chem. Interfacial Electrochem.* 263 (1989) 333–352.
- [62] L. Nadjo, J.M. Savéant, Electrodimerization: VIII. Role of proton transfer reactions in

## Chapter 5 – Biomimetic receptors for antibiotics electroensing

the mechanism of electrohydrodimerization formal kinetics for voltammetric studies (linear sweep, rotating disc, polarography), *J. Electroanal. Chem. Interfacial Electrochem.* 44 (1973) 327–366.





# Electrochemistry in milk

---

The use of electrochemical (bio)sensors for the analysis of antibiotics residues in milk is almost always preceded by pretreatments of the milk, physical or chemical in nature. To fully exploit the potentialities of these analytical tools for on-site, real sample analysis, the use of undiluted raw milk should be preferred. The work on real milk samples followed two parallel routes: (1) the development of a pretreatment protocol along with (2) the study of  $\beta$ -lactam antibiotics electrochemistry in undiluted raw milk. From the literature, two possible pretreatments based on the simultaneous extraction and deproteinization of milk samples have been selected (Holstage and Paniel protocol). Both are based on the addition of an organic solvent (acetonitrile ACN and isopropanol ISO) and a successive dilution of the extract in buffers. The detection of CFQ in milk was achieved with a simplified pretreatment protocol, applicable to on-site analysis.

To avoid sample pretreatments altogether, we also studied the electrochemistry of antibiotics in undiluted raw milk. We proved that a milk matrix supports electrochemistry, however with intensities of the oxidation currents being much lower than in buffer. One of the reasons identified for this decrease was the presence of chloride ions, which have a detrimental effect on the performance of the screen printed electrodes employed. Trying to overcome this problem, while keep using the low-cost and disposable screen printed electrodes, we devised a strategy based on the addition of a very high concentration of another salt ( $\text{KNO}_3$ ) to the undiluted raw milk. Further studies are in progress to ascertain the mechanism of said interactions, but the proposed protocol gave very good results so far. We were able to detect NAF, CFQ and CFU in the micromolar range at bare graphite SPE in undiluted raw milk. To the best of our knowledge this is the first report of electrochemistry of said antibiotics in undiluted raw milk.

Milk is a complex food matrix consisting of a water soluble part rich in proteins and sugars emulsified with lipids that constitute the fat fraction [1]. It is one of the most commonly tested real matrices in the field of bioanalytical chemistry, with focus on (bio)sensing applications, along with urine or blood [2–4]. Milk is readily available, can be easily handled and stored with many examples of pretreatment or sample preparation protocols known, all aiming to minimize matrix interferences. Commonly the milk is first deproteinized and/or defatted and then diluted with a

buffer or dH<sub>2</sub>O. Many different physical and chemical pretreatments are used [5], ranging from simple centrifugation [6] to solid phase extraction (SPE) [7], solvent or acid addition [8] to complex multi-composite reagents [9]. The direct analysis of raw, untreated milk is rare and most of these examples deal with the qualitative control of processed milk to verify the presence of adulterants such as melamine and urea [10–12] or liquid whey [13]; for the quantification of lactate [14,15] or progesterone [16] or to detect contaminants such as antibiotics [17].

As far as interfering compounds are concerned, proteins and fats can seize the target drug from the sample, entrapping it inside the structure of fat globules or protein micelles. This effect is related to the solubility of the target molecules and can be somehow foreseen, as for progesterone that is highly fat-soluble and thus prone to be sequestered by milk lipids [16]. Other common problems are fouling phenomena of the electrode surface; relatively large aggregates of fats and proteins can adsorb onto the electrode, hindering the electron transfer and decreasing the analyte signal [18]. Also water soluble components, such as inorganic salts and vitamins, can contribute to the matrix effect in different ways. For example some vitamins are electroactive and thus can contribute to the background signal of the blank or hinder the clear attribution of the redox peak of the target molecules [19]. For these reasons a pretreatment has to remove both seizing agents and possible electroactive compounds.

$\beta$ -lactam antibiotics tend to accumulate in the skim milk fraction [20], especially after intramammary administration of the drugs [21]. They will coexist in the hydrophilic phase of the milk along with other water soluble compounds such as whey proteins, sugars, vitamins and minerals. The total soluble salt concentration of milk is around 150 mM [22,23] which could act as supporting electrolyte for the electrochemical measurement. The supporting electrolyte plays a fundamental role in electrochemistry: it reduces the Ohmic drop effect and assures that the investigated system is only under diffusion control, suppressing the migration of electroactive species [24]. Moreover, the concentration and the nature of the electrolyte can influence the electrochemical response significantly [25,26].

In this chapter the detection of  $\beta$ -lactam antibiotics in milk will be attempted using different pretreatments, also in raw undiluted milk. The detrimental effect of chloride ions on the electrochemical oxidation of  $\beta$ -lactam antibiotics on commercial screen printed electrodes will be highlighted, and a strategy will be proposed to overcome this issue.

## Materials and methods

NAF, CFQ, CFU, ISO and ACN were purchased from Sigma Aldrich Ltd. Raw cow milk samples were obtained from the Instituut voor Landbouw-, Visserij- en Voedingsonderzoek (ILVO) (Melle, Belgium). All the other chemicals were analytical grade and used as received. All aqueous solutions were prepared using MilliQ water ( $R > 18 \text{ M}\Omega\text{cm}$ ). PB 0.1 M pH 6.8 was prepared by mixing stock solutions of 0.1 M  $\text{NaH}_2\text{PO}_4$  and 0.1 M  $\text{Na}_2\text{HPO}_4$ , purchased from Sigma Aldrich. 0.1 M phosphate buffer pH 2 was obtained by mixing stock solution of 0.1 M  $\text{NaH}_2\text{PO}_4$  and concentrated phosphoric acid. G-SPE were purchased from Dropsens (Metrohm, Belgium). All potentials are referred to the pseudo Ag internal reference electrode, which is -200 mV in respect to a saturated calomel electrode (SCE).

Glassy carbon (GC) electrodes (BASI, USA) were polished to a mirror finish with 0.3, 0.1 and 0.05  $\mu\text{m}$  alumina slurries and sonicated in MilliQ water to remove all the residues. These electrodes were used as WE in a conventional three-electrode cell setup with a platinum wire counter electrode and SCE reference electrode. Electrochemical measurements were performed with a PalmSens3 portable potentiostat connected with a MUX8-R2 Multiplexer controlled by the PsTrace5 software (PalmSens BV, The Netherlands) and with an Autolab potentiostat/galvanostat (PGSTAT 302N, ECOCHEMIE, the Netherlands) controlled by NOVA 1.1 software. CV was performed between -0.4 V and +0.6 V at 50 mV/s scan rate; EIS was performed between 100 kHz and 0.1 Hz with 50 frequencies per decade, amplitude of 0.01 V and bias potential determined by OCP; SWV was performed between +0.4 and +1.5 V, 1 mV step potential, 25 mV amplitude and different frequency values (5, 10, 25, 50 Hz). All results obtained by SWV are presented after baseline correction using the moving average algorithm to improve the visualization and identification of the peaks over the baseline.

## Milk pretreatments evaluation

CV studies were performed with a scan rate of 50 mV/s, using different potential ranges: from -1.2 to +1.5 V in presence of ACN and from -1.2 to +1.2 V with ISO. SWV measurements were carried out in the following conditions: step potential of 5 mV, amplitude of 50 mV and frequency of 50 Hz, a potential window from +0.4 to +1.3 V. Pre-treatments protocols were selected from the literature and are briefly described below. All milk samples were thoroughly homogenized before each experiment.

- Holstage extraction protocol [8]:
  - Initial addition of ACN (1:1) to the milk sample in a 2 ml vial. The sample was vortexed for 60 s and transferred in a 10 mL falcon tube.
  - A second addition of ACN (2:1) was performed, followed by mixing for 60 s. The precipitation of protein residue at the bottom of the tube was clearly observed.
  - The sample was centrifuged at 300 g for 5 min. The supernatant, a clear extract, was transferred to a clean 10 mL falcon tube.
  - The extract was then evaporated for 2 h using a stream of N<sub>2</sub> at RT to pre-concentrate the target.
  - After the pre-concentration, the extract was diluted with 0.1 M phosphate buffer (PB) pH 2.
- Paniel protocol [27]:
  - The sample was mixed with ISO (1:1) in 2 mL vial.
  - The mixture was then diluted with 0.1 M PB pH 2 and filtered with a 0.45 µm cellulose acetate membrane (Whatman) in a 10 mL syringe to remove the non-water soluble compounds dispersed in the supernatant organic phase.

The recovery study was performed on milk samples (1 mL each) spiked with 100 µM of CFQ concentration before the pretreatments. The difference between the measured concentrations and the theoretical one, for the different samples (average of three measurements) was used to determine the recovery rate for all protocols.

## Results and Discussion

### Electrochemical behaviour of ACN and ISO in 0.1 M PB pH 2 and whole milk

The pretreatment protocols chosen are based on the addition of an organic solvent and a successive dilution of the extract in buffer. To test their applicability, the electrochemical behaviour of the organic solvents involved was first investigated in combination with 0.1 M PB pH 2 [28,29]. ACN and ISO at different solvent:buffer ratios were analysed by CV on G-SPE.

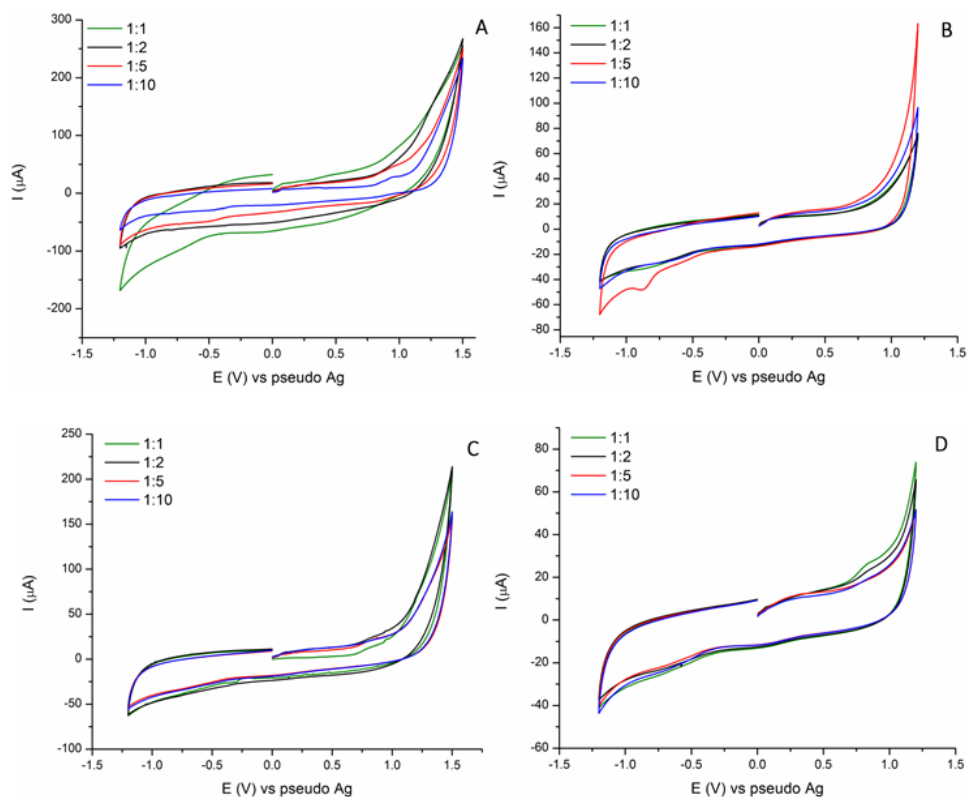


**Fig. 6.1** A) CVs of ACN:PB pH 2 binary mixture obtained at 50 mV/s; B) CVs of ISO:PB pH 2 binary mixture obtained at 50 mV/s; C) CVs of milk:ACN, 1:1 with different dilutions in PB pH 2 obtained at 50 mV/s; D) CVs of milk:ISO, 1:1 with different dilutions in PB pH 2 obtained at 50 mV/s (D).

Fig. 6.1A-B shows that no oxidation or reduction peaks are present in the blank at different solvent:buffer ratios. For ACN, an increase in the capacitive current was observed; the increase is proportional to the ratio of the solvent, underlining the increase in resistance to electron transfer. This is expected considering the dilution effect on the supporting electrolyte of the buffer; it is worth reminding here that the buffer has no added salt and relies only on the ions of the phosphate salts themselves. For the ISO no differences in the capacitive current were observed at different dilutions. No specific signal is observable in the region of interest, making both solvents, in combination with 0.1 M PB pH 2, suitable for the present application.

A second screening of milk:solvent, 1:1, solutions with increasing additions of 0.1 M PB pH 2 was performed. In this test, only the organic supernatant phase was analysed, while the white residues precipitated during the centrifugation were

discarded. The results, presented in Fig. 6.1D-C, show that it is possible to perform CV, with no particular high capacitive currents, suggesting that the possible fouling agents have been removed. In both cases, it is possible to observe small waves in the potential region between +0.8 and +1 V. These peaks can be related to electroactive components of the milk matrix, which are however disappearing with increasing buffer:extract ratio (as expected due to the dilution effect). Concerning the ISO:milk solutions in PB, it is possible to observe that the capacitive current is higher than for ISO:PB only. For 1:1 and 1:2 ratio of 0.1 M PB pH 2 dilutions, a peak at +1 V is clearly visible, its intensity decreasing at higher PB ratios until it disappears, as can be seen for the CV of the 1:5 and 1:10 solution. This first screening was needed because no literature about the electrochemical behaviour of this kind of mixtures was found. The electrochemistry of milk has been investigated only via the behaviour of different redox probes [30], but no complete studies regarding electrochemistry of milk in combination with organic solvents or buffers have been described.

### **Electrochemical behaviour of CFQ in ACN and ISO**

Even if the addition of organic solvents does not modify the pH of the buffer in a sensible way (with an experimental uncertainty on the pH value of  $\pm 0.4$ ) the electrochemical behaviour of the target CFQ was tested in presence of different solvent:buffer ratios to assure the reliability of the signal on which the target identification is based (oxidation peak at +0.6/+0.75 V). The different solvent:buffer solutions were spiked with 500  $\mu\text{M}$  of CFQ and analysed with SWV. In all the tested solutions, the analyte signal was found to be present even at a slightly different potential and with different current intensities (Fig. 6.2). For ACN the peak potential increases for 1:1 and 1:2 ratios, decreasing again for a higher dilution factor (1:5 and 1:10) (black squares in Fig. 6.2A). For ISO after an increase for the 1:1 dilution ( $E_p$  of +0.75 V) the value remain almost constant with only a small decrease for the 1:10 ratio (white dots in Fig. 6.2A).

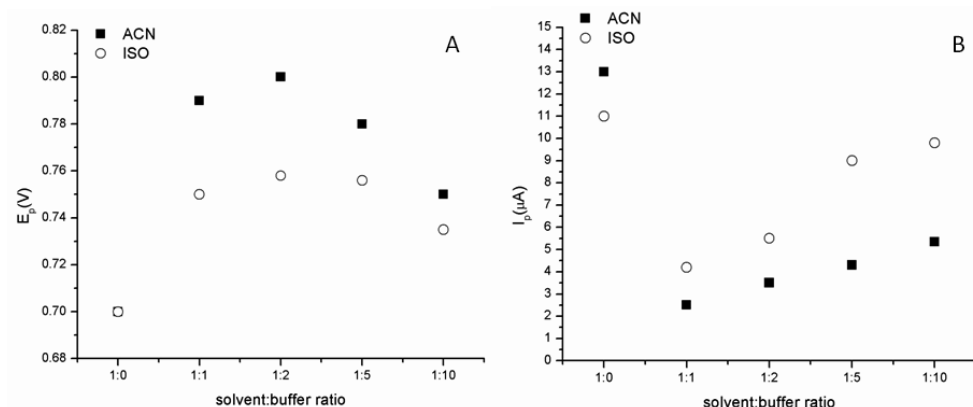


**Fig. 6.2**  $E_p$  vs. solvent:PB pH 2 ratio (A),  $I_p$  vs. solvent:PB pH 2 ratio (B). Data obtained from CVs of 500  $\mu$ M of CFQ in solvent:PB pH2 at different ratios with  $v=50$  mV/s.

In general, this variation is in the order of 0.04 V and it does not represent a problem for the identification of the target. Concerning the intensity of the signal, its variations are presented in Fig. 6.2B for both ACN and ISO. In presence of higher concentration of 0.1 M PB pH 2, for a constant CFQ concentration in the final solution, the intensity of the signal increase, even if never reaching the current of CFQ in pure buffer. The obtained results confirm the possibility to combine both solvents with the target in an eventual pre-treatment step.

### Simplified pre-treatment

The two pre-treatment protocols mentioned in the introduction were first tested as such to verify their ability to remove electroactive interfering species and assure the recognition of CFQ [8,31]. The obtained extracts were spiked with 500  $\mu$ M of CFQ before performing different dilutions with the 0.1 M PB pH 2. Also for this test, the results are presented in terms of  $E_p$  and  $I_p$  variations (Fig. 6.3A-B). The anodic peak potentials are in the range between +0.81 and +0.80 V for the ISO pre-treated samples and in between +0.75 and +0.78 V for the ACN ones. The peak current decreased with increasing amounts of buffer added, showing that the decrease is only due to dilution effects of the original CFQ concentration.



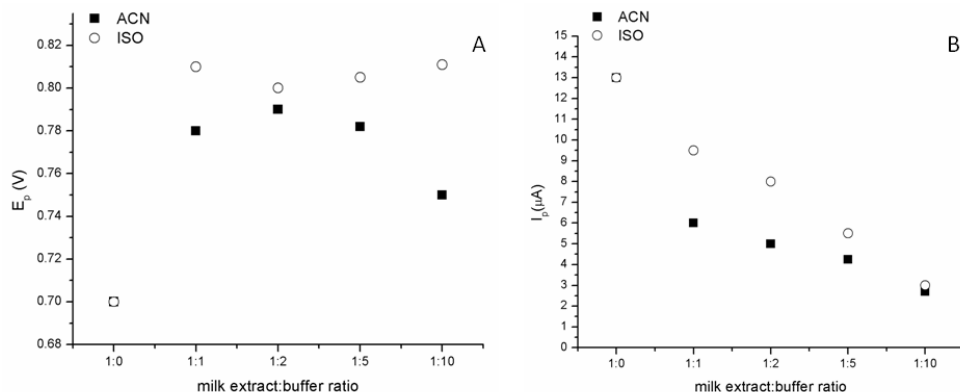


**Fig. 6.3**  $E_p$  vs. milk extract:buffer plot (A),  $I_p$  vs. milk extract:buffer plot (B). Data obtained from CVs of 500  $\mu$ M of CFQ in pre-treated milk extract with different PB pH 2 ratios at 50 mV/s.

From this comparison, it was possible to confirm the applicability of both protocols and the suitability of both solvents. Moreover, the 1:1 ratio between milk extract and buffer is already sufficient to obtain a good electrochemical signal for CFQ without diluting the samples too much.

The tested protocols (Holsatge and Paniel) were then simplified to a 1:1 solvent addition, followed by 15 min decantation, and filtration with a disposable syringe filter. These two simplified protocols were named New ACN and New ISO. The 15 min decantation was used to substitute the centrifugation steps proposed in the Holsatge protocol while the filtration step with the syringe was taken from the Paniel pre-treatment. The aim was to obtain an effective pre-treatment limiting as much as possible the need for laboratory equipment (like centrifuge) and the cost of the whole procedure. To evaluate the performance of the considered pretreatments a recovery study was performed spiking milk samples with 100  $\mu$ M of CFQ before each pretreatment. Since the dilution between milk extract and buffer is 1:1 for all the pretreatments, the final CFQ concentration detected is 50  $\mu$ M. In Fig. 6.4 is reported the percentage recovery for each pretreatment considering the dilution effect.

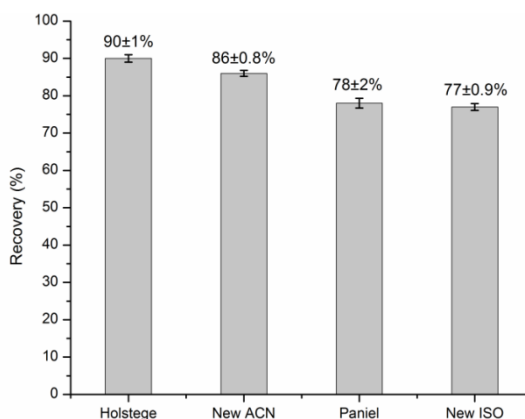


**Fig. 6.4** Comparison of the recovery rate for 100  $\mu\text{M}$  CFQ in pre-treated milk solutions with a 1:1 dilution in 0.1 M PB pH 2 using 4 different pre-treatment protocols. Error bars calculated on three repeated measurements. SD calculated on  $n=3$

The result for the first simplified pretreatment – New ACN – shows a small decrease (4%) in the recovery compared to the one obtained with the Holstage pretreatment (90±1%), also using ACN as solvent. The difference in recovery rate is less evident between the Paniel and the New ISO protocol (1.5%). However, this comparison allows to conclude that a simplified pretreatment is enough to obtain good results. An average recovery value of 86±0.8 % and 77±0.9% were obtained respectively using New ACN and New ISO, values in lines with the expected recovery rates for real sample analysis (60-140%) [32]. New ACN gives the best results in term of recovery and reproducibility and thus is most suitable in the present application. Also New ISO gave satisfying results; this pretreatment might be useful when the use of ACN is not possible for technological or safety limitation. For examples some inks for SPE are more sensitive to ACN compare to ISO. Also ISO is less a harmful solvent, thus more safe for the operator and the environment.

### **Electrochemistry in undiluted raw milk - Effect of chloride ions on $\beta$ -lactam antibiotics electrochemistry in buffer solutions**

The effect of the presence of chloride ions in the supporting electrolyte on the electrochemical fingerprint of  $\beta$ -lactams antibiotics on G-SPE is illustrated in Fig. 6.5. The peaks present can be ascribed to the oxidation of the active side chain of each antibiotic, namely the 2-ethoxy-1-naphthalene (2E1N) group for NAF at +1.1 V (Fig. 6.5A) and the thiazoximic side chain in the C7 position for CFQ and CFU at +0.5/0.6 V (Fig. 6.5B and C). For all antibiotics under study, and in the presence of chloride ions, a shift in the oxidation process towards more positive potentials is

observed coupled with a sensible decrease in current. Electrolytes containing a different anion, namely  $\text{KNO}_3$  and  $\text{Na}_2\text{SO}_4$ , did not affect the original electrochemical response obtained in the PB buffer solution. On the contrary, for NAF and CFQ, the addition of other electrolytes resulted in a slight increase in peak current.  $\beta$ -lactam electrochemistry is dependent on pH, with the best results obtained for acidic pH values (pH 4 for NAF [33] and pH 2 for CFQ and CFU [34]). Nevertheless, at pH 6.8, which is the usual pH of milk, all the considered antibiotics showed a clear electrochemical signal.

The shift in potential observed when  $\text{Cl}^-$  ions are present in the electrolyte solution can be explained by the reference electrode employed. The pseudo Ag reference of the G-SPE, in presence of  $\text{Cl}^-$ , will act as an Ag/AgCl reference, stabilizing the potential and shifting it towards positive values. However the effect on the peak intensity is more difficult to ascertain: the presence of the  $\text{Cl}^-$  ions could affect the working electrode surface or interact directly with the  $\beta$ -lactam antibiotics. Carbon screen printed electrodes are sometimes coated with a uniform layer of silver paste, to increase the conductivity and fabricate the contact to connect the electrode to the potentiostat. As already seen for the reference electrode made with Ag paste, this Ag layer might be influenced by the presence on chloride ions and affect the electrochemical determination of the antibiotics.

## Chapter 6 – Electrochemistry in milk

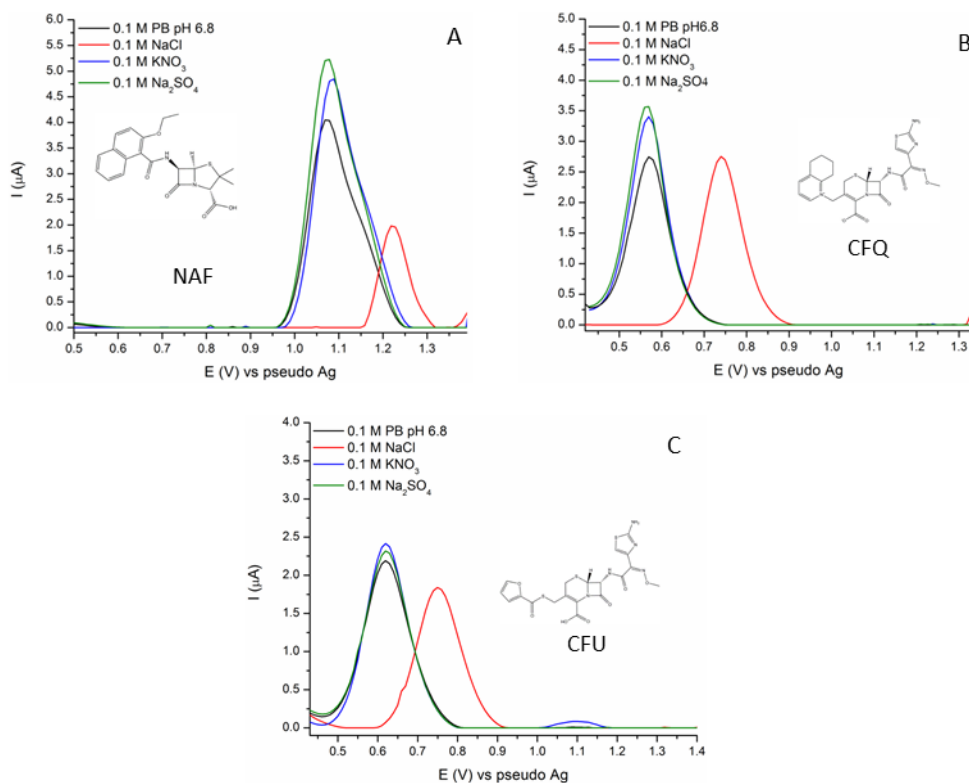


**Fig. 6.5** Representative SWVs for 500  $\mu\text{M}$  of NAF (A), CFQ (B) and CFU (C) in different buffer solutions; 0.1 M PB pH 6.8 (black line) and with the addition of 0.1 M NaCl (red line), 0.1 M  $\text{KNO}_3$  (blue line) and 0.1 M  $\text{Na}_2\text{SO}_4$  (green line). SWVs were recorded with a frequency of 10 Hz.

To ascertain whether the effect of  $\text{Cl}^-$  on the peak current intensity could be ascribed to some interaction with the G-SPE electrode, the experiment was repeated using a GC electrode as working electrode, SCE as reference and a platinum wire as counter electrode – conventional three electrodes cell setup.

## Chapter 6 – Electrochemistry in milk

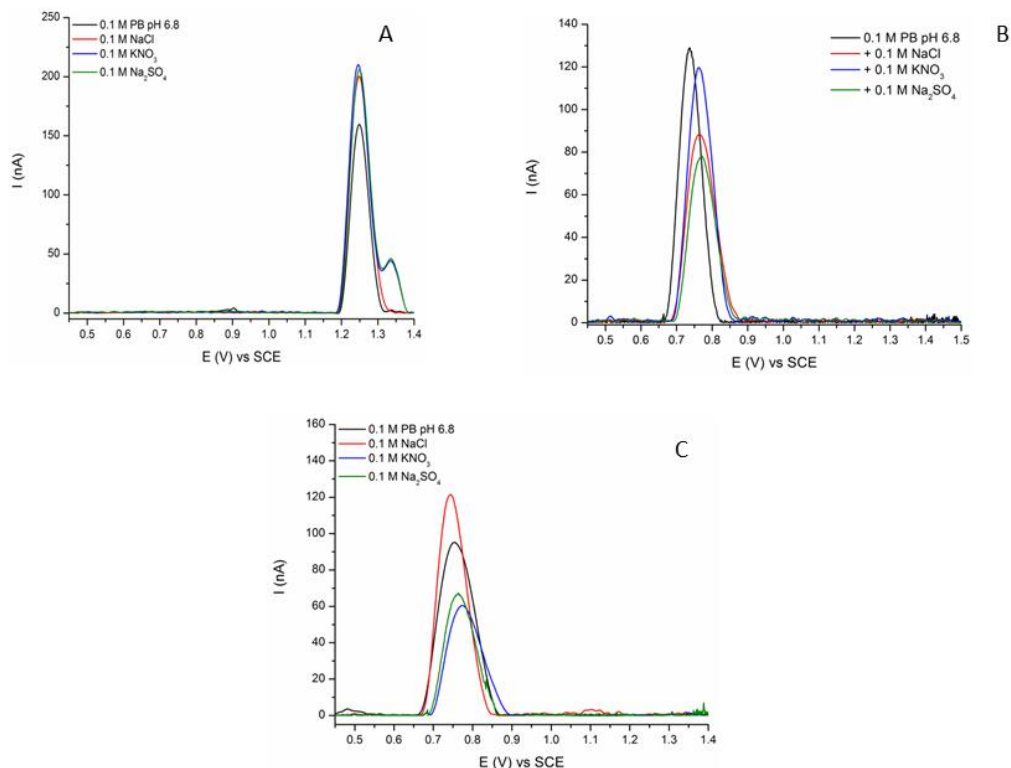


**Fig. 6.6** Representative SWVs for 100  $\mu\text{M}$  of NAF (A), CFQ (B) and CFU (C) in different buffer solutions at GC electrode; 0.1 M PB pH 6.8 (black line) and with the addition of 0.1 M NaCl (red line), 0.1 M  $\text{KNO}_3$  (blue line) and 0.1 M  $\text{Na}_2\text{SO}_4$  (green line). SWVs were recorded with a frequency of 10 Hz.

Fig. 6.6 shows the response of 100  $\mu\text{M}$  of each antibiotic at GC electrode in different buffers. For NAF oxidation (Fig. 6.6A) the peak intensity is comparable for each buffer salt composition, slightly higher than for PB pH 6.8. Another difference is that when 0.1 M  $\text{KNO}_3$  and 0.1 M  $\text{Na}_2\text{SO}_4$  are added to the PB another small peak appears at +1.35 V, probably related to the oxidation of the core penicillin structure. The comparison of oxidation signals for CFQ (Fig. 6.6B) shows a decrease of peak intensity for all the considered added salts. Looking at the average values obtained with replicate measurements (Table 6.1), performed with different GC electrodes, this decrease can be related to the uncertainty of the measurements and the conditions of the electrode surface more than to an effect of the salt on the antibiotics electrochemistry.

**Table 6.1.** Average  $I_p$  intensities for 100  $\mu\text{M}$  of NAF, CFQ and CFU at GC electrodes in different buffers. Average values and SD obtained from triplicate measurements with different electrodes. Current values are reported in nA.

	0.1 M PB pH 6.8	+0.1 M NaCl	+0.1 M $\text{KNO}_3$	+0.1 M $\text{Na}_2\text{SO}_4$
NAF	179 $\pm$ 20	200 $\pm$ 5	196 $\pm$ 4	203 $\pm$ 3
CFQ	154 $\pm$ 25	123 $\pm$ 22	115 $\pm$ 19	114.7 $\pm$ 10
CFU	111 $\pm$ 32	153 $\pm$ 31	124 $\pm$ 12	128 $\pm$ 12

For all the considered salts, the average current values for CFQ oxidation decreases from 154 nA of the pure buffer to around 120 nA. Therefore this small decrease is not caused only by the NaCl as seen for the screen printed electrodes. Instead for CFU the addition of NaCl causes an increase in the peak current intensity compared to the pure buffer, from 111 $\pm$ 32 nA to 153 $\pm$ 31 nA. For the other two salts tested the current intensity again decreases slightly with 124 $\pm$ 12 nA for  $\text{KNO}_3$  and 128 $\pm$ 12 nA for  $\text{Na}_2\text{SO}_4$  (see Table 6.1). The relatively high errors associated with the peak current values are probably due to the variability in the performances of the electrode surface for different GC electrodes and to the polishing protocol employed for their preparation.

The changes in current intensities on GC electrodes are present with all the added salts tested and not only with NaCl. This suggests that the specific effect of sodium chloride might be related to the interaction with the electrode surface. Considering the presence of Ag conductive paste below the working electrode, the chloride ions in solution can form AgCl on the working electrode surface, passivating it and reducing the current intensities.

### Electrochemistry of $\beta$ -lactam antibiotics in raw milk and with addition of $\text{KNO}_3$

The possibility of doing electrochemistry directly in raw milk was verified studying the behaviour of a well-known redox couple,  $[\text{Fe}(\text{CN})_6]^{3-/4-}$ . CVs of 2 mM of  $[\text{Fe}(\text{CN})_6]^{3-/4-}$  in 0.1 M PB pH 6.8 and in raw milk are shown in Fig. 6.7. The reversible redox reaction in buffer solution was compared to the one in raw milk. First of all it is possible to notice that the redox peaks of the mediator are present also in raw undiluted milk (green curve in Fig. 7); the reversibility of the redox reaction however is influenced by the matrix, with the  $\Delta E_p$  going from 157 mV in buffer to around 330 mV for the raw milk. Also the peak intensity decreases with a  $I_p^{\text{ox}}/I_p^{\text{red}}$  of 1.05 in buffer and 1.31 in raw milk. The ratio between the oxidation and reduction peak current can be used as an indication of the reversibility of the redox

process and it should be close to 1 for a fully reversible process [35]. This suggests that, even though it is possible as previously reported [30,36], the electrochemistry in raw milk is hindered by the complex matrix.

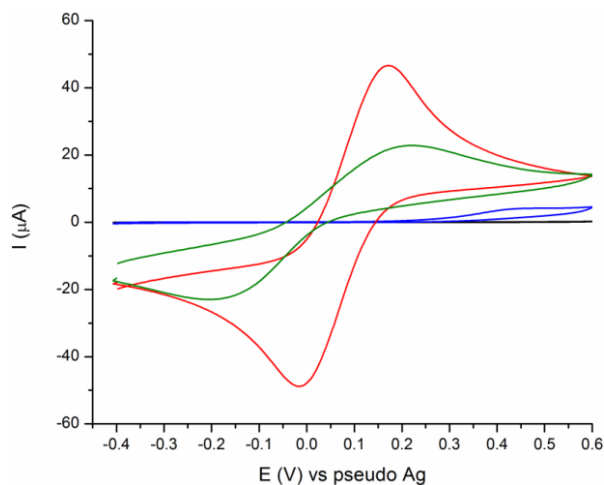


**Fig. 6.7** Blank CV for 0.1 M PB pH 6.8 (black curve) and raw milk (blue curve) and for 2 mM  $[\text{Fe}(\text{CN})_6]^{3-}/4^-$  in 0.1 M PB pH 6.8 (red curve) and in raw milk (green curve). The CVs were recorded at 50 mV/s.

To improve the direct electrochemical detection of  $\beta$ -lactam antibiotics, the addition of an high concentration of supporting electrolyte was tested. The added salts should improve the electrochemistry of the drugs both in respect to peak position and intensity. Different salts were tested, namely  $\text{Na}_2\text{SO}_4$ ,  $\text{KBr}$ ,  $\text{K}_2\text{CO}_3$ ,  $\text{K}_2\text{HPO}_4$  and  $\text{KNO}_3$ . Only the latter however possess the required characteristics: it dissolves easily in pure milk at concentration of 1 M, does not change the pH of the matrix and does not promote aggregation or precipitation of milk components. The addition of a very high concentration of supporting electrolyte should decrease the ohmic drop in the matrix: this effect was verified recording EIS in raw milk in presence or absence of 1 M  $\text{KNO}_3$ . The Bode modulus plot (Fig. 6.8) shows a decrease of the impedance at higher frequencies (black symbols) and concurrently the Bode phase plot evidenced a shift in phase from lower to higher frequencies (blue symbols) for the raw milk + 1 M  $\text{KNO}_3$  compared to the raw milk alone. The solution resistance ( $R_s$ ), extracted from the Bode plots, decreases from 236  $\Omega$  (raw milk) to 17.6  $\Omega$  (raw milk + 1 M  $\text{KNO}_3$ ).

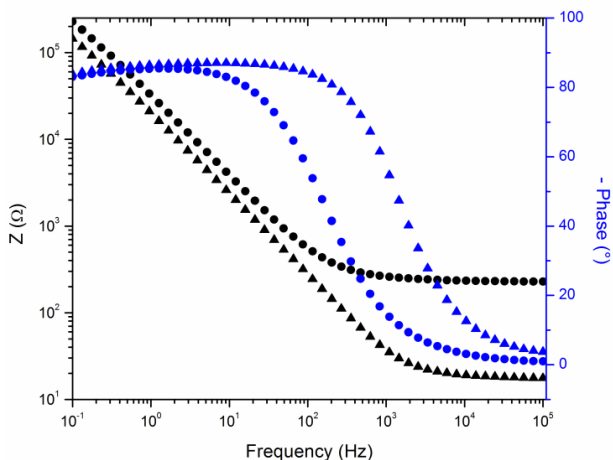


**Fig. 6.8** Bode modulus (black) and Bode phase plots (blue) for raw milk (dots) and raw milk + 1 M KNO<sub>3</sub> (triangles).

SWVs of the different antibiotics were recorded to study the effect of the addition of KNO<sub>3</sub> in the electrochemical oxidation of the considered antibiotics. The SWVs of raw milk with 500 μM of NAF, CFQ and CFU are shown in Fig. 6.9A along with the blank response of the matrix. The blank of the undiluted raw milk (black curve in Fig. 6.9A) presents a broad oxidation peak at *c.a.* +0.7 V and another at +1.3 V. The oxidation peak of NAF at +1.25 V (red curve in Fig. 6.9A) overlaps with the raw milk blank oxidation signal at +1.3 V. Also the peaks of CFQ and CFU at around +0.7 V are superimposed on the other oxidation signal of the blank, a broad peak at +0.7 V. Even if the antibiotic signal is detectable in milk, the peak position and intensity of the oxidation signal of raw milk hinders the detection of these residues in low concentrations (micromolar to nanomolar range).



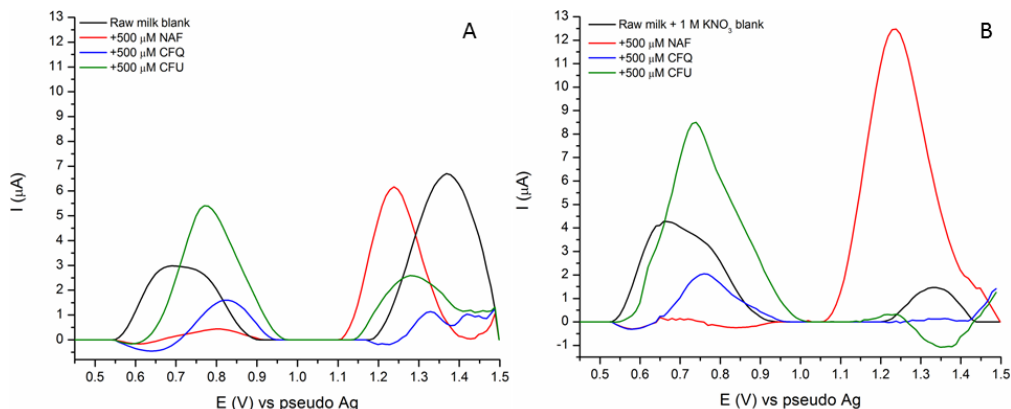


**Fig. 6.9** A) SWVs of blank raw milk (black line) and with addition of 500  $\mu\text{M}$  NAF (red line), CFQ (blue line) and CFU (green line). B) SWVs of blank raw milk + 1 M  $\text{KNO}_3$  (black line) and with addition of 500  $\mu\text{M}$  NAF (red line), CFQ (blue line) and CFU (green line). SWVs are recorded with a Freq. of 10 Hz and reported after blank subtraction.

SWVs recorded in raw milk with the addition of 1 M  $\text{KNO}_3$  are reported in Fig. 6.9B. The electrochemical signals of the raw milk are affected by the salt addition: the peak at +1.3 V has a smaller intensity and the shoulder of the peak at *c.a.* +0.75 V is less pronounced (black curve in Fig. 6.9B). However the salt effect is even more evident on the oxidation of the antibiotics: NAF oxidation peak shifts slightly towards less positive potentials and more important the current intensity increase (from 6  $\mu\text{A}$  to 13  $\mu\text{A}$ ). Also the oxidation peaks of both CFU and CFQ are more intense (from 8.5  $\mu\text{A}$  to 12.5  $\mu\text{A}$  and from 4  $\mu\text{A}$  to 6  $\mu\text{A}$ ); however the broad peak of the blank at +0.7 V is still present. Trying to improve the separation between the oxidations peaks of the raw milk and the ones of the antibiotics, the frequency of the SWV procedure was changed in the range between 5 and 50 Hz.

## Chapter 6 – Electrochemistry in milk

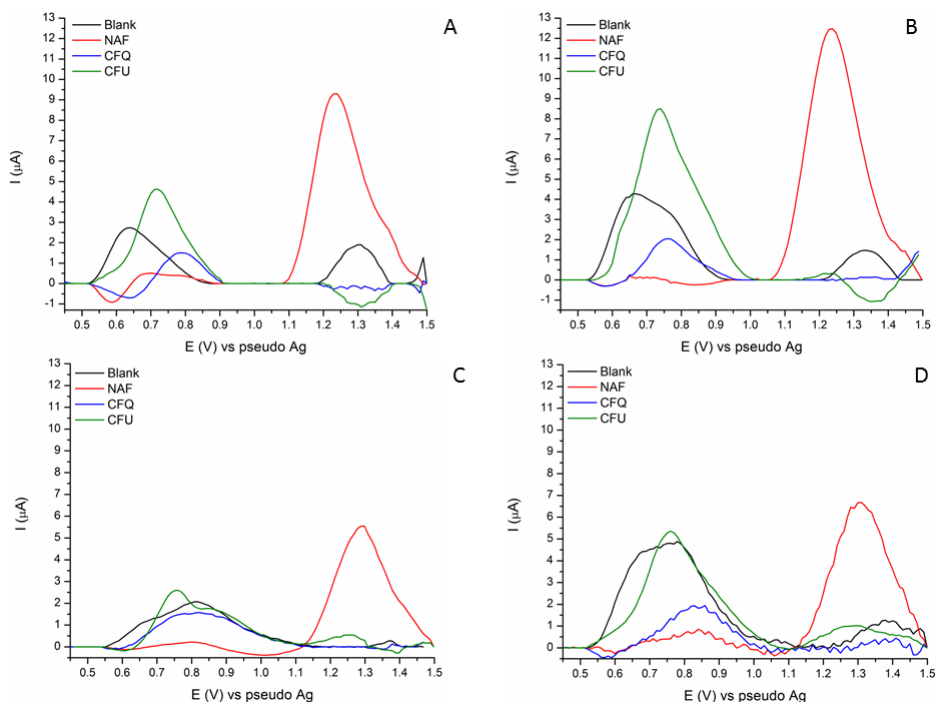


**Fig. 6.10** SWVs recorded in blank raw milk + 1 M  $\text{KNO}_3$  (black line) and with 500  $\mu\text{M}$  of NAF (red line), CFQ (blue line) and CFU (green line) at different frequencies: A) 5 Hz, B) 10 Hz, C) 25 Hz, D) 50 Hz. SWVs are reported after blank subtraction.

For lower frequencies (5 and 10 Hz) the separation between the peaks of the blank and the antibiotics is more pronounced than for higher frequencies (25 and 50 Hz) where the two set of peaks overlaps almost completely, especially for CFU and CFQ. At 5 Hz the oxidation peak of CFQ is clearly visible at +0.8 V, along the one of the blank raw milk at +0.6 V (blue curve in Fig. 6.10A). For higher frequencies these two peaks merge and thus the identification of CFQ signal is hindered. CFU oxidation peak is very intense for 10 Hz and the peak of the blank is visible as a shoulder at around +0.6 V (green curve in Fig. 6.10B). This behaviour is shared by NAF, whose peak at 10 Hz presents a shoulder at higher potentials that overlaps with the peak of the blank at +1.35 V (red curve in Fig. 6.10B). Based on these observations, it was chosen to build calibration plots for all the antibiotics in raw milk with 1 M  $\text{KNO}_3$  added, using a frequency of 10 Hz for CFU and NAF and 5 Hz for CFQ (Fig. 6.11). To calculate the current intensities, the SWV of the blank raw milk + 1 M  $\text{KNO}_3$  was subtracted from the SWVs of the different antibiotics, after moving average baseline correction. While NAF presented a linear dependence between current and

concentration in the given range, the fit for CFQ and CFU needs some more research. It seems that for CFU a response can be obtained only from c.a. 100  $\mu\text{M}$ , although seems to follow a linear response. For CFQ, a more complex fitting (e.g. sigmoidal dose/response or polynomial) from a concentration of c.a. 100  $\mu\text{M}$  is observed. This behaviour might be related to the complex milk matrix which affect the electrochemistry of the antibiotics and concurrently the electrode surface performances.

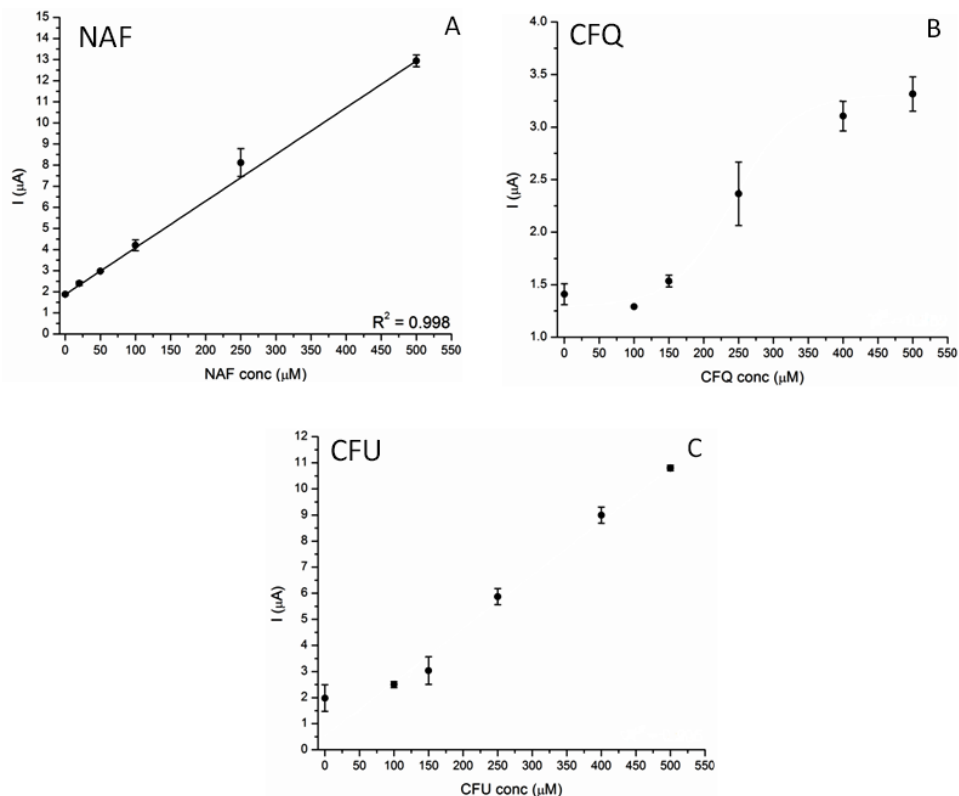


**Fig. 6.11** Calibration plot for NAF (A), CFQ (B) and CFU (C) in raw milk + 1 M  $\text{KNO}_3$ . SWVs for the calibration were recorder at 10 Hz for NAF and CFU and 5 Hz for CFQ. SD calculated on  $n=3$ .

## Conclusions

In this chapter, it was shown that both the original milk pretreatment protocols (Paniel and Holstege), and their simplified versions, can be successfully employed for the electrochemical determination of antibiotics in milk. The decrease in recovery rates for the New ACN and New ISO are offset by the simplified

pretreatment protocol, which does not require laboratory equipment and can be also performed on-site. Sample pretreatment for electrochemical analysis, while not ideal for commercial application, represent a viable alternative for quality control, also when compared to the more time consuming and complex pretreatment needed for traditional confirmatory methods such as HPLC. These simplified pretreatments, while developed for milk, can be possibly used for other food matrices such as meat or eggs. The interfering compounds will be removed by the solvent addition, while the filtration and subsequent buffer dilution will assure the presence of the target antibiotic in the water phase. More studies are however needed to identify where  $\beta$ -lactams accumulates, for example in meat and thus assuring the complete recovery of the antibiotics residues. Another point to consider is the use of solvents, which represent still a source of pollution and might be harmful for the final user if not properly handled.

With the idea of avoiding the use of solvents altogether, a strategy was developed that consisted on the addition of salt to the raw undiluted milk. With the proposed strategy is it possible to detect the investigated antibiotics on G-SPE in the micromolar range: the experimental LOD, which is the lowest concentration experimentally detected, is 20  $\mu\text{M}$  for NAF, 150  $\mu\text{M}$  for CFQ and 100  $\mu\text{M}$  for CFU.

The negative effect of the chloride ions, present in milk, on the performances of graphite screen printed electrodes was successfully neutralized by adding 1 M of  $\text{KNO}_3$  to the undiluted milk. The addition of salt to the milk is an easy and straightforward sample preparation protocol and does not include complex instrumentation or long waiting time. This method can be easily implemented for the analysis of  $\beta$ -lactam antibiotic residues, notwithstanding the need for more sensitive sensors. To the best of our knowledge, this is the first report of the direct electrochemical detection of these antimicrobial drugs in undiluted raw milk.

## Chapter 6 – Electrochemistry in milk

### References

- [1] R. Jenness, Composition of Milk, in: N.P. Wong, R. Jenness, M. Keeney, E.H. Marth (Eds.), *Fundam. Dairy Chem.*, Springer US, Boston, MA, 1988: pp. 1–38.
- [2] V. Gaudin, Advances in biosensor development for the screening of antibiotic residues in food products of animal origin – A comprehensive review, *Biosens. Bioelectron.* 90 (2017) 363–377.
- [3] M.A. Booth, H. Karaosmanoglu, Y. Wu, A. Partridge, CHAPTER 4 Biosensor Platforms for Detecting Target Species in Milk Samples, in: *Food Biosens.*, The Royal Society of Chemistry, 2017: pp. 71–103.
- [4] N. Raza, K.H. Kim, Quantification techniques for important environmental contaminants in milk and dairy products, *TrAC - Trends Anal. Chem.* 98 (2018) 79–94.
- [5] C. Blasco, Y. Picó, C.M. Torres, Progress in analysis of residual antibacterials in food, *TrAC - Trends Anal. Chem.* 26 (2007) 895–913.
- [6] G. Bacher, S. Pal, L. Kanungo, S. Bhand, A label-free silver wire based impedimetric immunosensor for detection of aflatoxin M1 in milk, *Sensors Actuators, B Chem.* 168 (2012) 223–230.
- [7] S.G. Dmitrienko, E. V Kochuk, V. V Tolmacheva, V. V Apyari, Y.A. Zolotov, Determination of the total content of some sulfonamides in milk using solid-phase extraction coupled with off-line derivatization and spectrophotometric detection, *Food Chem.* 188 (2015) 51–56.
- [8] D.M. Holstege, B. Puschner, G. Whitehead, F.D. Galey, Screening and mass spectral confirmation of  $\beta$ -lactam antibiotic residues in milk using LC-MS/MS, *J. Agric. Food Chem.* 50 (2002) 406–411.
- [9] H. Du Nguyen, T.T.L. Nguyen, K.M. Nguyen, A.M. Nguyen, Q.H. Nguyen, Amperometric detection of carbohydrates based on the glassy carbon electrode modified with gold nano-flake layer, *Anal. Chem. Res.* 5 (2015) 14–20.
- [10] M. Ezhilan, M.B. Gumpu, B.L. Ramachandra, N. Nesakumar, K.J. Babu, U.M. Krishnan, J.B.B. Rayappan, Design and development of electrochemical biosensor for the simultaneous detection of melamine and urea in adulterated milk samples, *Sensors Actuators, B Chem.* 238 (2017) 1283–1292.
- [11] H. Li, J. Somerson, F. Xia, K.W. Plaxco, Electrochemical DNA-Based Sensors for Molecular Quality Control: Continuous, Real-Time Melamine Detection in Flowing Whole Milk, *Anal. Chem.* 90 (2018) 10641–10645.
- [12] W.R. De Araujo, T.R.L.C. Paixão, Use of copper electrode for melamine quantification in milk, *Electrochim. Acta.* 117 (2014) 379–384.

## Chapter 6 – Electrochemistry in milk

- [13] S. Das, M. Sivaramakrishna, K. Biswas, B. Goswami, A low cost instrumentation system to analyze different types of milk adulteration, *ISA Trans.* 56 (2015) 268–275.
- [14] A.A.J. Torriero, E. Salinas, F. Battaglini, J. Raba, Milk lactate determination with a rotating bioreactor based on an electron transfer mediated by osmium complexes incorporating a continuous-flow/stopped-flow system, *Anal. Chim. Acta.* 498 (2003) 155–163.
- [15] E. Cortón, F. Battaglini, Effect of milk proteins on the behavior of a biosensor based on poly(allylamine) containing an osmium complex wired to redox enzymes: Part 1. Monoenzymatic configuration, *J. Electroanal. Chem.* 511 (2001) 1–7.
- [16] R.M. Pemberton, J.P. Hart, J.A. Foulkes, Development of a sensitive, selective electrochemical immunoassay for progesterone in cow's milk based on a disposable screen-printed amperometric biosensor, *Electrochim. Acta.* 43 (1998) 3567–3574.
- [17] S.M. Khor, G. Liu, J.R. Peterson, S.G. Iyengar, J.J. Gooding, An Electrochemical Immunobiosensor for Direct Detection of Veterinary Drug Residues in Undiluted Complex Matrices, *Electroanalysis.* 23 (2011) 1797–1804.
- [18] F. Fernández, K. Hegnerová, M. Piliarik, F. Sanchez-Baeza, J. Homola, M.P. Marco, A label-free and portable multichannel surface plasmon resonance immunosensor for on site analysis of antibiotics in milk samples, *Biosens. Bioelectron.* 26 (2010) 1231–1238.
- [19] M.D. Lovander, J.D. Lyon, D.L. Parr, J. Wang, B. Parke, J. Leddy, Critical Review—Electrochemical Properties of 13 Vitamins: A Critical Review and Assessment, *J. Electrochem. Soc.* 165 (2018) G18–G49.
- [20] H. Hakk, N.W. Shappell, S.J. Lupton, W.L. Shelver, W. Fanaselle, D. Oryang, C.Y. Yeung, K. Hoelzer, Y. Ma, D. Gaalswyk, R. Pouillot, J.M. Van Doren, Distribution of Animal Drugs between Skim Milk and Milk Fat Fractions in Spiked Whole Milk: Understanding the Potential Impact on Commercial Milk Products, *J. Agric. Food Chem.* 64 (2016) 326–335.
- [21] G. Ziv, F. Rasmussen, Distribution of Labeled Antibiotics in Different Components of Milk Following Intramammary and Intramuscular Administrations, *J. Dairy Sci.* 58 (2010) 938–946.
- [22] P.F. Fox, T. Uniacke-Lowe, P.L.H. McSweeney, J.A. O'Mahony, Chapter 5 Salts of Milk, in: *Dairy Chem. Biochem.*, 2015: pp. 241–270.
- [23] F. Gaucheron, The minerals of milk Frédéric, *Reprod. Nutr. Dev.* 45 (2005) 473–483.
- [24] S. Creager, 3 - Solvents and Supporting Electrolytes, in: C.G.B.T.-H. of E. Zoski (Ed.), *Handb. Electrochem.*, Elsevier, Amsterdam, 2007: pp. 57–72.
- [25] K. Sipa, M. Brycht, S. Skrzypek, The effect of the supporting electrolyte on the

## Chapter 6 – Electrochemistry in milk

- voltammetric determination of the veterinary drug nitroxinil, *J. Electroanal. Chem.* 827 (2018) 21–26.
- [26] N.G. Tsierkezos, U. Ritter, Influence of concentration of supporting electrolyte on electrochemistry of redox systems on multi-walled carbon nanotubes, *Phys. Chem. Liq.* 50 (2012) 661–668.
- [27] N. Paniel, G. Istamboulié, A. Triki, C. Lozano, L. Barthelmebs, T. Nougier, Selection of DNA aptamers against penicillin G using Capture-SELEX for the development of an impedimetric sensor, *Talanta*. 162 (2017) 232–240.
- [28] G. Moro, F. Bottari, N. Slegers, A. Florea, T. Cowen, L.M. Moretto, S. Piletsky, K. De Wael, Conductive imprinted polymers for the direct electrochemical detection of  $\beta$ -lactam antibiotics: The case of cefquinome, *Sensors Actuators, B Chem.* 297 (2019).
- [29] N. Slegers, A.L.N. Van Nuijs, M. Van Den Berg, K. De Wael, Cephalosporin Antibiotics: Electrochemical Fingerprints and Core Structure Reactions Investigated by LC-MS/MS, *Anal. Chem.* 91 (2019) 2035–2041.
- [30] S. Shrikrishnan, V. Lakshminarayanan, Electron transfer studies of redox probes in bovine milk, *J. Colloid Interface Sci.* 370 (2012) 124–131.
- [31] G. Istamboulié, N. Paniel, L. Zara, L.R. Granados, L. Barthelmebs, T. Nougier, Development of an impedimetric aptasensor for the determination of aflatoxin M1 in milk, *Talanta*. 146 (2016) 464–469.
- [32] E. Commission, Method Validation and Quality Control Procedures for Pesticide Residues Analysis in Food and Feed SANTE/11813/2017, (2017).
- [33] F. Bottari, G. Moro, N. Slegers, A. Florea, T. Cowen, S. Piletsky, A.L.N. van Nuijs, K. De Wael, Electropolymerized o-phenylenediamine on Graphite Promoting the Electrochemical Detection of Nafcillin, *Electroanalysis*. 0 (2019) elan.201900397.
- [34] N. Slegers, A.L.N. van Nuijs, M. van den Berg, K. De Wael, Cephalosporin Antibiotics: Electrochemical Fingerprints and Core Structure Reactions Investigated by LC-MS/MS, *Anal. Chem.* 91 (2019) 2035–2041.
- [35] M.C. Granger, The Influence of Surface Interactions on the Reversibility of Ferri/Ferrocyanide at Boron-Doped Diamond Thin-Film Electrodes, *J. Electrochem. Soc.* 146 (1999) 4551.
- [36] M. Nielen, H. Deluyker, Y.H. Schukken, A. Brand, Electrical Conductivity of Milk: Measurement, Modifiers, and Meta Analysis of Mastitis Detection Performance, *J. Dairy Sci.* 75 (2010) 606–614.





# Conclusions and perspectives

---

The present research project had three main objectives; (1) the study of the electrochemistry of  $\beta$ -lactam antibiotics to be coupled with (2) novel (bio)mimetic electrode modifiers for the (3) sensitive and selective detection of  $\beta$ -lactam antibiotics residues in milk.

Regarding the electrochemical fingerprints of  $\beta$ -lactam antibiotics, both cephalosporins and penicillins showed a rich electrochemistry. Each antibiotic presents different redox signals due to the oxidation of the core structure and different side chain groups. The combination between electrochemistry and HPLC-MS allowed to understand their oxidation mechanism and degradation pathway. Considering the penicillin class, we investigated the electrochemistry of nafcillin (NAF), one of the challenging antibiotic to detect with screening tests, and the isoxazolyl penicillins (ISOXA). NAF identification can be based on the oxidation peak at +1.25 V vs SCE, due to the oxidation of the side chain (2-ethoxy-1-naphthoic acid) conjugated with the core penicillin structure. For the ISOXA penicillins (oxacillin, cloxacillin, dicloxacillin and flucloxacillin) the oxidation peak at +0.8 V vs SCE of the isoxazolyl side chain can be used as a distinctive signal for the whole class. The electrochemical fingerprint of NAF and ISOXA penicillins is also useful to distinguish between the intact and degraded form of the antibiotic, as relevant changes in the voltammetric pattern are present when the core ring structure, responsible for the antimicrobial activity, is hydrolysed.

Concurrently we started the examination of suitable bio(mimetic) electrode modifiers, to enhance sensitivity and selectivity of the proposed direct electrochemical detection strategy. We investigated the possibility to obtain aptamers specific for  $\beta$ -lactam antibiotics. The chosen SELEX protocol was based on a modified version of the FLUMag Selex developed in the Sphere Research group at UAntwerpen. The selection was performed for both NAF and CFX, antibiotics difficult to detect with traditional screening tests. The yield of the first selection rounds (up to the tenth) for both NAF and CFX did not show an improvement in the binding capabilities of the selected pool, even varying several experimental conditions, such as precipitation protocol or dsDNA strand separation and recovery. We concluded that the employed protocol was not suitable for NAF and CFX. Therefore we devised a new variant of another selection strategy centred on GO.

GO-SELEX is based on the interaction between the ssDNA and the GO in solution. When the ssDNA binds to the target, the strand will leave the surface of the GO sheets. The interaction ssDNA-GO can be controlled, by varying experimental parameters such as pH, buffer composition, temperature and salt concentration. We are exploiting this effect to build a PCR-free selection strategy, based on different buffers with increasing stringency for the interaction between ssDNA and GO. Preliminary results showed that the proposed selection strategy is faster and requires less steps than traditional SELEX. Moreover, both the target and the ssDNA are free in solution, avoiding the need of immobilization on a solid support. The most interesting feature of this new selection strategy is the possibility to select the aptamer in the most suitable buffer for the intended final application, electrochemical detection in our case. Notwithstanding these encouraging preliminary results much work still needs to be done. On one hand it is necessary to verify the effect of other possible targets on the ssDNA-GO interaction and on the other hand to carry on the characterization of the obtained pool of fragments. In this way it will be possible to understand whether the obtained aptamers will show improved performance compared to traditionally selected ones.

In parallel with the aptamer selection, we critically evaluated the state-of-the-art in the field of  $\beta$ -lactam antibiotics aptasensing, by testing the affinity of all the aptamer sequences available. At the moment, only four aptamers for  $\beta$ -lactam antibiotics are described in literature: three different aptamer sequences for ampicillin (AMP4, AMP17, AMP18), two aptamers for benzylpenicillin (BBA1 and P8) and one for cefquinome (W1). We choose the ampicillin aptamers to validate a multi-analytical characterization protocol encompassing the use of ITC,  $^1\text{H-NMR}$  and nESI-MS to get a complete picture of aptamer binding mechanism. The results of this characterization survey were surprising; none of the three sequences, reported in the original article and used in many other studies afterwards, showed any sign of specific binding with the target ampicillin. Also the other three published aptamers for  $\beta$ -lactam antibiotics showed rather poor performances, in disagreement to what has been reported before, stressing once more the need for a shared multi-analytical validation strategy for aptamer performances. With our study we offer a robust and reliable protocol for aptamer binding characterization, especially when ultra-sensitive analytical applications are envisioned.

In a second part of the thesis, we focused on the development of alternative (bio)mimetic electrode modifiers. The use of synthetic receptors such as

molecularly imprinted polymers (MIPs) was investigated. We were able to select the best binding monomers for several  $\beta$ -lactam antibiotics by means of rational monomer design. This step was instrumental in obtaining sensitive and selective electropolymerized surface modifiers. We investigated two different strategies: first of all we undertook the development of a conductive imprinted polymer (C-MIP) for the direct electrochemical detection of CFQ with very good selectivity and limit of detection in the nanomolar range. Another approach based on the intrinsic interaction between monomer and antibiotics was employed, with the realization of a graphite screen printed electrode modified with poly(oPD) for the determination of NAF. These sensors were able to reach nanomolar concentration values and their robust and easy fabrication protocol bode well for commercial applications.

Lastly, the research activities were directed towards real sample analysis, i.e. milk in collaboration with ILVO. We developed a pre-treatment protocol for raw milk and investigated the electrochemistry of  $\beta$ -lactam antibiotics in undiluted raw milk. From the literature, two possible pre-treatments based on the simultaneous extraction and deproteinization of milk sample had been selected (Holstage and Paniel protocol). Both are based on the addition of an organic solvent (acetonitrile ACN or isopropanol ISO) and a successive dilution of the extract in buffer. The detection of CFQ in milk was achieved with both pre-treatment protocols, however, with lower sensitivity than in buffer. To avoid sample pretreatment in general, we also studied the electrochemistry of antibiotics in undiluted raw milk. We proved that the milk matrix supports electrochemistry, however with intensities of the redox signals much lower than in buffer. The presence of chloride ions, having a detrimental effect on the performance of the disposable screen printed electrodes employed, could explain this decrease. Trying to overcome this problem, we devised a strategy based on the addition of a very high concentration of another salt ( $\text{KNO}_3$ ) to the undiluted raw milk. The effect of said salt is two-fold. On one side it lowers the resistance of the solution and thus the background noise of the measurements. On the other hand, the  $\text{NO}_3^-$  anion complex the  $\text{Ag}^+$  cations released by the conductive paste of the screen printed electrode. Left unchecked and in presence of  $\text{Cl}^-$ , these  $\text{Ag}^+$  ions will form  $\text{AgCl}$  which, stabilizing the potential of the internal reference electrode, shifts the oxidation peak towards positive potential but can also passivate the working electrode surface. Further studies are in progress to ascertain the mechanism of said interactions, but the proposed protocol gave very good results thus far. We were able to detect NAF, CFQ and CFU in the

micromolar range at bare G-SPE in undiluted raw milk. At the best of our knowledge this is the first proof of electrochemistry of said antibiotics directly in undiluted raw milk.

The promises of electrochemical biosensors are still far from to be fulfilled. Only few of these analytical devices are used by industries and authorities and thus reached the market; while from a basic research point of view, huge improvements have been achieved in the last few years, regarding every aspect of those sensors. However, the efforts to achieve 'better' biosensors should be mitigated by the perspective on their potential for a real world application (responsible research and innovation); in this light MIPs and aptamers seem promising alternatives. Many limitations still remain however; MIPs need a deeper understanding of the characteristics and parameters affecting their performances and their - sometimes-poor selectivity should be improved, for example coupling them with other molecular recognition layers. A systematic and standardized approach to their synthesis is also required. As for the aptamers, the electroanalytical field needs more aptamers, 'better' aptamers. Most of the available aptamers are for bio-medical applications and yet the technology and the know-how are mature enough to tackle challenging targets, like antibiotics or other small molecules. A better understanding of aptamer-target binding mechanisms, along with reliable and accurate characterization techniques, is imperative. Limitations on the availability and the performance of these molecular recognition layers are the possible main cause of the lack of biosensors that can be easily implemented for real world applications. However, the combination of molecular modelling with electro polymerized electrode modifiers is the most promising alternative for direct electrochemical detection. These modifiers, in the form of conductive MIPs or polymer layers, already possess the required analytical characteristics, in term of selectivity and sensitivity, to be employed as monitoring tools for food quality control. Their easy and robust fabrication protocol, coupled with the use of inexpensive and commercially available SPEs, place them in a perfect spot for up-scaling and commercialization, considering also the wide availability nowadays of miniaturized potentiostats and user-friendly application for data collection and analysis.

Along with more robust bio(mimetic) electrode modifiers, one of the main challenge for the electrochemical community in the years to come is the design of sustainable analytical devices. To prevent e-waste growth and concurrently

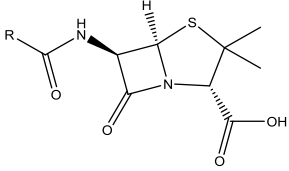
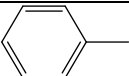
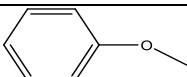
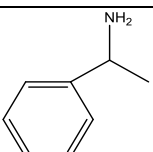
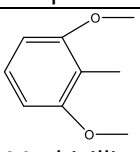
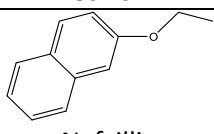
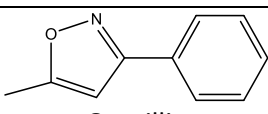
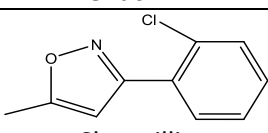
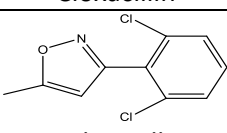
fostering the rapid development of new materials, the fabrication of biodegradable or recyclable electrodes seems the only promising alternative. From reproducibility to safety and reliability to cost-effectiveness and scalability, the mass production of environmentally friendly and completely recyclable sensors and biosensors should be posed as one of the main goals of the electro-analytical chemistry community for the years to come. Current possibilities are focusing on the implementation of either recycled or renewable materials for the substrates as well as for the electrodes themselves. The ultimate redesign goal is to grow towards a fully circular system, where re-use is mostly preferred. In a long term horizon, the development of completely biological sensors based on conductive microorganism such as cable bacteria could be envisioned, paving the road to biodegradable electronics or implantable diagnostic and therapeutic devices.



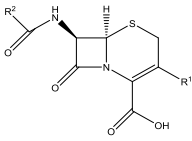
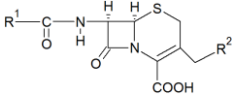
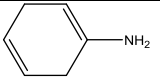
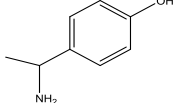
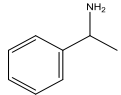
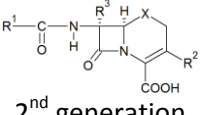
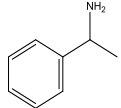
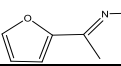
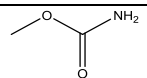
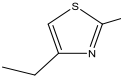
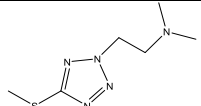
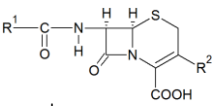
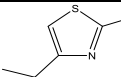
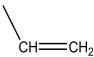
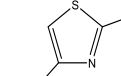
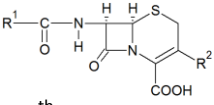
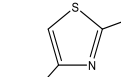
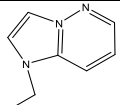
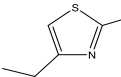
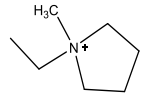
# Appendix

## Classification of $\beta$ -lactam antibiotics

**Table A1.** Classification of penicillins.

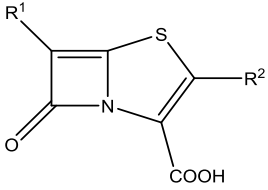
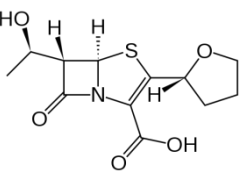
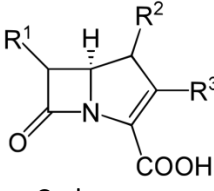
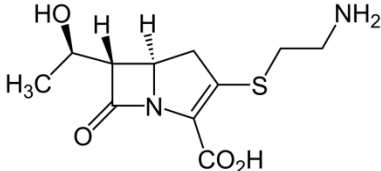
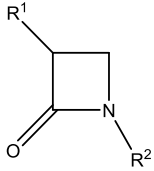
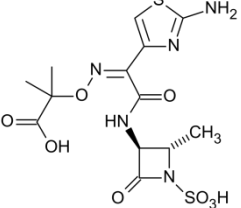
Class	R group
 <p data-bbox="252 1151 365 1180">Penicillin</p>	 <p data-bbox="719 567 857 595">Penicillin G</p>
	 <p data-bbox="719 681 857 710">Penicillin V</p>
	 <p data-bbox="725 872 857 900">Ampicillin</p>
	 <p data-bbox="723 1047 853 1075">Methicillin</p>
	 <p data-bbox="736 1199 835 1228">Nafcillin</p>
	 <p data-bbox="736 1332 840 1361">Oxacillin</p>
	 <p data-bbox="725 1485 853 1513">Cloxacillin</p>
	 <p data-bbox="715 1637 864 1666">Dicloxacillin</p>

**Table A2.** Classification of cephalosporins.

Class	Generation	R1	R2	Example
 <p><b>Cephalosporin</b></p>	 <p><b>1<sup>st</sup> generation</b></p>		-CH <sub>3</sub>	<i>Cephadrine</i>
			-CH <sub>3</sub>	<i>Cefadroxil</i>
			-CH <sub>3</sub>	<i>Cephalixin</i>
	 <p><b>2<sup>nd</sup> generation</b></p>		-Cl	<i>Loracarbef</i>
				<i>Cefuroxime</i>
				<i>Cefotiam</i>
	 <p><b>3<sup>rd</sup> generation</b></p>			<i>Cefdinir</i>
			-H	<i>Cefibuten</i>
	 <p><b>4<sup>th</sup> generation</b></p>			<i>Cefquinome</i>
				<i>Cefepime</i>



**Table A3.** Classification of other  $\beta$ -lactam antibiotics.

Class	Example
 <p data-bbox="329 485 416 519">Penem</p>	 <p data-bbox="806 476 954 510">Faropenem</p>
 <p data-bbox="288 704 450 738">Carbapenem</p>	 <p data-bbox="799 694 954 729">Thienamycin</p>
 <p data-bbox="288 942 456 976">Monobactam</p>	 <p data-bbox="806 961 954 995">Aztreonam</p>



# Abstract

In the broad context of food and environmental safety, the development of selective and sensitive analytical tools for the detection of  $\beta$ -lactam antibiotics in milk down to their Maximum Residues Limits (MRL), is still an open challenge. To address this need, the design of new bio(mimetic) electrochemical sensors was investigated in the present thesis. These sensors are based on the intrinsic electrochemistry of  $\beta$ -lactam antibiotics, taking advantages of the characteristic electrochemical fingerprints of the core structures and redox active side chain groups. The electrochemistry of nafcillin (NAF) and the isoxazolyl penicillins (ISOXA) was investigated, identifying the peculiar electrochemical fingerprint of each antibiotic, proving that it is possible to use electrochemistry for the selective detection of these antimicrobial drugs.

Once verified the applicability of a direct detection, different sensor configurations were tested mainly focusing on:

- the selection and validation of aptamers to be used as bioreceptors in the development of  $\beta$ -lactam biosensors;
- the design of biomimetic receptors, particularly molecularly imprinted polymers, and other synthetic electrode modifiers compatible with a direct detection strategy.

The selection of novel aptamers was performed following both a traditional FluMag SELEX protocol and a novel variant based on graphene oxide (GO). First results with the modified GO-SELEX are promising but more work still needs to be done to validate this novel approach. The few aptamers for  $\beta$ -lactam antibiotics, already reported in literature by other groups, were poorly characterized up to now. For this reason, a multi-analytical characterization protocol for aptamer binding studies was optimized and validated by focusing on aptamer AMP17 against ampicillin. The protocol combines ITC, nESI-MS and  $^1\text{H-NMR}$ . Very striking was the fact that the aptamer sequence did not show any sign of specific binding for its target, even if it was used in many other studies in the past. This thesis now offers a validated protocol for testing the affinity and binding capabilities of aptamer sequences.

In parallel, the functionalization of the electrode surface with polymer modifiers was studied. In particular we optimized a MIP electrochemical sensor based on 4-aminobenzoic acid for the direct electrochemical detection of CFQ. Another approach was tested based on the intrinsic affinity of NAF for an oPD

electropolymerized film on the electrode surface. Both sensors were found to be sensitive and selective for the detection of CFQ and NAF at MRLs in buffer solutions. The proposed protocols are robust and promising for technological transfer.

Lastly, the research activity was directed towards milk sample analysis following two parallel routes: the development of a pre-treatment protocol for raw milk, based on solvent addition (ACN or ISO), and the study of  $\beta$ -lactam antibiotics electrochemistry in undiluted raw milk with addition of  $\text{KNO}_3$  as supporting electrolyte. Both approaches gave encouraging results and the detection of NAF, CFQ and CFU in the micromolar range was achieved, with the second approach in undiluted raw milk.

# Samenvatting

Het ontwerp van een gevoelige en selectieve detectiemethode voor  $\beta$ -lactam antibiotica in zuivelproducten is tot op heden een uitdaging. In het kader van voedsel- en milieuveiligheid dient de bepaling tot op Maximum Residues Limits (MRL) niveau te gebeuren. Deze thesis biedt een oplossing in de vorm van nieuwe types bio(mimetische) elektrochemische sensoren. De sensoren maken handig gebruik van de unieke elektrochemische vingerafdruk van de  $\beta$ -lactam ringstructuur en de diverse redoxactieve zijketens. De elektrochemische mechanismen van nafcillin (NAF) en de isoxazolyl penicilines (ISOXA) zijn gedetailleerd onderzocht en laten toe om deze antimicrobiële stoffen selectief te detecteren.

Na de verificatie van de toepasbaarheid van de directe detectiestrategieën, is overgegaan tot het testen van verschillende sensor configuraties waaronder:

- de selectie en validatie van aptameren die gebruikt kunnen worden als bioreceptoren in de ontwikkeling van  $\beta$ -lactam biosensoren;
- de ontwikkeling van biomimetische receptoren; meer bepaald molecular imprinted polymers (MIPs) en andere synthetische lagen die directe detectie mogelijk maken.

De selectie van nieuwe aptameren is uitgevoerd met zowel de klassieke FluMag SELEX procedure als een nieuwe variant gebaseerd op grafeen oxide (GO). De eerste resultaten van het gemodificeerde GO-SELEX zijn veelbelovend, echter, validatie van deze nieuwe aanpak is vereist in verder onderzoek. De weinige aptameren voor  $\beta$ -lactam antibiotica, beschreven in de literatuur door andere groepen, zijn tot op heden slechts beperkt gekarakteriseerd. Met een geoptimaliseerde multi-analytische werkwijze, door gebruik te maken van ITC, nESI-MS en  $^1\text{H-NMR}$ , is de bindingssterkte van aptameer AMP17 met ampicilline getest. Opvallend was het gegeven dat AMP17 geen specifieke binding vertoonde, hoewel deze reeds in verschillende studies is gebruikt.

Alternatief is het gebruik van geïmmobiliseerde MIPs op basis van 4-amino benzoëzuur of elektro gepolymeriseerd o-phenylenediamine. Gevoelige en selectieve detectie van CFQ en NAF was mogelijk op MRL niveau. De voorgestelde protocollen zijn robuust en veelbelovend voor een technologische overdracht.

In een laatste fase werd onderzoek verricht naar de toepasbaarheid van de strategieën op reële melkstalen. Dit omvatte enerzijds de ontwikkeling van een voorbehandeling van ongepasteuriseerde melk op basis van solvent toevoeging (acetonitril of isopropanol). Anderzijds omvatte dit de elektrochemische studie van  $\beta$ -lactam antibiotica in onverdunde rauwe melk met additie van  $\text{KNO}_3$  als ondersteunend elektrolyt. Beide benaderingen gaven veelbelovende resultaten voor de detectie van NAF, CFQ en CFU, in onverdunde rauwe melk tot op micromolair niveau.



# Academic curriculum vitae

## Articles

F. Bottari, E. Daems, A.M. de Vries, P. Van Wielendaele, S. Trashin, R. Blust, F. Sobott, J. C. Martins, A. Madder, K. De Wael, *Do aptamers always binds? The need for a multi-faceted analytical approach when demonstrating binding affinity between aptamer and low molecular weight compounds*, in preparation.

G. Moro, F. Bottari, J. Van Loon, E. Du Bois, K. De Wael, L. M. Moretto, *Disposable electrodes from waste materials and renewable sources for (bio)electroanalytical applications*, Biosensors and Bioelectronics, 146, December 2019, 111758.

G. Moro, D. Cristofori, F. Bottari, E. Cattaruzza, K. De Wael, L. M. Moretto, *Redesigning an electrochemical MIP sensor for PFOS: practicalities and pitfalls*, Sensors (MDPI), October 2019, 19(20), 4433.

F. Bottari, G. Moro, N. Slegers, A. Florea, T. Cowen, S. Piletsky, A. Van Nuijs, K. De Wael, *Electropolymerized o-phenylenediamine on graphite promoting the electrochemical detection of nafcillin*, Electroanalysis, 26 August 2019.

G. Moro, F. Bottari, N. Slegers, A. Florea, T. Cowen, L. M. Moretto, S. Piletsky, K. De Wael, *Conductive imprinted polymers for the direct electrochemical detection of  $\beta$ -lactam antibiotics: The case of cefquinome*, Sensors and Actuators B: Chemical, Volume 297, 15 October 2019, 126786.

F. Bottari, L. M. Moretto, P. Ugo, *Impedimetric sensing of the immuno-enzymatic reaction of gliadin with a collagen-modified electrode*, Electrochemistry Communications, Volume 97, December 2018, Pages 51-55.

F. Bottari, R. Blust, K. De Wael, *Bio(inspired) strategies for the electro-sensing of  $\beta$ -lactam antibiotics*, Current Opinion in Electrochemistry, Volume 10, August 2018, Pages 136-142.

F. Bottari, K. De Wael, *Electrodeposition of gold nanoparticles on boron doped diamond electrodes for the enhanced reduction of small organic molecules*, Journal of Electroanalytical Chemistry Volume 801, 15 September 2017, Pages 521-526.

S. Pilehvar, C. Reinemann, F. Bottari, E. Vanderleyden, S. Van Vlierberghe, R. Blust, B. Strehlitz, K. De Wael, *A joint action of aptamers and gold nanoparticles chemically trapped on a glassy carbon support for the electrochemical sensing of ofloxacin*, Sensors and Actuators B: Chemical, Volume 240, March 2017, Pages 1024–1035.

F. Bottari, P. Oliveri, P. Ugo, *“Electrochemical immunosensor based on ensemble of nanoelectrodes for immunoglobulin IgY detection: Application to identify hen's egg yolk in*



*tempera paintings*” Biosensors and Bioelectronics, Volume 52, 15 February 2014, Pages 403-410.

#### *Oral Presentation*

F. Bottari, E. Daems, A.M. de Vries, P. Van Wielendaele, S. Trashin, R. Blust, F. Sobott, J.C. Martins, A. Madder and K. De Wael, *The affinity between aptamers and low molecular weight compounds: a cautionary tale*, 2<sup>nd</sup> European Biosensors Symposium, 18-21 February 2019, Florence, Italy.

G. Moro, F. Bottari, A. Florea, L. M. Moretto, K. De Wael, *Conductive Imprinted Polymers For The Direct Electrochemical Detection Of B-Lactam Antibiotics: The Case Of Cefquinome*, SMOBE 2018, Summer meeting on bio(mimetic) electrochemistry, 22-24 August 2018, Antwerp, Belgium.

G. Moro, F. Bottari, A. Florea, L. M. Moretto, K. De Wael, *Conductive Imprinted Polymers For The Direct Electrochemical Detection Of B-Lactam Antibiotics: The Case Of Cefquinome*, EUPOC 2018, Biomimetic polymers by Rational Design Imprinting and Conjugation, 20-24 May 2018, Como, Italy.

F. Bottari, K. De Wael, *Surface modifications of Boron Doped Diamond electrodes: “Soft” Electrochemical Pretreatments in Aqueous Buffers*, Summer meeting on Bio-electrochemistry, 17-19 August 2016, Antwerp, Belgium.

F. Bottari, K. De Wael, *Electrochemical pretreatment of Boron Doped Diamond Electrode for the determination of small organic molecules*, ESEAC MMXVI – 16<sup>th</sup> International Conference on Electroanalysis, 12-16 June 2016, Bath, UK.

F. Bottari, K. De Wael, *Electrochemical pretreatment of Boron Doped Diamond Electrode for the determination of small organic molecules*, ChemCys 2016, 16-18 March 2016, Blackenberge, Belgium.

F. Bottari, P. Oliveri, L. M. Moretto, P. Ugo, *Electrochemical immunosensor with nanoelectrodes ensemble for determination of IgY: identification of egg-yolk as binder in tempera paintings*, Summer meeting on Bio-electrochemistry, 17-20 August 2015, Antwerp, Belgium.

#### *Poster presentation*

G. Moro, N. Slegers, F. Bottari, L. M. Moretto, K. De Wael, *Conductive imprinted polymers for the direct electrochemical detection of  $\beta$ -lactam antibiotics: the case of cefquinome*, 2<sup>nd</sup> European Biosensors Symposium, 18 February- 21 February 2019, Florence, Italy.

F. Bottari, G. Moro, A. Florea, S. Piletsky and K. De Wael, *Graphite screen printed electrode decorated with electropolymerized o-phenylenediamine for the direct electrochemical*

*detection of nafcillin*, Summer meeting on Bio-electrochemistry, 22-24 August 2018, Antwerp, Belgium.

G. Moro, F. Bottari, N. Slegers, L. M. Moretto, K. De Wael, *Exploiting the Intrinsic Electroactivity of B-Lactam Antibiotics: A Biomimetic Sensor for Cefquinome in Milk*, 2-7 September 2018, 69th Annual Meeting of the International Society of Electrochemistry, Bologna, Italy.

F. Bottari, K. De Wael, *Surface modifications of Boron Doped Diamond electrodes: electrochemical pretreatments for sensing of drugs and antibiotics*, 67<sup>th</sup> Meeting of the International Society of Electrochemistry, 21-26 August 2016, The Hague, The Netherlands.

F. Bottari, K. De Wael, *Influence of the electrochemical pretreatment of boron-doped diamond electrode for the detection of  $\beta$ -lactam antibiotics*, 7<sup>th</sup> International Workshop on Surface Modifications for Chemical and Biochemical Sensing, 6-10 November 2015, Pultusk Castle, Poland.

K. De Wael, S. Pilehvar, F. Bottari, *Pinhole permeation of self-assembled ssDNA monolayer on gold electrodes*, 7<sup>th</sup> International Workshop on Surface Modifications for Chemical and Biochemical Sensing, 6-10 November 2015, Pultusk Castle, Poland.

*Reviewer*

Bioelectrochemistry

Colloids and Surface B: Biointerfaces

Sensors and Actuators B: Chemical

Helyion

Biosensors (MDPI)

Polymers (MDPI)



# Acknowledgments

First of all I would like to thank my promoters, prof. Karolien De Wael and prof. Ronny Blust for giving me the opportunity to work on this engaging project for the last 4 years.

Many other people made this thesis possible and I would like to acknowledge their invaluable help for my research. I am grateful to prof. Alexander van Nuijs from Pharmaceutical Science at UA for the MS experiments; Dr. Freddy Dardenne from SPHERE research group at UA, Stella Givanoudi and Dr. Johan Robbens from ILVO for their help with the SELEX; prof. Frank Sobott and Elise Daems from BAMS research group at UA for the nESI-MS experiments; Anne-Mare de Vries, prof. Annemieke Madder and prof. José Martins from UGhent for the NMR and the help with aptamer characterization; Dr. Pieter van Wielendaele, prof. Anne Marie Lambeir and prof. Ingrid de Meester from Biomedical chemistry group at UA for allowing me to work with the ITC instrumentation and their guidance; prof. Sergey Piletsky and Dr. Todd Cowen from Leicester University for the rational monomer design and Dr. Wim Reybroeck from ILVO for his help with milk samples.

Next I am thankful for having spent these last 4 years with all my colleagues, former and current: Cheryl, Liselotte, Mats, Shahid, Gert, Stijn, Steven, Geert, Anca, Saranya, Elise, Jonas, Victoria, Noelia, Karen, Dmitrii, Stas, Vanoushe, Devin, Hanan, Camila, Ermanno, Ehab.

A special thanks to Rui, that had the dubious pleasure of reading and correcting the first draft of this thesis!

Another special thanks to Giulia, for teaching me as much as I taught her.

Thanks to all my “academic” friends that became more than colleagues: Oli, Nick, Alba, Frederick, Stefano and Andrea. Thank for all the time spent together.

Thanks to all my “non-academic” friends that are like my second family here in Antwerp: Chiara, Rita, Winny, Luigi, Maja, Kat, Aya, Carlos, Jonas, Gogo, Andrea and Peter.

And of course thanks to my family who always supported me.

